University of Adelaide
Faculty of Engineering, Computer & Mathematical Sciences
School of Mechanical Engineering
Mech Eng 4135: Honours Project

E.D.W.A.R.D.

Electric Diwheel With Active Rotation Damping

Authors:
Christopher Dyer
Kane Fulton
Jonathon Harvey
Evan Schumann
Tao Zhu

Supervisor:
Ben Cazzolato

November 25, 2009

Executive Summary

This report details the design and construction of an Electric Diwheel With Active Rotation Damping (EDWARD) as well as the implementation of active control methods and system proving. A review of current and previous diwheel designs is conducted and the final design of EDWARD presents several novel improvements, both to the mechanical design and the handling of the system. Mechanical improvements feature an isolated inner frame utilising automotive spring dampers and the design is minimalistic, clean and aesthetically pleasing. Motion of the diwheel is achieved through the use of two DC electric motors, providing a much faster response to commands than previous petrol systems. The diwheel's two DC motors are driven through the use of a dual H-bridge motor controller which receives a pulse-width-modulated signal from a microprocessor. A number of integrated sensors, including a gyrosensor, accelerometer and two encoders are used to measure the behaviour of the diwheel and are used to implement active control of the system. Acceleration, deceleration and steering are controlled by a joystick which is read by the microprocessor.

Slosh control has been implemented in EDWARD to reduce the intrinsic rocking motion during harsh acceleration and deceleration and the success and viability of this control is detailed. Inversion control which aims to invert the driver and inner frame upside down and maintain this unstable position, has been modelled and shown to be feasible for application on the physical system. Implementation of inversion control in the future is proposed and would allow the driver to drive the diwheel in its inverted state.

At the time of this report, the authors are unaware of any other fully operational electric diwheels, and no diwheels implementing any form of active control exist to date. This has created the opportunity to explore new grounds in the field of active control as applied to non-linear vehicles by providing a fun, fully functional and visually impressive prototype. The group have achieved all core project goals, as well as a number of extension goals.

Disclaimer

This report is the work of the five authors named below. Any information that has been obtained from other authors has been respectively cited where used.

Christopher Dyer

Kane Fulton

Jonathon Harvey

Evan Schumann

Tao Zhu

Acknowledgements

Firstly we would like to acknowledge Associate Professor Benjamin Cazzolato for his indelible enthusiasm and support throughout the project. We would also like to thank Philip Schmidt who was an integral part of the design of the system electronics, and the source of many ideas. Furthermore we would like to thank Silvio De Ieso. Finally we would like to sincerely thank Bob Dyer who has assembled the physical system EDWARD with great skill and patience.

Contents

Executive Summary iii

Disclaimer v

Acknowledgements vii

1 Introduction 1

2 Background 3
- 2.1 Previous Designs . . . 3
  - 2.1.1 Outer Wheel . . . 5
  - 2.1.2 Tyre . . . 7
  - 2.1.3 Inner Wheel . . . 7
  - 2.1.4 Idler Wheel . . . 8
  - 2.1.5 Drive System . . . 8
  - 2.1.6 Steering . . . 10
  - 2.1.7 Brakes . . . 10
  - 2.1.8 Seating and Harness . . . 10
  - 2.1.9 Conclusion . . . 11
- 2.2 System Dynamics and Research . . . 11
- 2.3 Slosh Control . . . 12
  - 2.3.1 Previous Work . . . 12
  - 2.3.2 Relevance of Studies . . . 12
  - 2.3.3 Application to the Diwheel . . . 13
- 2.4 Yaw Control . . . 13

3 Design Specification 15
- 3.1 Project Goals . . . 15
- 3.2 Functional Requirements . . . 17
- 3.3 Technical Performance Measures . . . 18

4 Component Selection 21
- 4.1 Mechanical Brake Selection . . . 21
- 4.2 Brake Lever . . . 23
- 4.3 Outer Wheel . . . 24
- 4.4 Seating and Harness . . . 25
- 4.5 Drive-wheel . . . 27
- 4.6 Motors . . . 28

4.7 Motor controller . . . 30
4.8 Batteries . . . 31
4.9 Processor . . . 31
4.10 Gyrosensor . . . 33
4.11 Accelerometer . . . 34
4.12 Steering Control . . . 35

5 Electrical Hardware **37**
5.1 Motor Controller . . . 38
5.2 Power Board . . . 40
5.3 Power Control Board . . . 41
5.4 Ignition Circuit . . . 41
5.5 Current Sensors . . . 42
5.6 Gyrosensor and Accelerometer Board - *Sensor Board* . . . 44
5.7 Encoder Sensors . . . 46

6 Mechanical Design **49**
6.1 Space Frame Design . . . 50
6.1.1 Dynamics . . . 50
6.1.2 Ergonomics . . . 52
6.1.3 Final Design of the Space Frame . . . 52
6.1.4 Electronics Box . . . 53
6.1.5 Battery Box . . . 54
6.1.6 Joystick Mounting . . . 54
6.2 Finite Element Analysis . . . 54
6.2.1 Idler Wheel Contact Problem . . . 54
6.2.2 Idler FEA Results and Conclusions . . . 56
6.2.3 Space Frame Analysis . . . 57
6.2.4 Space Frame FEA Results and Conclusions . . . 57
6.3 Outer and Inner Wheel Design . . . 58
6.3.1 Design Criteria and Aim . . . 59
6.3.2 Concept Solutions . . . 59
6.3.3 Final Design of the Inner Wheel . . . 67

7 Control System Design **73**
7.1 Analytical Derivation of the System Dynamics . . . 73
7.1.1 Mechanical Dynamics . . . 73
7.1.2 Euler-lagrange Derivation . . . 74
7.1.3 Electrical Dynamics . . . 78
7.1.4 Linearised Dynamics . . . 79
7.1.5 Summary of Assumptions . . . 81
7.1.6 Model Parameters . . . 81
7.2 Simmechanics Derivation of the System Dynamics . . . 81
7.2.1 Main Block Diagram . . . 82
7.2.2 Inner Frame . . . 82

7.2.3 Drive System . . . 83
7.2.4 Outer Wheels . . . 85
7.2.5 Results . . . 85
7.2.6 Visual Simulation Using VRML . . . 85
7.2.7 Final VRML Model . . . 88
7.3 Speed Control . . . 90
7.3.1 Open-loop Speed Control . . . 90
7.4 Yaw Control . . . 91
7.4.1 Derivation of Yaw Dynamics . . . 92
7.4.2 Open-loop Yaw Step Response . . . 94
7.4.3 Closed-loop Yaw Response . . . 94
7.5 Slosh Control . . . 96
7.6 Inversion Control . . . 99
7.6.1 Design of Fuzzy Swing-up Controller . . . 100
7.6.2 Balancing Controller . . . 102
7.6.3 Combining the Swing-up and Balancing Controller . . . 104
7.6.4 Controllability and Observability of the Linearised System . . . 104

8 Software Design 107
8.1 Overview of Software and Design Methodology . . . 107
8.2 Input and Output data . . . 108
8.3 Steering and Motor Control . . . 109
8.4 Measuring Motor Speed . . . 109
8.5 Measuring Inner Frame Angle and Slosh Rate . . . 109
8.5.1 Sensor Fusion using a Kalman Filter . . . 114
8.5.2 Performance of the Kalman Filter . . . 115
8.5.3 Arctangent Function . . . 115
8.6 Implemention of the Control Systems . . . 116
8.6.1 Slosh Control . . . 116
8.6.2 Swing-up Control . . . 117
8.7 Additional Functions . . . 117
8.7.1 Using the SD card . . . 117

9 Experimental Results and System Integration 119
9.1 System parameter identification . . . 119
9.2 System Tests . . . 120
9.2.1 Open-loop slosh . . . 121
9.2.2 Closed-loop slosh control . . . 121
9.2.3 Positive Feedback Swing-up Controller Test . . . 124
9.3 Software and Electrical Issues . . . 125
9.4 Hardware Issues . . . 126

10 Final Design Analysis 127
10.1 Summary of Goals and Achievements . . . 127
10.1.1 Mechanical Goals . . . 127

10.1.2 Electrical and Electronic Goals . . . 128
10.1.3 Miscellaneous Goals . . . 130
10.1.4 Extension Goals . . . 130
10.2 Cost Analysis . . . 133

11 Summary **137**
11.1 Future Work . . . 137
11.2 Conclusion . . . 138

References **139**

A Publications Arising from this Thesis **143**

B Appendix **155**
B.1 Hertzian Idler Wheel Contact . . . 155
B.2 Drive-wheel Hub Bolt . . . 157
B.3 Mechanical Design Dynamic Analysis . . . 158
B.4 Anthropometrics . . . 160

C FMEA, Risk Analysis and SOP **163**

D Mechanical Drawings **183**

1 Introduction

A diwheel is a vehicle which consists of a two large outer wheels that completely encompass an inner frame. The inner frame is free to rotate within the wheels, and is typically supported by a common axle or idler wheels which roll on the inner surface of the wheels. The outer wheels are driven from the inner frame and forward motion is achieved through a reaction torque generated by the eccentricity of the centre of gravity of the inner frame. Diwheels, like their more popular cousins the monowheel, have been around for almost one and a half centuries (Cardini 2006). Each of these platforms suffer from two common issues affecting driver comfort those of slosh and tumbling (also known as gerbiling). Slosh consist of the oscillation of the inner frame, and it occurs in all monowheels and diwheels, where the centre of gravity of the inner frame is offset from the centre line of the wheels. It is very noticable as these platforms typically have low damping between the wheel and the frame in order to minimise power consumption during locomotion. In addition, during severe braking or acceleration the inner frame may tumble relative to the earth centred frame, which affects the ability of the driver to control the platform.

The aim of the project was to design and build an electric diwheel and to implement several control strategies to modify its dynamics. The first was a slosh controller, with the purpose of minimising the rocking motion that occurs as the vehicle is accelerated or decelerated when applying torque to the drive-wheels. This was deemed necessary after viewing videos of monowheels and diwheels in operation. If implemented correctly it would also allow maximum deceleration of the vehicle if necessary, which occurs when the centre of gravity of the inner frame is horizontally aligned to the centre of the outer wheels. The project was subsequently called the Electric Diwheel With Active Rotation Damping, and the vehicle was nicknamed Edward. Another control mode was also considered with the aim to make the ride more exciting. This involved a swing-up controller followed by a balancing controller, together termed an inversion controller. The purpose of this controller was to invert the driver and balance the inner frame, enabling the driver to drive around upside down.

A literature review was undertaken to evaluate previous diwheel and monowheel designs from which the design of Edward was to improve. Using these designs as a basis, an original mechanical concept design of a diwheel was produced and subsequently constructed. The outer wheels were rolled and welded stainless steel tube with a rubber strip bonded on the outer rolling surface. An inner frame supports the driver who is held in place by a five-point racing harness. The inner frame runs on the outer wheels with three nylon idlers that are coupled to the inner frame by suspension arms, which act to provide some suspension and also maintain a constant contact force between the idlers and the wheel. Two brushed DC motors each drive (via sprockets and a chain) a small motorcycle drive-wheel which contacts the inner radius of the outer wheel. Thus the vehicle can be driven forwards and backwards using a combined voltage applied to the motors, and can be steered when the motors are driven differentially. The vehicle was made drive-by-wire, where the driver controls the vehicle via a joystick which

interfaces with a microprocessor. A mechanical hand brake operates calipers on the drive-wheels. Three sensing systems were implemented: a solid state gyrosensor (for measuring the slosh rate of the inner frame), a solid state DC coupled accelerometer (for state estimation of pitch angle) and incremental encoders on the two drive-wheels.

The conceptual design of EDWARD was commenced in parallel with the design of an electrical control system. The open-loop and closed-loop control strategies, which were to be implemented on a microcontroller unit (MCU), were designed following the derivation of the dynamics for the diwheel. The dynamics, which have not been presented elsewhere, have been derived using the Lagrangian approach, and SIMMECHANICS™ using a mechanical based approach. Measured parameters of EDWARD were used in a virtual reality simulation for which the open-loop response and various closed-loop responses were simulated. The concept of using feed-back control strategies to actively reduce the slosh of the inner frame has never before been demonstrated. EDWARD has proven to be an exciting vehicle which showcases a strong mechanical engineering component, and will be used to demonstrate automatic control at the University of Adelaide.

The following report details the methods and efforts taken to achieve the construction of EDWARD. Initially, a background to the project is presented in Chapter 2, where the mechanical design and control of previous diwheels and monowheels is reviewed. Chapter 3 specifies the goals of the project with regard to functional requirements and performance measures. The mechanical and electric components purchased for use in EDWARD are described in Chapter 4 while the electrical hardware designed to support the implementation of control on diwheel is described in Chapter 5. Chapter 6 discusses the mechanical aspects of the diwheel, and the concepts developed throughout the design process. Chapter 7 contains the design of the control strategies of slosh and inversion and presents the derivation of the uncoupled yaw and translation dynamics. Chapter 8 describes the design of the software implemented on the MCU which achieves both user and active control of the diwheel. The results achieved during the testing of the diwheel and it subsystems are presented in Chapter 9. An analysis of the final design of EDWARD in the context of the project goals is provided in Chapter 10. Chapter 11 concludes the report and lists possible future work which appears relevant to continuing the success of EDWARD.

2 Background

A literature review is essential for the design of an electronic diwheel as it creates a basis for system integration, part design and component selection. The following chapter presents a review of a number of which demonstrate what has already been achieved towards the design of a diwheel.

2.1 Previous Designs

From a review of existing diwheel's mechanical components, a report and assessment of systems in previous diwheel designs was conducted. Previous monowheels, which use similar systems to that of a diwheel, were also considered. An internet based academic search revealed no literature directly relating to the mechanical design of a diwheel, however there exist many designs outside the formalisation of academia. For the purpose of the discussion of the mechanical system a diagram labelling the relevant components in shown in Figure 2.1. The term *inner frame* will be used to refer to the inner wheel and space frame, which together constitute all components which rotate inside the outer wheels.

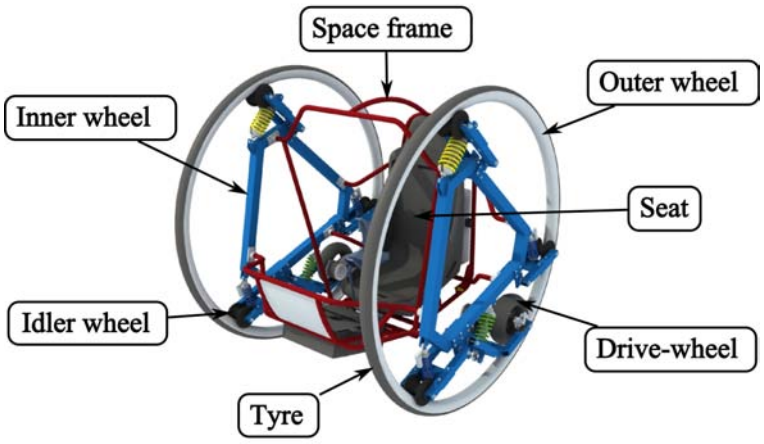

Figure 2.1: Components of a diwheel

Modern designs of diwheels and monowheels have been used only on a small non-commercial scale as backyard projects and attractions. Perhaps the closest use of the diwheel principle in commercial applications is the prototype of André Costa, winner of the 3rd Peugeot Design Competition (Serious-wheels 2005). Details of the system's design have not been made public. However, the concept design is described in a Peugeot press release (Serious-wheels 2005) and

can be seen in Figure 2.2. This highly stylised vehicle prototype is not a true diwheel, as it is stabilised by two spheres which act as front wheels.

Figure 2.2: The Peugeot Moovie, (Serious-wheels 2005)

Patent archives contain many old monowheel and diwheel designs with details of their intended mechanical realisation. Detailed description of a diwheel concept and its working subsystems is presented in the 1947 Belgian Patent: "Two-wheeled vehicle supportive of each other" (Vereycken 1947). This diwheel was said to have been constructed and designed by Ernest Fraquelli (Unknown 1935) and can be seen in Figure 2.3.

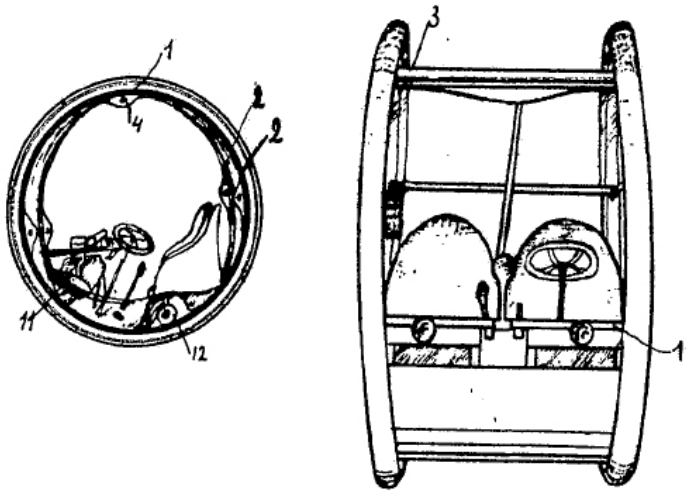

Figure 2.3: A schematic from a Belgian patented diwheel, (Vereycken 1947)

Dave Southall, a senior lecturer in embedded systems at Manchester Metropolitan University in the United Kingdom, has previously made a petrol powered monowheel and

is currently completing an electric diwheel. Southall's diwheel is, to the authors knowledge, the only other electric diwheel in development. Correspondance with Dave Southall has been useful for ascertaining detailed knowledge of some of the problems he has encountered with construction of his diwheel. Other relevant constructions include the Rocket Roaster by Kerry Mclean and a petrol powered diwheel by Jonas Bjorkholtz (Di-wheels 2009)

2.1.1 Outer Wheel

The outer wheel is used to make rolling contact with the surface of the road. Similar to conventional bike and car tyres, its function is to support the loads of the structure upon the road, as well as provide some vibration and shock isolation from the variation in road surface. Manufacturing a large outer wheel is problematic because the outer wheel must be capable of enduring contact pressures between the wheel and the road and between the outer wheel and the idler wheels. Under operational loading, local deformation must be kept to a minimum and the wheel's circular profile must be maintained.

Many diwheel manufacturers have constructed the outer wheel from tubular metal. The wheel is typically metal tube or section, rolled and joined to form a rigid ring. The Rocket Roadster made by Kerry Mclean shown in Figure 2.4, features a tubular aluminium wheel. The wheel is rolled into a ring and then cut and welded. It is then held flat, heated and annealed until it is round (Parks 2005).

Figure 2.4: The Rocket Roadster by Kerry Mclean (pictured), (Parks 2005)

The Trinity, constructed by Dave Southall (Figure 2.5) uses a rolled and welded steel

wheel. A tubular wheel allows the contact between the outer wheel and the ground to remain at a single point when the wheel is tilted. In order to provide steering, a monowheel's outer wheel must maintain contact with the ground at a single point. However, this is not required in the operation of a diwheel as the wheels are permanently upright. The Swedish diwheel (Figure 2.6), uses a rolled C-channel section for its wheel, which has a flat outer surface.

Figure 2.5: The Trinity by Dave Southall (pictured) (Southall 2009)

Figure 2.6: Diwheel by Swedish Jonas Bjorkholtz (Di-wheels 2009)

The diameter of the outer wheel influences the dynamics of the diwheel system and its overall size and mass, while constraining the space for the passenger and equipment. The size of the wheel limits the use of existing wheel and tyre arrangements that are of conventional dimensions, which would provide the system with a convenient pneumatic tyre. The diameter of the wheel is large, ranging from 1.96 metres in the Swedish diwheel (Figure 2.6), to 0.914 metres, the diameter of a mini-monowheel by laFrance Bressen shown in Figure 2.7. The height (and approximate wheel diameter) of the Peugeot Moovie (Figure 2.2) is 1.54 meters. The Peugeot Moovie's body extends past the diameter of the wheels to house externally mounted spheres, providing further stability and preventing tumbling.

Figure 2.7: The mini-monowheel of laFrance Bressen, (Wiley 1988)

2.1.2 Tyre

The tyre of a diwheel system is required to isolate the wheel from the roughness of the road and provide traction for propulsion. Conventional tyres are typically made from rubber, which provides excellent grip. The Belgian patent, (Vereycken 1947), presented a custom pneumatic solution which provided significant vibration isolation (Figure 2.8). Figure 2.8 shows the wheel using a custom tubeless tyre and rim arrangement modified with a flange for rolling contact with the supporting idler wheels. The Swedish diwheel does not use any tyre and the steel wheels make direct contact with the road. The mini-monowheel of laFrance Bressen (Figure 2.7) uses a tractor tyre modified for use in the monowheel design. With the use of existing wheels the tyre is already integrated into the wheel and requires no further customisation for use in a diwheel. Larger tractor wheels and tyres have been used in the design of several monowheels shown on the Museum of Retro Technology website (Monowheels 2009).

Figure 2.8: Construction of the patent of Vereycken, (Unknown 1935)

2.1.3 Inner Wheel

The inner wheel (see Figure 2.1) is a rigid structure supporting the guidance and drive mechanisms of the outer wheel and connects to the main frame. Typical monowheel designs require

this system to accommodate the seating of the passenger as featured in the monowheels shown in Figures 2.4 and 2.7. However, a diwheel does not require the seating of the passenger in either inner wheel. The inner wheel design of a diwheel then, has an additional function of supporting an inner frame of the vehicle where the passenger is seated. The design of a monowheel often uses a circular rolled inner wheel (see Figure 2.4) which is segmented for the mounting of functional elements. This design is also used in diwheels (see Figure 2.5) for the function of providing a circular frame structure.

If the inner frame is restricted from rolling by mechanical means, then the function of the inner wheel changes. The load is then always concentrated at the lower part of the inner wheel and the function of the inner wheel is to support the frame only at this point. This concept is featured in GBO Design-Engineering's concept of a diwheel (GBO 2005) as shown in Figure 2.9.

Figure 2.9: A pedal powered diwheel concept vehicle, (GBO 2005)

Another design concept used for the inner wheel is a spoked wheel which then attaches to an axle, and bypasses an inner wheel to attach to the space frame. This design does not need idler wheels to guide the outer wheel, instead it uses a large hub and axle. The inner frame then hangs and pivots from the axle.

2.1.4 Idler Wheel

The function of the idler wheels is to support and guide the outer wheel. The idlers make contact with the outer wheel at certain points along its profile. This contact has been solved through a variety of solutions. The Trinity (Figure 2.5) uses custom idler rollers made from nylon with inset bearings (Southall 2009). This solution is also used in the Rocket Roadster by Kerry McLean (Figure 2.4). The Vereycken diwheel uses a similar idler wheel with a square inner profile (Figure 2.10). Another solution for guiding idler wheels is shown in Figure 2.11 of Ben Wilson's version of a monocycle (Dez 2008). This design uses two thin wheels similar to roller blade wheels either side of a tubular inner wheel.

2.1.5 Drive System

The drive-wheel system provides a means of transferring the torque of the motor or engine to the outer wheels. In the design of a wheel with an axle, coupling of the wheels to the driven

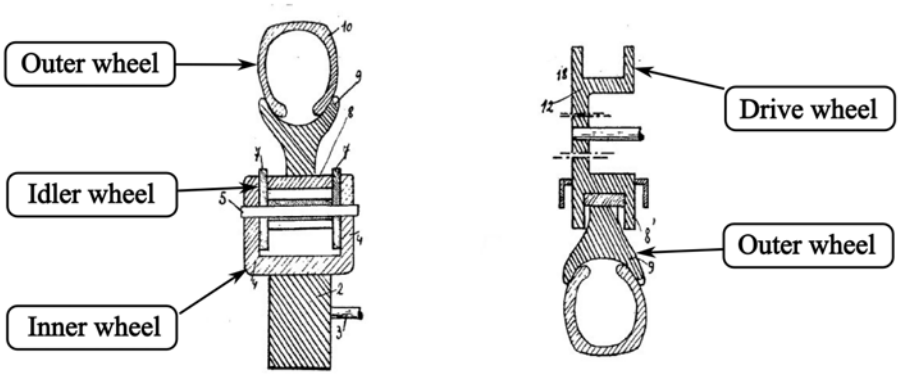

Figure 2.10: A cross section of: left: an idler wheel mechanism, and right: a drive-wheel used to guide and drive the outer wheel, respectively. (Vereycken 1947)

Figure 2.11: Drive wheel and idler wheel detail of the Ben Wilson monocycle, (Dez 2008)

axle is required. However, in the design of a centre-less wheel, the drive mechanism requires the transference from the drive-shaft to the large outer wheel. Components of this system may include drive-wheels or cogs. As part of the drive system, the outer wheel acts as the internal gear annulus in a planetary gear system, with the drive-wheel as a single planet. The planet rotates around a common axis of the planet and annulus when accelerating or decelerating.

One form of drive system that transmits power to the wheel is a toothed drive gear within the wheel which meshes with the outer wheel. This design is featured in many patented monocycles seen on the Museum of Retro Technology website (Monowheels 2009). Another form of drive is a traction between a drive-wheel and the outer wheel. This design is used in The Trinity (Figure 2.5). A possible problem with a friction drive is that the driving torque is limited by the possibility of slipping between the outer wheel and the drive-wheel. The source of propulsion is commonly a petroleum engine, featured in the designs of Vereycken (Figure 2.3), Kerry

Mclean (Figure 2.4) and Bressen (Figure 2.7). The diwheel by Edouard Vereycken (Figure 2.3) is differentially driven by a petrol engine. The differential allows the use of a single engine by distributing the propulsion to each wheel, while enabling the independent rotation of each wheel through a braking system. Other forms of power include pedal, as in the monocycle by Ben Wilson (Figure 2.11), and electric motors as featured in the Moovie (Figure 2.2) and the Trinity (Figure 2.5).

2.1.6 Steering

Steering of the diwheel requires the separate and controlled drive of each wheel, and has been achieved through many methods. The steering of Edouard Vereycken's diwheel is controlled by a steering wheel rotated by the passenger, much the same as in an automobile. Vereycken's design featured brake shoes housed within each drive-wheel, which, when the steering wheel is turned, are activated accordingly to slow the drive-wheels. This then governs the distribution of propulsion though the means of a mechanical differential (Vereycken 1947). The Peugeot Moovie (Figure 2.2) uses variable control of the electric drives on each of the wheels to achieve steering and remarkable manoeuvrability (Serious-wheels 2005). This allows swift and complete yawing of the vehicle while stationary.

The control of the diwheel structure is influenced by its dynamics which are mainly constrained by it's geometry and the distribution of mass. Rotational motion of the diwheel's inner frame relative to the earth-centred frame is termed *slosh* and a complete revolution is termed *tumbling* or *gerbiling*. The designs of many monowheels avoid this behaviour by having a centre of mass far from the centre of rotation. This can be achieved by adding mass to the inner frame, as was done by Kerry Mclean (Parks 2005), or by designing the seating position and engine mount far from the centre of rotation. However, if intended, gerbiling can be facilitated in a diwheel by keeping the centre of mass close to the central axis.

2.1.7 Brakes

Mechanical braking systems aim to remove rotational and translational kinetic energy from the vehicle. In the case of the diwheel, this action may also convert translational energy into rotational energy of the inner ring, which may resulting in gerbiling. Mechanical braking systems need to be mounted to the drive-wheel axle or the outer wheel. Often the drive-wheel is acted on directly. Cable drawn disc brakes are used in the design of The Trinity (Figure 2.5) mounted directly to the hub of the drive-wheel. The Vereycken diwheel (Figure 2.8), also uses brake pads which are applied to the drive-wheels, essentially acting as a disc brake.

2.1.8 Seating and Harness

Passenger integration presents a challenge in a diwheel where the dynamics and mechanics pose serious safety issues. If the diwheel accidentally or deliberately is provoked to gerbil, the passenger may remain upside down for sometime and must be properly restrained. Previous models of diwheels and monowheels have not required such security and have relied on the centre of mass being far away from the centre of rotation in order to keep to occupant upright. The Trinity (Figure 2.5) uses a 5-point racing harness anchored on the frame in combination

with a go-kart seat. Seats used in previous designs are varied, including the use of motorcycle seats, go-kart seats and automotive seats. Diwheel and monowheel seating has also been constructed from panelling integrated into the frame (Figure 2.8). The seat and harness places significant influence on the human occupant. During operation the forces on the occupant due to acceleration may cause damage if the occupant is unrestrained or in incorrect posture. Therefore the use of a seat and harness combination must be considered with due care to occupant safety.

2.1.9 Conclusion

The mechanical components reviewed in this section give an overview of the previous designs and methods used to form a functional diwheel. Each design must be considered in the context of its desired function and behaviour before use in the design of EDWARD. Another factor in considering previous designs is that none have yet implemented an electronic feedback control system, and that the EDWARD diwheel is the first of its kind.

2.2 System Dynamics and Research

The diwheel is comprised of two wheels which are connected to an inner wheel that is rigidly connected to a central space-frame, where the driver of the vehicle is seated. Each of the two wheels may be independently driven by an appropriate drive system which applies torque to the wheels.

In the lower equilibrium position, the combined mass of the inner frame and rider sits below the rotational axis of the outer wheels. When a torque is applied to the wheels via the drive system, the inner frame will be displaced by a reaction torque. This continues until the weight of the displaced center of gravity counteracts the torque due to gravity. Rotation of the center of gravity is generally considered unfavourably, as harsh braking or acceleration robs the diwheel of its forward acceleration.

When the drive-wheels are driven at different speeds, the diwheel will rotate about a vertical axis. This steering can be controlled by a differential drive scheme and is very practical.

If the center of gravity of the diwheel is rotated 180 degrees from the neutral position, the characteristics of the system resemble that of an inverted pendulum. The pivot point is then located at the central axis of the wheels, and the line connecting the axis and the combined Center of Gravity acts as a virtual rigid link, provided the Center of Gravity remains static relative to the inner frame. In order that the upper unstable equilibrium point is controlled, several tasks must be addressed:

- The Center of Gravity must be moved from the lower to the upper equilibrium
- The Center of Gravity must be balanced at the upper position
- The diwheel must maintain balance against disturbances; including those induced by trajectory following

Because the use of the inverted pendulum in control systems is well established, many of these issues have been addressed in the literature. A discussion of the control to be used in the proposed inversion controller is given in Section 7.6.

2.3 Slosh Control

The implementation of control in the project aims to diminish the rocking of the driver within diwheel inner frame which occurs during harsh acceleration and deceleration. This rocking motion is similar in dynamics to the sloshing of liquid that occurs in containers of fluid undergoing lateral acceleration and deceleration. Liquid slosh is evident in many systems such as vehicles containing tanks of fuel, submarines and rockets. When the vehicle accelerates or brakes, the fuel undergoes oscillatory motion until the acceleration ceases and the liquid slosh decays to equilibrium. The effects of liquid slosh on a system's dynamics have been investigated with increasing interest as the implications of the problem have been found to be significant in systems such as satellites, spacecraft, and large ships (Nichkawde et al. 2004).

2.3.1 Previous Work

Although much work has been done on deriving the dynamics of liquid slosh for various container shapes and fill levels (Nichkawde et al. 2004; Aboel-Hassan et al. 2009; Dodge 2000; Gandhi et al. 2009), little work has been published on the active control of slosh. Liquid slosh control has been attempted at ranging levels of complexity. A basic form involves implementing physical baffle plates within the liquid vessel to dampen the flow of the liquid and hence help to suppress the slosh (Modaressi-Tehrani et al. 2007). Designs of this form are predominantly based on experimental results and utilise Computation Fluid Dynamics (CFD) software to analyse the slosh in a tank before, and after the addition of various types of baffles (Modaressi-Tehrani et al. 2007).

A more complex form of slosh control involves the use of input-shapers. This method of control uses the flexible modes of a system to cancel out residual vibration by altering the reference signal sent to the actuator, through the addition of self destructive impulses (Aboel-Hassan et al. 2009). In reference to slosh control, this method sends an altered speed control curve to the motor to prevent the excitation of the liquid slosh modes. This does not require any form of sensory data to shape the control input making it cheap and relatively simple, however it results in a control system that is not very robust and very sensitive to disturbance and modelling errors (Aboel-Hassan et al. 2009).

A more robust and effective form of slosh control uses sensors to measure system states and implements control loops to adaptively control the input signal sent to the plant actuators. Although this method requires more complex system equipment and a more comprehensive model of the dynamics of the system and its slosh production, it provides much better suppression of slosh over a much larger range of system tasks and is much less sensitive to disturbances. This control has been implemented in systems such as the ball and hoop system (Wellstead and Readman) and the two-degree-of-freedom (2DoF) slosh control rig (Gandhi et al. 2009).

2.3.2 Relevance of Studies

For the purpose of implementing slosh control on the diwheel, the dynamics of the system during slosh need to be derived. This then provides the ability to model the system and tune a control system to it. Liquid slosh has been approximated as a suspended pendulum by Gandhi et al. (2009) for their derivation of the dynamics of a two degree of freedom actuation slosh rig

and by Nichkawde et al. (2004) for their derivation of the dynamics of a coupled slosh vehicle. The Ball and Hoop system is also an approximation of slosh similar to a pendulum where the ball is the pendulum mass which rolls freely inside a rotating hoop (Wellstead). This system is very closely related to the structure of the diwheel. It has also been outlined in Dodge's 2000 revision of Abramson et al's 1996 paper, *Dynamic Behavior of Liquids in Moving Containers*, that slosh is well represented by a pendulum whose mass oscillates relative to the tank. The structure of the diwheel resembles a combination of both the pendulum and ball and hoop systems making the literature mentioned useful in aiding with the derivation of slosh dynamics of the diwheel.

Dynamic slosh control was implemented and investigated for both the two-degree of freedom (2DoF) actuation slosh rig and the ball and hoop system (Gandhi et al. 2009). The ball and hoop system investigates the use of a simple proportional feedback controller, feeding back the slosh angle. Although this showed promising results in suppressing the slosh of the ball, the best slosh suppression results required long hoop position settling times (Wellstead and Readman). The Slosh rig used a Proportional-Integral-Derivative (PID) controller integrated with another controller. The aim of the 2DoF slosh rig was to reduce the forces on a body arising from liquid slosh. To accomplish this, the forces were fed back to the controller which then determined the desired trajectory of the actuators. This trajectory was then controlled using a PID controller, feeding back the position of the actuators. Using this control structure, the liquid slosh was considerably suppressed for an oscillating excitation of the tank (Gandhi et al. 2009). This literature provides constructive insight into the types of control methods to use in the suppression of slosh in the diwheel.

2.3.3 Application to the Diwheel

All relevant literature reviewed for the project regarding slosh and slosh control used the Lagrangian method, and the Euler-Lagrange equations to determine the dynamics of the system. This method is straightforward and relatively simple to perform, making it the preferred method for the derivation of the diwheel's dynamics.

It is probable that the slosh control to be implemented on the diwheel will consist of a form of PID control, in keeping with the methods used for the ball and hoop system and 2DoF slosh rig. The results of the Ball and Hoop control system suggests that a purely proportional controller feeding back the slosh angle may be sufficient in providing satisfactory control and rider comfort. Should purely proportional control not provide sufficient results, a Proportional-Derivative (PD) controller controller may be necessary.

2.4 Yaw Control

Yaw control regulates the rate at which the diwheel turns about its vertical axis. The implementation of yaw control will reduce the undesired yawing of the diwheel whilst it is travelling in a straight line and will also allow the turning of the vehicle to be smooth and responsive. Recent research on closed-loop yaw control has been conducted for a number of vehicles including a bicycle (Zheng and Anwar 2009) and an automobile (Esmailzadeh et al. 2003). However the most relevant research to the diwheel has been done by Baker et al. (2005) and Tarakameh and

Shojaie. Motion of these vehicles is achieved by the rotation of two individually driven wheels. The small differences in the velocity of each wheel causes an undesirable drift whilst the desired trajectory is a straight line. This effect can be minimised by implementing a closed-loop yaw controller. The effective implementation of yaw control is achieved by calculating the dynamics of the system, determining its open-loop response and designing a closed-loop controller to improve this response.

Previous research on the dynamics of differentially driven robots has been conducted by Tarakameh and Shojaiewho used a Newton–Euler method to obtain the dynamics for a differentially driven system. However these dynamics did not consider lateral slip. The dynamics of a Segway type vehicle were calculated by Baker et al. (2005) who produced a detailed steady state model.

Yaw control may be achieved either by open-loop or closed-loop. Because open-loop systems do not employ the use of feedback they suffer from inaccuracies induced by steady state errors as shown by Cooney et al. (2004). Their mobile platform, with four Mecanum wheels was an autonomous vehicle. This meant that, whilst in operational, no user input was available. Consequently the vehicle was unable to counter the slip between wheels and driving surface. As such there were variations between the desired yaw rate and the actual yaw rate and for this reason a closed-loop system was implemented. The closed-loop system received feedback through a visual dead reckoning method using two optical mice mounted on the bottom of the robot which provided x and y displacement and the yaw angle as feedback. This method when combined with a PID controller, produced an improvement of two orders of magnitude in the yaw angle step response when compared to the open-loop. However this type of feedback is not viable for the diwheel, as the outer wheels and inner frame are free to rotate relative to each other.

Baker et al. (2005) constructed a co-axial, two wheeled Segway vehicle that used encoders for yaw control feedback. Measuring the angular velocity of each motor allowed a yaw rate to be estimated. This method of feedback proved successful in keeping the two wheeled segway travelling in a straight line.

3 Design Specification

EDWARD is a complex mechanical and electrical system, containing many components that closely interact with each other. Figure 3.1 shows a basic System Hierarchy Diagram of the diwheel system and its components. Proper integration of all of the system components is important to achieve the project goals. In order to achieve these goals each subsystem has an associated functional requirement that must be satisfied. To confirm that these functional requirements have been met there must be a way to assesses each component and this is provided in the form of a number of Technical Performance Measures.

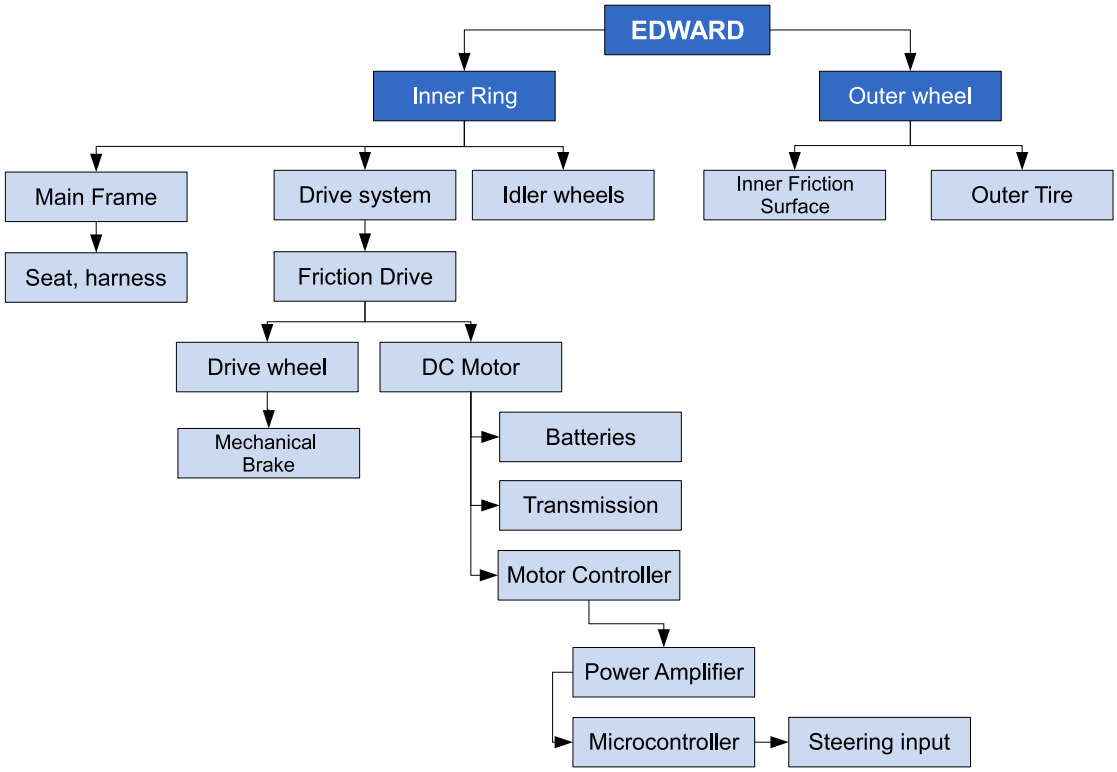

Figure 3.1: System Hierarchy Diagram

3.1 Project Goals

The project goals are objectives that are intended to be achieved in the final design. These goals are divided into mechanical, electrical / electronic, miscellaneous and extension goals. All goals

in the former three categories must be achieved in order to satisfy the project contract, while the extension goals are optional. It is for this reason that the extension goals have purposefully been posed as difficult to achieve and are not required for the normal operation of an electric diwheel. The following is a summarised form of these goals.

Mechanical goals:

- Create a concept solution for an electrically driven diwheel
- Build a diwheel to be driven by two DC motors including a frame to support one person and systems equipment
- Implement a mechanical braking system

Electrical / Electronic goals:

- Achieve open-loop differential yaw control
- Achieve open-loop speed control
- Implement a dynamic braking system
- Accomplish closed-loop slosh control
- Implement adjustable acceleration and deceleration ramps
- Implement a battery compensation unit

Miscellaneous goals:

- Build a mathematical model of system / state space model
- Create a virtual simulation of the diwheel

Extension goals:

- Implement a regenerative braking system
- Use state control of the pitch angle
- Achieve closed-loop yaw rate control
- Build a method for dynamically stabilized pitch
- Design an alternate tire for the wheel

3.2 Functional Requirements

The functional requirements are requirements that must be met by the various systems on the project. These requirements have sub-requirements that must be achieved by the components. The Functional requirements, sub-requirements and components are listed below.

- Provide traction with the road surface
  - Outer wheel tire
- Seating of the driver and support of the electronic components
  - Main space frame
  - Seat and harness
- Suspension of the main space frame
  - Inner ring assembly
- Read user input commands
  - X, Y-axis data from the Joystick
  - Processor
- Provide power to the system
  - Batteries
- Supply power to the system's components
  - Power distribution board
  - Signal distribution board
- Convert stored electrical energy into rotational motion
  - Electric motor
  - Convert motor rotation to translational velocity
    - Transmission
    - Drive-wheel
    - Outer wheel
- Brake the drive-wheel
  - Hand lever
  - Disk brake, calliper, cables
  - Limit switch to indicate braking to the processor
- Provide the option of slosh control to driver

    - Measure slosh rate of the inner frame
        * Gyrosensor
        * Accelerometer
    - Control slosh rate of the inner frame
        * Processor
        * Slosh controller
        * Motor controller
- Provide yaw control to the driver
    - Measure yaw rate of system
        * Encoder
    - Control yaw rate of system
        * Processor
        * Control circuit
        * Motor controller
- Dynamic Braking
    - Determine when to activate dynamic braking
        * Joystick
    - Activate dynamic braking
        * Processor
        * Dynamic braking circuit
        * Motor controller
- Measure battery voltage
    - Resistive voltage divider
    - Processor
- Display battery level
    - Processor

3.3 Technical Performance Measures

The technical performance measures are used to determine whether the functional requirements have been met and are given in Table 3.1.

Table 3.1: Technical Performance Measures

Goal	Sensor	What is Measured	Minimum Requirement	Unit
Open-loop yaw control				
Differential drive	Encoders	Yaw rate of the diwheel	1.5	rad / sec
Brake				
Mechanical brake	Stop watch	Braking time from full speed to zero	10	sec
Electrical braking	Stop watch	Braking time from full speed to zero	10	sec
Open-loop speed control				
Drive forwards	Encoders	Speed of the diwheel	10	km / hr
Drive backwards	Encoders	Speed of the diwheel	5	km / hr
Closed-loop slosh control	Gyrosensor / accelerometer	The reduction of the sloshing of the inner ring when compared to the open-loop response	20	%
Dynamically stabilized pitch	Stop watch / gyrosensor / accelerometer	Time elapsed while the diwheel's inner frame is inverted to 180 degrees	30	sec
Closed-loop yaw control	Encoders	The step response for a maximum yaw rate.	50	%

4 Component Selection

4.1 Mechanical Brake Selection

While electrical braking can be applied to the drive-wheel via the motors in normal braking situations for added safety and for additional braking capability, a mechanical brake can be used. Brake systems often use frictional forces to apply a stopping torque to the drive system. Disc and drum brakes are two types of brake systems common in modern vehicles. Other types of brakes include caliper brakes used in bicycles which brake directly onto the rim of the wheel, whereas disc and drum brakes operate within the drive system of the vehicle.

Hydraulic disc brakes were considered because of their ability to apply an even distribution in a hydraulic line to independant wheels, which would eliminate the possibility of differential braking. However, hydraulics were dismissed as being too expensive and a cable drawn disc brake has been chosen. The cable disc brake is intended to be used with a mini-moto wheel hub and has been chosen in conjunction with the drive-wheel for its simplicity and to reduce cost. A photo of the purchased brake caliper is shown in Figure 4.1a. A SolidEdge model of the brake disc rotor chosen is shown in Figure 4.1b. As each drive-wheel is rotating independently of the other, independent brakes have been used on each drive-wheel.

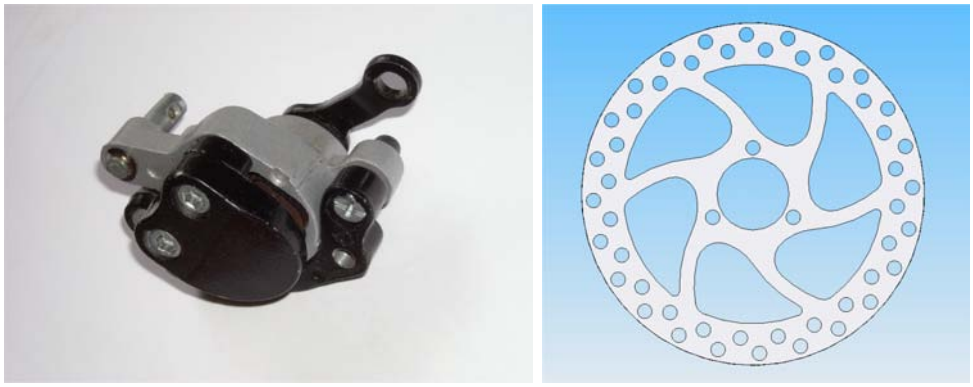

(a) Brake caliper

(b) SolidEdge model of the brake disc rotor

Figure 4.1: Mechanical brake chosen for use in EDWARD

Brake Performance

The performance of a disc brake system depends predominantly on the size of the brake pads, and the radius and force at which the brake pads are applied to the brake rotor. The measured specifications of the purchased brake caliper and rotor are shown following.

- Brake pad height: 16mm
- Proportion of the rotor the brake pad covers: 18 degrees
- Radius of the brake rotor: 70mm

The equation for the torque available from a disc brake with uniformly worn brake pads is shown below (Shigley and Mischke 2004, p.831).

$$T = \frac{1}{2}(\theta_2 - \theta_1)\mu p_a r_i (r_o^2 - r_i^2) \tag{4.1}$$

The definition of the geometric terms of this equation are shown in Figure 4.2. The other terms are defined as:

- T: Braking torque [Nm]
- μ: Coefficient of friction of the brake pads
- p_a: Maximum allowable applied pressure on the disc pads [Pa]

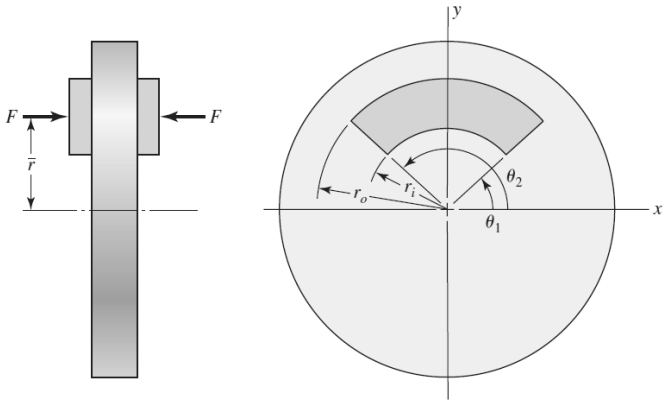

Figure 4.2: Geometric definitions of a disc brake system (Shigley and Mischke 2004, p.830).

The material of the brake pads is a dry sintered metal. The coefficient of friction and maximum allowable pressure of this material are $\mu = 0.3$ and $p_a = 2$MPa respectively (Shigley and Mischke 2004, p.842). The maximum allowable pressure of this material relates to its ability to withstand pressure without being damaged. The available torque from the chosen brake system is

$$T = \frac{1}{2} \times (18 \times \frac{\pi}{180}) \times 0.3 \times 2 \times 10^6 \times 0.054 \times (0.07^2 - 0.054^2), \tag{4.2}$$

$$T \approx 10\text{Nm}. \tag{4.3}$$

This torque value represents an upper limit that the brakes are capable of applying to each drive-wheel. The brake calipers chosen operate using a cam mechanism for which data is not available. This makes analysis of the actual braking capability untenable. The upper limit of the braking torque is then an estimate only and is on the same order as the maximum torque applied to the drive-wheel by the motors.

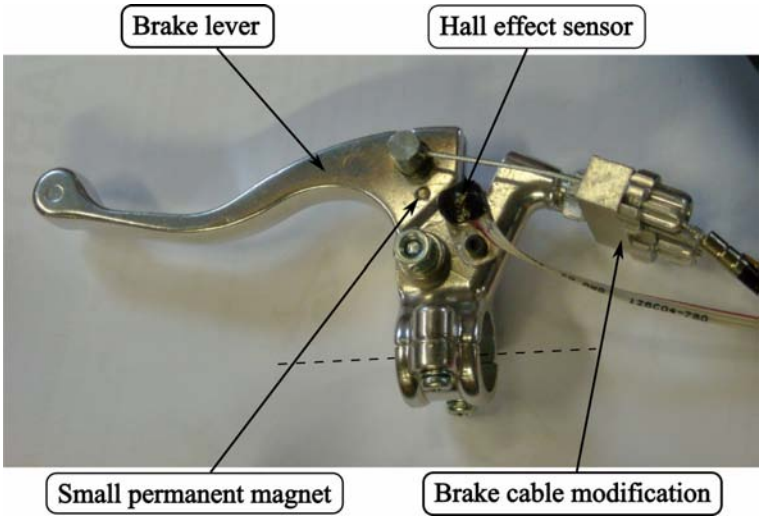

Figure 4.3: Hand operated cable lever chosen for use in EDWARD

4.2 Brake Lever

The mechanical brake is to be operated by the occupant. A foot operated brake which was considered in the diwheel preliminary report (Dyer et al. 2009), was determined to be unergonomic due to the restricted movement of the occupant's legs. A single hand operated brake lever was then chosen to operate the cable drawn brakes. The brake lever chosen was a motorcycle cable drawn lever shown in Figure 4.3. The lever shown was subsequently modified to accommodate both cables from each brake and to distribute even tension between the two cables.

Signaling Operation of the Brake

The application of the mechanical brakes must be registered by the processor in order to prevent driving whilst braking. Braking the drive-wheel while it is being driven will cause the control systems to sense a drop in speed of the wheels for which it must compensate by trying to increase the speed of the motors. The solutions proposed to sense the operation of the brake lever include a normal micro limit-switch and a Hall effect sensor. The Hall effect sensor is a transducer which has an analogue output voltage which is altered in the presence of a magnetic field. A Hall effect sensor may be used as a proximity switch due to its highly non-linear output signal in the presence of a strong local magnetic field. Such a magnetic field may be created by a small permanent magnet. Because a limit switch would be invasive to the physical operation of the brake lever, the simpler solution was to use a Hall effect sensor to sense the proximity of the lever arm when not in operation. A Hall effect sensor, shown in Figure 4.4, was set in epoxy resin on a small bracket that screws into the brake lever base and a small permanent magnet was set into a drilled recess within the brake lever arm (see Figure 4.3).

Figure 4.4: A Hall Effect sensor used in sensing the operation of the brake lever (scale: approximately 15mm lengthwise) .

4.3 Outer Wheel

The outer wheels of the diwheel provide rolling support of all other components of the diwheel. They also determine the maximum outer diameter of the diwheel. The outer wheels mate with the idler wheels and are in rolling contact with them. Some common solutions for a diwheel's outer wheel are reviewed in Section 2.1. A pneumatic outer wheel was determined to be unfeasible as a suitable component does not exist and would be expensive to manufacture. Subsequently, the solution of rolling a tubular wheel was chosen. Analysis of the strength of these wheels in rolling contact with the idler wheels can be seen in Section 6.2. As the outer wheels must be in rolling contact with the idler wheels, the outer wheel must be partially exposed. If this section were coated with paint in order to prevent corrosion, it is likely to be worn by the idler wheels and would crack and fail. Because of this, the outer wheels were chosen to be rolled from stainless steel piping: 50mm nominal bore (60.3mm OD) schedule 40 (wall thickness of 3.91mm). The piping was rolled to an outside radius of 1500mm and cut and welded to form a ring. The completed outer wheels with a rubber tyre adhered to the outer surface are shown in Figure 4.5.

Figure 4.5: The finalised assembly of rolled stainless steel tube and rubber tyre to form the outer wheel

Outer Wheel Tyre

The tyre of the diwheel is required to provide traction and vibration isolation between the wheel and the road. It also eliminates the rigid rolling contact between the wheel and the ground. The tubular wheel chosen requires a compliable surface to be attached to the outer radius. The compliable surface must provide grip and wear resistance and must bond well to a metallic surface. From email correspondence with ALLIED RUBBER on the 23^{rd} March 09, natural rubber was recommended as the most feasible option. As budgetary constraints limit the selection of many components, sponsorship was sought while looking for potential rubber suppliers. Sponsorship was recieved from RUBBERTEX PTY. LTD. for the adhesion of 6mm thick rubber strips to the outside of the wheels. The method used by RUBBERTEX was to firstly prepare the outer surface of the wheels by buffing them. A steel primer was used before two coats of an adhesive. The rubber strips were pre-cut from a sheet of a product called Chemoline 4. Chemoline 4 is a Butyl based synthetic rubber which has a bonding skin layer which is revealed when a protective film is peeled away. The rubber was applied as one continuous length and joined at its ends using a lapped joint (Figure 4.6).

Figure 4.6: The lapped join of the continuous rubber strip of the outer wheel tyre

4.4 Seating and Harness

The occupant is required to be constrained in various angles of rotation due to the dynamics of the diwheel system. Allowing for the accomplishment of the extension goal to remain upside down and considering that the diwheel may gerbil if large accelerations are allowed, the seat and harness must afford proper constraint. The seat and harness must work in combination to sufficiently restrain the occupant and must therefore be integrated to do so. Furthermore, safety is paramount in selecting a seat and harness and designing an integrated system due to the risk presented in the operation of the diwheel.

A regular automotive seat belt consists of a three point harness, which outside of collision situations provides little support through a retraction system. Racing harnesses consist of three, four, five or six point harnesses (Figure 4.7) which are designed to provide constraint of the occupant during operational loadings. Common safety problems involved with the use of a harness include, submarining, pressure injuries and spinal injuries (States et al. 1970). Submarining occurs when the harness is pulled up and the lap strap becomes positioned above the abdomen. The occupant's pelvis is then allowed to move forward putting pressure on the soft abdomen. The three and four point harness can lead to submarining because the abdomen may slide down beneath the belt. Therefore a 5 or 6 point harness is required to constrain the passenger when sliding forward, and to increase the restraint by holding the abdomen and shoulder straps down. The restraint of the occupant also relates to how far the upper anchorage is mounted above the shoulders. If these points are too far above the shoulders they provide little to no vertical restraint of the occupant.

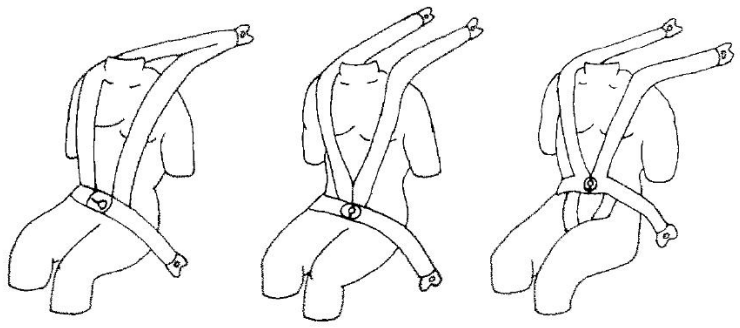

Figure 4.7: Left: Inverterd Y-harness (three-point harness). Middle: Four-point harness. Right: Five or six-point harness. (Ottoson and Lovsund 1989)

A racing harness combined with a regular seat can lead to submarining due to the lack of body support (Ardoino 1984). Racing harnesses constrain the occupant well when used with a racing seat. Further protection is added by using a racing seat through appropriate holes in the seat which allow the harness to better fit the human form. These seats may be constructed using a tubular frame and panel board covered with cushioning. Advanced versions of racing seats are made from fiberglass or a Carbon/Kevlar composite. These provide an advantage of weight reduction over the tubular framed racing seats.

Due to budget and feasibility constraints the cheaper go-kart seats, when compared to the racing seats, were previously considered a suitable solution (Dyer et al. 2009). While a go-kart seat was used in initial designs of the space frame, due to the lack of upper back support it was later deemed inadequate. A racing seat, which provides upper back and side support, was therefore purchased to be used in conjunction with a 6 point racing harness to provide safe and adequate restraint during the operation of the diwheel. A polyethylene car racing seat was chosen as an inexpensive alternative to more expensive tubular framed or composite seats. The JAZ 400 Polyethylene racing seat used in the final construction of Edward is shown in Figure 4.8. The racing harness chosen for use in Edward was a 6 point VELO TRS Magnum racing harness shown in Figure 4.9.

Figure 4.8: The JAZ 400 polyethylene car racing seat chosen for use in EDWARD

Figure 4.9: The 6 point VELO TRS Magnum racing harness chosen for use in EDWARD

4.5 Drive-wheel

The method chosen to drive the outside wheel was a friction drive system. This is required because the outer wheel is a rolled tubular structure. The friction drive system requires an appropriately sized wheel with a high friction compliable surface in order to form rolling contact with the inner surface of the wheels and provide sufficient traction so that the drive-wheel does not slip. The drive-wheel selected for this function was a mini-moto rear wheel hub and tyre because it is appropriately sized and is an inexpensive, off-the-shelf component. The drive-wheel is a cast aluminium hub with a pneumatic tube and tyre, providing compliance with

the wheel with a constant contact pressure. This tyre is slick having no tread, which provides a continuous friction surface. Among these features the drive-wheel was also chosen as it had accompanying disc brakes, axles, bearings and chain and sprocket drives for possible use. Further specifications of the wheel include:

- Tyre Width: 90mm
- Measured outside diameter approximately: 275mm
- Rim diameter 6.5 inches
- Maximum tyre pressure: 250 kPa

For the purpose of friction driving the outer wheel, a pneumatic tyre is useful. When the tyre is pressurised at maximum pressure the contact friction will be minimised while the rolling resistance will also be at a minimum. The pressure may be lowered to achieve higher frictional force, however an increase in rolling resistance will also occur. Figure 4.10 shows a photograph of the drive-wheels used in EDWARD. The hub has an inset housing for a bearing. The axle supports the inner runs of the bearings and passes through the hub. The brake disc is attached to the hub by three 4mm bolts. An analysis of these bolts for their adequacy of strength is given in Appendix B.2.

Figure 4.10: The mini-moto drive-wheels chosen for use in EDWARD

4.6 Motors

This section presents a brief overview of the motor selection, although Dyer et al. (2009) discuss the selection in more detail. DC motors were chosen over AC motors because power is provided to the motors by the batteries. AC motors may be used with batteries, but require an inverter which increases the cost and complexity of the motor controller. The major criteria for the choice of motors included:

- Cost
- Performance
- Integration with motor controller

After selecting DC motors, the choice was made between brushed and brushless. Brushless DC motors do not require physical brushes to make contact with the commutator in order to drive the motor, resulting in less friction and heat during operation (Ellis 2000). This gives brushless motors the advantage over brushed motors in performance - providing higher torque, speed and power efficiency (Ellis 2000). However driving a brushless motor is more complicated than a brushed motor as commutation must be achieved electronically (Ellis 2000). This requires the use of a more complex motor controller, which needs close matching to the motor. Brushed DC motors are much simpler in design and can be therefore utilised with relatively simple controllers.

The main driver for the choice of motors is cost, due to the project's limited budget, and the increased complexity of both the motor and controller for brushless DC motors results in a much higher cost compared with the equivalent brushed DC motor. It was deemed that the reduction in performance of the brushed motors in comparison to brushless motors was less significant in the application than the reduction in cost, and hence brushed DC motors were chosen for use in the project. Following the decision on the type of motor, a motor suitable for the diwheel application was sourced.

Through past experiences and communications with motor providers, it was recommended that a 24V motor of at least 300 Watts was used. Although Dyer et al. (2009) describe several candidate motors, the final motor chosen for the system is shown in Figure 4.11. These motors are rated at 900 Watts each, and provide 2.2Nm of torque at 34 Amps. The final motor was not geared, so that the backlash in the transmission was minimized, requiring the design of a transmission system.

Figure 4.11: Picture of the final motor (monsterscoopterparts.com 2009)

4.7 Motor controller

The motor controllers were originally not a purchased item, instead being manufactured by the University of Adelaide's electrical workshop. However during testing the fabricated controllers failed, and the selection of a commercial-off-the-shelf motor controller was mandated. This controller is discussed in more detail in Section 5.1. Despite the fact that the initial motor controller was not chosen, its electrical topology was. In order to be capable of driving the motors forwards and backwards as well as applying braking torque in the forward and reverse directions, a 4-quadrant controller was required. Dyer et al. (2009) describe an alternative to the final choice of a 4-quadrant H-bridge, which consisted of a controller using two contactors arranged as a *double-pole double-throw* switch. Although this solution was a viable one, it was decided that its bandwidth would be limited due to the slow switching of the mechanical relays and was not pursued further.

The H-bridge controller topology was chosen for its:

1. Simplicity and robust design
2. Varied and simple switching schemes
3. Four quadrant (4QD) operation

and was to be controlled through Pulse Width Modulation (PWM) of the four switches according to a particular switching scheme. Dyer et al. (2009) discuss in detail the numerous switching schemes available to the user when switching a H-bridge which include:

- Sign magnitude
- Locked antiphase
- Active field-collapse
- Modified active field-collapse
- Synchron collapse

After considering the normal operation of the diwheel, the *Sign magnitude* drive was deemed the most suitable switching option as it is commonly used when the direction of the motor does not change frequently. Using this drive scheme regenerative braking was an option and Dyer et al. (2009) describe its implementation. However, as discussed in Section 5.1, the final motor controllers did not allow access to the transistors in the H-bridge, instead being controlled by one of three methods, Analog, R/C control or Serial control.

4.8 Batteries

The selection of the motors was the main driver for the choice of batteries to be used in the diwheel. The batteries needed to provide adequate voltage for the required motor speeds and supply sufficient current to achieve adequate torque at high loads. Several types of batteries were considered for use and details of the advantages and disadvantages of the candidate types are analysed by Dyer et al. (2009) which guided the decision on the final battery selection.

A summary of the battery types considered is shown in Table 4.1 which has been compiled using battery specifications supplied by an online battery retailer[1] and a battery selection guide (Jaycar 2001). The main considerations for the battery selection were cost and capacity. SLA Gel batteries provided the cheapest solution which met the needs of the project and were selected for use in the diwheel. These are shown in Figure 4.12. Each of the four batteries purchased were 12V, Gel SLA batteries rated at 26Ah and weighing 8.2kg each.

Table 4.1: Summary of Battery Properties

Battery Type	Capacity	Current Source	Ease of Charge	Size/Weight	Mounting Angle	Cost
SLA	High	High	Simple	Very large, Very heavy	0-90°	Cheap
SLA Gel	High	High	Simple	Very large, Very heavy	360°	Cheap
NiMH	Low	Medium	Complex	Large, Medium Weight	360°	Expensive
NiCad	Low	Low	Complex	Large, Medium Weight	360°	Expensive
LiPo	Low	High	Complex	Small, Light	360°	Expensive
Li-ion	Low	Medium	Complex	Small, Light	360°	Expensive
LiFePO4	Low	Very High	Complex	Very Small, Light	360°	Very expensive

4.9 Processor

In order to control the diwheel, a controller in the form of a microprocessor is required. The processor chosen for the design was the M9S12DG256, manufactured by Freescale Semiconductor. This microprocessor is utilised in the Dragon12-Plus (known as the *Dragonboard*) a development board produced by Wytec. The board is replete with a number of peripherals that have been choosen to demonstrate the capabilities of the S12 microprocessor. A selection of processor capabilities is listed below:

- 16 bit processor, with ability to perform 32 bit operations

[1] (http://www.batteryspace.com/)

Figure 4.12: Sealed-Lead-Acid battery source for use in the project (Jaycar 2009)

- 8-channel, 8-bit PWM modules or 4-channel 16-bit PWM modules
- Enhanced Capture/Compare timer module, allowing flexible timing
- Up to 91 digital input-output lines
- 3 Serial-Peripheral Interfaces
- 2 Serial Communication Interfaces
- 2, 8-channel ADCs with 8 or 10 bit resolution
- Assembly instructions for use with fuzzy control

These features make the HCS12 microprocessor a versatile choice for control. The Dragonboard has been designed predominantly to bring out a number of the processors features, and add peripherals useful for debugging and prototyping such as:

- Liquid Crystal Display
- LEDs
- 7-segement display
- Piezo-electric Speaker
- Keypad input

This board has been extensively in past Honours projects because of its versatility and flexible programming interface.

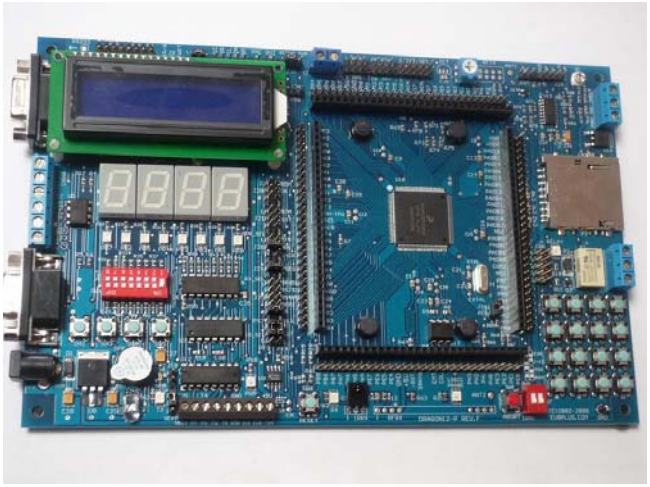

Figure 4.13: The Dragonboard development board, manufactured by Evbplus

4.10 Gyrosensor

In order to provide the system with active slosh control, sensory feedback is needed to measure the angular velocity of the inner frame. There are several types of gyrosensors (gyros) that measure angular rate. These include spinning gyrosensors, laser gyrosensors and vibrating gyrosensors. The most suitable type of gyrosensor to the project application is a vibration gyrosensor or *MEMS* gyrosensor. These are small, cheap and commonly available. They provide very good accuracy and although most are influenced by temperature, many also measure the temperature to provide compensation for its effects.

The gyro was sourced from SparkFun, an online supplier commonly used in previous final year control projects. The gyros have standard fullscale limits on the angular rate: 50, 150, 300 and 500deg/sec being common - and the correct specification had to be matched to the project's application. Choosing a gyro with a low limit of angular rate provides finer resolution with less sensitivity to noise. If this limit is too low however, the sensor may saturate and an important state of control is lost. A gyrosensor with a 300deg/sec limit was chosen to suit the expected range of angular rates of the diwheel. In order to maximise options for optimising the measurement signal, a gyro that provided both digital and analog outputs was chosen. It was anticipated that an analog to digital conversion of the angular rate within the sensor itself would involve less noise and hence provide a more accurate signal.

The gyrosensor selected came mounted on a breakout board, making connections to its pins simple through use of a header. An image of the gyrosensor selected is shown in Figure 4.14. Specifications of the gyro are given below:

- full scale range: 300deg/sec
- operating voltage: 4.75-5.25V
- zero rate output (nominal bias): 2.5V
- temperature measurement (compensation for digital)

- single axis
- digital (serial port interface) and analog output

Figure 4.14: Gyrosensor Breakout board (Sparkfun.com 2009)

4.11 Accelerometer

In order to allow for the inverted pendulum mode of operation of the diwheel, a measure of the angular position of the centre of gravity of the inner frame is needed. This could be obtained by integrating the angular rate from the gyrosensor discussed in Section 8.5. However, as the gyrosensor is prone to drift creating low frequency fluctuations, another sensor is needed to obtain an accurate measure of angular position. An accelerometer can be used as a tilt sensor, measuring the angle at which it is rotated about one of its axes. These values are commonly accurate at low frequency rates of rotation yet lose accuracy at higher frequencies (Baker et al. 2005). Combining the advantages of both accelerometer tilt sensor and gyrosensor provides a method of accurately determining the angular position over a broad range of frequencies. The two sensors can be used in conjunction through the use of Kalman Filter as outlined in Section 8.5.

The major parameter driving the selection of the accelerometer was the range of operation. This range is usually specified in term of the gravitational acceleration with common full scale ranges of 1.5g, 2g, 4g and 6g. Although accelerometers with greater range than this are available, they suffer reduced resolution. For the diwheel project, it was deemed that anything more than 6g was quite excessive.

Sourcing the accelerometer from SparkFun with an aim to minimise cost resulted in the the accelerometer shown in Figure 4.15 already mounted on a breakout board. The accelerometer measures changes, both static and dynamic in the acceleration of 3 mutually perpendicular axes and has selectable full scale ranges, making it very versatile. Setting the full scale range to 1.5g provides the highest sensitivity, but 2g has been chosen as the sensitivity. The accelerometer has the following specifications:

- Variable full scale range: 1.5g, 2g, 4g and 6g
- Triple axis measurement

- Operating voltage 2.2V-3.6V
- Sensitivity 860-185mV/g (depending on range selection)

Figure 4.15: Accelerometer Breakout board (Sparkfun.com 2009)

4.12 Steering Control

Steering of the diwheel can be easily accomplished using a number of techniques. The design of a diwheel from an electrical stand-point makes steering and control more flexible, particularly because steering can be completely controlled by signals arising from a microcontroller.

Several steering methods were considered by Dyer et al. (2009). A computer joystick was chosen for the final user control, as it is the simplest, cheapest and most compact option. A joystick has a small space envelope, which is particular important for mouting on the inner space frame. It comes with several generic buttons, and provides two-axis control in a design that is immediately familiar to users. Computer joysticks are also very cheap, provided only coarse control (in comparison to industrial joysticks) is adequate. Purchase of an industrial joystick, which are particularly robust, is not an option for project EDWARD due to budget constraints. The joystick chosen for the project is a Logitech Attack 3, shown in Figure 4.16

Figure 4.16: Logitech Attack 3 Computer Joystick (Global Systems Solutions 2009)

Most computer joysticks are the USB variety and designed for 'plug-n-play'. This means they possess are a USB controller with flashed drivers. For the project, connection to the microcontroller via USB is not a simple process, since the USB protocol is very complicated to implement. The alternative is to use the actual sensors in the joystick, which can be read as analog voltages into the Analog-to-digital converter (ADC) of the Dragonboard.

A two-axis joystick generally contains two potentiometers attached to the stick in a *gymbal* arrangement. Pushing the stick forward or pulling backward, only changes the resistance of a y-axis potentiometer, for example; while pulling left or right changes the voltage of a x-axis potentiometer. The two potentiometers share a common ground and common voltage and are thus in parallel. The signals from each potentiometer are derived from the respective wiper voltages according to the simple voltage divider formula. The Logitech Attack 3 joystick comes with 11 buttons, a rotary potentiometer and a two-axis stick. It is cheap, sturdy and equally comfortable to both left and right handed users. A discussion of the electrical connections to the Dragonboard can be found in Section 8.3.

5 Electrical Hardware

This chapter presents an overview of the electronic hardware used on the diwheel system. The arrangement of the electrical hardware in the control box is shown in Figure 6.7. The electrical hardware consists of a number of components:

- Motor controller
- Power board
- Power control board
- Ignition circuit
- Current sensors (located on the underside of the electronics box)
- Gyrosensor and accelerometer board - *sensor board*
- Encoder sensors

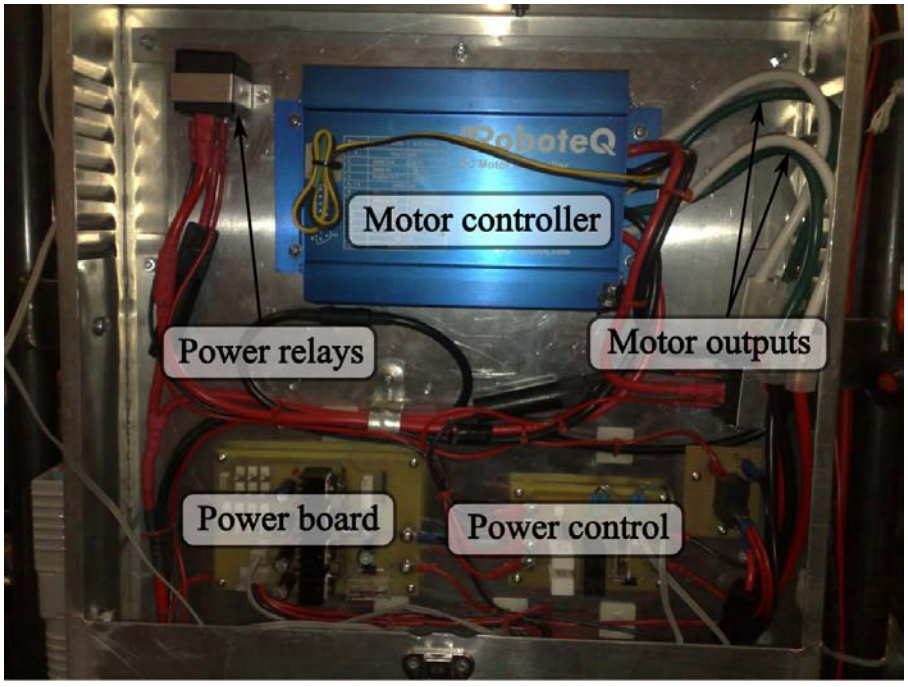

Figure 5.1: Arrangement of electrical hardware in the control box

5.1 Motor Controller

The motor controller lies between the microcontroller and the motor itself. It is required to apply the correct voltage, and sink or source the required current in order to achieve the microcontroller's desired speed and torque commands.

The motor controller can be *active* or *passive*, in the former case the motor controller contains internal circuitry which converts speed / torque commands from some simple setpoint such as a resistor into the appropriate output. The alternative is a motor controller which derives control signals from the microcontroller itself - such a motor controller acts as a *power amplifier*.
Generally the intelligent controller is slightly inflexible, as it is usually tailored to a particular application. This project requires a good deal of flexiblility in terms of the motor controller since it has several proposed modes of operation:

- Free-running mode
- Slosh control mode
- Inverted mode

In the free-running mode, it is more intuitive for the user to control speed, rather than acceleration, while inverted mode may require torque control. The voltage applied to a DC motor with no load determines its speed, while the current controls the motor's torque (Hughes 2006). Dyer et al. (2009) present two controller possibilities, a contactor controller and H-bridge controller. The decision for the motor controller was motivated by the following factors:

- Cost
- Power-handling capability
- Ease of control
- Performance with regard to control goals.

and resulted in the design of a H-bridge motor controller adapted from the Open Source Motor Controller H-bridge design. The motor controller board is shown in Figure 5.2. This controller was designed for 4-quadrant operation as was specified in the project goals. Unfortunately during testing of the motors with the batteries, one of the controllers failed because a number of the Mosfets transistors overheated. This was later investigated as being caused by PWM control of the motors, which has the effect of causing higher currents to flow within the motor (and hence through the motor controller) due to the flyback effect of the motor's inductance.

Because the inadequacy of the initial motor controllers was identified at a late stage in the project, a more robust motor controller was promptly sought after. The controller shown in Figure 5.3 was removed from a previous project that was no longer in active use. The controller is a AX2850HE Roboteq dual H-bridge controller which runs from 12-43V. It is for this reason that the full 48V bus voltage (provided by the four batteries) could not be used. The controller can be controlled via three methods: Analog control, standard R/C control and serial control.

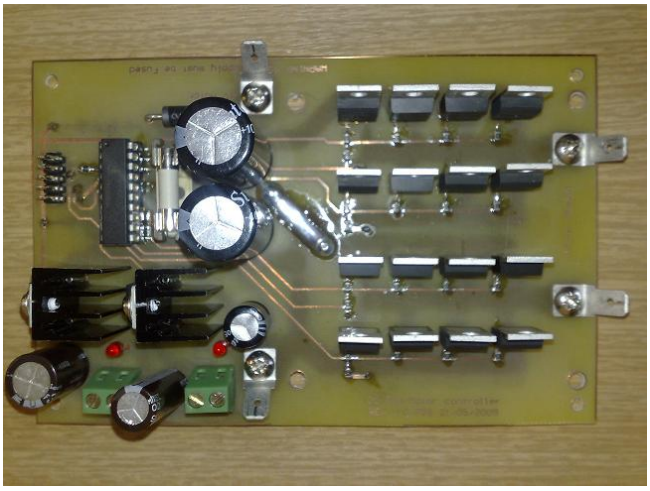

Figure 5.2: Initial H-bridge motor controller

Synthesis of a R/C compatible PWM signal was the simplest to program using the Dragonboard and was pursued first. Clark et al. (2005) describe several issues with the process of controlling the ROBOTEQ controller, however none of these issues were faced during testing. Use of R/C control restricts the use of some of the optional inputs to the controller, such as those which disable the internal power MOSFETS but has been completely adequate in providing control over the motors. As the ROBOTEQ controller contains an internal processor, several system parameters may be set by flashing the controller's internal memory using a dedicated computer program. Such parameters as, maximum current and acceleration rate could be customised in the program. However because the project only required a *power amplifier* most of these parameters were zeroed or set to values that removed intelligent operation from the controller.

Figure 5.3: ROBOTEQ dual H-bridge motor controller (Picture from Clark et al. 2005)

5.2 Power Board

Power to the vehicle is provided by the series connection of three 12V batteries. The initial design featured the series-parallel arrangement of the batteries to provide a larger current supply at 24V. However simulations involving the inversion control scheme described in Section 7.6 showed that the lower system voltage of 24V made the swing-up of the inner frame harder to achieve. Some of the advantageous features of a series-parallel arrangement of the batteries, such as even power consumption, easy recharging and simple voltage monitoring continue to apply, however the higher bus voltage was taken as a preference in the selection of the battery arrangement.

Power to the system is provided by a Power Board, which provides the numerous required system voltages. The diwheel system requires the following working voltages:

- 9V regulated supply for the Dragonboard
- 5V regulated supply for the gyrosensor / encoder sensors
- 3.3V regulated supply for the accelerometer
- 12V regulated supply for the current sensor
- 36/48V connections for each motor

Power at 36V is fed directly from the batteries through two high-current horn relays to the motor controllers. These relays are controlled by the Power Control Board described in Section 5.3. The single ROBOTEQ motor controller is connected to the series connection of three batteries providing 36V through the high current relays. The Power Board also takes an unregulated 24V input from the series connection of two batteries and generates the regulated system voltages.

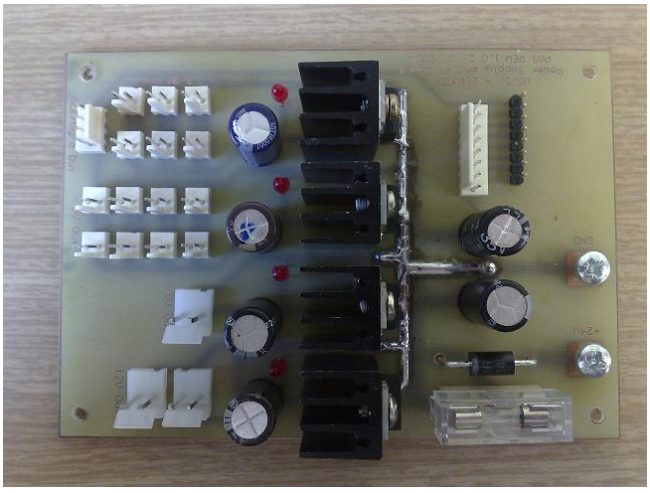

Figure 5.4: Power board use to provide regulated voltages to system components

5.3 Power Control Board

To increase safety of the system and add redundnacy, a power control board has been added to give the driver control over the power to the motors. This power control board implements an emergency stop button and a start button to form an emergency shut-off circuit.

The emergency shut-off circuit consists of a *mushroom button*, which opens two relays when pressed, cutting power to both motors. It is not essential that power be removed from the power distribution board, which may continue to operate and so the stop circuit only cuts power to the motor controller allowing the Dragonboard to continue running. In this situtation, a signal is sent to the Dragonboard indicating that power has been removed from the motors. The emergency shut-off circuit is powered from 24V, while the relays are fed 12V and require around 0.5A in order to latch. In order to return power to the motor controller once the emergency stop button has been pressed, the stop button must be deactivated followed by the activation of the start button.

The Power Control Board also accomodates the battery monitoring circuit which provides the Dragonboard with a signal proprtional to the voltage level of the batteries. This is used in an attempt to maintain maximum responsiveness of the motors as the battery voltage drops. The battery monitoring cicuit consists of two resistors in series, forming a voltage divider, outputting an analog signal bewteen 0V and 5V to be read through an ADC on the Dragonboard. The resistor values were chosen such that 0V into the Dragonboard represented 0V across the batteries, and 5V into the Dragonboard represented 26V across the batteries (as each of the 2 batteries may be charged up to 13V). The resistors chosen for the battery monitoring system were

$$\begin{aligned} R_3 &= 56k\Omega \\ R_4 &= 12k\Omega \end{aligned}$$

In the actual implementation, only two thirds of the bus voltage is measured by the voltage divider. The assumption is that the estimated voltage level of fraction of the battery voltage is proportional to the entire voltage. The battery voltage may be viewed on the Dragonboard LCD through use of the menu system, in contrast to initial designs involving the voltage being dispayed on an external bar graph using a bar graph driver.

5.4 Ignition Circuit

During periods where the diwheel is not in operation, it is necessary to implement a method of isolating the batteries and cutting off power to all electronics to prevent discharging of the batteries. This is implented using an ignition circuit which consists of a key switch, a relay and a circuit breaker.

The 400A key switch is located exterior to the control box and is the main point of isolation between the batteries and electronics. The 100A circuit breaker is connected in series with the ignition and will trip, removing power to the electronics in the event that current in excess of 100A is drawn from the batteries. A relay inside the control box provides power to the Power Control Board once the ignition switch has been activated.

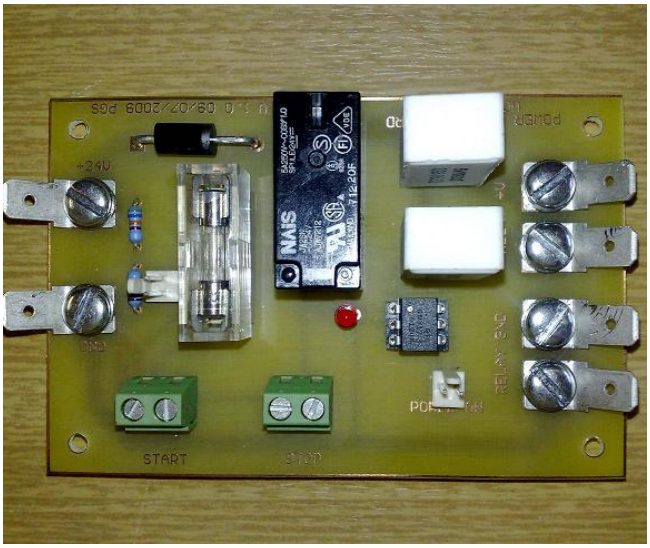

Figure 5.5: Power control board which controls power to the motor controller (and therefore motors)

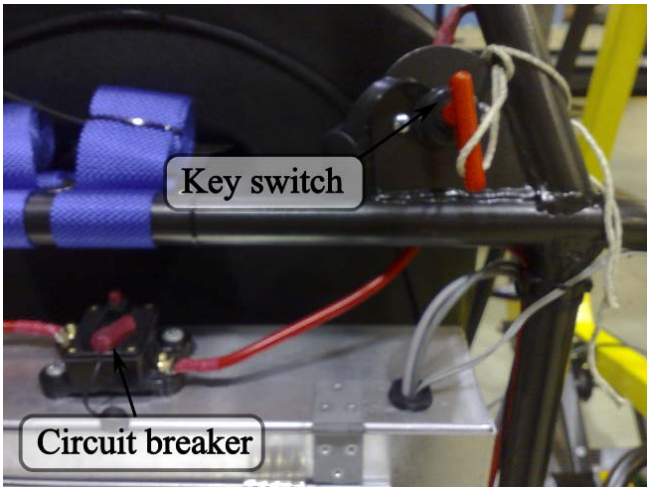

Figure 5.6: The key switch and circuit breaker which form part of the ignition circuit

5.5 Current Sensors

The current sensors may be used to sense the motor current for feedback or monitoring. However at this stage they have not been actively used in the design due to delays in the project. Typical current sensor designs usually place a current sensing resistor either in series with the motor, or in the lower legs of the H-bridge. The motor current causes a measurable voltage drop across the resistor which is then fed into a differential amplifier. Due to the high currents drawn by the motors, these resistors become quite specialised and therefore expensive. Another solution is to use a dedicated IC, as described in (Dyer et al. 2009)

Why current sensing?

Current sensing is useful in controlling the torque produced by the motors, as this torque is proportional to current for permanent magnet DC motors (Hughes 2006). However, the motor torque can be estimated from the following formula:

$$\omega = \frac{V}{k_t} - \frac{R_a \tau}{k_t^2}$$

where

- ω is the motor speed
- V is the armature voltage
- k_t is the motor torque constant
- R_a is the motor armature resistance
- τ is the motor electrical torque

This relationship indicates that torque (τ) may be estimated from knowledge of the motor speed (ω) and the voltage applied to the motor (V). This estimate is slightly problematic because it is determined partially by the load and partially by the duty cycle of the applied PWM. The motor back emf can be estimated from the back emf constant, k_e, of the motor, but these measurements may not be very accurate, especially since the motor speed is quantised and inaccurate at low speeds. The alternative is to measure the current in the motor torque directly where

$$\tau = k_t \cdot I$$

Usually this is achieved by placing a sense resistor either in series with the motor or in both low legs of the H-bridge. However frequent switching of the transistors due to PWM creates noise transients which are fed through to the common differential amp. Dyer et al. (2009) present a discussion of two amplifier ICs: LTC6103 and LTC6014 (produced by Linear Technology) which provide a bidirectional load monitoring circuit with differential output, or single-ended output, respectively. Two representative circuits using these amplifiers are shown in Figure 5.7.

However, due to the high currents associated with high motor torques, heat dissipation from the sense resistor can easily exceed hundreds of watts. This requires the use of large, expensive sense resistors, which significantly degrade system integration. The solution is to measure the current indirectly using a hall-effect sensor. These sensors make use of the principle of electromagnetic interaction by passing the load current carrying wire through the sensor. The magnetic field produced by the current-carrying wire induces a smaller proportional current in windings of the hall-effect sensor which can then be converted to a voltage by passing it through a resistor. Figure 5.8 shows the current sensor board, of which there are two mounted on the diwheel. Each sensor is capable of measuring currents ranging from -150A to 150A and requires a supply voltage between 12V and 15V. The current sensor board uses a INA126 differential amplifier and ICL7660S charge pump IC for providing the required negative voltage to the current sensor.

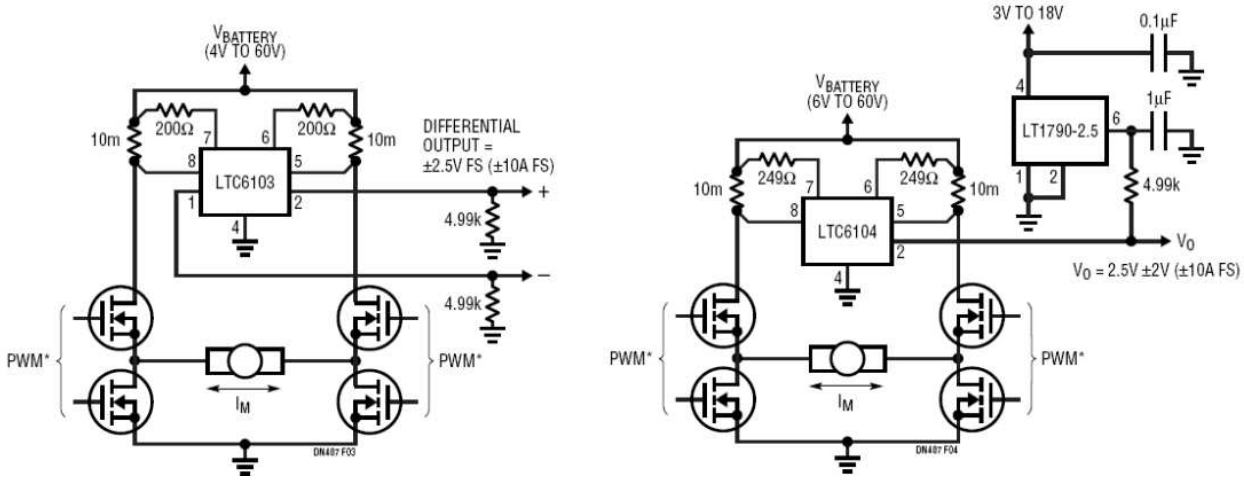

Figure 5.7: Differential output using LTC6103 (Left), Single-ended output using LTC6104 (Right), (Munson 2006)

The output from the current sensor board is a voltage between 0-5 Volts representing the current flowing. Performance of the current sensor is shown in Figure 5.9.

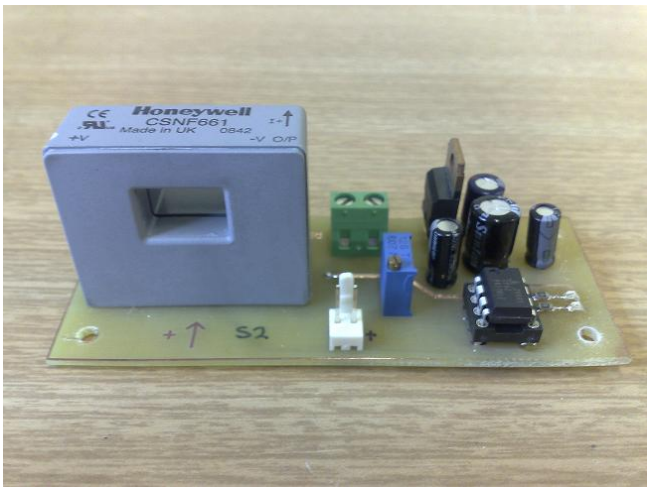

Figure 5.8: One of the current sensor boards

5.6 Gyrosensor and Accelerometer Board - *Sensor Board*

The gyrosensor and accelerometer have been combined together on the sensor board to form a simple *attitude reference system* as shown in Figure 8.3. This board simply contains the two breakout boards of the gyrosensor and accelerometer described in Section 4.10 and Section 4.11 as well as a number of headers which connect directly to pins on the two breakout boards. The red DIP switch is used to select the sensivity of the accelerometer. Use of the sensor board on EDWARD is described in Section 8.5.1.

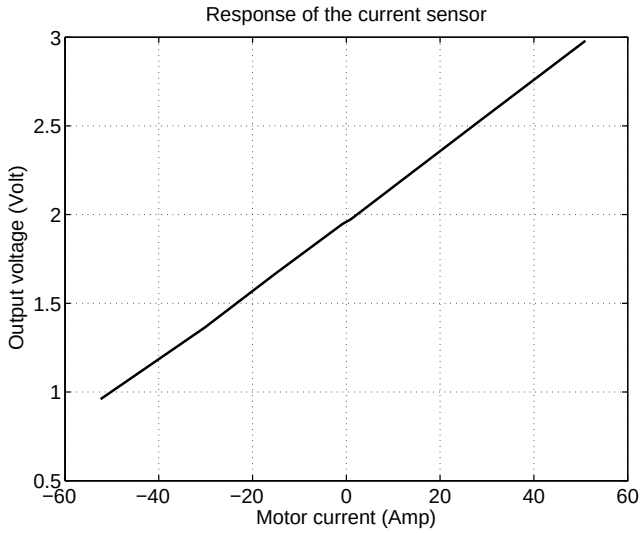

Figure 5.9: Performance of the current sensor board

The mounting of the sensor board needed to take into consideration the axes of operation of each sensor. The accelerometer measures acceleration on three orthogonal axes, and as such could be mounted in any orientation. Orientating the accelerometer with one axis horizontal, however, meant that only measurements of the remaining two axes were required to measure the slosh angle. The gyrosensor measures angular rates about one axis only and so this axis must be aligned parallel to that of the rotational axis of the inner frame (axis through the centre of the outer wheels). The two sensors were mounted on the sensor board in a fashion such that the gyrosensor axis was parallel to one of the accelerometer axes, resulting in only two accelerometer axis readings being required. To align the gyrosensor axis with the inner frame's axis of rotation, the board required mounting on a surface that would always remain in the xy-plane. The inner wall of the electronics box was chosen as a suitable mounting point.

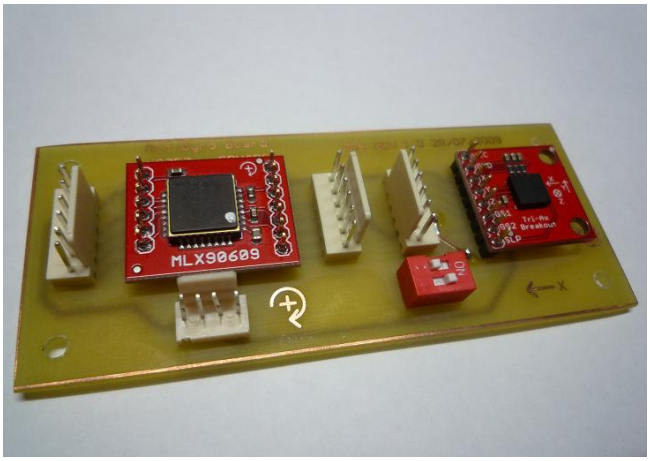

Figure 5.10: Picture of the sensor board with the gyrosensor and accelerometer

5.7 Encoder Sensors

The velocity measurement was required to provide speed and yaw feedback with direction, to the closed-loop control systems. Typical devices measure the angular velocity of a rotating part which may then be converted into a desired system velocity measurement using proper scaling. Accessible rotating parts of the system included the motor, sprocket, the chain and the brake's disc. A number of speed measurement devices were considered, including tachometers, resolvers and encoders. A tachometer made from a brushed DC motor was dismissed early in the design as it was thought that the wear of the brushes would become an issue after extended use, so that the part would need replacing. However, this option may be returned to in a future design, as the speed measurement is likely to be quite accurate.

Although resolvers provide adequate feedback they require oscillator circuits to produce the speed measurement. Encoders provide a feedback in a digital form with a greater noise immunity and do not require a complicated control circuit. Encoders were found to be costly when purchased as integrated units. The encoder units typically include bearings, an encoder sensor and encoder disc, and are designed to be mounted directly onto the motor shaft. However such sensors were found to be too costly for the design.

By utilising the brake's disc a cost effective encoder sensor was made using a pair of photo-detectors. The two common forms of encoder sensors are optical and magnetic. Magnetic encoder sensors were found to be unable to sense the holes in the brake's disc, because the disc was made of steel. Suitable optical sensors were sourced from the University of Adelaide. These optical sensors were of low cost and were mounted on the rotating arm providing speed feedback by sensing the holes in the brake's disc. A photograph of the optical encoder sensor is shown in Figure 5.11.

Encoders work by producing two digital pulse trains which are 90 degrees out of phase. In the design, the pulse trains are produced when a hole passes between the photo-detector. The phase difference may be used to determine the direction of rotation and is achieved by placing one of the sensors slightly ahead of the other. The frequency of either pulse train is proportional to the angular speed of the brake's disc. The encoder sensor can also be used as position measurement sensor by counting the number of pulses and multiplying the number by the angular distance between the holes in the disk brake's rotor. However because the control systems did not require an absolute measure of position, this feedback has not been implemented.

The encoder sensors were mounted on a circuit board to allow the sensors to be correctly located so that the two pulse trains were 90 degrees out of phase. The arrangement is shown in 5.12. A steel plate was constructed so the encoder sensors board could be located as close to the disc's holes without fouling the disc. The plate was then screwed into the arm with four screws.

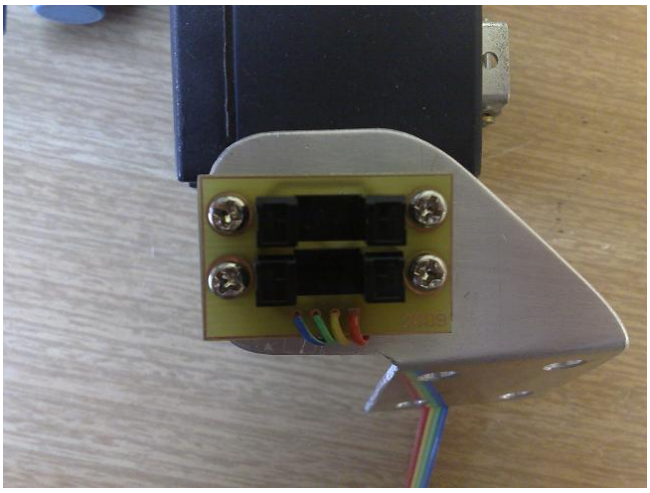

Figure 5.11: Encoder sensors made from two infrared photo detectors.

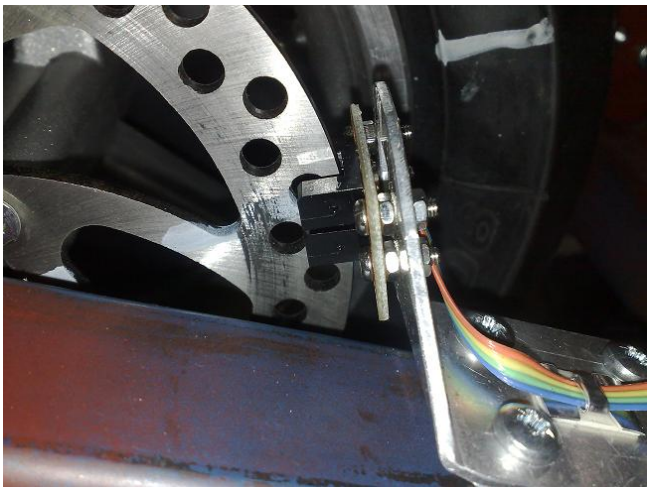

Figure 5.12: Location of the encoder sensors on the brake disc

6 Mechanical Design

The final constructed prototype of the diwheel is pictured in Figure 6.1. The construction of the physical system was completed by the University of Adelaide's Mechanical Engineering Workshop, with the manufacture of a number of parts being outsourced. The final construction varied slightly from the initial concept design where certain details were incomplete or could be manufactured more easily another way. The drawings created in order to construct the diwheel are found in Appendix D.

Figure 6.1: A photograph of the constructed diwheel

The features of the final conceptual design of the diwheel are labeled in Figure 6.2. The concept design includes a tubular outer wheel driven by traction from the drive-wheel. The electric motors turn the drive-wheel through a chain transmission. The outer wheel is guided and supported by nylon idler wheels and a suspension system. The space frame includes mounting locations for a racing seat and harness, as well as a battery and electronics box. The joystick is attached to a retractable mounting plate and the brake lever is secured on the space frame. The mechanical design of the diwheel was separated into two sections. The first section consists of the mechanical structure and components that exist between the left and right wheels, named the space frame. The second section includes the outer and inner wheel design, including the drive and suspension system. The detailed design of these two sections will be discussed in this chapter.

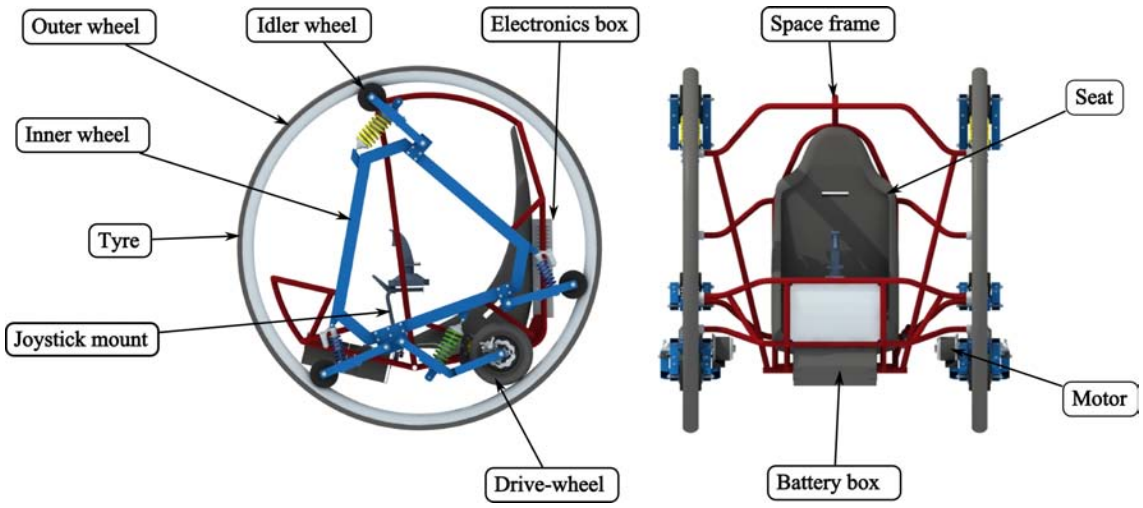

Figure 6.2: Labeled render of the final diwheel concept design

6.1 Space Frame Design

The space frame of the diwheel structure is a rigid network providing support for the passenger, mounted control systems, electronics and batteries. The space frame must be designed with consideration for a number of functional requirements. A functional design tree, showing the hierarchy of the design components for consideration, is shown in Figure 6.3. The dynamics of the system determines the required mass distribution of the diwheel as well as the functional stability of the frame. The ergonomics provided to the driver affect component spacing and sizing, around which the design of the supporting frame is based. The loading requirements of the frame are derived from the passenger and battery loading as well as the system's self weight and dynamic loading. Furthermore, the loading on the system is dynamic because of the ability of the inner frame to rotate. Budgeting constraints will also have a large influence on the design of the frame, requiring the frame to be easily manufactured using inexpensive parts. The designs presented in the following sections culminate in the final assembly diagram of the space frame shown in Figure 6.4.

6.1.1 Dynamics

The distance of the center of gravity of the diwheel from its center of rotation affects the manner in which the vehicle will roll. The project goals will depend on the ease with which the inner frame is capable of rotating within the outer wheels. The required dynamics are a compromise between the ability of the system to rotate and the stability required for effective slosh control. To initially estimate the required eccentricity of the center of gravity a simplistic energy approach was taken, where the diwheel's kinetic energy traveling at 8km/hr is converted into potential energy in a braking situation to invert the diwheel. This calculation can be found in Appendix B.3, and gives an initial design value for the eccentricity of the center of gravity of the diwheel of 0.29 metres.

The dynamics driving the design of the width between wheels of the diwheel is a worse case yawing situation. If one wheel locks and the diwheel yaws about one wheel, then a centrifugal

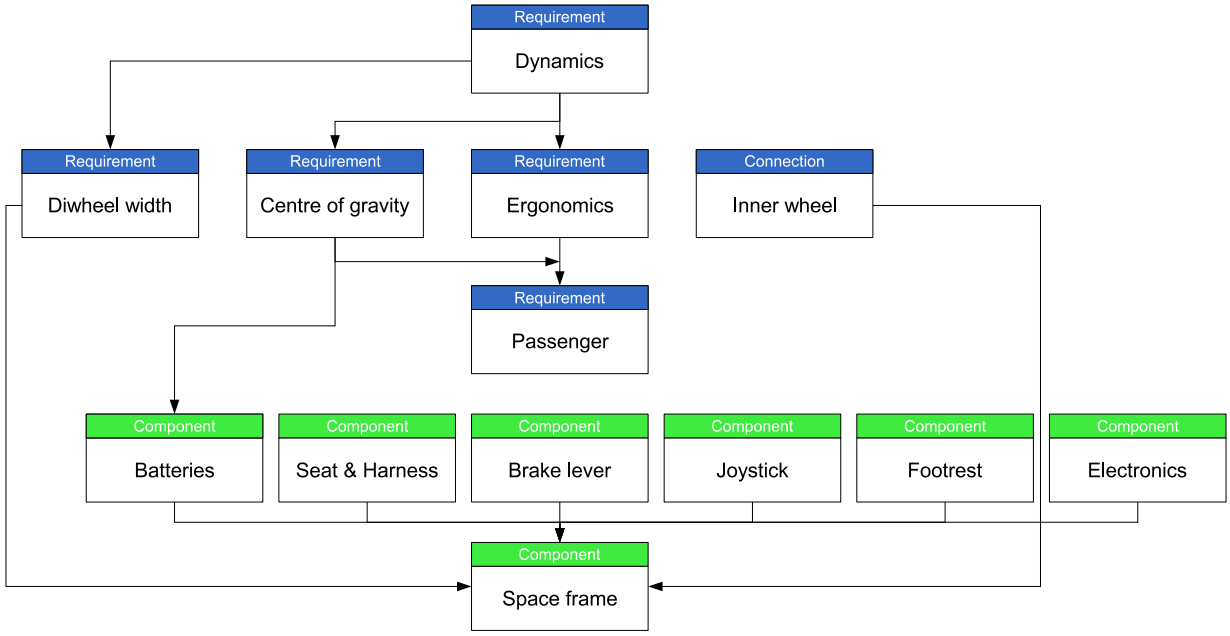

Figure 6.3: Functional diagram of the space frame

Figure 6.4: Assembly of the final concept design of the space frame

force created from this rotation must balance with the weight of the diwheel to keep both wheels on the ground. The calculation for this can be found in Appendix B.3, and gives an approximate initial width of 1.2 metres.

6.1.2 Ergonomics

Due to the variability of the human form, a system to be used by different individuals must accommodate many various statures. The space frame structure has several design features that interact with the occupant. The sizing and location of these features requires careful consideration in order to safely accommodate a variety of typical users.

Anthropometrics

Anthropometrics is the measurement of humans from which statistical predictions on the variations in human proportions can be made. This data is often used in designs that require human interaction. For the design of the diwheel a comprehensive database has been selected from NASA's Man-Systems Integration Standards (Christensen et al. 1995). Dimensions of the human form used from this document in the design of the space frame can be found in Appendix B.4. Figure 6.5 illustrates the use of anthropometric data in sizing the space frame. Similarly, a mannequin was used also used in the design process (Figure 6.5), which had similar dimensions to the anthropometric data found in Appendix B.4.

Figure 6.5: The use of anthropometric data, left: the lines drawn are of human dimensions and right: a mannequin is positioned in the space frame

6.1.3 Final Design of the Space Frame

The final concept of the space frame design has been refined from concept designs presented in the preliminary report (Dyer et al. 2009). The final design has a focus on passenger safety while being easily fabricated. In the interest of occupant safety, a Finite Element Analysis study of the integrity of the space frame design was performed (Section 6.2). The final concept design of the space frame uses tubular framing and is shown in Figure 6.6. The seat and harness selected in Chapter 4 have been incorporated into this design. The harness is bolted to two rails under the seat and the harness straps are fed through holes in the seat and are looped around tubing of the frame. The harness is also connected to a gusset plate which strengthens the frame

using two eye bolts. The brake lever is mounted to a tubular bar extending from the main space frame. The battery and electronics box are mounted underneath the passenger's legs and behind the seat respectively. The overall design of the space frame consists of a ladder frame which begins at the feet of the occupant and extends around the seat to a roll cage protecting the occupant's head. The framing running between the wheels of the diwheel are bent to meet the inner wheel at connecting brackets. The brackets weld to the space frame and bolt to the inner wheel enabling the inner wheel and space frame to be separated.

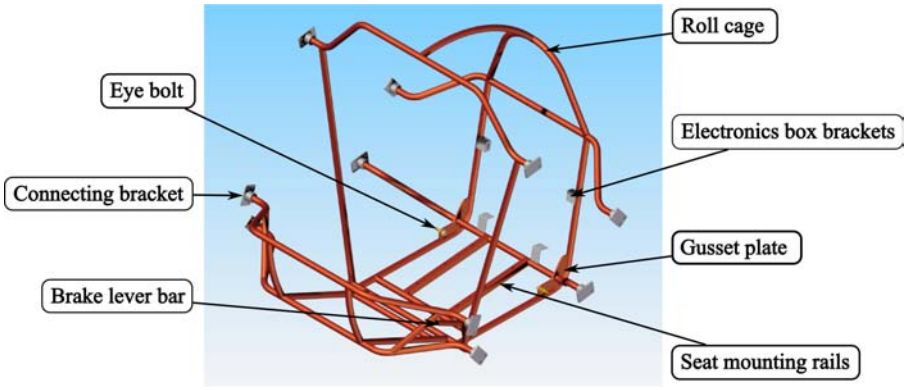

Figure 6.6: Final space frame design concept

6.1.4 Electronics Box

An electronics box is incorporated in to the space frame for the housing and protection of the control electronics of the diwheel. The final design shown in Figure 6.7 is a folded Aluminium sheet metal box with a lid that pivots open. A removable electronics mounting plate is fastened in the box with spacers in between. The electronics box is ventilated by incorporating a 12 Volt DC 60mm diameter computer fan placed on the inside of a louvered panel of the box.

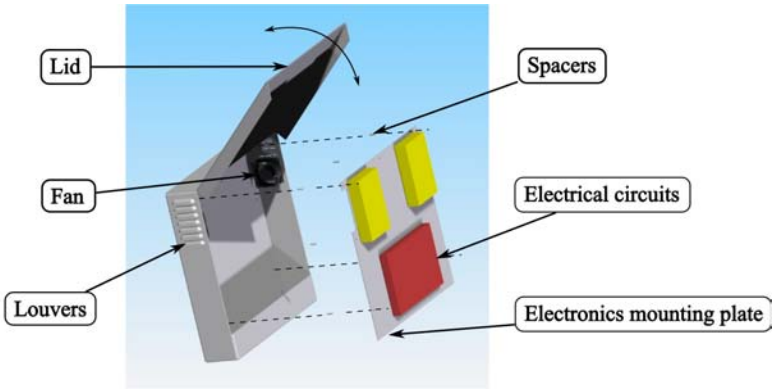

Figure 6.7: Final concept of the electronics box

6.1.5 Battery Box

The batteries chosen represent a significant proportion of the weight of the diwheel and must be supported accordingly. These batteries are mounted below the footrest in an open box constructed of folded sheet steel which is bolted to the space frame structure. The battery enclosure has a lid fastened by wing nuts to allow easy access to the batteries. The battery terminals are exposed when the lid is secured so that they can be connected and charged directly.

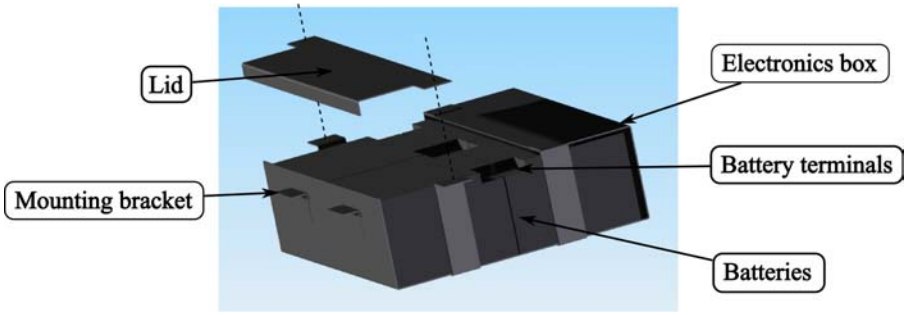

Figure 6.8: Final concept of the battery box

6.1.6 Joystick Mounting

The joystick used for the diwheel's user control input needs to be mounted rigidly in an ergonomic location. The relative frailness of the joystick's structure prevents it from taking any loads and the harness should deter the occupant from loading the joystick. To prevent any overloading of the joystick, it was designed that it be mounted on a pivoting structure which provides support for the joystick in its intended operational location and retracts when the occupant enters and exits the seat, or when a significant load is placed on the joystick. The final concept design of the joystick mounting is shown in Figure 6.9. The joystick mounting plate is connected to a pivoting tube which runs inside and is supported by two brass bushes. The brass bushings clamp onto the pivoting tube and secure it in place using two bicycle seat quick lock clamps.

6.2 Finite Element Analysis

Finite Element Analysis (FEA) of the diwheel was used to analyse the contact between the tubular outer wheel and idler wheel, and the space frame structure. The following is a summary of the FEA performed on the diwheel.

6.2.1 Idler Wheel Contact Problem

The contact experienced between the tubular outer wheel and idler wheel is rolling contact between two elastic bodies. However, dynamic rolling contact was outside the scope of the investigation and so the contact was considered static. The problem is then similar to a Hertzian

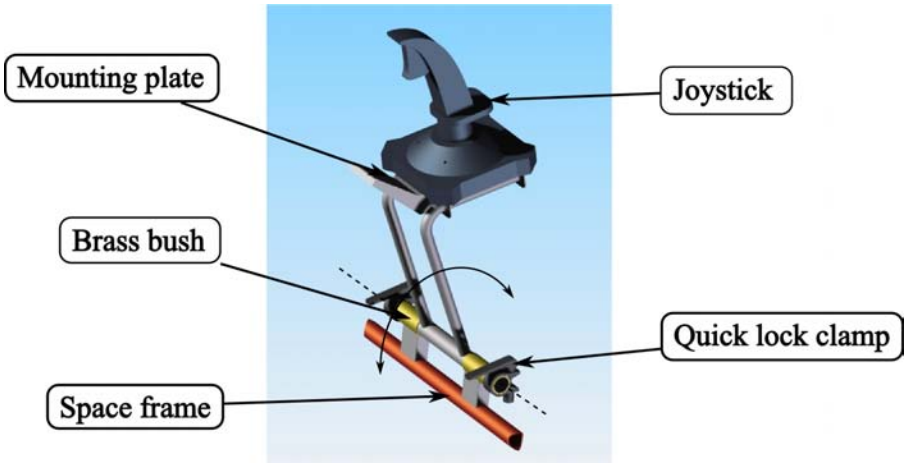

Figure 6.9: Final design of the joystick mounting

contact problem for which there are solutions between curved surfaced solid bodies in contact. In this investigation the FEA model was developed from the conceptual design of the diwheel. The material properties and loads were estimated and used in a model of the idler and outer wheel (see Figure 6.10) in ANSYS, the FEA software used. The material of the outer wheel and idler wheel are Stainless Steel and Nylon 6,6 respectively. The important properties of a material in the FEA and calculation of elastic non-linear contact problems is the Young's Modulus, E, and Poisson's ratio, v. The properties of Nylon 6,6 were $E = 2$GPa and $v = 0.39$ (Tilley 2004 p.301). For this investigation the standard properties of steel were used as $E = 200$GPa and $v = 0.3$. The friction caused by movement between both surfaces was modeled using the friction coefficent between steel and nylon of $\mu = 0.5$. The maximum loading to be simulated on a single idler was determined by considering the situation where the diwheel is inverted placing all load on one ilder wheel. If the mass of the diwheel is overestimated at 250kg and is dispersed between two wheels, and considering the pretension in the other spring-dampers, a conservative maximum loading on a single idler was estimated at 200kg (2000N). These material properties and loadings were used in a model (Figure 6.10) where the single idler and outer wheel contact were cut along two symmetry planes.

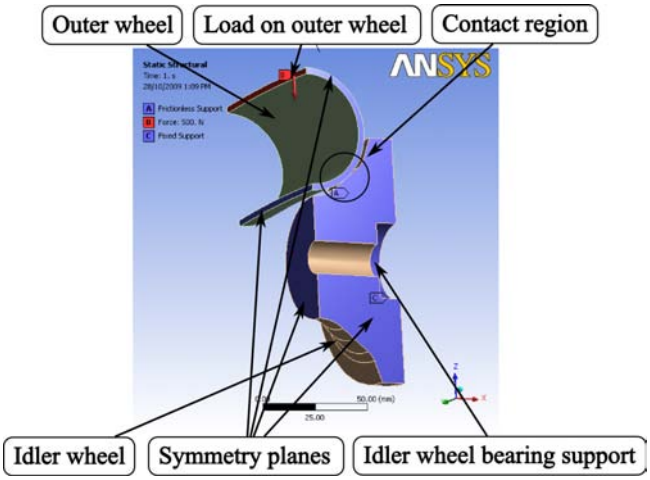

Figure 6.10: FEA idler wheel contact setup

6.2.2 Idler FEA Results and Conclusions

The results extracted from the solved ANSYS model were compared and validated with the calculated results from Hertzian contact theory found in Appendix B.1. A solved model displaying a contour plot of the shear stress is shown in Figure 6.11. The principle results from this model include:

- Maximum shear stress occurs in the steel: $\tau_{max} = 88.0\text{MPa}$
- Maximum shear stress in the idler wheel: $\tau_{max} = 52.6\text{MPa}$
- Maximum contact pressure: $p_a = 97.2\text{MPa}$
- Hertzian contact theory results predict a maximum shear in material with the lower stiffness (Nylon): $\tau_{max} = 33.3\text{MPa}$
- Hertzian contact theory predicts a maximum contact pressure: $p_a = 104.1\text{MPa}$

The conclusions that may be deduced from these results are based on the maximum shear stress criterion, comparing the resultant shear stress to half that of the material's yield stress:

$$\tau_{max} \leq \tau_{maxAllow} = \frac{\sigma_y}{2} \tag{6.1}$$

The yield strength of steel used in this comparison is $\sigma_{Sy} = 250\text{MPa}$, and the yield strength of Nylon 6,6 as given in ISO527 is $\sigma_{Ny} = 60 - 90\text{MPa}$ (Nyl 2009). As Stainless Steel was the actual material used for the outer wheels, these results were only intended to be used as a guide in the design process. Furthermore, the effects of work hardening on the outer wheel during the rolling process have not been considered in this section. Finally the following points are important:

- Local high contact stresses indicate that the contact zones of the idler and outer wheel are expected to deform and wear during operation

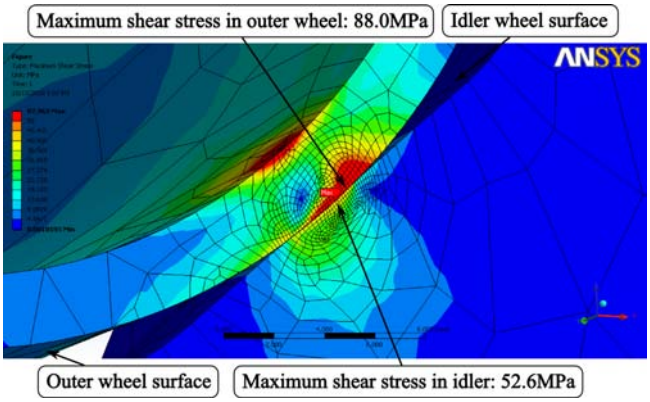
Maximum shear stress in outer wheel: 88.0MPa
Idler wheel surface
ANSYS
Outer wheel surface
Maximum shear stress in idler: 52.6MPa

Figure 6.11: Shear stress contour plot of the idler (lower body) and outer wheel (upper body) contact

- High stresses in the outer wheel when compared to half the yield stress of steel indicated the possibility of local deformation in the event of an impulse overload
- It was recommended that thicker walled piping be used for the outer wheels (this will also increase the inertia of the outer wheels making the inner frame more susceptible to slosh)

6.2.3 Space Frame Analysis

FEA was performed on the structure of the space frame. The purpose of this investigation was to determine how the space frame would distribute loading when in operation, to identify areas of concentrated stress, and to assess the viability of the design. The material of the space frame modeled was 25mm OD steel tubing with a 2mm thickness. The properties of steel used were a Young's modulus of $E = 200$GPa, Poisson's ratio of $v = 0.3$ and a yield stress of $\sigma_y = 250$MPa. The loading of the space frame considered was the static weight of one passenger and other components overestimated to be 200kg. These loads were applied at two points at the location of the seat mounting. A half model of the space frame was created in ANSYS using the plane of symmetry between the wheels of the diwheel. The model was also simplified by not modeling the details of each joint in the space frame. A contour plot of the Von Mises stresses of the solved FEA model is shown in Figure 6.12.

6.2.4 Space Frame FEA Results and Conclusions

The results obtained from the solved FEA model of the space frame are illustrated in Figure 6.12. The stresses described in the following list are Von Mises stresses. The results obtained were:

- Excessive stresses due to bending found around the seating area were ignored because of the point loading used in the model
- Maximum stress in the tubing at the connecting brackets was found to be 45MPa

- Maximum stress was found around the seat mounting rails of 65MPa

The Von Mises stresses found can be directly compared with the yield stress of the material, $\sigma_y = 250$MPa. Thus the following conclusions, and improvements as a result of the FEA performed, were made:

- A safety factor of approximately 4 was achieved in the analysed design
- An excessive load factor is sufficient in conpensating for overloading during extraneous operation of the diwheel (Genta and Morello 2009).
- The framing supporting the seat was improved in order to not subject the space frame tubing to excessive bending loads
- The final tubing used for the space frame was a heavier grade: Onesteel's Tubeline CHS 26mm OD medium grade (2.6mm wall thickness)

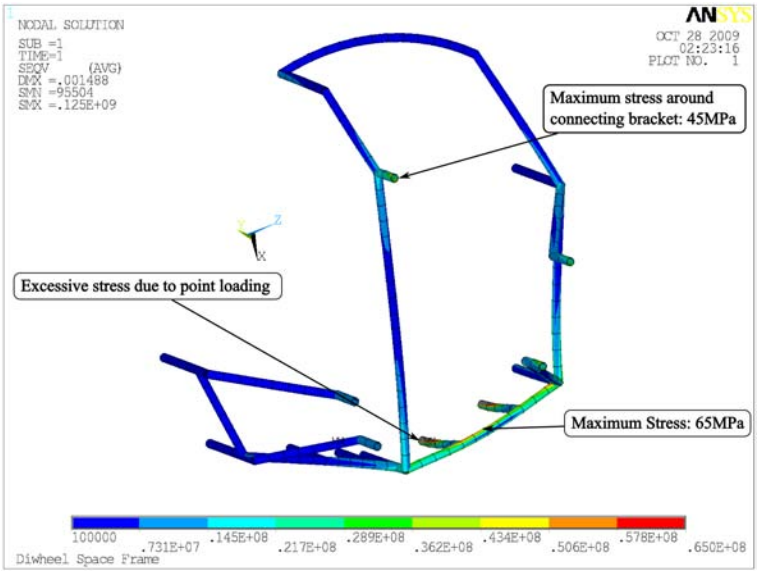

Figure 6.12: Von Mises stress contour plot of the space frame

6.3 Outer and Inner Wheel Design

The role of the outer and inner wheels is to provide rolling contact between the inner frame and the drive system of the diwheel and therefore form the foundation of the load support. As such care must go into the design of this system to ensure minimum rolling friction, maximum drive-wheel traction and structural integrity.

6.3.1 Design Criteria and Aim

The principle design function of the diwheel system is to carry one person in the forward and reverse direction and stands as a concept solution for a future transportation vehicle. The design of a diwheel is concerned with three main aspects:

1. Safety
   Safety is the one of the primary elements of the design of a consumer vehicle. The structure must be robust and durable. In order to protect vehicle occupants, proper harnessing should be included and the vehicle structure should be designed to withstand and absorb all or part of energy in the event of an impact. The design aim for safety is to provide for the securing of a harness to the inner-frame and also proper constraint for the user if the diwheel is allowed to become inverted.

2. Function and performance
   Basic function and performance include the diwheel's top speed, its stability and the comfort afforded to the user. The initial requirements of these performance measures include a minimum operating speed of 10 km/hr, the ability to perform steady turns at different radii and the capability to reduce the driver sensation of road disturbances.

3. Cost
   Cost in a design project is one of the principle drivers of the project outcome, and this remains the case for project EDWARD. The design should be made in accordance with budget constraints. For the project, the budget is particularly tight. In the design phase, this is the primary consideration for the selection of candidate parts. Because cost is directly related to component quality, it is challenging to make the design functionally sound while minimizing cost. The aim of the project is to successfully achieve the primary project goals and to accomplish as many extension goals as the budget allows.

6.3.2 Concept Solutions

To achieve the design aims mentioned in the previous section, several concept designs have been made and assessed. Improvements to the concepts have been made based on comments and advice from the project Supervisor as well as a number of manufacturing companies. In the designs that follow, only a single side of the diwheel system is shown, as the other side is designed to be symmetrical.

Design Overview and Description of Concept Solution 1

Figures 6.13 and 6.14 show the initial concept for the rotating diwheel system. In this design, the outer wheel is made of a rolled industry I-beam. Four caster wheel assemblies (Figure 6.14) travel on the inner flange of the I-beam, establishing support for further installations on the caster assemblies. In Figure 6.14, the four caster rollers (the four small sized rollers with black rubber tyre and gray rim) are designed to take the inward radial load (along the outer wheel radial direction pointing towards the wheel's center of rotation) and the long silver roller is designed to bear the outward radial load. The two flanges on either side of the longer

roller help maintain the position of the caster assemblies along the axial direction of the outer wheel. Housing of all rolling elements is achieved by two bent metal plates with a 10 millimeter thickness.

Figure 6.13: Concept design 1 - Overview

Figure 6.14: Concept design 1 - Caster exploded view

The drive-wheel tensioning mechanism envisaged for Concept 1 is shown in Figure 6.15. The tensioning mechanism was not developed past this stage and is only a representation of the tensioning system. The design of the tensioning system is similar to those of the caster

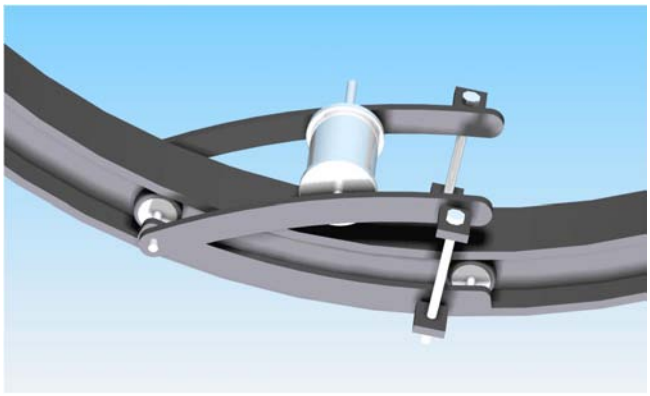

Figure 6.15: Concept design 1 - Drive-wheel tensioning mechanism

assemblies. In Figure 6.15, the longer roller with flanges represents the drive-wheel with a motor connection shaft. The four smaller rollers function in the exact same way as the caster assemblies. The contact force between the drive wheel and I-beam surface can be controlled by adjusting the tensioning bolts. Advantages of this design are that this system is self-locating and able to support itself and the motor assembly (not shown in the figure).

Design Evaluation of Concept Design 1

In concept design 1, the outer wheel is manufactured from an industry I-beam through rolling process. The large moment of inertia of an I-beam makes this outer wheel design extremely robust and durable. The caster assembly design enables casters to be locked in both directions (inwards and outwards in outer wheel radial direction) so that derailment, where the inner frame loses connection with outer wheel, is impossible. However, the fatal problem for this design is faced during manufacturing. Through advice from the project Supervisor and rolling companies it was quickly discovered that rolling an I-beam is complicated and cannot be easily achieved without structural distortion. This is because the inner flange of the beam is subject to buckling when rolled. In addition, the rollers required for the caster assemblies were unable to be sourced. Since this design contains major risks in manufacturing phase, no further design improvements were made to this concept.

Design Overview and Description of Concept Design 2

Concept design 2 as shown in Figure 6.16, uses a rectangular inner frame. One idler roller (red) is located at each corner to support to the frame and allow the required rotational movement while constraining the frame in the outer wheel axial direction. The frame beam members are formed by Rectangular Hollow Sections (RHS) and connected by trapezoidal gusset plates with bolts. Instead of bolt connection, weld joints were also considered as a possible solution.

The profile of idler roller and roller bracket is shown in Figure 6.17. This roller design uses a V-channel concept combined with a flat channel bottom. The flat center part of the roller is designed to both share part of the vertical radial load as well as reducing the risk of initiating cracks due to the wedge effect (explained in Figure 6.18). Slots on the brackets make the idler position adjustable to fit the outer wheel and allow slight deformation of it.

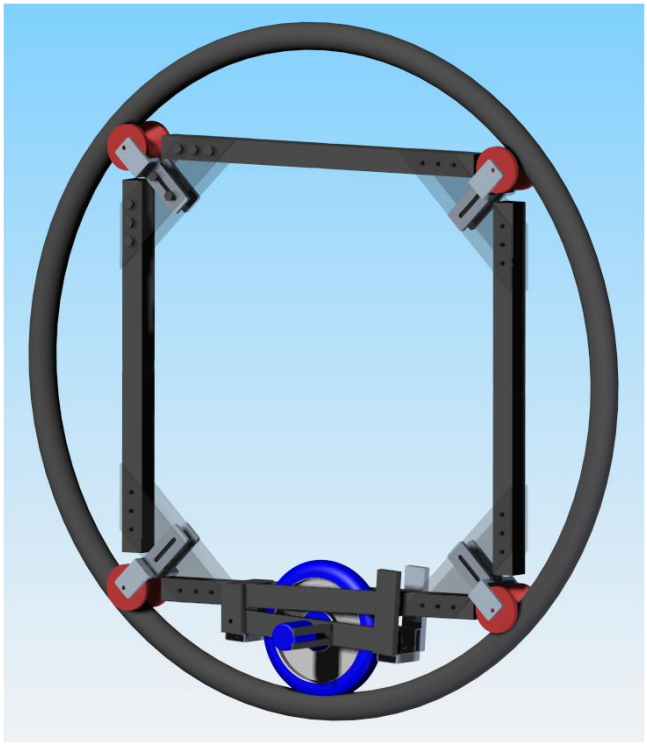

Figure 6.16: Concept design 2 - Overview

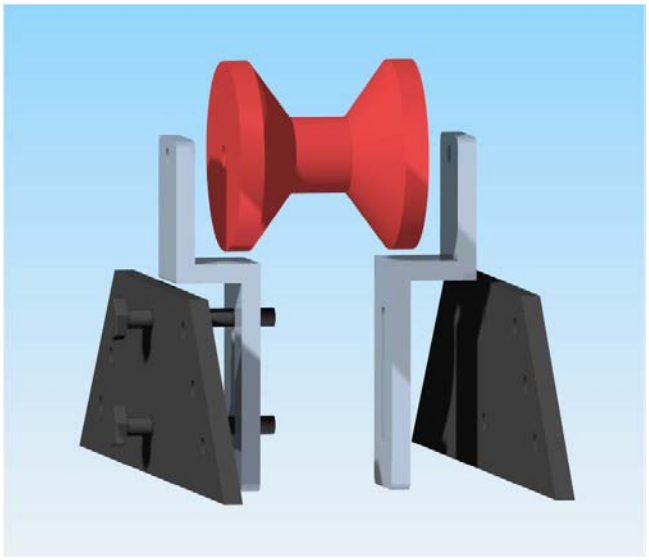

Figure 6.17: Concept design 2 - Idler roller assembly exploded view

This concept design has a new drive-wheel tensioning system as shown in Figure 6.19 which better fits the design frame. The tensioning system is made from a number of simple RHS sections to minimize cost. Spring connections will need to be fitted on the right side (labeled) to provide a securing force on the wheel shaft. Holes on the left side columns provide a pivot point for the drive-wheel assembly to swing up and down.

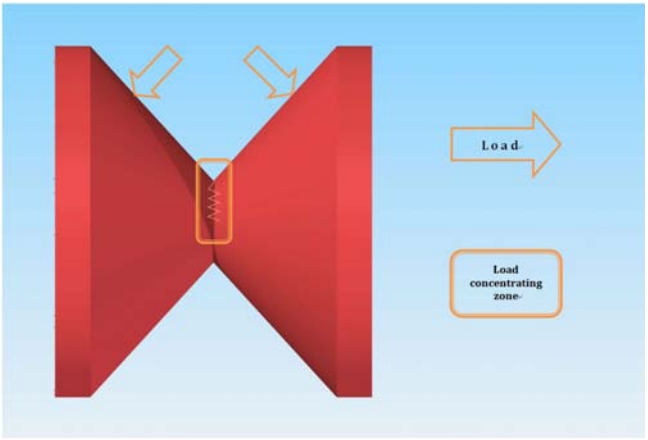

Figure 6.18: Wedge effect caused by a load on the idler

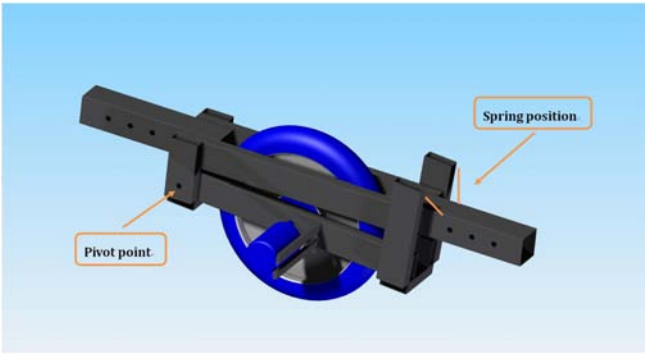

Figure 6.19: Concept design 2 - Drive-wheel tensioning mechanism

Design Evaluation of Concept Design 2

This design has some fatal problems. Firstly, the idler roller assembly brackets are connected to frame gusset plate by bolts meaning that cyclic loading and vibration introduced by a rough road surface may loosen the bolts and cause the whole frame to fall due to idler roller derailment. There is, therefore, a major risk of failure which may result in human injury and severe structural damage. This problem may be resolved by using Nyloc nuts. However, position of idler rollers may require adjustments due to structure deformation or roller wear. This can not be done with Nyloc nuts since they are not removable. The design also lacks a tensioning system on the idler wheel, hence this would require the outer wheel to be rolled with great accuracy in order to avoid misalignment between the outer wheel and idler rollers. However, higher manufacturing accuracy dramatically increases the wheel rolling process cost. In addition, deformation due to impact loading resulting from a fluctuating road surface may also cause misalignment issues between the wheel and idlers.

Another problem is raised by the drive-wheel tensioning system. The tensioning design, which is shown in Figure 6.19, does not includes a damping device to dissipate vibrational energy in the drive system. This might influence motor operation or the accuracy of sensor feedback.

Overall, this design possesses improvements from the previous concept design in terms of its manufacturing simplicity. However, a number of obvious problems may be catastrophic during operation. In addition to the possible failure modes, the design is "not a visually attractive solution" according to meritous sources.

Design Overview and Description of Concept Design 3

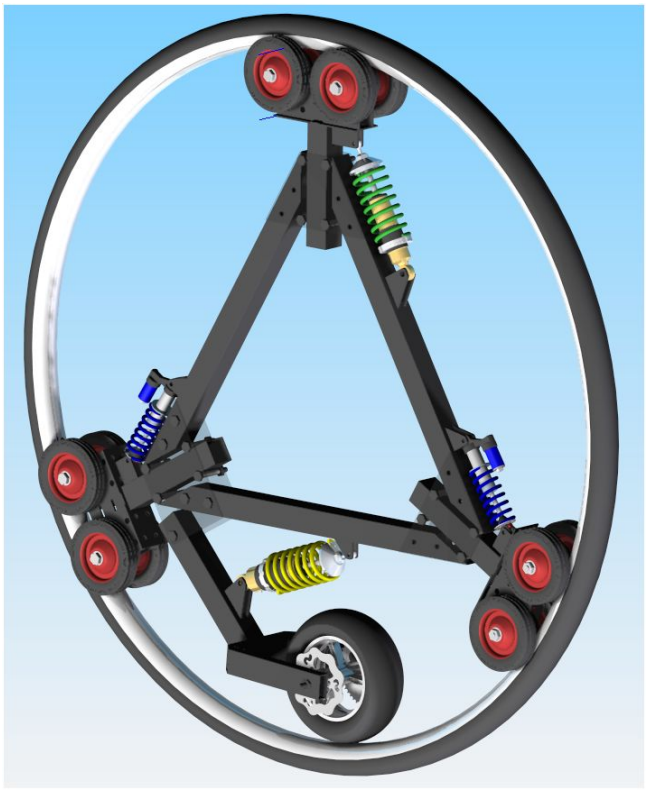

Figure 6.20: Overview of Concept design 3

The third concept design is shown in Figure 6.20. The major improvement achieved in concept design 3 is the integration of a suspension system on all idler wheel assemblies and the bottom drive-wheel swing arm. All components included in the proposed caster assemblies could be sourced from Bunnings Warehouse. The frame remains to be made from RHS but connected in a triangle manner rather than the rectangular connection used in concept design 2. At this stage of the design, the drive-wheel, brake disc and sprocket had been sourced from various suppliers and drawings of each component include in the design. The caster wheel assemblies at the vertices of the triangular frame are free to slide in the outer wheel radial direction. The constraint system of the caster assemblies contains a seriess of bolts and sleeves. This is shown in detail in Figure 6.21. In Figure 6.21, the silver coloured tubes (bolt sleeves) run on the shank surface of the bolts. The supporting bolts are lubricated to allow free rotation of the sleeves. The slide system setup is similar to that of plain bearings but with a longer axial length. The Roller wheel assembly has been designed from items available from a local hardware store. More details of the caster assembly are included in Figures 6.22, 6.23, 6.24.

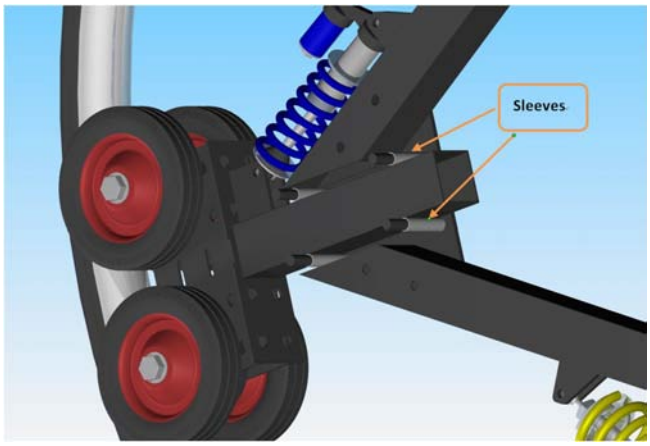

Figure 6.21: Concept design 3-Caster assembly slide path

All the parts appearing in the figures of the caster assembly were available for purchase and no work-shop labour was required.

Figure 6.22: Concept design 3 - Parts list of warehouse caster assembly

Design Evaluation of Concept Design 3

Concept design 3 has many major improvements. It is not only more visually attractive but also better performing. The design includes all the advantages developed from previous concepts and improves on or eliminates some of the defects identified earlier. The installation of a suspension system makes the vehicle more comfortable to ride as well as providing a higher tolerance on the outer wheel rolling accuracy. The spring dampers force the caster wheels to follow the outer wheel's profile closely and no-slip condition is achieved. Another advantage of concept design 3 is that all caster components are available to be purchased from local stores. Therefore, workshop usage and lead-time are avoided.

The design has some problems which required improvement. The friction force in the caster

Figure 6.23: Concept design 3 - Off-the-shelf caster assembly

Figure 6.24: CAD model of the roller assembly

assembly sleeve systems will wear out the supporting bolts rapidly. This is not desirable as the design lacks robustness. In addition, the center wheels in the roller wheel assembly (the middle smaller sized wheels in between of the red wheels in Figure 6.24), which support a major part of the radial load (alone the caster assembly shaft), do not contain any thrust bearings. This means the constraint plates on both sides will rub against it. This is very unfavorable when the vehicle is operated at high speed since the both sides of center wheels will heat up due to

friction causing increased wear. Another major problem is that the actual load on the center caster wheels is only marginally below their designed capacity, which may result in failure under small impact loads, such as the load experienced when running over a small bump.

6.3.3 Final Design of the Inner Wheel

Design Overview

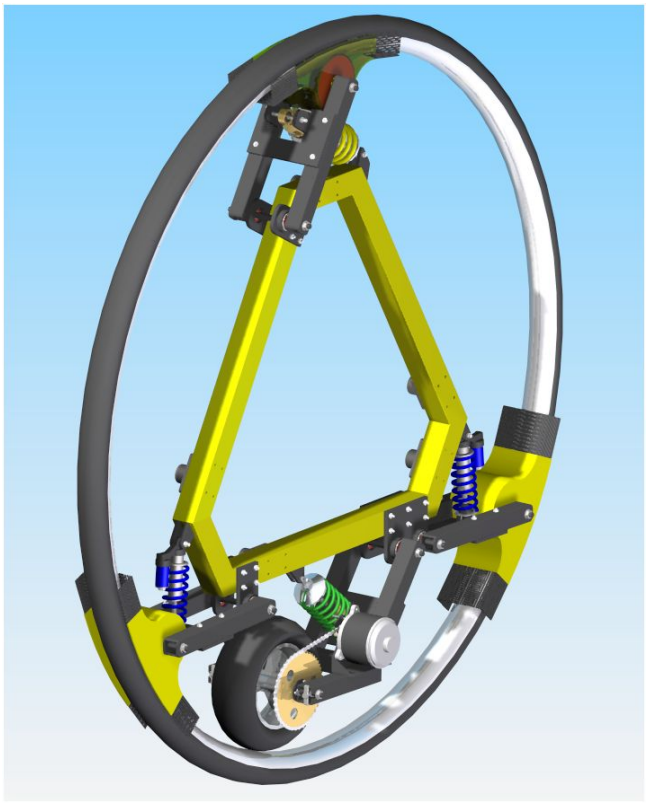

Figure 6.25: Overview of the final design.

The final design possesses major improvements over previous suspension and bearing system arrangements, and is shown in Figure 6.25. Radial movement of the suspension structure (such as in Concept Design 3 where sleeves were used to constrain caster assemblies to move in outer wheel radial direction) has been replaced by a H-bridge bracket structure. Ball bearing pivot joints are utilised for the suspension bridge and inner frame connection, which provides excellent joint flexibility and load capacity.

Inner Wheel Design

The inner frame has a triangular shaped profile due to a triangle's geometric stability. The six sides are chosen to be 50mm RHS with a 2mm wall thickness according to RHS dimension selection and is given in Appendix . The maximum load on each side of the wheel is estimated to be approximately 3000N. This estimation takes into consideration the static weight of system

components and one operator as well as dynamic loads due to non-linear structure movements. In the estimation a worst case, load of 3000N was placed as a point load at the center of the 0.8m RHS (the longer sections of the 6 frame sections in Figure 6.26) as this is the load

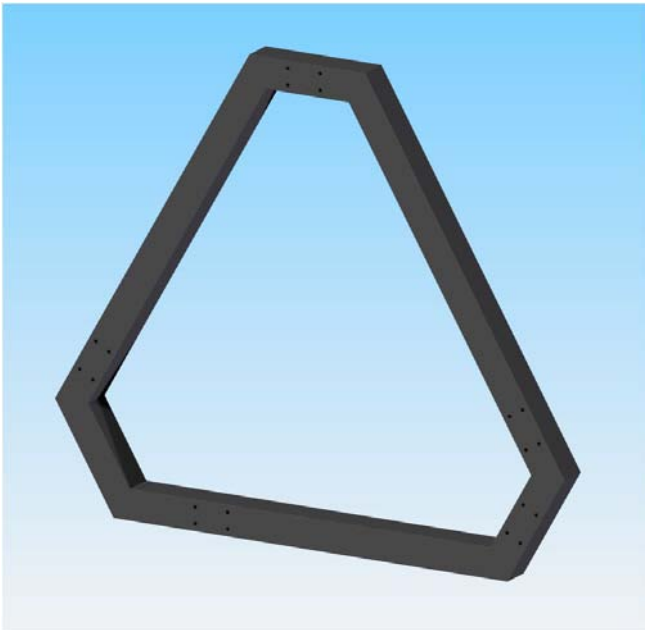

Figure 6.26: Final design - Triangular inner frame

condition which results in the largest deformation. The corresponding maximum deflections are calculated for a series of tabulated RHS (Refer to 'SHS selection', Appendix C).

For the load condition on this frame, torsional rigidity is also an important aspect to consider since the frame needs to withstand torque from the four attached swing arms due to vehicle turning. In this case, relatively large side width RHS is preferred since the moment of inertia of RHS increases significantly with the side width. Due to this reason, a 50mm side width was selected. Structural weight is another important issue. The wall thickness of RHS should be as thin as it can practically be. Therefore, 1.6mm thickness was initially selected. However, all external attachments with the frame were to be connected by bolts, which need to be supported by the thin walls of the RHS frame. The wall thickness should also be chosen with consideration of bolt tear out. It has been advised by the Adelaide University Workshop that, from the manufacturing experience, 2mm is the minimum wall thickness for this load condition. Therefore the wall thickness of RHS has been changed to 2mm in the final design.

Suspension Design

Figure 6.27 shows an overview of suspension structure design. In the final suspension design, the swing arm structure is used instead of the radial slip structure proposed in Concept Design 3. This change makes the design more durable and optimizes the damper performance since the dampers are designed to work in conjunction with a linkage system where the damper-arm relationship is perpendicular. On the suspension arms, 8mm square plates are used to connect

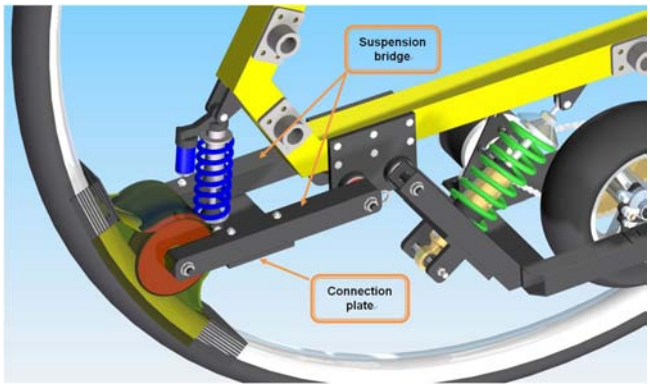

Figure 6.27: Final design - Detail of the suspension configuration

dampers to suspension arms and reinforce the geometrical stability of suspension bridges at the same time.

The suspension bridge beams are also formed by RHS with size 35x35mm. The dimensions of the beams are calculated to ensure that all idlers are able to maintain contact with outer wheel so that "derailing" will not occur. For ease of assembly and adjustment, connections are through bolts. Nyloc nuts are used to ensure they remain tight.

Bearing Selection

Bearing are used on critical joints and axles, as shown in Figure 6.28. In the system, the bearings take mainly two types of load, radial and thrust. The radial load is due to the system's static and dynamic weight, impact forces from road surface and pre-tension from damper springs. The bending moment on suspension bridge due to vehicle turning contributes mainly to thrust load on the bearings. Some of the dynamic loads are not possible to predict without testing on the real vehicle structure, so a large safety factor of 5 has been included in the bearing selection process.

From the load analysis, the load condition on bearings has been classified as a *combined load*. According to SKF bearing selection criteria (Appendix), deep grove ball bearings were selected. All bearings for the swing arm pin joints and suspension pin joints are chosen to be 37mm outer diameter, 12mm inner diameter and 12mm boss width. Selection is based on the bearing static and dynamic load capacity (refer to SKF deep grove ball bearing catalog).

Idler Roller Design

The idler rollers are a critical component in the system as they support inner frame and allow it to rotate within the outer wheels. Therefore, the rollers have to be rigid and durable. Nylon has excellent abrasion resistance and is mechanically strong (Riegel 2003), which makes it a perfect material for the idlers. Roller profile is calculated based on force distribution. The roller surface profile was divided into 3 zones, A, B and C (as shown in Figure 6.29). Zone A is the contact surface between the idler roller and outer wheel. It has a wall angle of 39

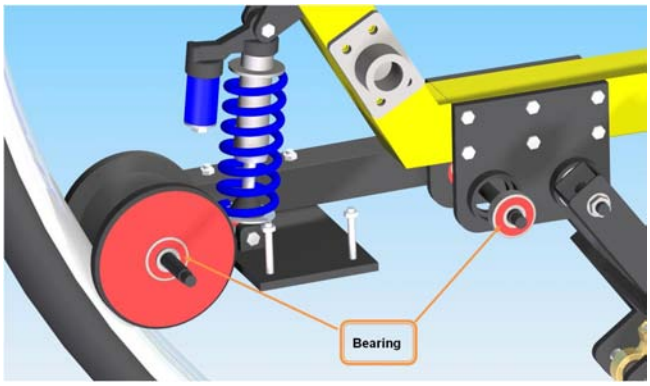

Figure 6.28: Final design - Bearing selection

degrees. The wall angle is calculated according to ratio of maximum radial and thrust load on the roller. The 39 degree angle allows the resultant force of maximum radial and thrust load to be perpendicular to the Zone A idler surface. Zone B has a curved profile to minimize the wedge effect and load concentration (explained in Figure 6.18) on the idler's center spot. The curved profile is tangential to both the Zone A idler surfaces on both sides of the roller. Zone C has a steeper angle than Zone A. The purpose of the steeper angle is to prevent derailing from occuring when the centripetal force on the vehicle is excessive.

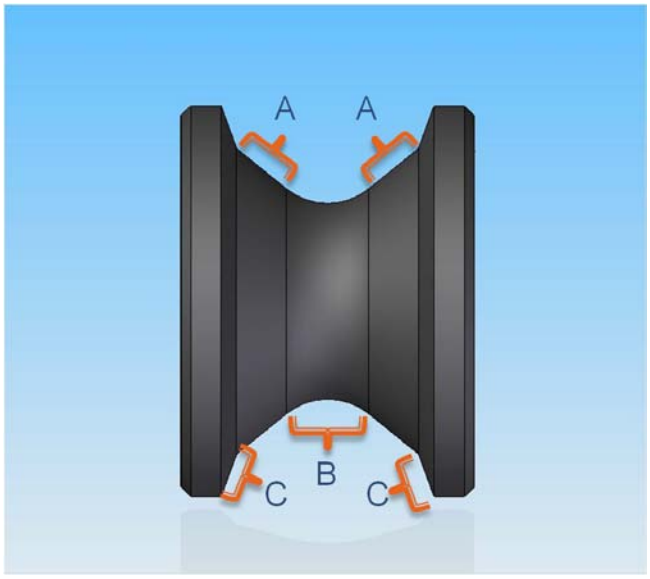

Figure 6.29: Idler wheel profile

Drive System

To achieve the desired speed goal without significantly reducing starting torque, a drive system is required to transmit power from the motor to drive-wheel in a ratio of approximately 1:7 (shown in Figure 6.30). For the required transmission ratio, both chain and belt drives are

effective. The drive system backlash should be kept small in order to allow transmission of the motor torque to the drive-wheel to be smooth. This requirement narrows the belt drive selection to toothed belt drives, which are significantly more expensive than a chain drive. Due to the high cost of a toothed belt drive, a chain drive has been chosen. The sprockets have been purchased at C&A Complete Drive Solutions. According to the supplier's stock, sprockets with 73 and 11 teeth have been chosen.

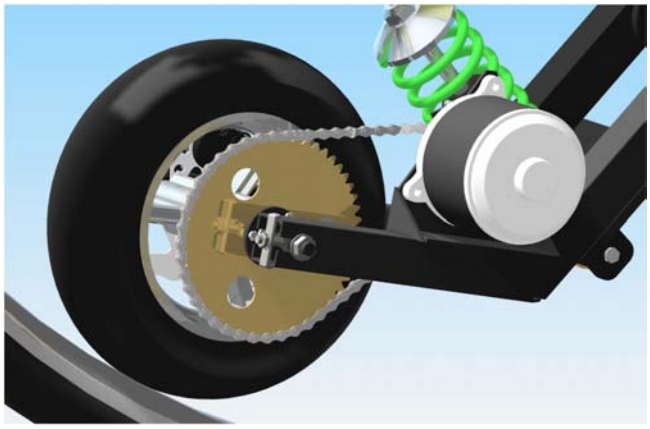

Figure 6.30: Final design - Chain drive

Idler Guards

A plant risk assessment is a compulsory component required by OHS and other legal documents. Through the risk analysis and assessment, the idler wheels were found to be potentially dangerous to human hands. Incidents may occur under certain circumstances if a person makes contact with the inner side of outer-wheel when the vehicle is being driven or being manually moved. Since the sharp edged Nylon idlers are pushed towards the outer wheel by the spring dampers with high force magnitude, hand injury due to idler run-over could be potentially irreversible. Therefore, it became essential to enclose the idlers in protective guards.

The design requirement for the idler guards was to eliminate the possibility of making hand contact with the idlers. This could be achieved by either warning the person in advance of grabbing the wheels or setting up physical barriers which block the access paths to idlers. However a human's response time, in this case, is not fast enough for the person to remove their hand before it reaches the idler. Therefore, the latter method was chosen for idler guard design.

Figures 6.31 and 6.32 show the design of the idler guard. The idler is fully enclosed in a profiled 3mm thick aluminum shield, and the access path (the gap between the guard and the outer wheel) to idler has been sealed by folded industry brushes.

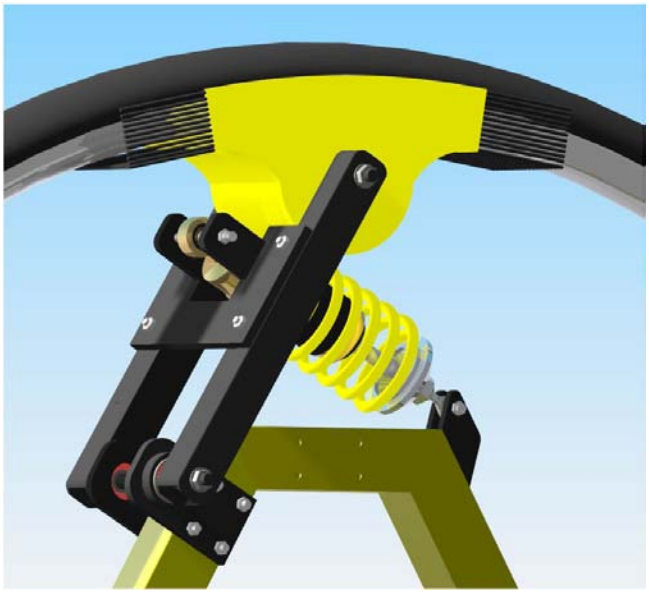

Figure 6.31: Final design - Idler guards

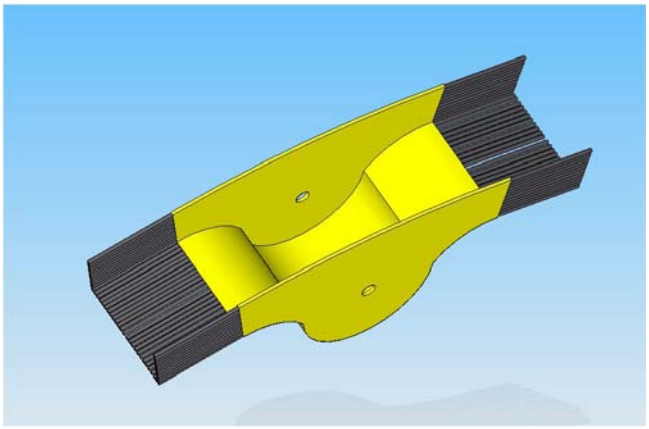

Figure 6.32: Final design - Idler guard detail view

7 Control System Design

Often the aim of control is to improve a system's dynamics by altering the open-loop performance until it meets a number of required design specifications. However, in the case of EDWARD a number of the proposed control strategies are not only envisaged to improve the performance of the system, but also to provide a novel platform for control systems which has not been developed before. The first principle control aim is to implement closed-loop slosh control as discussed in Section 7.5. This control is used to suppress oscillations of the inner frame during normal operation. It was noted during testing that the sloshing motion of the inner frame does indeed make the system harder to control, making a slosh controller desirable for improving user comfort, and the handling of the diwheel. A second major control aim, though initially proposed as an extension goal due to its difficulty, is to implement an inversion controller which can swing the inner frame upside down, and a balancing controller to keep it there. Such a combination of controllers is described in Section 7.6. The remainder of the chapter presents the results of the two modelling routes taken to verify the diwheel's dynamics with two degrees-of-freedom.

7.1 Analytical Derivation of the System Dynamics

The dynamics are defined as the effect that forces and torques have on the motion of a system. In the case of the diwheel, the system dynamics determines the behaviour of each element of the diwheel, as a result of torques supplied to the drive-wheels from the motors. The derivation of the diwheel's dynamics has been performed using two separate methods for the purpose of verifying the final solutions of each and to increase confidence in the accuracy of the results.

The two methods used were an analytical, energy based approach using the Euler-Lagrange method, and a mechanical block diagram (visual) based approach using the SIMMECHANICS TOOLBOX in MATLAB.

7.1.1 Mechanical Dynamics

The analytical method for deriving the dynamics of the diwheel uses the Euler-Lagrange equations. This energy based method is relatively simple to apply to the diwheel and has been applied to other similar dynamic systems such as the Furuta inverted pendulum (Astrom 2000) and a monocycle (Martynenko and Formal'skii 2005b).

In order to derive the dynamics of the system, the bodies of interest of the diwheel must be defined. In the interest of deriving the dynamics of the diwheel for the purpose of slosh and inversion control, the motion of the system has been restricted to the xy-plane. This simplification can be made assuming the slosh and inversion occurs predominantly in this plane, and that any yaw does not have a significant effect on the slosh/inversion dynamics.

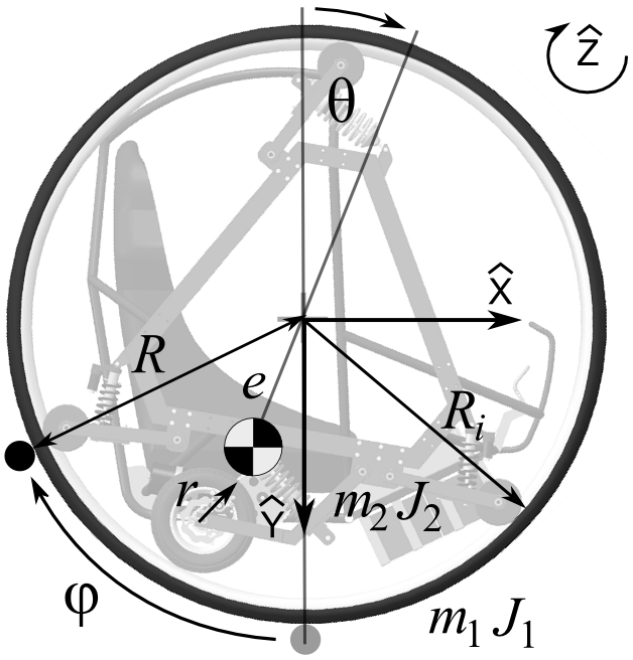

Figure 7.1: Schematic side-on view of the diwheel

To make this simplification, the left and right drive and outer wheels are each combined into a single entity with the assumption that both sets of drive and outer wheels rotate at equal speeds. The schematic in Figure 7.1 shows a side-on view of the diwheel, representing the simplification into the single plane.

The coordinate frame of the system follows the right handed convention and is located at the diwheel's centre of rotation. The x-axis is defined as positive to the right (in the forward direction of the diwheel) and the y-axis is positive down. Rotations about the z-axis are defined as positive clockwise. The two masses, m_1 and m_2 represent the two bodies of interest of the diwheel, where m_1 is the combined mass of the left and right outer wheels, and m_2 is the mass of the inner frame inlcuding a driver and the mass of the drive-wheel assembly. Both bodies have a moment of inertia J_1, J_2 about the centre of rotation of the diwheel. To define the drive transmission, the three radii are defined such that R, R_i are the inner and outer radii of the outer wheels respectively, and r is the radius of the drive-wheel. The eccentricity of the centre of mass of the inner frame assembly from the centre of rotation of the diwheel is given as e.

The model has three coordinates given by φ; the rotation of the outer wheels about the z-axis, θ; the rotation of the inner frame assembly about the z-axis (slosh angle), and x; the horizontal translation of the diwheel centre from an earth centred reference frame. Both the rotation of the outer wheels and the inner assembly are taken from a zero datum given by the positive y-axis. As the horizontal translation of the diwheel is dependent on the rotation of the outer wheels, the system can be classified as having two degrees of freedom.

7.1.2 Euler-lagrange Derivation

The Euler-Lagrange approach follows this basic process:

1. Define the potential and kinetic energies of each body of the system in terms of its coordinates (θ and φ in the diwheel's case).

2. Find the Lagrangian, L, given by the difference in the kinetic and potential energies of the system
$$L = E_k - E_p. \tag{7.1}$$

3. Apply the Euler-Lagrange Equations given by
$$\frac{d}{dt}\left(\frac{\partial L}{\partial \dot{q}_i}\right) - \frac{\partial L}{\partial q_i} = F_i, \tag{7.2}$$

where q_i are generalised coordinates and F_i are generalised forces. This yields an expression describing the systems dynamics of the form
$$\mathbf{M}(\mathbf{q})\ddot{\mathbf{q}} + \mathbf{C}(\mathbf{q}, \dot{\mathbf{q}}) + \mathbf{G}(\mathbf{q}) = \mathbf{F}. \tag{7.3}$$

Velocities

To define the kinetic energy of the system, the rotational and translational velocities of each body are found. The rotational velocities, $\dot{\varphi}$ and $\dot{\theta}$ are the angular velocities of the outer wheels and the inner frame assembly respectively. The translational velocity of the centre of gravity (CoG) of the outer wheels (body 1) in the x-direction is
$$v_{1x} = R\,\dot{\varphi}, \tag{7.4}$$

and there is no translation in the y-direction for body 1. The translational velocity in x-direction of the CoG of the inner frame assembly (body 2) is
$$v_{2x} = R\,\dot{\varphi} - \dot{\theta}\,e\,\cos(\theta)\,, \tag{7.5}$$

and the corresponding velocity in y-direction of the inner frame CoG is
$$v_{2y} = -\dot{\theta}\,e\,\sin(\theta)\,. \tag{7.6}$$

The magnitude of the velocity of the inner frame CoG is thus
$$|v_2| = \left(\left(R\,\dot{\varphi} - \dot{\theta}\,e\,\cos(\theta)\right)^2 + \dot{\theta}^2\,e^2\sin(\theta)^2\right)^{\frac{1}{2}}. \tag{7.7}$$

Kinetic Energies

With the translational and rotational velocities, the kinetic energies of each body and thus the entire system may be found. The rotational energy of the outer wheels is
$$E_{1r} = \frac{J_1\,\dot{\varphi}^2}{2}, \tag{7.8}$$

where J_1 is the *combined* moment of inertia of both wheels about their centre. The translational energy of the outer wheels is

$$E_{1t} = \frac{R^2\,\dot{\varphi}^2\,m_1}{2}. \tag{7.9}$$

Now the rotational energy of the inner frame is

$$E_{2r} = \frac{J_2\,\dot{\theta}^2}{2}, \tag{7.10}$$

where J_2 is the moment of inertia of the inner frame about the centre of rotation of the diwheel. Lastly, the translational energy of the inner frame CoG is

$$\begin{aligned} E_{2t} &= \frac{1}{2} m_2 v_2^2 \\ &= \frac{m_2\,\left(\left(R\,\dot{\varphi} - \dot{\theta}\,e\,\cos(\theta)\right)^2 + \dot{\theta}^2\,e^2\,\sin^2(\theta)\right)}{2}, \end{aligned} \tag{7.11}$$

where $N = \frac{R}{r}$ is the ratio of outer wheel radius R to drive-wheel radius r.

Thus the total kinetic energy of this system is

$$\begin{aligned} E_k &= E_{1r} + E_{1t} + E_{2r} + E_{2t} \\ &= \frac{m_2\,\left(\left(R\,\dot{\varphi} - \dot{\theta}\,e\,\cos(\theta)\right)^2 + \dot{\theta}^2\,e^2\,\sin^2(\theta)\right)}{2} \\ &\quad + \frac{J_1\,\dot{\varphi}^2}{2} + \frac{J_2\,\dot{\theta}^2}{2} + \frac{R^2\,\dot{\varphi}^2\,m_1}{2}. \end{aligned} \tag{7.12}$$

Potential Energy

As the outer wheels move only in the xz-plane, they maintain a constant potential energy. Therefore the total potential energy (assuming zero potential energy at $\theta = 0$) is related to the change in height of the CoG of the inner frame and is given by

$$E_p = e\,g\,m_2\,\left(1 - \cos(\theta)\right), \tag{7.13}$$

where g is the gravitational acceleration.

Lagrangian

Now, with the total kinetic and potential energy of the system, the Lagrangian, $E_k - E_p$, may be found.

$$\begin{aligned} L &= \left(\frac{J_1}{2} + \frac{R^2\,m_1}{2} + \frac{R^2\,m_2}{2}\right)\,\dot{\varphi}^2 \\ &\quad - R\,e\,m_2\,\cos(\theta)\,\dot{\varphi}\,\dot{\theta} + \left(\frac{m_2\,e^2}{2} + \frac{J_2}{2}\right)\,\dot{\theta}^2 \\ &\quad - e\,g\,m_2 + e\,g\,m_2\,\cos(\theta)\,. \end{aligned} \tag{7.14}$$

It is desirable to reduce the size of this equation to make further maths operations neater. This may be done by collecting the constants before state variables and replacing each of the expressions with a single coefficient. Performing this simplification yields

$$L = \frac{\hat{J}_1}{2}\dot{\varphi}^2 + a_R \cos(\theta)\,\dot{\varphi}\dot{\theta} + \frac{\hat{J}_2}{2}\dot{\theta}^2 + a_g\,(\cos(\theta) - 1)\,, \tag{7.15}$$

where $\hat{J}_1 = J_1 + R^2\ (m_1 + m_2)$ is the effective moment of inertia of the wheel and inner frame about the contact point with the ground, $\hat{J}_2 = J_2 + e^2\, m_2$ is the effective moment of inertia of the inner frame about the centre of the wheels, with regard to the coupled motion of the inner frame and wheels; and $a_R = -R\, e\, m_2$ and $a_g = e\, g\, m_2$ are constants of convenience.

Euler-Lagrange equations

With the Lagrangian determined, the Euler-Lagrange equations may be applied to yield the system dynamics in the form

$$\frac{d}{dt}\left(\frac{\partial L}{\partial \dot{\theta}}\right) - \frac{\partial L}{\partial \theta} + b_{12}(\dot{\theta} - \dot{\varphi}) \;=\; -\tau, \tag{7.16}$$

$$\frac{d}{dt}\left(\frac{\partial L}{\partial \dot{\varphi}}\right) - \frac{\partial L}{\partial \varphi} + b_{12}(\dot{\varphi} - \dot{\theta}) + b_1\dot{\varphi} \;=\; \tau, \tag{7.17}$$

where b_{12} is a viscous damping coefficient related to the relative velocities of the inner frame (θ) and the outer wheel (φ), b_1 is the viscous damping constant associated with the wheel rolling (and is surface dependent) and τ is a differential torque applied to both the inner frame and the outer wheel by the drive-wheel/motor assembly.

Evaluating the terms for θ

$$\frac{d}{dt}\left(\frac{\partial L}{\partial \dot{\theta}}\right) = \hat{J}_2\,\ddot{\theta} + a_R\,\ddot{\varphi}\,\cos(\theta) - a_R\,\dot{\varphi}\,\dot{\theta}\,\sin(\theta) \tag{7.18}$$

$$-\frac{\partial L}{\partial \theta} = \sin(\theta)\,\left(a_g + a_R\,\dot{\varphi}\,\dot{\theta}\right). \tag{7.19}$$

Evaluating the terms for φ

$$\frac{d}{dt}\left(\frac{\partial L}{\partial \dot{\varphi}}\right) = -a_R\,\sin(\theta)\,\dot{\theta}^2 + \hat{J}_1\,\ddot{\varphi} + a_R\,\ddot{\theta}\,\cos(\theta) \tag{7.20}$$

$$-\frac{\partial L}{\partial \varphi} = 0. \tag{7.21}$$

Differential Equations

With each term evaluated, the governing differential equations of the diwheel are given by

$$-\tau = \hat{J}_2\,\ddot{\theta} + b_{12}\,\left(\dot{\theta} - \dot{\varphi}\right) + a_g\,\sin(\theta) + a_R\,\ddot{\varphi}\,\cos(\theta) \tag{7.22}$$

and

$$\tau = \hat{J}_1\,\ddot{\varphi} + b_{12}\,\left(\dot{\varphi} - \dot{\theta}\right) + b_1\dot{\varphi} - a_R\,\dot{\theta}^2\,\sin(\theta) + a_R\,\ddot{\theta}\,\cos(\theta)\,. \tag{7.23}$$

It should be noted that the above differential equations are similar to the equations of motion derived for the monowheel by (Martynenko and Formal'skii 2005a; Martynenko 2007) with the exception of both damping terms, b_1 and b_{12}. It is also similar to that for the self-balancing two-wheel mobile robots (Grasser et al. 2002; Ruan and Cai 2009) and the ballbot (Lauwers et al. 2006), the difference being that the gravitational term acts to stabilise the diwheel whereas in the "inverted pendulum" robots, the gravitational term causes instability.

Solution to the Differential Equations of the Mechanical System

The system of differential equations may be solved in terms of $\ddot{\theta}$ and $\ddot{\varphi}$ to give

$$\begin{aligned}\ddot{\theta} &= -\frac{1}{D_1}\Bigg(\left(\hat{J}_1 + a_R\cos(\theta)\right)\left(\tau + b_{12}(\dot{\theta} - \dot{\varphi})\right)\\ &- a_R\cos(\theta)\,b_1\dot{\varphi}\\ &+ a_R^2\sin(\theta)\cos(\theta)\,\dot{\theta}^2 + \hat{J}_1 a_g\sin(\theta)\Bigg),\end{aligned} \tag{7.24}$$

where

$$D_1 = \hat{J}_1\,\hat{J}_2 - {a_R}^2\cos^2(\theta)\,, \tag{7.25}$$

and

$$\begin{aligned}\ddot{\varphi} &= \frac{1}{D_1}\Bigg(\left(\hat{J}_2 + a_R\cos(\theta)\right)\left(\tau + b_{12}(\dot{\theta} - \dot{\varphi})\right) - \hat{J}_2 b_1\dot{\varphi}\\ &+ \hat{J}_2 a_R\sin(\theta)\,\dot{\theta}^2 + a_R a_g\sin(\theta)\cos(\theta)\Bigg).\end{aligned} \tag{7.26}$$

7.1.3 Electrical Dynamics

The mechanical dynamics presented assume a torque input into the system. However, as Permanent-magnet DC electric motors have been used to power the diwheel, the control input into the system is the voltage applied to the motors to produce a torque. It has been assumed that the electrical inductance of the motors, L_m, is sufficiently small it may be neglected, and therefore the current in the motor coil is an algebraic function of the supplied voltage V_m and motor speed $\dot{\theta}_m = N n_s(\dot{\varphi} - \dot{\theta})$, and is given by

$$R_m i + K_m\dot{\theta}_m = V_m, \tag{7.27}$$

where R_m is the resistance of the motor armatures in parallel, K_m is the motor torque constant (which is equal to the back EMF constant for SI units) for both motors, $N = \frac{R}{r}$ is the ratio of the wheel radius to drive-wheel radius and n_s is the drive ratio from the motor sprocket to drive-wheel sprocket (as a chain drive has been used to transmit power from the motors to the drive-wheel). The differential torque acting on the wheel and the inner frame generated by the motor in terms of the armature current is given by

$$\tau = N n_s K_m i. \tag{7.28}$$

Combining Equations (7.27) and (7.28) gives the differential torque in terms of applied voltage

$$\tau = N n_s K_m \left(V_m - N n_s K_m (\dot{\varphi} - \dot{\theta}) \right) / R_m. \tag{7.29}$$

Inserting Equation (7.29) into Equations (7.22) and (7.23) yields the differential equations of the fully coupled electro-mechanical system. By performing these substitutions equations (7.24) and (7.26) may be rewritten in terms of an input voltage to the motors to give

$$\begin{aligned} \ddot{\theta} &= -\frac{1}{D_1}\Bigg(- a_R \cos(\theta)\, b_1 \dot{\varphi} + \left(\hat{J}_1 + a_R \cos(\theta) \right) \\ &\times \left(\frac{N n_s K_m}{R_m} V_m + (b_{12} + b_m)(\dot{\theta} - \dot{\varphi}) \right) \\ &+ a_R^2 \sin(\theta)\cos(\theta)\,\dot{\theta}^2 + \hat{J}_1 a_g \sin(\theta) \Bigg), \end{aligned} \tag{7.30}$$

where $b_m = \frac{(N n_s K_m)^2}{R_m}$ is the effective damping from the back EMF, and

$$\begin{aligned} \ddot{\varphi} &= \frac{1}{D_1}\Bigg(\hat{J}_2 b_1 \dot{\varphi} + \left(\hat{J}_2 + a_R \cos(\theta) \right) \\ &\times \left(\frac{N n_s K_m}{R_m} V_m + (b_{12} + b_m)(\dot{\theta} - \dot{\varphi}) \right) \\ &+ \hat{J}_2 a_R \sin(\theta)\,\dot{\theta}^2 + a_R a_g \sin(\theta)\cos(\theta) \Bigg). \end{aligned} \tag{7.31}$$

7.1.4 Linearised Dynamics

In order to be able to apply typical control tuning techniquies to the diwheel system, a linearised model of the non-linear dynamics was required. The dynamics of the plant were linearised about two operating conditions; the downward (stable) position and the upright (unstable) position as the control modes were required to operate about these positions.

Linearising about downward position

Using a Jacobian linearisation, the non-linear dynamics given by Equations (7.24) and (7.26) about the downward position $\theta = \dot{\theta} = \varphi = \dot{\varphi} = 0$ may be approximated by the linear state equations

$$\dot{\mathbf{x}} = \mathbf{A}\mathbf{x} + \mathbf{B}u, \tag{7.32}$$

where $\mathbf{x} = \begin{bmatrix} \theta & \varphi & \dot{\theta} & \dot{\varphi} \end{bmatrix}^T$ is the state vector, $u = \tau$ is the plant input and the state and input matrices are given by

$$\mathbf{A} = \frac{1}{{a_R}^2 - \hat{J}_1\hat{J}_2} \times \begin{bmatrix} 0 & 0 & {a_R}^2 - \hat{J}_1\hat{J}_2 & 0 \\ 0 & 0 & 0 & {a_R}^2 - \hat{J}_1\hat{J}_2 \\ \hat{J}_1 a_g & 0 & (\hat{J}_1 + a_R)b_{12} & -(\hat{J}_1 + a_R)b_{12} - a_R b_1 \\ -a_g\, a_R & 0 & -(\hat{J}_2 + a_R)b_{12} & (\hat{J}_2 + a_R)b_{12} + \hat{J}_2 b_1 \end{bmatrix}$$

and

$$\mathbf{B} = \frac{1}{{a_R}^2 - \hat{J}_1\hat{J}_2} \begin{bmatrix} 0 \\ 0 \\ (\hat{J}_1 + a_R) \\ -(\hat{J}_2 + a_R) \end{bmatrix}. \tag{7.33}$$

The poles of linearised dynamics in the lower equilibrium position are at $s = 0, -0.22 \pm 2.59i, -0.26$, with the complex poles having a damping ratio of $\zeta = 0.083$. The transfer function from torque, τ, to slosh angle, θ, exhibits one zero on the origin which is expected as at the steady state $\theta(s \to 0) \to 0$. It is interesting to note that the transfer function from τ to outer wheel angle, φ, exhibits two purely imaginary zeros at $s = \pm 3.44i$. The presence of purely imaginary zeros is similar to that found in other systems exhibiting slosh such as the ball and hoop system (Wellstead and Readman). The implication is that if the motor is driven with a sinusoidal input at the frequency of the zeros, then the wheel will stand still and only the inner frame will move

Note that for the case of a voltage input, $u = V_m$, then the damping term arising from the differential velocity of the frame and wheel increases from $b_{12} \to b_{12} + b_m$ (resulting in open loop poles at $s = 0, -0.34 \pm 2.55i, -0.37,$) and the state input matrix $\mathbf{B}$ needs to be multiplied by $\frac{N n_s K_m}{R_m}$.

Linearising about upright (inverted) position

Linearising the non-linear dynamics given by Equations (7.24) and (7.26) about the upright position $\theta = \pi$, $\dot{\theta} = \varphi = \dot{\varphi} = 0$ gives the linear state equations

$$\mathbf{A} = \frac{1}{{a_R}^2 - \hat{J}_1\hat{J}_2} \times \begin{bmatrix} 0 & 0 & {a_R}^2 - \hat{J}_1\hat{J}_2 & 0 \\ 0 & 0 & 0 & {a_R}^2 - \hat{J}_1\hat{J}_2 \\ -\hat{J}_1 a_g & 0 & (\hat{J}_1 - a_R)b_{12} & -(\hat{J}_1 - a_R)b_{12} + a_R b_1 \\ -a_g\, a_R & 0 & -(\hat{J}_2 - a_R)b_{12} & (\hat{J}_2 - a_R)b_{12} + \hat{J}_2 b_1 \end{bmatrix}$$

and

$$\mathbf{B} = \frac{1}{{a_R}^2 - \hat{J}_1\hat{J}_2} \begin{bmatrix} 0 \\ 0 \\ (\hat{J}_1 - a_R) \\ -(\hat{J}_2 - a_R) \end{bmatrix}. \tag{7.34}$$

The poles of this plant are at $s = 0, -0.25,\ 2.27, -3.07$. Note that for the case of a voltage input, $u = V_m$, then the damping term arising from the differential velocity of the frame and

wheel increases from $b_{12} \rightarrow b_{12} + b_m$ (resulting in open loop poles at $s = 0, -0.34, 2.12, -3.40$) and the state input matrix $\mathbf{B}$ needs to be multiplied by $\frac{Nn_sK_m}{R_m}$ as was done for the downward linearisation case.

7.1.5 Summary of Assumptions

In deriving the dynamics of the diwheel, several assumption have been made to simplify the model. A summary of these assumptions is given here.

- The motion is restricted to the xy-plane
- Friction is limited to viscous friction, and the Coulomb friction arising from the idler rollers is neglected
- The suspension arms are fixed, keeping the centre of gravity of the inner frame a fixed distance from the centre of the wheels
- The inductance of the motor is negligible and therefore the current is an algebraic function of voltage and motor speed
- The rotational and translational inertia from the motors and drive-wheels has been included in the inner frame
- The energy associated with the rotational velocity of the drive-wheel is considered negligible
- There is no slip between the drive-wheels and the outer wheels
- There is no slip between the outer wheels and the ground

7.1.6 Model Parameters

The parameters used for the model, and thus the controller designs, are detailed in Table 7.1. Most parameters were estimated from the Solid Edge model of the diwheel (and driver) with the exception of the damping terms which were measured. The motor parameters were source from supplier data.

7.2 Simmechanics Derivation of the System Dynamics

In order to verify that the dynamics of the two degree-of-freedom (DoF) found in Section 13 are correct, a model of system was also completed using the SIMMECHANICS toolbox in MATLAB. In comparison to the energy-based analytical method of Section 13, the SIMMECHANICS model derivation utilises a block-diagram approach to describing the system dynamic behaviour which requires:

- The identification of separate bodies with mass and inertia
- Defining relationships between each body (DoF) using *joints*
- The measurement of joint/body displacements, velocities and accelerations

Table 7.1: Parameters used to define the model. Note that the terms for the wheels and motors account for both acting together.

Part	Parameter	Value
Wheels	m_1	50.3 kg
	J_1	26.1 kg.m^2
Frame	m_2	218 kg
	J_2	48.4 kg.m^2
Lengths	R	720 mm
	$R_i \approx R$	720 mm
	r	140 mm
	e	160 mm
Damping	b_{12}	30 Nm.s/rad
	b_1	12 Nm.s/rad
Motor	V_{sat}	36 V
	R_m	0.314 Ohms
	L_m	0.3 mHenry
	K_m	65 mNm/A
Transmission	$N = \frac{R}{r}$	5.14
	N_s	7

7.2.1 Main Block Diagram

A view of the main SIMMECHANICS block diagram is shown in Figure 7.2. The main block diagram consists of three interconnected entities, the inner frame assembly, the combined two outer wheels and the drive assembly. The connection between the inner frame and the outer wheels is assumed to be solely via the drive system consisting of the drive-wheel and the motor and transmission.

7.2.2 Inner Frame

The block diagram of the inner frame assembly is shown in Figure 7.3. Beginning at the left of the diagram, the block diagram consists of a *Machine Environment* block connected to a *Ground* block. This is the root of the SIMMECHANICS model, and there is only one connection to the *Machine Environment* block. The physical constraints placed on the inner frame body consist of two degrees of freedom with respect to the Earth (Ground) centered reference frame: one rotational (revolute) and one translational (prismatic). The two degrees of freedom describe the behaviour of the inner frame as being able to rotate freely within the outer wheels, and translate parallel to the ground in a vertical plane. The *Body DOF* block in SIMMECHANICS requires the axes about which the DoFs are applied. Following the derivation in Section 13 the rotational DoF is applied about the z-axis, while the translational DoF is along the x-axis. An initial condition (the IC block) has been included so that an initial translational velocity, rotation velocity or rotational angle of the inner frame may be set at the start of a simulation. Two sensors are connected to the *Body DOF* block each of which measures the kinematic state

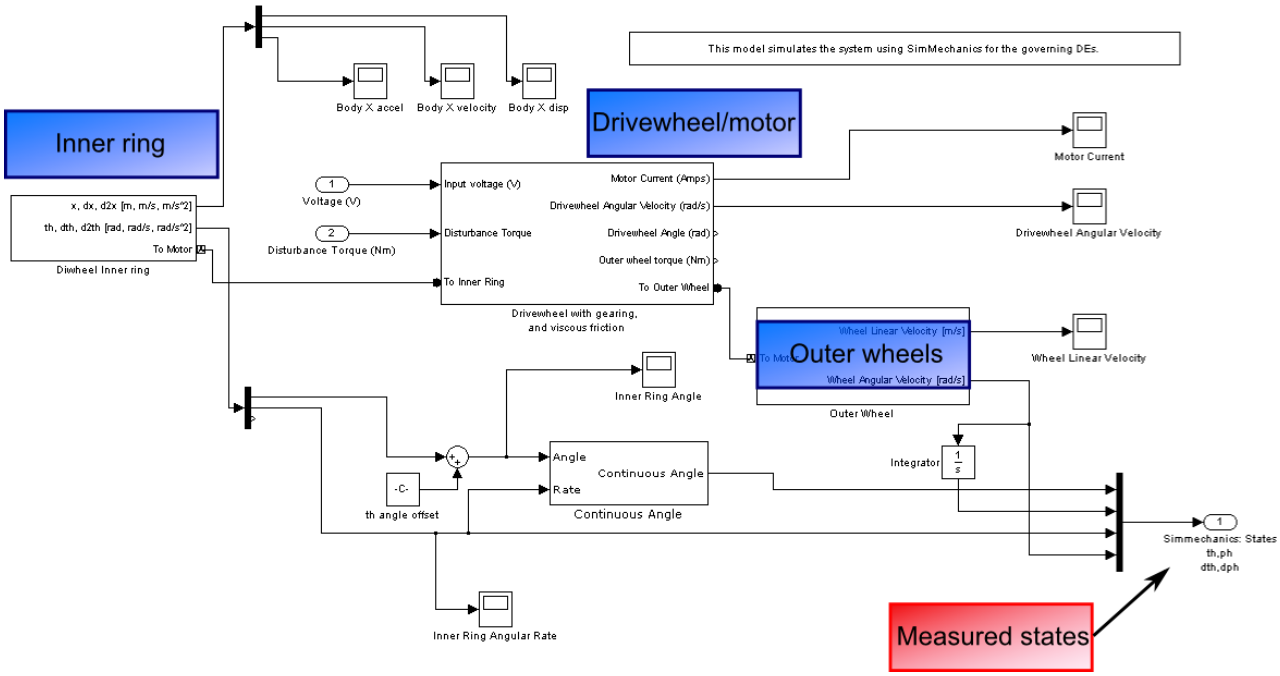

Figure 7.2: The main SIMMECHANICS block diagram

of each DoF. These measurements can be viewed on *Scopes,* and exported to MATLAB for analysis.

7.2.3 Drive System

The SIMMECHANICS model of the drive system shown in Figure 7.4 models the behaviour of the friction drive-wheel as a joint between the inner frame and the outer wheels. In MATLAB's SIMMECHANICS toolbox, forces and torques may only be applied through joints, and the drive system block diagram models this by applying the torque produced by the motors to a *Joint Actuator* which actuates the drive-wheel joint. The motor torque is derived from an algebraic equation relating torque to speed and the applied armature voltage, which is discussed in Section 7.3.1. Any inertial or damping properties associated with the chain drive transmission have been omitted from the block diagram model, following the derivation of Section 13. The block diagram also contains both voltage and current limits used to simulate the limited supply voltage and current ratings on the diwheel. During initial simulations, when the dynamics were being verified against each other, these limits were relaxed to $(-\infty, \infty)$ volts and amps, respectively.

On the left-hand side of Figure 7.4, a sensor block is connected to *Base* of the drive-wheel joint. The sensor measures the *differential* angular velocity of the outer wheels with respect to the inner frame. Assuming the drive-wheel does not slip along the inside of the outer wheels, the angular velocity of the drive-wheel is N times this measured value. The only friction effects included in the block diagram is the viscous damping caused by the differential motion of the inner frame within the outer wheels. This damping consists of friction due to the idler wheels, as well damping in the transmission.

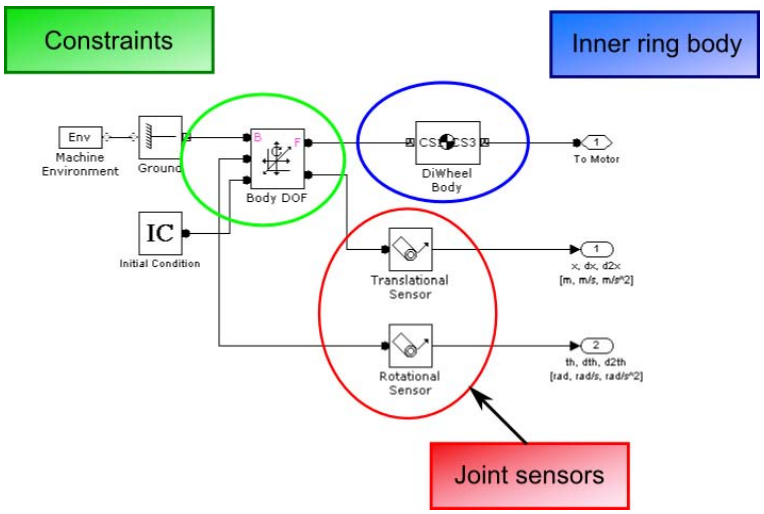

Figure 7.3: Inner frame SIMMECAHNICS block diagram

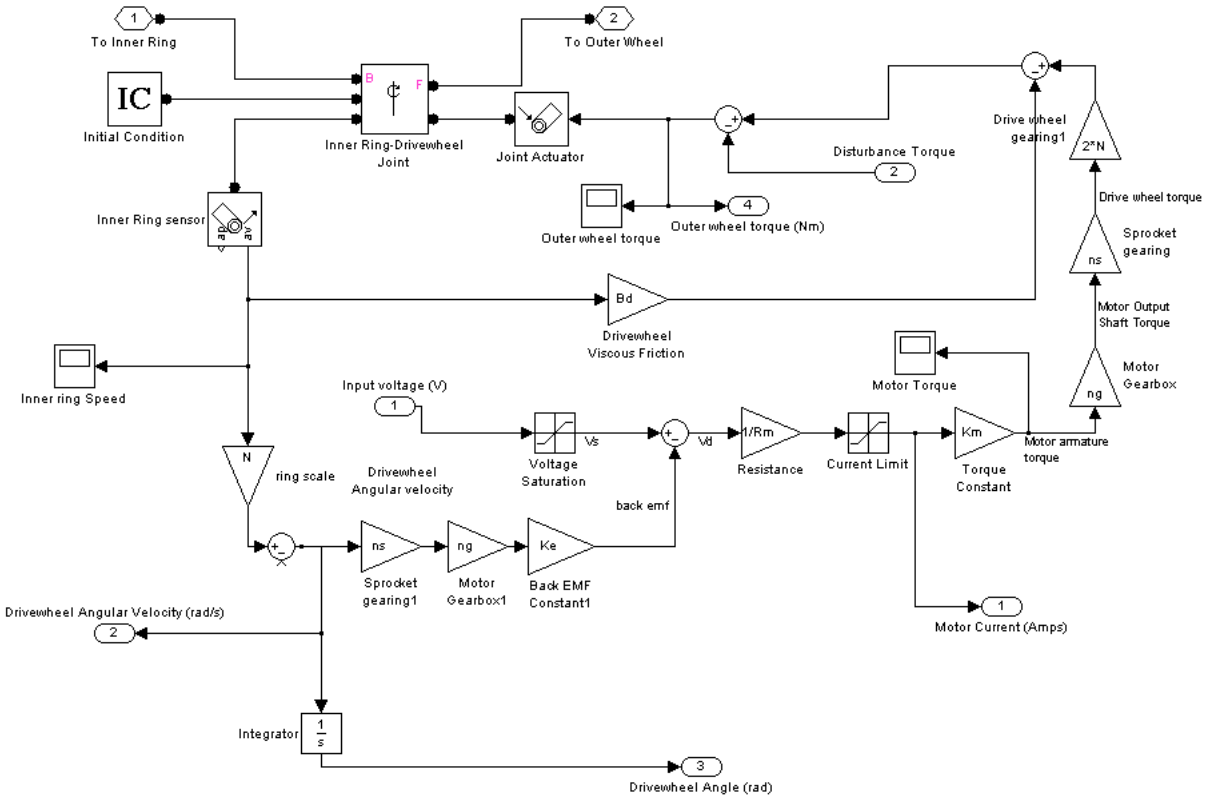

Figure 7.4: SIMULINK block diagram of the drive system including motor dynamics

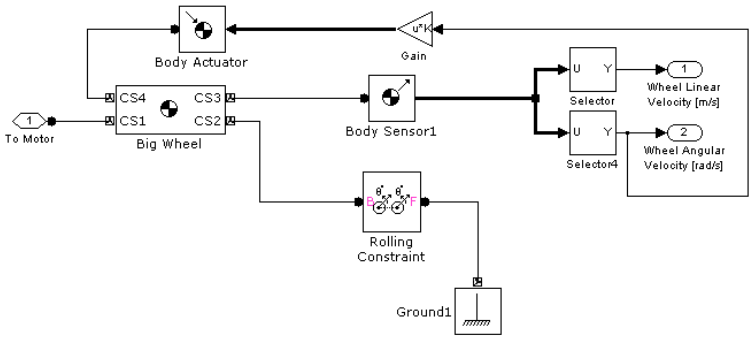

Figure 7.5: Block diagram of the combined outer wheels

7.2.4 Outer Wheels

Because both the analytical and SIMMECHANICS models restrict motion of the diwheel to one plane, the two outer wheels are assumed by this model to be rotating at one speed. Therefore, the model combines the two wheels into a single wheel with twice the inertia of one wheel. Figure 7.5 shows the basic block diagram. At the left of the diagram, the *To Motor* input which arises from a connection to the drive-wheel joint connects to a body block that contains the mass and inertia of the two wheels. To the right of this block are a *Body Sensor* and *Rolling Constraint*. The body sensor is capable of measuring all coordinates and derivatives of the outer wheel. However in Figure 7.5, the measured quantities are restricted to the wheel's linear velocity, $\dot{x}$ and its angular velocity, $\dot{\varphi}$. The rolling constraint is used to tell SIMMECHANICS that the wheel's linear and angular velocities are algeraically related, i.e.: $\dot{x} = \dot{R}\varphi$. This stipulates that the outer wheel maintains *pure rolling contact* with the ground. In reality, the outer wheels will never slip before the drive-wheel does, because it is the traction between the drive-wheel and the inner surface of the wheels that provides the reactive torque. The feedback through the gain block models the rolling damping of the outer wheels.

7.2.5 Results

The reason for verifying the dynamics of the analytical solution is to ensure that any simulations performed with either set of dynamics, are a realistic representation of the true physical system. The two DoF models described in this section and Section 13 are only representations of this diwheel's behaviour in the absence of any turning (yaw) motion about the y-axis. However for the purpose of the Slosh and Inversion control systems described in Sections 7.5, the models form a solid basis for simulation and controller testing.

7.2.6 Visual Simulation Using VRML

In order to assist the design process further, the dynamic models derived in Section 13 and 7.2 were to be simulated in conjunction with a *Virtual Reality* simulation, which formed one of the principle project goals. The virtual reality simulation was achieved by utilizing MATLAB's VRML TOOLBOX. The initial task involved exporting a simplified version of the final CAD assembly model to a WRL file which contains a purely text-based representation of all 2D/3D

primitives of the three-dimensional model. The second task required the grouping of individual primitives into assemblies of the diwheel, and finally into *transform* groups which produces a part hierarchy so that the motion of a parent part has the correct effect on child parts.

The result is a file which contains groups associated with the following assemblies on the diwheel:

- Left and right wheel
- Left and right drive-wheel
- Inner frame, including the space frame, seat, idlers and spring dampers as well as other non-critical parts

This structure allows visual simulation of the diwheel using the states derived from either the analytical or SIMMECHANICS. Figure 7.6 shows the result of this task.

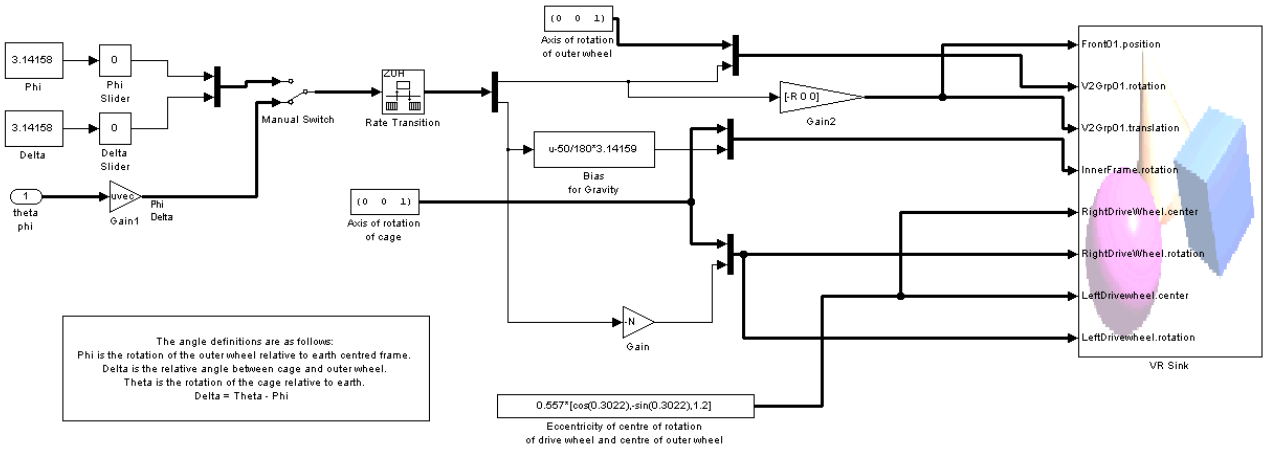

(a) VRML Block Diagram

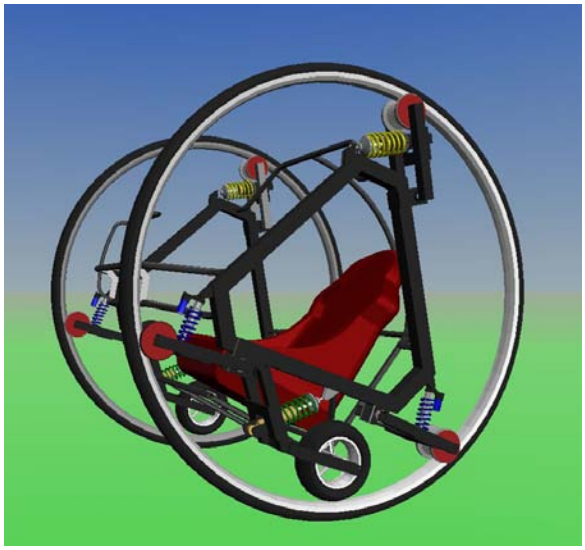

(b) Image of the VR Model

Figure 7.6: The VRML models

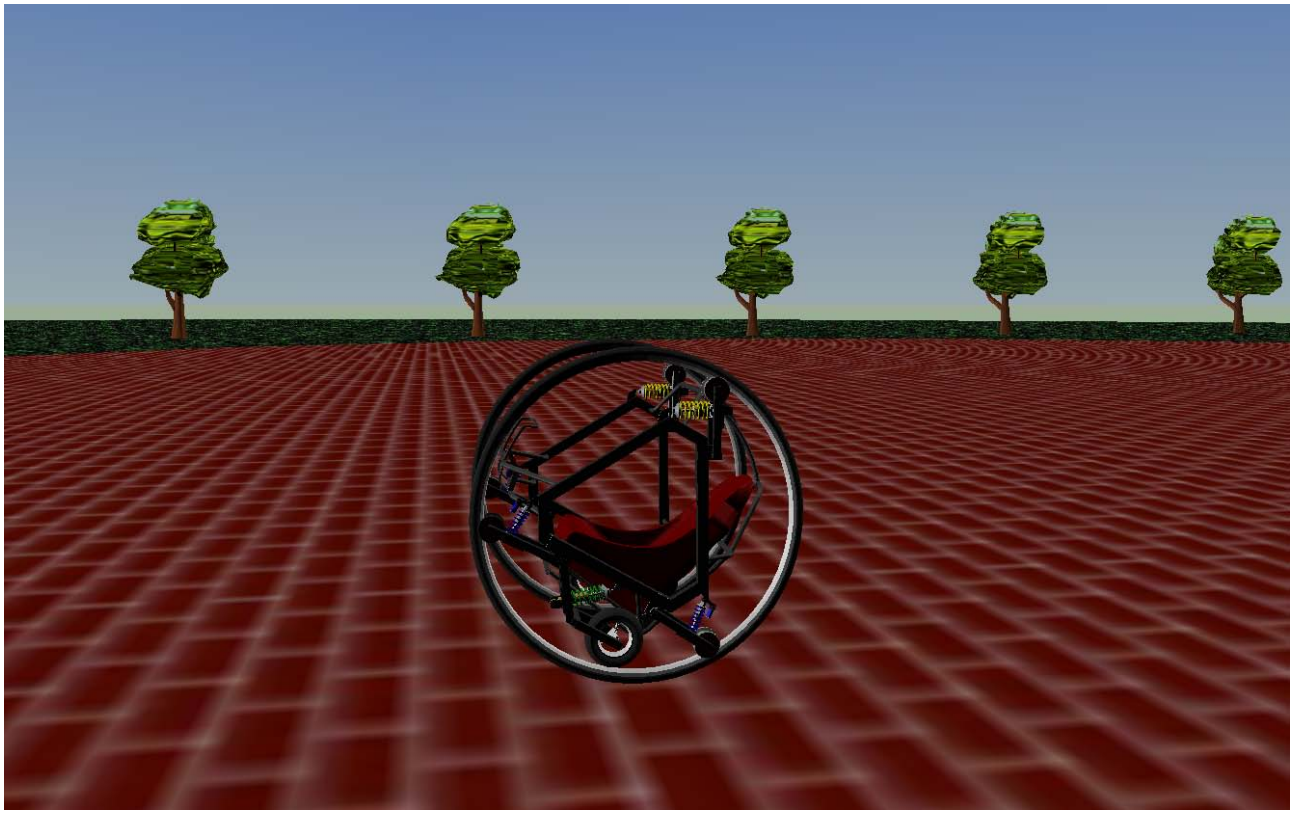

Figure 7.7: Image of the final VRML simulation

7.2.7 Final VRML Model

The initial VRML model was used only as a verification tool to ensure that the dynamics that had been derived for the two DoF model were correct. The system's behaviour was visualised for each control mode in a single plane of motion. To accomplish the core goal pertaining to the VRML model, the final VRML enviroment required a modelling of the diwheel's behaviour for all command inputs. This encompassed the two DoF dynamics of the initial VRML model as well as the response of the system to a yaw command.

To achieve this goal with an aim to keep the system dynamics as simple as possible, the yaw dynamics were considered as being uncoupled from the two DoF dynamics described in 13. This allowed the initial dynamics to remain the same while another set of dynamics was run in parallel to alter the heading and position of the diwheel in the virtual reality environment. In order to view the results of the updated VRML model, a joystick identical to that used on the physical diwheel was integrated to allow the user to drive the virtual diwheel in the same fashion as the physical system, as well as giving the user opportunity to test each control mode without stopping the simulation. To improve the visualisation of the speed and movement of the diwheel as well as allowing the option of a tracking camera view, the environment in which the diwheel runs was updated. Simple ground textures and trees were added to give indication of speed and yaw rate resulting in the VRML environment displayed in Figure 7.7. A view of the highest level mask of the final VRML model incorporating all the operating features of the physical system excluding mechanical braking is shown in Figure 7.8.

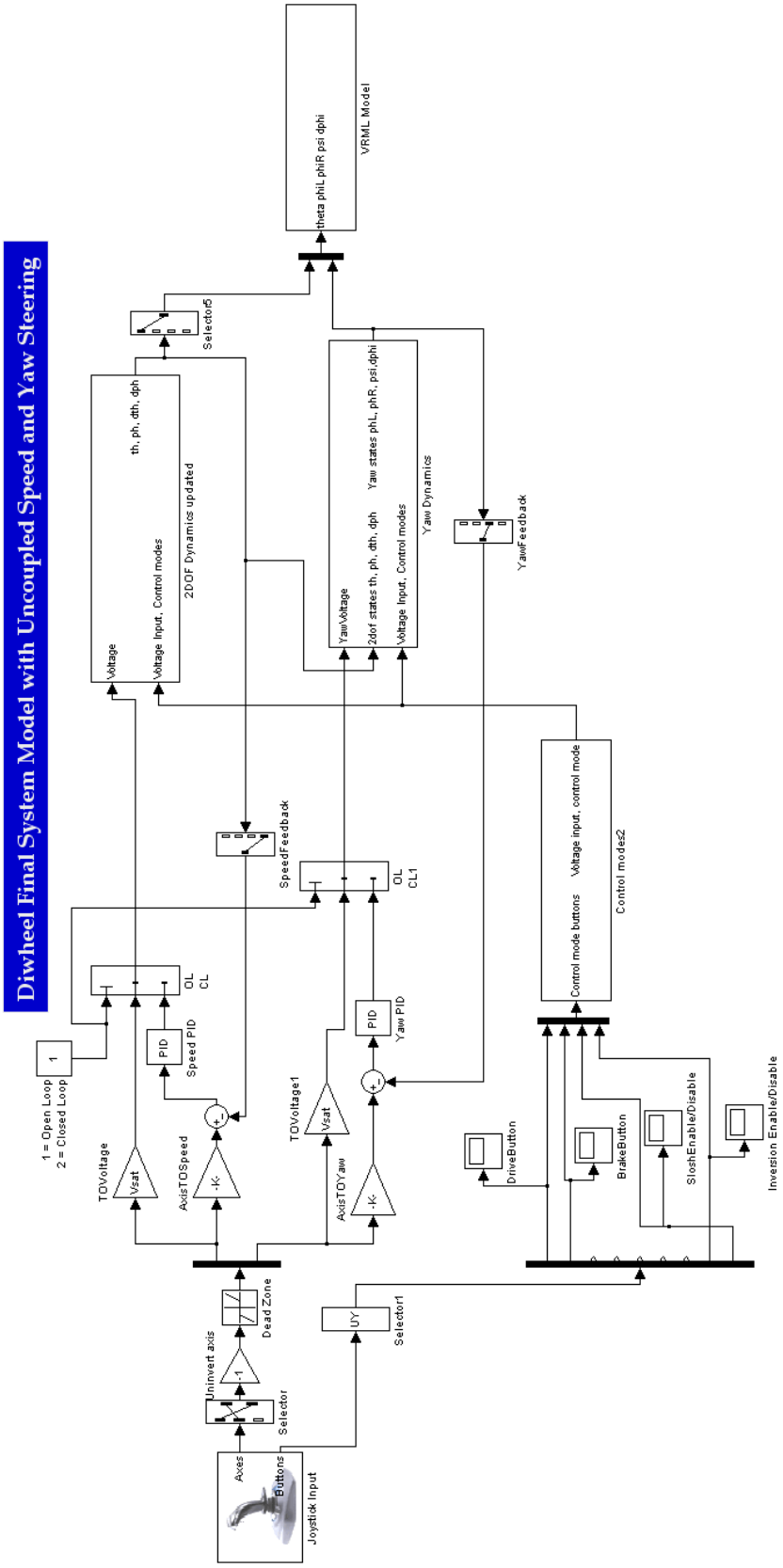

Figure 7.8: Final simulink model including the uncoupled yaw and inner frame dynamics

7.3 Speed Control

The requirement for speed control, is essential - without it, the diwheel is static and uninteresting. Speed control can be achieved via *open-loop* or *closed-loop* control. In the case of open loop control, a voltage is applied to the armature of the motors by the motor controllers as described in Section 5.1. The basic effect is that the motor speed increases as the applied voltage is increased. However a Permanent magnet DC motor cannot achieve equal speeds for all conditions. For example, if the load applied to the motor is increased, the steady-state speed will be reduced (Hughes 2006).

Closed-loop control augments the open-loop system by providing negative feedback from a sensor. For the case of closed-loop speed control the sensed output is the average velocity of the two wheels: $\frac{1}{2}(\dot{\varphi}_L + \dot{\varphi}_R)$ which is inferred by the encoder measurements. The closed-loop system then forms the error between the desired speed and the measured speed, and uses the error to increase or decrease the voltage applied to the left or right motors. Closed-loop speed control becomes necessary if the load on one wheel is dramatically different from the other,

7.3.1 Open-loop Speed Control

As discussed above open-loop speed control does not require feedback, and simply uses the inherent properties of the two DC motors to control their speed. Assuming the mechanical dynamics of the motor, such as inertia and friction, are small negligible in comparison to the inertia of the drive-wheel / outer wheels (in fact they are $< 1\%$), then behaviour of an *armature-controlled DC motor* is summarised by the differential equations:

$$L\frac{di}{dt} + Ri + k_e\dot{\theta} = V$$

$$\tau = k_t i$$

which describe the change in current (i) and motor speed ($\dot{\theta}$) due to a voltage (V) applied to the armature, and the electrical torque (τ) produced by the armature current. If the torque produced by the motor is zero (no load), then the motor speed is directly proportional to the voltage:

$$\dot{\theta} = \frac{1}{k_e}V$$

This relationship then provides the possibility of using an open-loop system to control the diwheel's speed, purely by altering the average voltage applied to each motor.

Transfer function between voltage and $\dot{\varphi}$ at the lower equilibrium

The dynamics of Section 13 assume the input into the system is a torque input, which does not correctly resemble the behaviour of the DC motors, which are voltage controlled devices. Because the motor electrical dynamics are important and are not negligible, they must be accounted for in the design. Assuming the motor inductance is negligible with regard to the remaining system poles (i.e., the electrical time constant is much lower than any mechanical

time constant), the relationship between the motor voltage, its angular speed and the torque produced is given algebraically by:

$$\tau_m = \frac{V k_t}{R_m} - \frac{k_t k_e \omega_m}{R_m} \tag{7.35}$$

where $k_e$is the back-EMF constant of the motor.

The motor torque is increased by the transmission ratio, n_s and then further increased by the drive ratio, $N = {}^{R}/_{r}$ - the ratio of the wheel radius to that of the drive-wheel radius. As described in Section 13, the motor speed is proportional to the differential angular velocity ($\dot{\delta}$) of the outer wheels and the inner frame, and proportionality is:

$$\omega_m = N n_s \delta = N n_s \left(\dot{\varphi} - \dot{\theta}\right)$$

Therefore the coupled torque applied to the outer wheels and inner frame is:

$$\tau = \frac{N n_s}{R_m}\left(V k_t - k_t k_e N n_s \left(\dot{\varphi} - \dot{\theta}\right)\right) \tag{7.36}$$

Augmenting the dynamics derived in 13 by including the electro-dynamic torque of Equation 7.36 produces the transfer function of Equation 7.37 between the input voltage and average wheel speed, $\dot{\varphi}$:

$$\frac{\dot{\varphi}(s)}{V(s)} = \frac{0.0247s^2 + 0.00105s + 0.3101}{s^3 + 0.9903s^2 + 7.124s + 1.977} \tag{7.37}$$

which has a steady-state gain of ${}^{0.3101}/_{1.977} = 0.1569$ rad/s/volt. This is equivalent to a top speed of $24 \times 0.1569 \times 0.72 \times 3.6 = 9.76$ km/hr at 24 Volts. This is quite different from the top-speed predicted simply due to the back-EMF of the motor which predicts a top speed of: $3100\text{rpm} \times 2\pi \times 0.72 \times 3.6/(5.14 \times 7 \times 60) = 23.39$ km/hr . This large discrepancy is caused by the large damping due to the differential motion of the inner frame inside the wheels - principally due to idler friction and is likely to decrease as the system is bedded in.

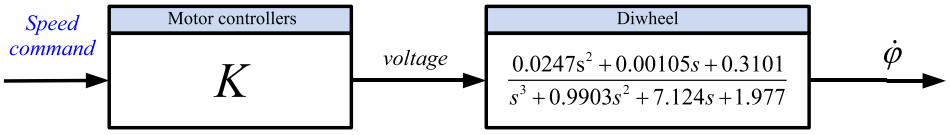

Figure 7.9: Block diagram of open-loop speed control

7.4 Yaw Control

Yaw control is required to manoeuvre the diwheel. Open-loop and closed-loop yaw control provide feasible options for controlling the yaw rate. Each option uses a differential drive system to create a yaw rate. However a closed-loop system uses feedback to minimise the error between the desired yaw rate and actual yaw rate. The yaw rate is determined by the difference in the wheels angular velocities divided by the distance between them

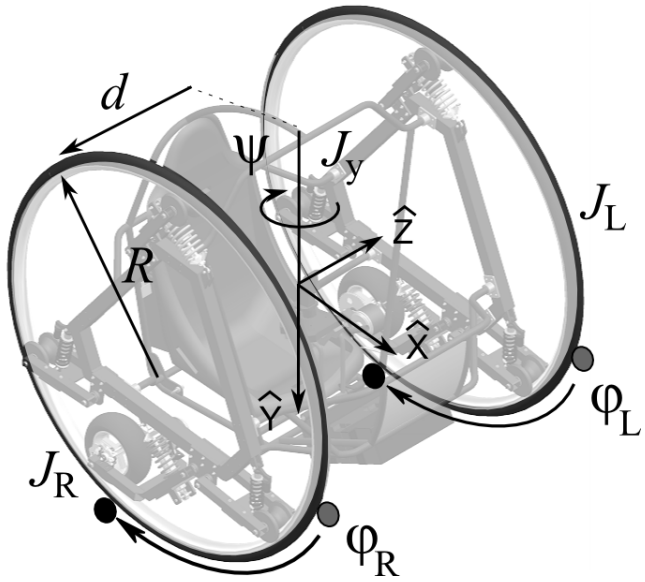

Figure 7.10: Schematic of the diwheel used in yaw dynamics derivation

$$R\frac{\dot{\varphi}_L - \dot{\varphi}_R}{L} \tag{7.38}$$

by providing equal but opposite incremental voltages to each motor, the diwheel's speed remains unaffected. This allows individual control of both the yaw rate and speed.

7.4.1 Derivation of Yaw Dynamics

In order to design a yaw controller an approximate mathematic model of the diwheel's yaw dynamics was developed. The model has been simplified by assuming that inertia about the yaw axis is constant and that the inner frame does not slosh. In fact, if each drive-wheel is driven at the same speed, then no sloshing of the inner frame will occur. The yaw rate (ψ) is achieved by rotating the left and right wheels at $\dot{\varphi}_L$ and $\dot{\varphi}_R$ respectively. This meant that the yaw rate was controlled by the differential velocity supplied to both wheels by the motors. This model was simplified further due to the symmetrical nature of the diwheel about the x, y plane which allowed the two outside wheels to be grouped together. Figure 7.10 shows a schematic used for the derivation.

The following symbols were used in the derivation of the yaw dynamics

- $\varphi_\triangle$ – is the difference in angle between the left and right wheel ($\varphi_R - \varphi_L$)
- V_R – is the voltage applied to the right motor
- V_L – is the voltage applied to the left motor
- $V_\triangle$ – is the difference in voltage applied to each motor ($V_R - V_L$)
- ψ – is the yaw (heading) angle

- $J_W = J_L + J_R$ – is the combined inertia of the wheels about their rotational axis
- B – is a viscous damping term proportional to the differential wheel velocity
- F_w – is the force produced at the ground by the differential velocity of the wheels
- K_y – is a gain which determines how much of the system voltage is reserved for yaw motion

The yaw angular rate is given by

$$\dot{\psi} = \frac{R \times \dot{\varphi}_{\triangle}}{d} \tag{7.39}$$

Differentiating gives

$$\ddot{\psi} = \frac{R \times \ddot{\varphi}_{\triangle}}{d} \tag{7.40}$$

The sum of the moments for the wheel is given by

$$J_W \ddot{\varphi}_{\triangle} - B\dot{\varphi}_{\triangle} - R \times F_w = \tau \tag{7.41}$$

The sum of the moments for the diwheel is given by

$$J_y \ddot{\psi} - d \times F_w = 0 \tag{7.42}$$

Combining Equation 7.41 and 7.42produces

$$J_y \ddot{\psi} - d\frac{J_w \ddot{\varphi}_{\triangle}}{R} + d\frac{B\dot{\varphi}_{\triangle}}{R} = -d\frac{\tau}{R}$$

Substituting Equation 7.40gives

$$\left(J_y - J_w\left(\frac{d}{R}\right)\right)\ddot{\psi} + B\left(\frac{d}{R}\right)\dot{\psi} = -d\frac{\tau}{R} \tag{7.43}$$

The differential torque of the motor is given by combing the torque of both motors

$$\tau = 2N_s N\frac{k_t V_{\triangle} - k_e k_t N_s N\frac{d}{R}\dot{\psi}}{R_m} \tag{7.44}$$

Combining with 7.43 produces

$$\frac{R_m}{2N_s N}\left(\left(\left(\frac{R}{d}\right)J_y - \left(\frac{d}{R}\right)J_w\right)\ddot{\psi} + \left(B\left(\frac{d}{R}\right) + 2k_e k_t N_s^2 N^2\frac{d}{R_m}\right)\dot{\psi}\right) = k_t V_{\triangle} \tag{7.45}$$

Taking the Laplace transform produces

$$\frac{\psi(s)}{V_{\triangle}(s)} = 2\frac{k_t N_s N}{R_m}\frac{1}{\left(\left(\left(\frac{R}{d}\right)J_y - \left(\frac{d}{R}\right)J_w\right)s^2 + \left(B\left(\frac{d}{R}\right) + 2k_e k_t N_s^2 N^2\frac{d}{R_m}\right)s\right)} \tag{7.46}$$

Differentiate to give the yaw rate

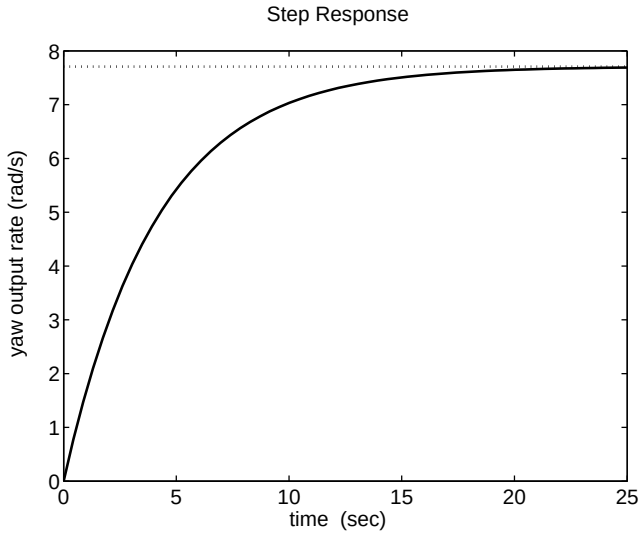

Figure 7.11: Open-loop yaw response for a 14.4V step input

$$\frac{\dot{\psi}(s)}{V_{\triangle}(s)} = 2\frac{k_t N_s N}{R_m} \frac{1}{\left(\left(\left(\frac{R}{d}\right) J_y - \left(\frac{d}{R}\right) J_w\right) s + \left(B\left(\frac{d}{R}\right) + 2k_e k_t N_s^2 N^2 \frac{d}{R_m}\right)\right)} \tag{7.47}$$

Substituting values for the estimate system parameters produces

$$\frac{\dot{\psi}(s)}{V_{\triangle}(s)} = \frac{12}{92.15s + 22.42} \tag{7.48}$$

7.4.2 Open-loop Yaw Step Response

The open-loop dynamics given by Equation 7.48 have a steady state gain of 0.535 rad /s / V. The effective maximum differential voltage is 14.4 Volts which is determined by taking the product of the maximum voltage, K_y (control weighting given to yawing motion) and 2 (because it is a differential system) which gives $36 \times 0.2 \times 2 = 14.4$ Volts. This produces a maximum yaw rate of 7.71 radians per second under no load. However this response has a two percent settling time of 16.1 seconds as shown in Figure 7.11. The two percent settling time is defined as the time it takes for the output to be constantly within a two percent error band of its final value. This result can be improved by using a closed loop system with a compensator.

7.4.3 Closed-loop Yaw Response

A closed loop system is usually only required for high accuracy applications as suggested by Santana et al. (2002). However as yaw control is responsible for improving the safety of the driver reducing the two percent settling time is desirable. This can achieved by using a compensator which utilizes yaw rate feedback.

The yaw rate is first converted into a G-force of the centripetal acceleration by 7.49 where m_3 is the mass of the driver and r_1 is the distance between the driver's head and the center

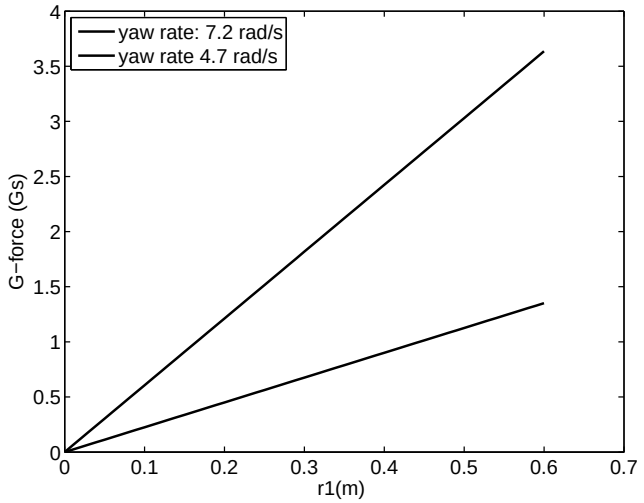

Figure 7.12: Magnitude of G-forces for yaw rates

of the diwheel. Ashcroft (2002, pg. 235) states that if a person experiences a force greater than 3G's they start to temporarily lose vision. This effect is not desirable and in order to reduce the magnitude of centripetal acceleration on the driver the maximum yaw rate must be reduced. Figure 7.12 highlights the G-forces on the driver with the original maximum yaw rate (7.2 radians / s) and the proposed maximum yaw rate (4.7 radians / s). As shown the original yaw rate exceeds 3G's at 0.495m from the center meaning the driver would need to be enclosed in the circle formed by this radius.

In order to eliminate the need to keep the driver in this circle a new maximum yaw rate was selected (4.7 radians /sec). This rate produces a maximum G-force of 1.351G's at 0.6m away which is low enough that the driver does not experience any undesirable effects. Thus in order to produce a 4.7 radians per second response for a 14.4 Volt input a compensator with a proportional component was required.

$$F = \frac{(m_1 + m_2) \times r_1 \times \dot{\psi}^2}{m_3 \times 9.81} \tag{7.49}$$

The compensator selected for yaw control is a PD controller with low pass filter. This compensator reduces the maximum yaw rate and also decreases the settling time. The transfer equation of this compensator is found in Equation 7.50. The closed-loop step response is depicted in Figure 7.13, which highlights a settling time of 6.01 seconds. This closed-loop settling time shows a 10.09 second reduction when compared to than the open-loop settling time.

$$G(s) = \frac{3.807s + 0.9065}{2.4s + 1} \tag{7.50}$$

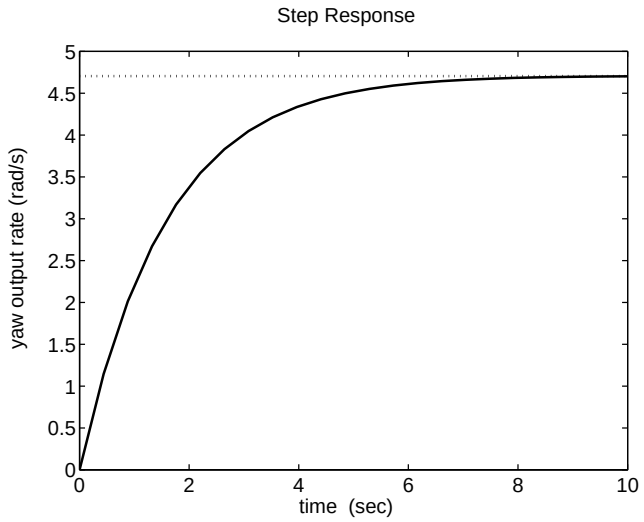

Figure 7.13: Closed-loop yaw response for a 14.4V step input

7.5 Slosh Control

Slosh control forms one of the principle project goals and aims to reduce the large amount of rocking (sloshing) of the inner frame which is an intrinsic property of the diwheel's open-loop dynamics. By limiting the sloshing motion of the inner frame, the driver will be able to experience a much smoother ride. As mentioned in Section 2.3 previous methods of actively controlling slosh have generally employed some form of a Proportional Integral Derivative (PID) control using feedback of some of the states of the system. Examples include the 2DoF slosh rig (Gandhi et al. 2009) and the ball and hoop system (Wellstead and Readman). Proceeding in a similar fashion to these implementations of slosh control, a form of PID controller has been designed for the diwheel.

During operation of the diwheel, the centre of gravity must be displaced by some angle (slosh angle, θ) in order for forward or reverse motion to occur. During harsh acceleration and braking, the inner frame will slosh and oscillate until it reaches a steady state angle. This steady state angle will be non-zero in the case that the diwheel is to be driven at constant non-zero velocity as a reaction torque (supplied by the offset centre of gravity) is required for the diwheel to overcome the external/internal load caused by friction. Because friction dictates that an angular offset is required for translation to occur, it is desirable that the slosh control aims to reduce the slosh angular rate rather than the slosh angle. The aim of slosh control is to improve the settling time of the slosh angular rate, and reduce oscillations of the inner frame about the steady-state slosh angle.

Not all three components of a standard PID controller were included in the slosh controller as some terms were deemed unnecessary. The integral component of a PID controller is used to reduce the steady-state error of the output which, in the diwheel's case, is the slosh angular rate. As the inner frame reaches a steady state angle offset with a constant input voltage, the angular rate will also converge to zero, without the need for integral control. The derivative component aims to reduce overshoot of the output (in this case the angular rate and hence also the slosh angle) and was considered for use in the slosh controller. However utilising

purely proportional control of the angular rate showed reasonable results in simulations of the controllers in SIMULINK and the use of derivative control was dismissed in an attempt to keep the controller as simple as possible.

The use of a purely proportional controller for slosh suppression was also outlined by Wellstead and Readman on their ball and hoop system. The ball and hoop system exhibits dynamics very closely related to those of the diwheel, although there is no translation of the ball and hoop system and the output is a desired hoop angular position rather than a desired hoop angular rate (as is the case in the diwheel). The slosh controller for the ball and hoop system used proportional feedback of the slosh angle rather than the angular rate, which is understandable as the system output is the hoop position where no slosh angle offset will be present at steady state.

To determine appropriate slosh controller gains, a linearised transfer function between the motor voltage, V, and the slosh angular rate, $\dot{\theta}$, was utilised. This transfer function was derived from the linearised matrices about the lower equilibrium position and is given in transfer function form as

$$\frac{\dot{\theta}(s)}{V(s)} = \frac{-0.1249s^2 + 0.0105s}{s^3 + 1.03s^2 + 7.124s + 2.478}. \tag{7.51}$$

The transfer function of Equation 7.51 was loaded into the SISO DESIGN GUI in MATLAB to provide a simple method of altering the controller gains and viewing the step response. The root locus of this transfer function is shown Figure 7.14 where the closed-loop pole locations are denoted by the pink squares. A live updated step response of the transfer function was viewed and the proportional feedback gain was altered until a reasonable step response of the slosh angular rate was achieved. The slosh controller proportional gain was chosen as

$$K_p = 31, \tag{7.52}$$

giving the slosh angular rate step response in Figure 7.15. A comparison of the open-loop step response between the motor voltage and the slosh angle and the closed-loop controlled step response is shown in Figure 7.16. It can be seen that with the slosh controller implemented, the oscillations of both the slosh angle and slosh angular rate have been significantly reduced and the inner frame has reached its steady state position following a trajectory that is much more comfortable for the driver.

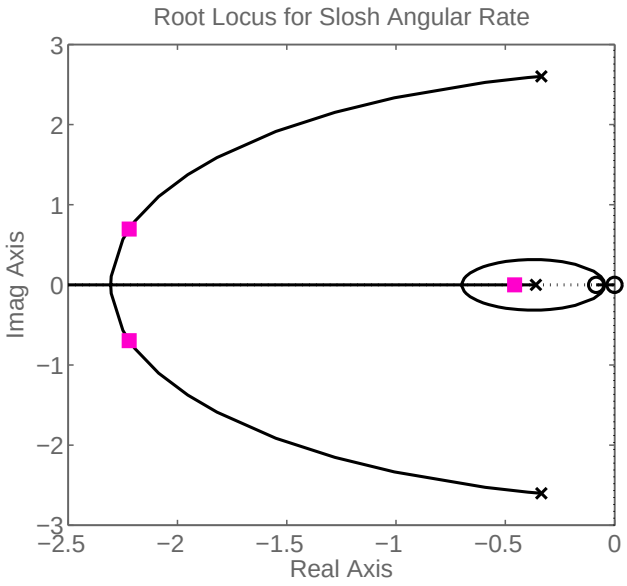

Figure 7.14: Root locus for voltage to slosh angular rate transfer function showing closed-loop pole locations (indicated by pink squares).

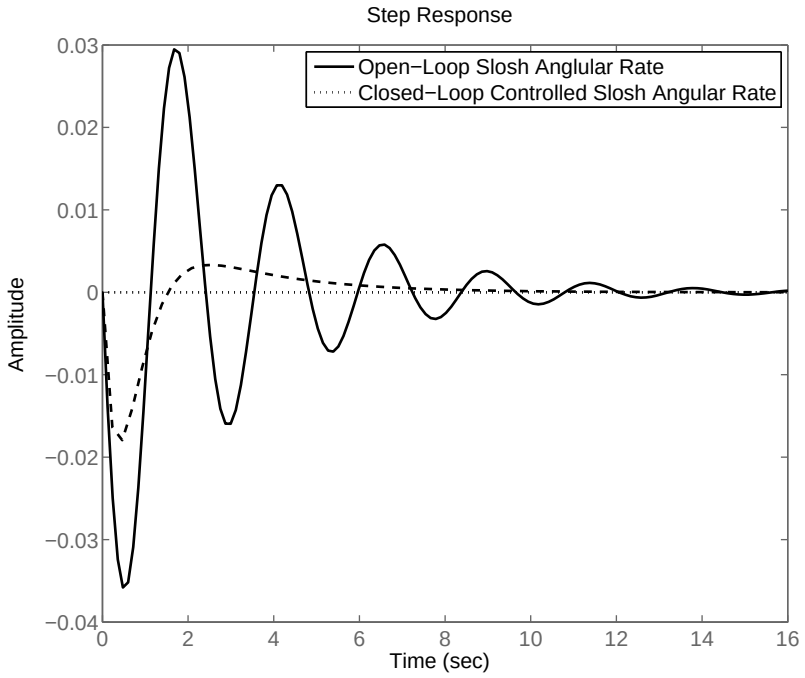

Figure 7.15: Closed-loop step response of open-loop slosh angular rate for voltage input and closed-loop with slosh controller gain $K_p = 31$.

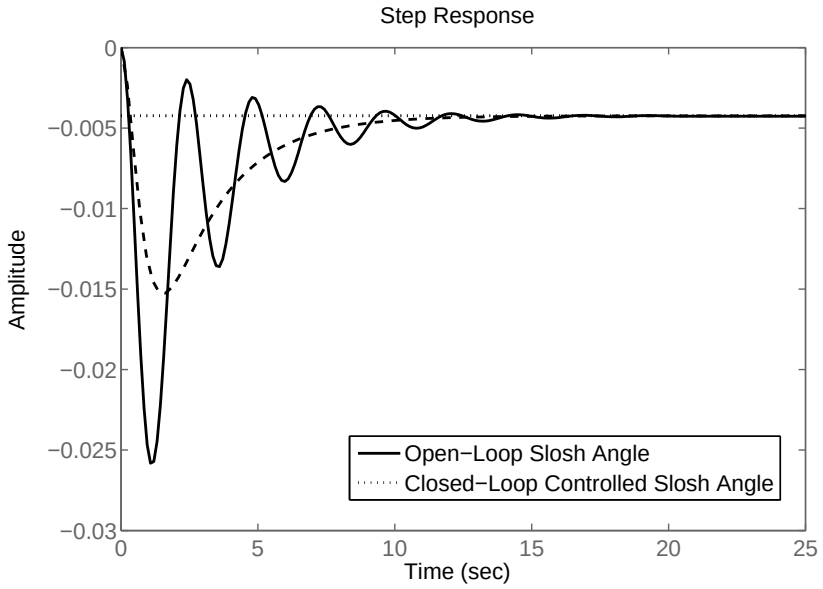

Figure 7.16: Closed-loop step response of open-loop slosh angle for voltage input and closed-loop with slosh controller gain $K_p = 31$

7.6 Inversion Control

The purpose of inversion control is to swing the inner frame upside down, and keep it there. Typical approaches to this task have divided the problem into separate swing-up and balancing controllers. Typically the swing-up controller is used to pump energy into the system so that the energy of the inner frame (or pendulum) is increased to that of the upper equilibrium. Astrom (2000) describe such an energy pumping approach, achieved by differentiation of the Lagrangian of a single pendulum system. A non-linear control law of $u = ng.sign(E - E_0)\,\dot{\theta} cos\,\theta$ was used, which increased the pendulum's energy towards E_0 at the inverted position. While energy-based control laws appear frequently in the literature, they are not always amenable to the problem of swinging up a mechanical system because differentiation of the Lagrangian often produces a complicated control law.

Swing-up can also be achieved using such strategies as *fuzzy control.* Chang et al. (2007) describe fuzzy controllers for both the swing-up and balancing control of a planetary train type inverted pendulum. Their fuzzy swing-up controller consists of pure *bang-bang* control, with only two rules and two membership functions. However, such a fuzzy controller cannot be used on the diwheel because the magnitude of torque applied to the inner frame is decreased due to the gravity spring as the angle of the inner frame increases. A more complicated fuzzy swing-up controller is presented by Muskinja and Tovornik (2006), who have designed a fuzzy-multiswing swing-up controller for a small inverted pendulum on a cart. Their control input consists of a voltage applied to a permanent magnet DC motor, which parallels the control available on Edward. Because of the voltage input, the acceleration of the pivot point is not constant for all motor speeds. Instead, the effective magnitude of acceleration was used to determine their control gains.

Balancing control as applied to inverted pendulum systems has been achieved using the *linear quadratic regulator (LQR)* (Chang et al. 2007; Lauwers et al. 2006; Muskinja and Tovornik 2006) as well as *fuzzy distributed pole assignment* techniques which use fuzzy controllers to perform pole placement (Tao et al. 2008).

This section will present the design of a fuzzy swing-up controller and a LQR balancing controller for use on EDWARD. In further sections a discussion is given as to the ability to perform trajectory tracking when the inner frame is balanced upside down as well as issues with feedback of the entire state vector.

7.6.1 Design of Fuzzy Swing-up Controller

This section describes the design of a fuzzy swing-up controller. The history and detail of the method behind the application of fuzzy control will not be treated in depth. The authors recommend (Jantzen 1998) as a good introduction to the design of fuzzy controllers.

Design of the fuzzy swing-up controller was carried out using MATLAB'S FUZZY LOGIC TOOLBOX. This allowed the controller to be quickly designed and tested with minimum difficulty. The first part of the design required the specification of the membership functions. Because the objective of swinging up the inner frame does not require the diwheel as a whole to restrict its translational motion (to limit φ) this did not feature as an input. This is in contrast to Muskinja and Tovornik (2006), as well as others, who have placed restrictions on this state because of the restricted travel on their platform. Instead, the fuzzy controller uses two of the system's states:

- θ - the position of the inner frame with respect to the gravity vector
- $\dot{\theta}$ - the angular velocity (slosh rate) of the inner frame

to produce a control signal. As discussed in Section 7.6 the membership functions consist of functions which describe how much an input belongs to a number of input categories. If the number of membership functions is large, it is usually possible to produce a fine and relatively exact control signal, but the complexity involved may become increasingly high. Alternatively, the fuzzy controller may be realised with fewer membership functions with a possible loss of performance such as poor robustness.

The input membership functions for θ and $\dot{\theta}$ were designed following the reasoning of Muskinja and Tovornik (2006). More membership functions were used for the angle of the inner frame, than for the angular rate in order to provide finer control to the inner frame angle. A single voltage output membership function was used, consisting of five singleton sets corresponding to $[-36, -18, 0, 18, 36]$.

Standard names used in the design of FUZZY-CONTROLLERS were given to each of the input and output membership functions such as: POSITVE SMALL (PS), NEGATIVE BIG (NB), POSITIVE MEDIUM (PM); and the sign of both inputs followed from the reference frames assigned in Section 13.

The angle input, θ, was divided into six membership functions:

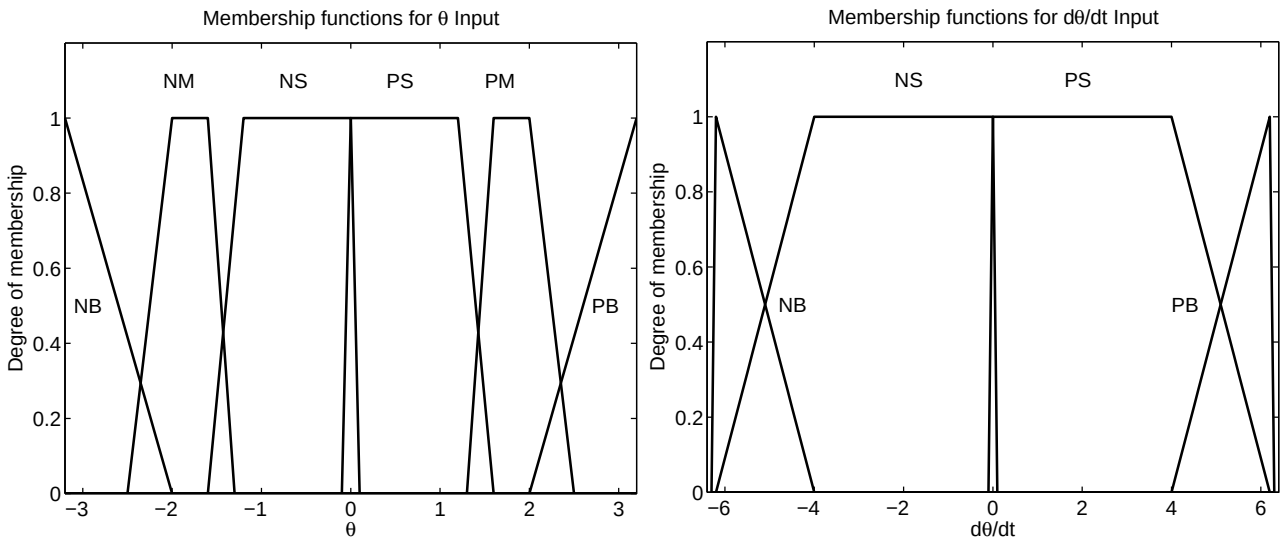

(a) (b)

Figure 7.17: Fuzzy controller Membership functions

- Negative Big (NB)
- Negative Medium (NM)
- Negative Small (NS)
- Positive Small (PS)
- Positive Medium (PM)
- Positive Big (PM)

and consists principally of three types of angle: small, medium and big. Small angles correspond to angles close to the stable equilibrium of the inner frame - the state of the inner frame at rest. Medium angles are close to the 90° positions, and big angles are close to the 180° inverted position. The limits used in Muskinja and Tovornik (2006) were taken as a starting point.

Rules

The Rules used in the fuzzy swing-up controller are given in Table 7.2. All rules follow the format of:

$$\text{If } (\theta = \text{PS}) \text{ AND } (\dot{\theta} = \text{PS}) \text{ then } (V_m = \text{NB})$$

Table 7.2: Fuzzy rules

Rule 1	If (θ = PS) & ($\dot{\theta}$ =PS) then (V_m = NB)
Rule 2	If (θ = NS) & ($\dot{\theta}$ = NS) then (V_m = PB)
Rule 3	If (θ = PS) & ($\dot{\theta}$ = NB) then (V_m = PB)
Rule 4	If (θ = NS) & ($\dot{\theta}$ = PB) then (V_m = NB)
Rule 5	If (θ = PM) & ($\dot{\theta}$ = PB) then (V_m = NB)
Rule 6	If (θ = NM) & ($\dot{\theta}$ = NB) then (V_m = PB)
Rule 7	If (θ = PM) & ($\dot{\theta}$ = PS) then (V_m = NB)
Rule 8	If (θ = NM) & ($\dot{\theta}$ = NS) then (V_m = PB)
Rule 9	If (θ = PM) & ($\dot{\theta}$ = NB) then (V_m = NB)
Rule 10	If (θ = NM) & ($\dot{\theta}$ = PB) then (V_m = PB)
Rule 11	If (θ = PB) then (V_m = PS)
Rule 12	If (θ = NB) then (V_m = NS)
Rule 13	If (θ = PB) & ($\dot{\theta}$ = PB) then (V_m = Z)
Rule 14	If (θ = NB) & ($\dot{\theta}$ = NB) then (V_m = Z)

7.6.2 Balancing Controller

The balancing controller is used to capture the inner frame as it is brought to within 10 degrees of the inverted position. The balancing controller has been designed as a basic full state-feedback regulator. This allows all of the poles of the open-loop system at the inverted position to be moved into the left-hand side of the complex plane. The effect of relocating any of the unstable poles is to provide a stable response to any impulses exerted on the inner frame when it is inverted.

This section will describe the control system used to balance the inner frame upside-down as well as application to the diwheel itself.

Full state-feedback regulator

Figure 7.18 shows the simplest block diagram used for the controller. It consists of a full state-feedback regulator which ensures all closed-loop poles are stable at the inverted position. This means that any sufficiently bounded impulse exerted on the inner frame when inverted will produce a bounded output for all of the system's states. The system model contains the A matrix which determines how the state vector evolves due to the internal dynamics of the system, and the B matrix which determines how the states are affected by the actuators. Because there is only one input to the system, u is a scalar. The control input consists of the motor torque which is applied differentially to the inner frame and outer wheels.

The C matrix maps the system states to outputs measured by sensors.

Linear Quadratic Regulator

The feedback gains for relocating the closed-loop poles have been determined using the linear quadratic regulator (LQR) approach. This approach has been used successfully in the inverted pendulum problem and its many variants (Chang et al. 2007; Lauwers et al. 2006; Muskinja and

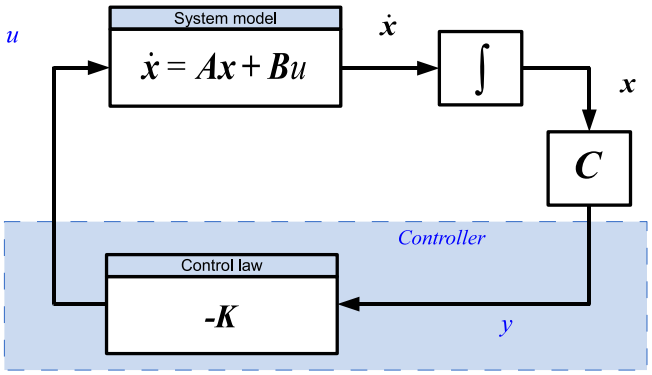

Figure 7.18: Basic State-feedback regulator

Tovornik 2006). Determination of the required feedback gains, K, requires the minimisation of a *performance index* or *cost function:*

$$J = \int_0^\infty \left(\mathbf{x}^\mathbf{T}(\tau)\mathbf{Q}\mathbf{x}(\tau) + \mathbf{u}^\mathbf{T}(\tau)\mathbf{R}\mathbf{u}(\tau) \right) d\tau \tag{7.53}$$

Such a solution for the matrices, Q and R is termed *optimal*. The matrices Q and R were determined using Bryson's rule, which suggests diagonal matrices such that

$$\begin{aligned} Q_{ii} &= 1/(\text{max acceptable value of} [x_i]^2) \\ R_{ii} &= 1/(\text{max acceptable value of} [u_i]^2) \end{aligned}$$

The states θ, and $\dot{\theta} - \dot{\varphi}$ as well as the control input were restricted to 15 degrees, 2100RPM and 36 volts, respectively:

$$\mathbf{Q} = \begin{bmatrix} q_1 & 0 & 0 & 0 \\ 0 & 0 & 0 & 0 \\ 0 & 0 & q_2 & -q_2 \\ 0 & 0 & -q_2 & q_2 \end{bmatrix} = \begin{bmatrix} 15 & 0 & 0 & 0 \\ 0 & 0 & 0 & 0 \\ 0 & 0 & \frac{1}{220^2} & -\frac{1}{220^2} \\ 0 & 0 & -\frac{1}{220^2} & \frac{1}{220^2} \end{bmatrix} \tag{7.54}$$

and the effort penalty was

$$R_1 = \left(\frac{1}{36} \right)^2 \tag{7.55}$$

with cost function:

$$J = \int_0^\infty \left(q_1\theta^2 + q_2 \left(\dot{\theta} - \dot{\varphi} \right)^2 + R_1 V_m^2 \right) dt \tag{7.56}$$

Solving the continuous algebraic Riccati equation returns the optimal control gains

$$\mathbf{k} = [\ -190 \quad 0 \quad -45 \quad -13\ ]. \tag{7.57}$$

It is important to note that the stabilisation of the inner frame in the inverted position does not require a measurement for φ, which is important if this state is not measured.

7.6.3 Combining the Swing-up and Balancing Controller

The SIMULINK block diagram of the combined swing-up and balancing controller is shown in Figure 7.19. If the *Control Mode* is set to 3, the second multiport switch feeds the third input through to the *Control Voltage* output. The system states (2DoF) are fed into a *Fuzzy Logic Controller* as well as a block which determines if θ is within 10 degrees of the inverted position. If θ is less than ± 10 degrees, the first multiport switch feeds the second input through to the second multiport switch, which consists of the balancing control gains multiplied by the states, $K * u$. If θ is not within 10 degrees of the inverted position, the *Fuzzy Logic Controller* determines the control output in accordance with the membership functions and rules described in Section 7.6.1. The modular arithmetic and bias functions given in Figure 7.19 are required because the normal definition of $\theta = 0$ is at the stable equilibrium, and not the inverted position. Without performing this modular arithmetic, the fuzzy controller would see a discontinuity in θ around $-\pi, \pi$. The modular arithmetic shifts the θ zero datum for the fuzzy controller to the inverted position.

Figure 7.20 shows the performance of the fuzzy swing-up and balancing controller simulated in SIMULINK using an estimate of system parameters. As can be seen, the swing-up controller swings the inner frame upside down in around 14 seconds, at which point the balancing controller captures the inner frame and stabilises it.

7.6.4 Controllability and Observability of the Linearised System

Because there is only one input into the 2DoF - the differential motor torque, it is important to determine the controllability of the system's states. Controllability refers to the ability of the control inputs to bring the system to any desired state in finite time. It is determined by calculating:

$$\mathbf{C_o} = \begin{bmatrix} \mathbf{B} & \mathbf{AB} & \mathbf{A^2B} & ... & \mathbf{A^{n-1}B} \end{bmatrix} \tag{7.58}$$

where, the $\mathbf{A}$ and $\mathbf{B}$ matrices are the linearised state matrices given in Section 13. If $\mathbf{C_o}$ has full rank, then the system is completely controllable. For both the inverted and stable linearised systems, the controllability matrix has full rank, and the two linearised systems are *controllable*. This means that, using only the combined motor voltage input, all system states can be transferred to a desired final state in a finite time (however this time may be long due to damping).

Observability refers to the ability to estimate the states which are not directly measured by the sensors. The minimum number of sensors to be used on the diwheel are the gyrosensor and accelerometer. Using only these two sensors, the output matrix $\mathbf{C}$ becomes:

$$\mathbf{C} = \begin{bmatrix} 1 & 0 & 0 & 0 \\ 0 & 0 & 1 & 0 \end{bmatrix} \tag{7.59}$$

calculating the Observability matrix:

$$\mathbf{O_b} = \begin{bmatrix} \mathbf{C} & \mathbf{CA} & \mathbf{A^2} & ... & \mathbf{CA^{n-1}} \end{bmatrix}^T \tag{7.60}$$

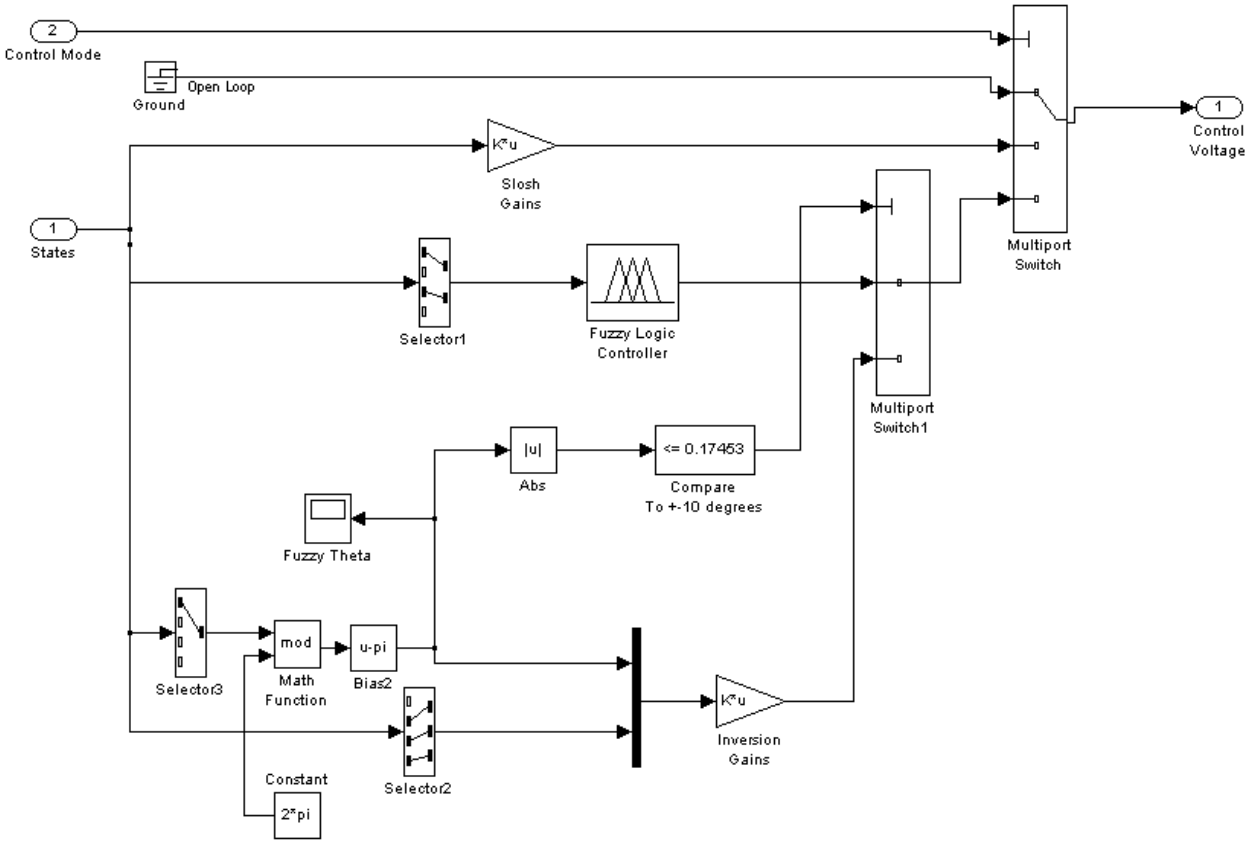

Figure 7.19: Fuzzy swing-up with Balancing Controller SIMULINK Model

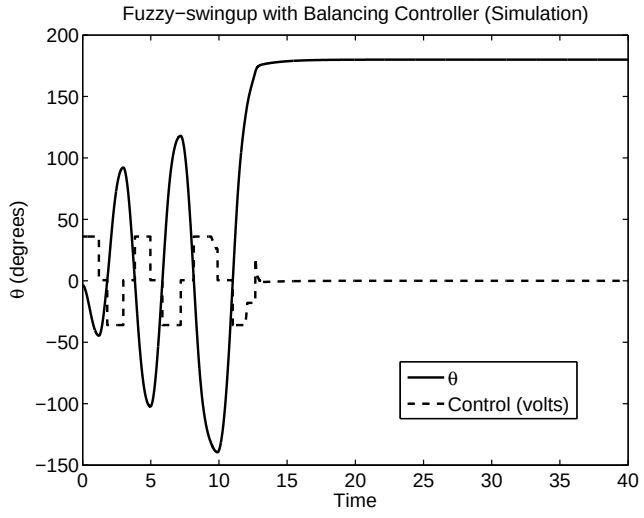

Figure 7.20: Simulation of the Fuzzy swing-up and LQR Balancing Controller

gives:

$$\mathbf{O_b} = \begin{bmatrix} 1 & 0 & 0 & 0 \\ 0 & 0 & 1 & 0 \\ 0 & 0 & 1 & 0 \\ 0 & 0 & -1.0851 & 1.1763 \\ ... & 0 & ... & .. \end{bmatrix} \tag{7.61}$$

although the entire observability matrix is not given in Equation 7.61, the point to note is that the second column is zero. This means that the second state, φ, is unobservable and cannot be estimated purely based on the gyrosensor and accelerometer measurements (i.e., $\dot{\theta}$ and θ, respectively). However, because the balancing controller does not require φ, this is not a big issue and an observer could be designed for the system which determines $\dot{\varphi}$ based on the two sensor measurements. Such an observer has not been designed at this stage, but would be a valuable future addition to the system, especially if measuring the drive-wheel / motor speed was problematic.

8 Software Design

This chapter describes the software as implemented on the Dragon12-Plus processor including the design methodology, inputs and outputs required by the system, and techniques used to process sensor data. Finally, a number of useful non-project specific additions are described which improve the system's flexibility.

While techniques of software implementation using a Real-Time Target or use of a DSpace controller have been used successfully in past projects for implementation of control on a microprocessor, it was decided early in the project that all software development would be done in C or assembly, programming the microprocessor directly. The reason for this was chiefly in the added control over the compilation process. The Real-Time Target, a Matlab toolbox written by Dr Frank Wornle (formerly of the University of Adelaide), which converts a Simulink model directly into runnable C-code has been used in the past by Clark et al. (2005); Baker et al. (2005), to implement control on the HCS12 microcontroller found on the Dragon12-Plus. They report several issues with the conversion of Simulink models to runnable code, especially those arising from the order of block compilation. For this reason a complete system coded purely in C has been created.

The software for the platform has been coded in Freescale's Code Warrior IDE, using as a basis, the Learning By Example (LBE) stationery (Haskell and Hanna 2009). The LBE stationery contains a number of functions useful to quickly activate and use many of the peripherals onboard the Dragonboard especially the LCD, which has been heavily used for debugging and eventually as a basis for user feedback in the form of a menu system.

8.1 Overview of Software and Design Methodology

The software used in the project has employed modular design. Functions, variables and definitions are collected into a C source and header file with a name which describes their function in the system. In many cases a number of these file pairs can be grouped together to form independent tasks required by the software. The following briefly describes these groups.

Sensor

Consists of adc (.c and .h), gyro and accel files. These files are used to sample the sensors connected to the Analog-to-digital converters on the board. The gyro and accel files are currently used to scale the raw sensor data for use in the control system.

Data Logging and Processing

Consists of SDCARD, ANGLE, SCItoMatlab, and FRTYPE. SDCARD provides functions for writing and reading to the SD-card while SCItoMatlab has been used predominantly for periodic data logging (using a Real-Time-Interrupt). ANGLE contains code to implement the Kalman Filter described in Section 8.5.1 and FRTYPE contains code to implement a fractional, fixed point data type as well as a number of other useful macros.

Control

- steeringControl
  - Implements open-loop speed and steering control and contains unimplemented code for closed-loop steering control.
- PID
  - This file contains a number of control structures for use in future. Unfortunately, due to time constraints, these structures could not be used to their full potential and the control implementation remains to be streamlined in future.

8.2 Input and Output data

This section briefly describes the connections required for inputs and outputs on the system:

Joystick

The joystick consists of two separate input systems: the axis potentiometers (X, Y) and the inputs which are connected to a circuit within the joystick that determines which button is pressed. The X-axis (red) and Y-axis (yellow) are connected to PAD02 and PAD03, respectively. The following list presents the connection of the remaining joystick wires.

- Purple - PH0
- Orange - PH1
- Brown - PH4
- White - PH5
- Blue - PH6
- Yellow - PH7

The joystick axis data is read from an ADC, while the buttons states are read from a function called *readJoystickButton.*

Brake Depressed

This circuit connects to PH3 and brings the pin high when the brake lever is pulled.

Motor Controller Outputs

At this stage the ROBOTEQ motor controllers are controlled by two PWM outputs connected to PP3 (grey wire) and PP7 (purple wire).

8.3 Steering and Motor Control

Steering and speed control is currently achieved through open-loop control using the joystick. A flowchart of the function that implements this control is shown in Figure 8.1. This function is called at 50Hz by a timer interrupt.

8.4 Measuring Motor Speed

The speed of each motor is measured by the encoders as discussed in Section 5.7. The speed is calculated using a constant time elapsed method from Li et al. (2005). This method utilizes multiple registers from the Enhanced Capture Timer including the Pulse Accumulators A (PT7) and B (PT0) one for each encoder, PT6 and PT1 as an input capture of the second pulse train of each encoder and timer 4 as an output compare timer, providing sampling instances. Each pulse counter is sampled in succession commencing simultaneously with the timer on the falling edge of the pulse train. After a specified time has elapsed (Tel, timer 4) the code awaits the falling edge. Upon the next falling edge the time elapsed and pulse count are recorded and the other pulse train (PT6 or PT1) digital value for the same encoder is sensed. A value of zero indicates the motor is rotating clockwise and a value of one indicates it is rotating anticlockwise. These values are used to estimate the speed of the motor. This process is repeated for each encoder in succession as shown in Figure 8.2.

This method worked effectively for most frequencies however an adaptive sampling interval should be implemented to gain better results for all speeds of the motor. This method adjusts the sampling period (Tel) to match the last pulse count (Lygouras 2000) and can improve the accuracy of the speed estimates. Because the constant time elapsed method uses interrupts these interrupts should be given a lower priority to the other interrupts which run the control loops.

8.5 Measuring Inner Frame Angle and Slosh Rate

This section describes the integration of sensors to measure the inner frame's angle with respect to the gravity vector, and its angular velocity (slosh rate). These measurements are required for the slosh and inversion control systems. Two sensors are located on EDWARD to provide measurements of these two states (θ, $\dot{\theta}$), a two-axis accelerometer and a single-axis gyrosensor (Figure 8.3).

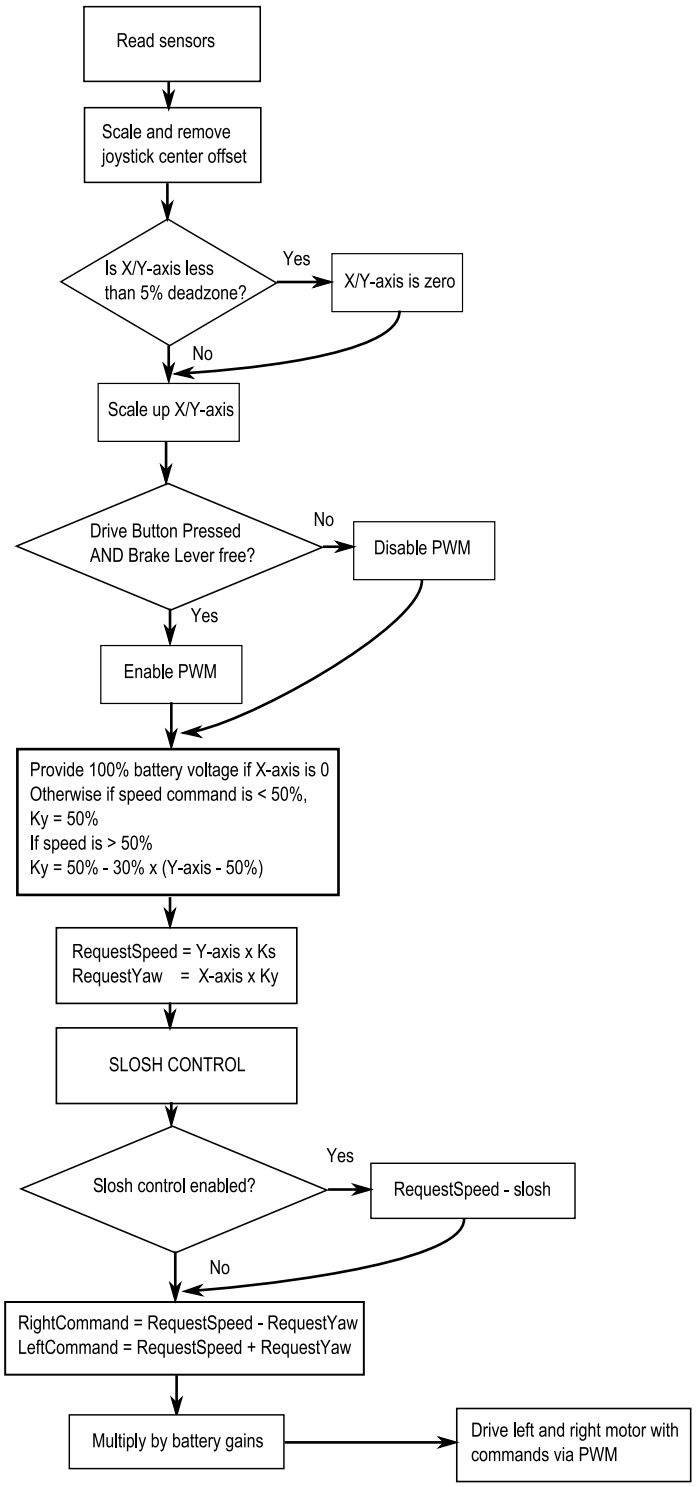

Figure 8.1: Flowchart of the steering function used to drive the diwheel with open-loop control

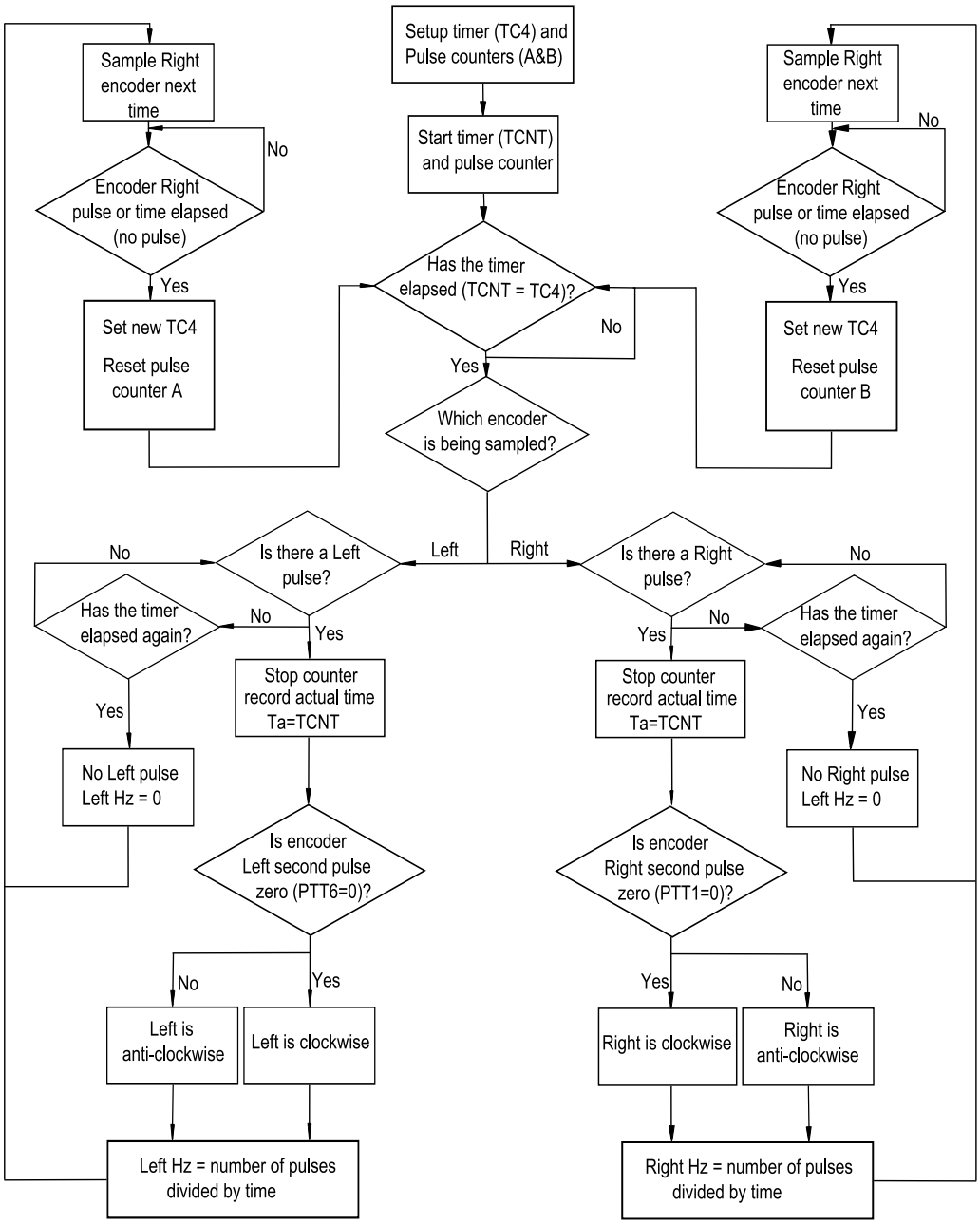

Figure 8.2: Flowchart of the algorithm used to measure encoder speed

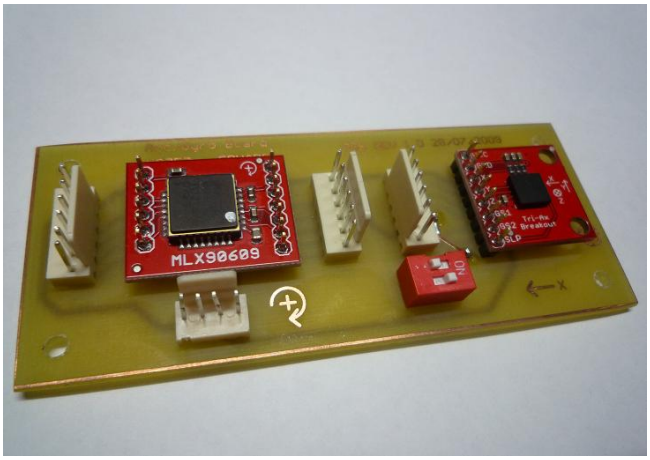

Figure 8.3: Sensor board combining a gyrosensor and two-axis accelerometer

The accelerometer measures the projection of the gravity vector onto its two axes, as shown in Figure 8.4. As the inner frame rotates with respect to the gravity vector, a larger reading will be measured on either the x-axis or y-axis of the accelerometer. The angle estimate of the inner frame is then given by:

$$\theta^{accel} = atan\left(\frac{accelerometer\, y}{accelerometer\, x}\right) \tag{8.1}$$

While the arctangent function can correctly estimate the inner frame angle based on the projection of gravity onto each axis, it suffers increased noise when the magnitude of the readings on either axis becomes small (i.e., near 0° and 90°). For this reason, the accelerometer should be orientated at 45° at the neutral position (lower equilibrium) if possible. Unfortunately, the accelerometer estimate for θ is affected by noise since the accelerometer cannot distinguish between the static acceleration of the gravity and dynamic acceleration of the inner frame. The fidelity of the angle estimate given by the accelerometer is highest at *low-frequencies* (especially at dc), but becomes useless at high frequencies (Guerra 2008). For this reason, a gyrosensor can be used to provide a better estimate of the inner frame angle at higher-frequencies. The gyrosensor outputs a reading proportional to the angular rate of the inner frame, which may be integrated to estimate θ:

$$\theta^{gyro} = \int_{T_1}^{T_2} (gyrosensor)\, dt \tag{8.2}$$

The issue with the gyrosensor, however, is that it has a non-zero bias error, which generally increases with temperature. When this bias is integrated for low frequency changes in $\dot{\theta}$, the estimate for θ eventually increases in error until it becomes useless. However, a gyrosensor can perform well for high frequency changes in $\dot{\theta}$, especially if the bias error can be estimated and corrected for.

By combining the two sensors together, good performance at low frequencies (utilising the accelerometer) and high frequencies (using the gyrosensor) can be achieved. Several methods can be used to achieve this *sensor-fusion*:

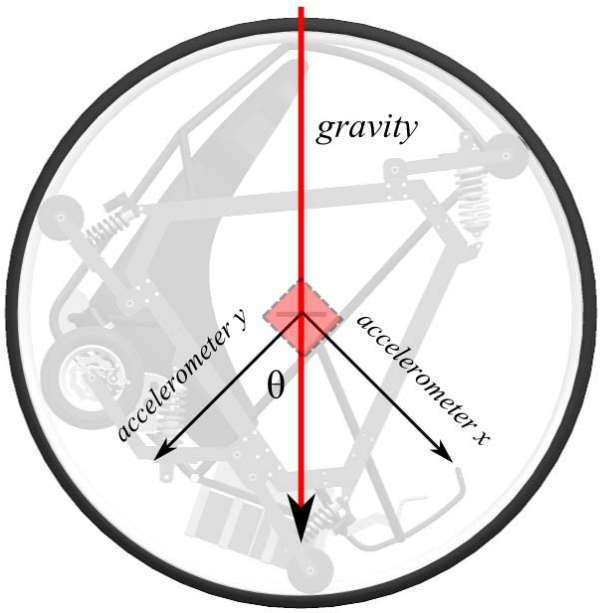

Figure 8.4: Use of the two-axis accelerometer to measure pitch

- Complementary Filter:
  - Combines the accelerometer estimate and gyrosensor (integrated) estimate through low-pass and high-pass filters, respectively.
  - Generally slower than other techniques
  - Cannot track gyrosensor bias
  - Simple implementation
- Kalman Filter
  - Produces an optimal estimate of the states which minimises the process noise and sensor covariances
  - Can track gyrosensor bias
  - Only considers linear systems
- Extended Kalman Filter
  - Similar to the Kalman Filter, but extended to non-linear time-varying state matrices
  - Complicated

The alternative to combining the two sensors together is to use an *Inertial Measurement Unit* (IMU) which contains gyrosensors and accelerometers and sensor processing within a convenient package. However, IMUs are very expensive devices, and a more affordable solution is desirable.

8.5.1 Sensor Fusion using a Kalman Filter

The gyrosensor and accelerometer have been fused using a simple Kalman Filter which estimates the inner frame angle and gyrosensor bias. The two inputs to the Kalman Filter (KF) consist of the biased gyrosensor reading, $\dot{\theta}^{gyro}$ and the angle estimate given by the accelerometer, θ^{accel}. The state equations used to describe the sensor states are given by:

$$\mathbf{x_{i+1}} = \mathbf{A}\mathbf{x_i} + \mathbf{B}u \tag{8.3}$$

$$\begin{bmatrix} \theta_k \\ \dot{\delta}_k \end{bmatrix} = \begin{bmatrix} 1 & -dt \\ 0 & 1 \end{bmatrix} \begin{bmatrix} \theta_{k-1} \\ \dot{\delta}_{k-1} \end{bmatrix} + \begin{bmatrix} dt \\ 0 \end{bmatrix} \dot{\theta}^{gyro}_{k-1} + w_{k-1} \tag{8.4}$$

and:

$$\mathbf{y_{i+1}} = \mathbf{C}\mathbf{x_i} \tag{8.5}$$

$$\theta^{accel}_k = \begin{bmatrix} 1 & 0 \end{bmatrix} \begin{bmatrix} \theta_k \\ \dot{\delta}_k \end{bmatrix} + v_k \tag{8.6}$$

where dt is the time between gyrosensor readings, w_{k-1} is the process noise and v_k is the noise of the accelerometer measurements (in radians). As shown in Equation 8.4, the model of the states consists of the inner frame angle θ_k and gyrosensor bias, $\dot{\delta}_k$. The first step of the Kalman filter consists of the *Prediction step* which estimates the change in states determined by the state matrix, and the change in the covariance matrix:

$$\mathbf{z}_k = \begin{bmatrix} \theta^-_k \\ \dot{\delta}^-_k \end{bmatrix} = \begin{bmatrix} 1 & -dt \\ 0 & 1 \end{bmatrix} \begin{bmatrix} \theta_{k-1} \\ \dot{\delta}_{k-1} \end{bmatrix} + \begin{bmatrix} dt \\ 0 \end{bmatrix} \dot{\theta}^{gyro}_{k-1} \tag{8.7}$$

$$\mathbf{P}^-_k = \begin{bmatrix} 1 & -dt \\ 0 & 1 \end{bmatrix} \mathbf{P}_{k-1} \begin{bmatrix} 1 & 0 \\ -dt & 1 \end{bmatrix} + \mathbf{Q} \tag{8.8}$$

where $\mathbf{P_{k-1}}$ is the covariance matrix, which measures how well the sensors or model are estimating the states, and $\mathbf{Q}$ is the process noise covariance matrix, which measures the covariance of the states due to modelling uncertainties.

Measure and update The measure and update step calculates the *Optimal Kalman gain* which minimises the process and measurement covariances, providing a optimal estimate of the system's states. The result of this step is an optimal estimate for the inner frame angle θ_k and the gyrosensor bias, $\dot{\delta}_k$.

$$\mathbf{K}_k = \mathbf{P}^-_k \begin{bmatrix} 1 \\ 0 \end{bmatrix} \left(\begin{bmatrix} 1 & 0 \end{bmatrix} \mathbf{P}^-_k \begin{bmatrix} 1 \\ 0 \end{bmatrix} + \mathbf{R} \right)^{-1} \tag{8.9}$$

$$\begin{bmatrix} \theta_k \\ \dot{\delta}_k \end{bmatrix} = \begin{bmatrix} \theta^-_k \\ \dot{\delta}^-_k \end{bmatrix} \mathbf{K}_k \left(\theta^{accel}_k - \begin{bmatrix} 1 & 0 \end{bmatrix} \begin{bmatrix} \theta^-_k \\ \dot{\delta}^-_k \end{bmatrix} \right) \tag{8.10}$$

$$\mathbf{P}_k = \left(\mathbf{I} - \mathbf{K}_k \begin{bmatrix} 1 & 0 \end{bmatrix} \right) \mathbf{P}^-_k \tag{8.11}$$

8.5.2 Performance of the Kalman Filter

The process noise covariance matrix, $\mathbf{Q}$ is a measure of the variance of the two states with respect to errors and uncertainties in the state model. It is generally difficult to select appropriate values for the elements of $\mathbf{Q}$, especially if the states are not independent. For application on the diwheel, the $\mathbf{Q}$ matrix was tuned to the following, with the assumption that the two states were independent:

$$\mathbf{Q} = \begin{bmatrix} var(\theta_k) & 0 \\ 0 & var(\dot{\delta}_k) \end{bmatrix} = \begin{bmatrix} 0.03 & 0 \\ 0 & 0.08 \end{bmatrix} \tag{8.12}$$

it was noted during testing that increasing the magnitude of the diagonal terms of $\mathbf{Q}$ made the Kalman Filter trust the accelerometer measurement more than the gyro and noise susceptibility was increased, although the response of the filter was good. Making the magnitude of the diagonal terms of $\mathbf{Q}$ smaller (but keeping their ratio the same) allowed the filter to smooth noise in the accelerometer estimate of the angle (using the atan function), though small steady-state errors between the filter estimate of θ and the accelerometer estimate were noted, especially when the angle was changed rapidly. Therefore smaller terms in $\mathbf{Q}$ tend to make the Kalman Filter less capable of tracking fast changes in θ. The $\mathbf{R}$ matrix, which is simply the measurement noise of the accelerometer was set at 0.9 rad.

The main issue with the filter implementation, is that the $\mathbf{Q}$ and $\mathbf{R}$ matrices are hard to choose realistically, especially from a quantitative perspective. In future a thorough analysis of these parameters should be taken to ensure the filter performance is a robust as possible.

A MATLAB script was written to receive data from the processor, which consisted of the arctangent of the accelerometer axes readings and the Kalman Filter estimate of the angle of the sensor board, both of which were calculated in floating point format. The MATLAB script was also paired with an artificial horizon which provided visual feedback of the sensor board angle. Figure 8.5 shows the performance of two Kalman Filters, one implemented on the processor (green) and the other implemented in MATLAB (blue). These plots were produced by rotating the board and shaking it at 10 and 13 seconds. The red plot is the estimate of θ using the arctangent of the two accelerometer readings. As can be seen, several portions of the accelerometer estimate are noisy, corresponding to vibration of the sensor board at those times. The green and blue plots show reduced noise (better estimate), which is the principle aim of the Kalman Filter. As the accelerometer measurement becomes noisy, the filter automatically prefers data from the gyrosensor. Between 15 and 17 seconds the board was rotated towards 180 degrees. Because the two-argument arctangent function (atan2) has a range of $[-\pi, \pi]$, the angle returned by the function is discontinuous at $-\pi, \pi$. For this reason, the filter should not be used close to this region of the function or the zero-datum should be adjusted by using modular arithmetic or physically orientating the sensor board differently.

8.5.3 Arctangent Function

The implementation of the two argument arctangent function on a microcontroller can be achieved in a variety of ways, but it is generally undesirable to rely on compiled libraries, since they dramatically increase code-size, are slow (though accurate, as they generally use a power

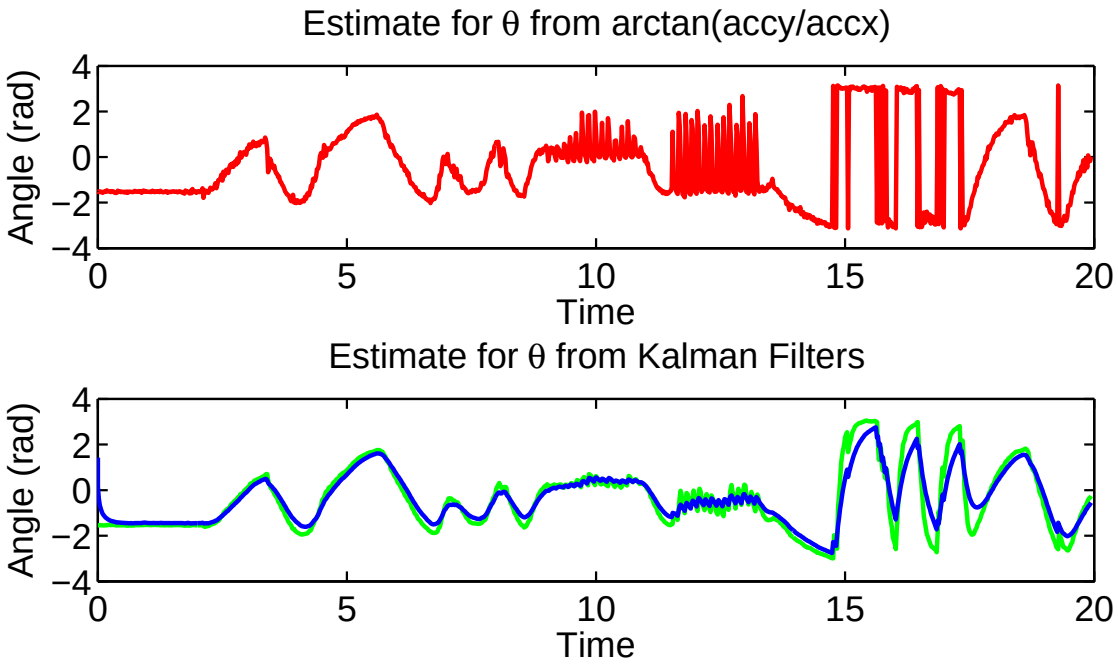

Figure 8.5: Performance of the Kalman Filter. Top: Estimates for θ using accelerometer. Bottom, green: Implementation on the Dragonboard. Bottom, blue: Kalman Filter in MATLAB

series method) and cannot be altered by the user. For this reason a two argument arctangent (atan2) function was created for use on the dragonboard. The implementation adapts the method presented in (Lyons 2005, pp. 547-549) which divides the unit circle into octants, and uses an approximation of *atan2* for $0 - 45°$ with a maximum error of 0.26°. Two such atan2 functions were implemented in code, a fixed point version and floating point version. The functions can be found in *angle.h*

8.6 Implemention of the Control Systems

Although time constraints have restricted the implementation of all the controllers described in Chapter 7, a basic proportional feedback controller was implemented to provide slosh control. The idea was to simply feed back a control gain proportional to the slosh angular rate using negative feedback. By changing the sign of the gain (and increasing its magnitude) an effective swing-up controller was produced which relied on making the closed loop poles of the system unstable. The results of both of these controller are discussed in Chapter .

8.6.1 Slosh Control

The form of slosh control implemented to date is the simplest. The pseudocode required for this control is:

$$K_{sloshgain} = -31.0 \tag{8.13}$$
$$slosh = \frac{gyro \times K_{sloshgain}}{36} \tag{8.14}$$
$$sloshcommand = slosh \times K_s \tag{8.15}$$

8.6.2 Swing-up Control

By simply altering the sign of Equation (8.13), the system becomes unstable and automatically swings the inner frame upside down.

8.7 Additional Functions

A number of additional functions have been implemented on the Dragonboard. They include:

- A basic button driven menu system
- Functions to use the SD-card circuits provided on the board

8.7.1 Using the SD card

Because of the delays faced during the project, the implementation of a flexible data logging method on the microprocessor has not been fully completed. However, functions for reading and writing to the SD-card were implemented and successfully tested. The SD-card is used to provide the system with an almost unlimited amount of non-volatile storage, though typically 1GB is all that is envisaged at this stage, because higher capacity cards have not been tested.

The SD card protocol comes in two varieties, however only one is ever used without proper licensing. Such a protocol is standard SPI. The Dragonboard provides SD card interface circuits which connect to PM2, PM3 and PM4 providing *Write Enable, Card Detect* and *Chip Select* input/outputs. The card is written to and read from using the SPI on Port S, using pins 4, 5 and 6. The process of reading and writing to the card is as follows:

- Ensure a card is inserted (check that PM3 is low)
- Initialise the card by running SD_init(), and ensuring it returns 0
- For writing, populate the global array, *buffer* with data
  - Call SD_writeSingleBlock(x), where x is the number of the 512 block of data to be written to
- For reading, call SD_readSingleBlock(x), where x is the number of the 512 block to be read
  - The data read is stored in the global array, *buffer*

The code used to interface with the SD-card via the SPI protocol was modified from code available at

www.dharmanitech.com

9 Experimental Results and System Integration

The following chapter displays and discusses the experimental results derived from testing the control systems implemented on the physical diwheel. This chapter also contains descriptions of solutions to problems encountered in the integration of EDWARD's electrical, software and hardware systems.

9.1 System parameter identification

To provide an accurate mathematical model of the diwheel, several parameters incorporated in the dynamics of the diwheel needed to be determined. Many of these parameters were determined from the 3D CAD model of the diwheel after care was taken to ensure material properties of components were accurately applied in the model. These parameters included, the mass and centre of gravity of each body of interest, along with the moments of inertia of each body about the rotational axes (slosh and yaw axes). Parameters that were unable to be found from the CAD model were the damping terms associated with the rolling friction between the inner frame and the outer wheels, and the rolling friction between the outer wheels and the ground.

The damping terms were determined through physical testing by recording live data and using an oscillation decay method. To determine the damping term associated with the sloshing of the inner frame, b_{12}, the following method was applied.

1. The diwheel was set up with no power and seating a driver.
2. The inner frame was rotated by some arbitrary angle and held (by another group member).
3. A video camera was started to record the sloshing behaviour.
4. The inner frame was released and allowed to slosh down to the lower equilibrium position.
5. Recording was ended and the footage sent to a computer.
6. The initial angular offset was determined by measuring the angle between the centre of the top idler wheel and the vertical at the moment before release of the inner frame as shown in Figure 9.1a.
7. The footage was then run until the inner frame reached the peak of its oscillation about the equilibrium position. The new angle between the same idler and the vertical was measured and recorded as shown in Figure 9.1b. The time of this peak was also recorded.

8. Step 7 was repeated for each subsequent peak until the diwheel returned to its lower equilibrium position.

9. The zero position angle was also recorded.

10. The logarithmic decrement, δ, was determined using

$$\delta = \frac{1}{n} \ln \left(\frac{x_i}{x_{i+n}} \right) \; n = 1, 2, ...$$

where n is the number of peaks being measured across (angles must be on the same side of the equilibrium level), and x_i is the amplitude of the peak.

11. The damping ratio ζ, was then found using

$$\zeta = \frac{\delta}{\sqrt{4\pi^2 + \delta^2}}.$$

12. The average period, T, between peaks was found using the recorded times and was used to find the natural frequency, ω_n by

$$\omega_n = \frac{2\pi}{T}.$$

13. The corresponding damping term in the mathematical model presented in Section was then tuned until the dynamics revealed poles exhibiting this damping ratio and natural frequency.

To measure the damping term associated with the rolling friction between the outer wheels and the ground, clamps were added on either side of the idlers, effectively locking the inner frame to the outer wheels. The testing process was conducted in the same manner to determine the second damping term.

The system parameters used in the mathematical model are given in Chapter 7 and simulations have showed close matching of the sloshing behaviour between the model and physical system. This suggests that system parameter identification methods have produced adequate results.

9.2 System Tests

To measure the success of the implementation of control on the physical system, a test method was required to provide quantitative results of the diwheel's behaviour with, and without control. These tests were used to measure the level of accomplishment of the goals related to the implementation of control in the project. In order to further verify the mathematical model used to simulate the diwheel's sloshing behaviour, a number of tests were performed. Data for $\dot{\theta}$ from the gyrosensor was recorded at approximately 50Hz for 10 seconds, producing 500 data points. After the data had been recorded it was sent to MATLAB using a function accessible from the menu on the Dragonboard. Though functional, this method of logging is not particularly convenient and in future, the system could be setup to log all data to the SD-card in the desired format, and send or transfer it to a computer in one go. Both open-loop and closed-loop testing was performed to give an indication of the suitability of slosh control on the platform.

(a) (b)

Figure 9.1: Damping tests

9.2.1 Open-loop slosh

The first slosh control test was an open-loop step response, applying approximately 24V to both motors for 10 seconds with a 60kg driver. Figure 9.2 shows the response for θ and $\dot{\theta}$. Because the accelerometer was damaged at this stage, the estimate for the inner frame angle has been calculated using numerical integration of the slosh angular rate, $\dot{\theta}$. The bias of the slosh angular rate was noted as -0.3326 rad/s, and was accounted for before the integration was performed. Although the bias of the gyrosensor will increase with time, this constant approximation is justified as the bias increases slowly over time. Unfortunately during testing, data logging of the control signal was overlooked, and has not been recorded. However, the driver of the diwheel attempted to maintain a constant input command by holding the joystick fixed. From experience it was estimated that approximately 30V was applied to the motors.

9.2.2 Closed-loop slosh control

The second test included a basic proportional controller using negative feedback of the slosh angular rate as described in Section 7.5. The slosh angular rate was measured by the gyrosensor in the same manner as the open-loop testing. It should be noted that, as the sign of the input torque and slosh angle are opposite, the feedback gain was implemented as positive rather than negative. However, the effect of the gain was that of negative feedback. To discern whether the slosh controller gain tuned from the simulated model of the diwheel was applicable to the physical system, three different controller gains were tested. The results of the closed-loop slosh controller for these three feedback gains are given in Figures 9.3, 9.4, and 9.5. It can be seen from comparison of the closed loop responses for each controller gain, that the simulation tuned controller gain of $K_p = 31$, gives the best results. This gives further evidence of the ability of the simulated mathematical model to accurately describe the physical system's behaviour.

The maximum slosh angle from Figure 9.2 was -1.2 rad. Comparing this result to Figure 7.16 allows a comparison of the dynamic model with the physical system to be made. Because Figure 7.16 was a step response for 1V, the increase in amplitude from -0.025 rad to -1.2 rad

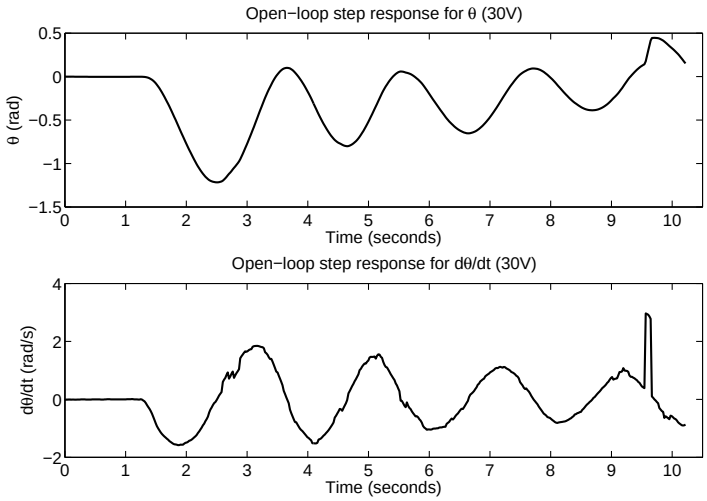

Figure 9.2: Open-loop step response with 60kg driver at 30 volts

predicts that the voltage input in the test was $1.2/0.025 = 48$V. This is impossible as the full voltage available during testing was 36V. The discrepancy may be caused an underestimation of the differential damping in the model. This increase in damping (friction) has the following result:

- The speed of the motor decreases, reducing the back-emf
- More current flows in the motor due to the greater armature voltage, increasing motor torque
- The increased torque causes a larger reaction torque due to gravity, therefore increasing θ

Therefore, according to this test, the model's differential damping, b_{12}, is closer to:

$$b_{12} = 30 \times \frac{1.2}{0.025 \times 30} = 48 Nm.s/rad,$$

assuming a voltage of 30V was applied.

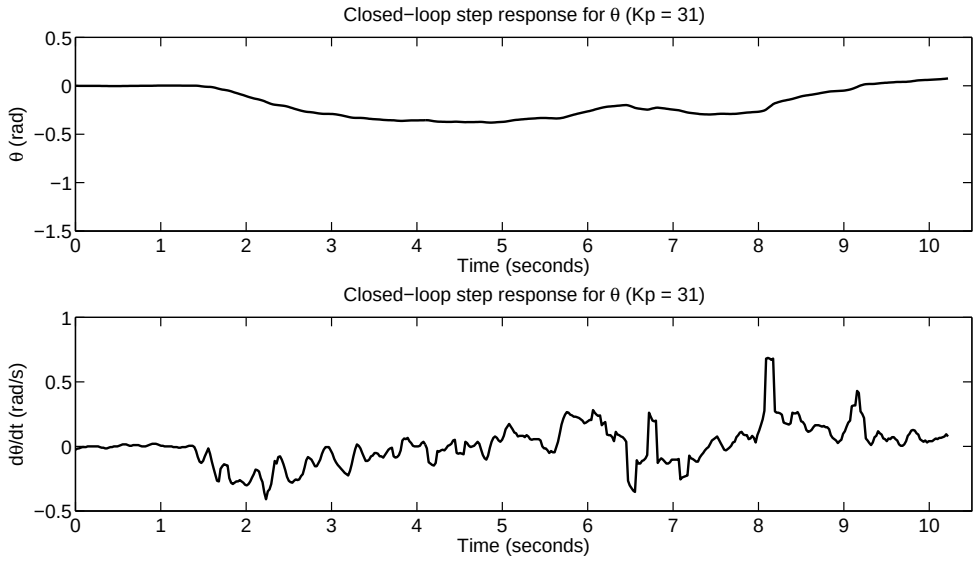

Figure 9.3: Closed-loop slosh control with proportional feedback, $K_p = 31$

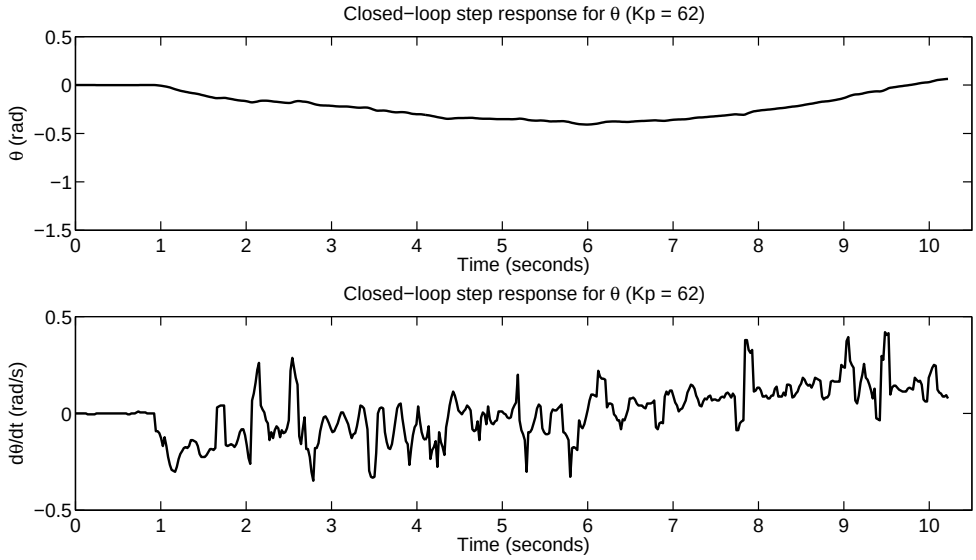

Figure 9.4: Closed-loop slosh control with proportional feedback, $K_p = 62$

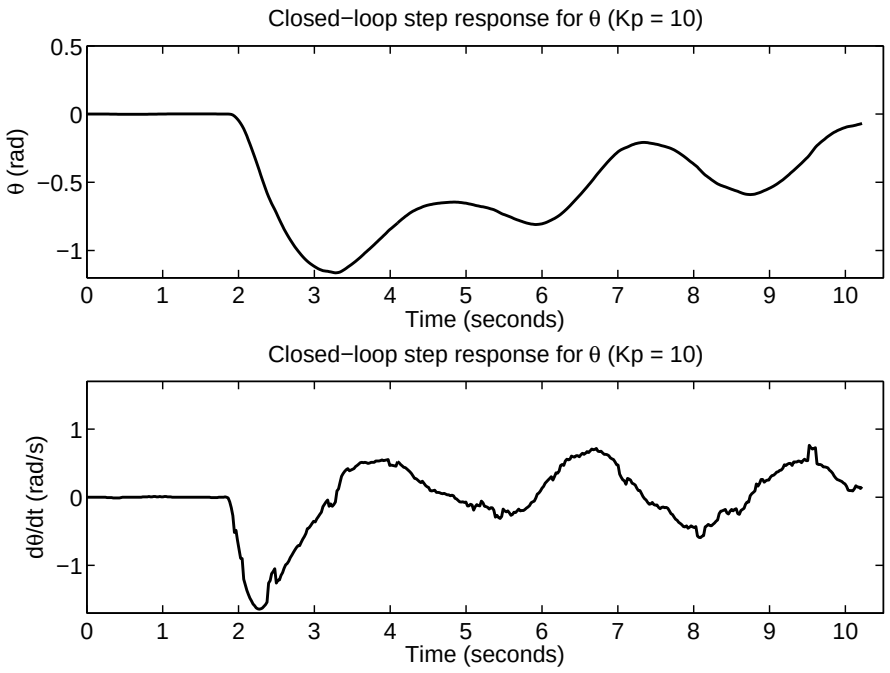

Figure 9.5: Closed-loop slosh control with proportional feedback, $K_p = 10$

9.2.3 Positive Feedback Swing-up Controller Test

An earlier hypothesis suggesting that changing the sign of the slosh controller gains would cause the system to go unstable, and hence swing the inner frame up, was inadvertently tested during the testing of the slosh control. The required sign of the negative feedback gain was initially difficult to discern due to the opposite directions of the input torque and the movement of the inner frame, and the dependence on the orientation of the gyrosensor. For this reason, the required sign was determined using trial and error. The gain was initially set as $K_p = 31$ and testing showed no perceivable slosh control. To ensure that the controller was in fact being implemented in software correctly, the gain was increased by an order of magnitude to $K_p = 310$. Testing the slosh controller with this gain resulted in the diwheel becoming unstable due to the non-zero gyro bias, with the inner frame being inverted in one and a half swings. This positive feedback response can be seen in Figure 9.6 which shows that the inner frame angle exceeds $\pi = 3.142$ radians at around 2.5 seconds. While this indicated that the sign of the feedback gain was incorrect it demonstrated the effectiveness of using positive feedback to swing the inner frame upside down. The concept of this form of swing up control was considered early on in the project but was initially dismissed, due to presumptions that the system damping would be too high and that the control signal would be too weak due to the sinusoidal slosh angular rate. For this reason, a fuzzy control swing-up controller was kept as a primary swing-up control method. However it is not known at this time whether the positive feedback swing-up controller was linear, or whether it was swinging between full positive and full negative voltage in a form of *bang-bang* control.

Although there is potential in this form of swing-up control, using positive feedback along

does not allow the level of control of a fuzzy controller. For the balancing controller to capture the inner frame at the inverted position, the inner frame must not be rotating too fast as it reaches the inverted position. Inverting and multiplying the slosh controller gain does not provide as high a level of control as the fuzzy controller, which remains the preferred method of swing-up control.

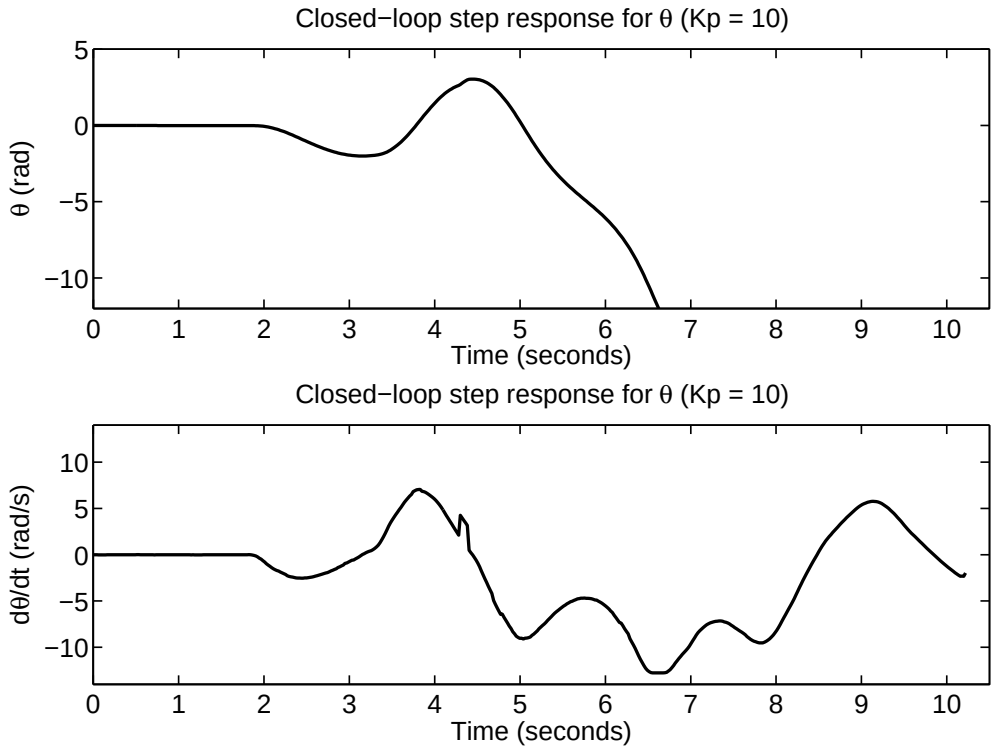

Figure 9.6: Closed-loop positive feedback controller

9.3 Software and Electrical Issues

The initial motor controllers were developed based on an open source motor controller, and constructed by the University of Adelaide electrical workshop. However, during the initial stages of testing several MOSFET transistors overheated and were consequently destroyed as shown in Figure 9.7. This was attributed to the PWM control of the motors, which causes large currents to flow within the motor controller as discussed in Section 5.1. The motor controllers were replaced with an off-the-shelf motor controller that featured a dual high current H-bridge controller. This system required additional software design to be implemented on the Dragonboard before it was functional, which caused minor delays. The main issue with the current controller is that it is only rated at a maximum voltage of 43 Volts where the intended bus voltage was 48 Volts. By removing one battery from the series connection the effective bus voltage was reduced to 36 Volts. Simulations of the diwheel at this voltage were conducted and

it was found the diwheel would still be able to achieve inversion. It was decided to not remove the unused battery as it provided a useful distribution of weight.

Creating an effective encoder on the brake disc from two optical sensors was problematic. The disc brake's misalignment caused fouling between it and the optical sensors. This was overcome by removing excess casing from between the transmitter and receiver of the optical sensors. Reading the brake disc did not provide equal on and off periods, which would make the second sensor redundant, if the sensor was not correctly spaced. This meant directional feedback was an issue. The encoders were sampled in succession with a constant elapsed time method. This method provided accurate results during individual testing. However it uses multiple interrupts and as such inhibits the main functions of the Dragonboard including speed and yaw control. Consequently due to this effect and time delays they were not implemented into the main program.

Figure 9.7: Motor controller board destroyed

9.4 Hardware Issues

The initial design of the diwheel proposed that the idler wheels be exposed with no external shroud. However, as discussed in Section 6.3.3 the risk of leaving them exposed was identified during the diwheel's construction. The design discussed in Section 6.3.3 was the result of this realisation and caused delays in other project priorities by several weeks. An initial prototype of the idler wheel guard was constructed from rigid sheet aluminium and contacted the outer wheel at various locations, inducing a debilitating rolling resistance. Subsequently, the rigid guard was modified to provide clearance with the outer wheel. This created a dangerous gap, exposing the idler wheel and not solving the issue. Flexible materials such as rubber hosing, agricultural piping and nylon brushes, were then considered to bridge this gap and to completely guard the idler wheels from human contact. The nylon brushes succeeded in fulfilling the design requirements of the guard and were used without further deliberation.

10 Final Design Analysis

10.1 Summary of Goals and Achievements

The project goals were divided into Mechanical and Electrical/Electronic goals at the initial stages of design. The level of accomplishment of these goals, at the time of this report, is outlined here.

10.1.1 Mechanical Goals

Create a concept solution for an electrically driven diwheel

A number of CAD designs will be created and reviewed. The cheapest solution shall be chosen for further development.

Throughout the design process, 3D CAD models of the diwheel were continually being produced and improved upon as outlined in Chapter 6. The final CAD design was chosen on the basis of cost, ease of manufacture, ergonomics and aesthetics. The CAD models presented indicate that this goal has been accomplished.

Build a diwheel to be driven by two DC motors including a frame to support one person and system equipment

This goal will be verified by a final demonstration of the system concept according to the project outcomes. The structural integrity of the frame shall be verified by performing FEA incorporating nominal loadings.

Proceeding from the completion of the final designs of the diwheel, construction of the physical system was commenced. This goal has been achieved as illustrated through the construction of a fully-operational the diwheel presented in Chapter 6. The results of the FEA of the space frame is also provided in this section, verifying the structural integrity of the frame.

Implement a mechanical braking system

The diwheel shall be capable of stopping safely at top speed without assistance from the motors. The mechanical braking system shall consist of two disc, drum or caliper brakes each capable of stopping a wheel. The mechanical brake shall be capable of stopping the vehicle during a loss of electrical power.

A mechanical braking system involving two caliper brakes (on on each drive wheel), has been implemented on the diwheel providing mechanical braking in addition to dynamic electrical

braking. The two calipers are controlled by a single hand brake lever which operates two brake discs directly coupled to the two drive-wheels as outlined in Section 4.2. In the event of loss of power to the motors as a result of some fault or the emergency stop button being pressed, the mechanical brakes may be applied to bring the diwheel to a stop. A safe stopping distance may be achieved through controlled use of the mechanical brake and care should be taken not brake so hard that the inner frame locks with the outer wheels. In the event that locking occurs, the diwheel will tend to tumble and may not stop within a safe stopping distance. Ensuring that the driver is well informed of the optimal braking procedures sees the requirements of this goal being met.

10.1.2 Electrical and Electronic Goals

Open-loop differential yaw control

The rate of yaw shall be controlled by analog data sampled by the MCU from the steering system. The diwheel shall be capable of turning through user control with repeatable results and consistent operation. The nature of the steering control shall be intuitive to the user.

Steering of the diwheel has been achieved through the use of a joystick as described in Section 8.3. A minimalistic approach was taken to the user control of the diwheel, and both forward and reverse operation along with steering was implemented using the joystick. The steering command signal is sent to the Dragon board and provides repeatable turning rates. Following full operation of the diwheel, the steering control was found to be intuitive allowing the driver to quickly learn how to control the diwheel.

Open-loop speed control

The forward and reverse speeds of the vehicle shall be controlled by analog data sampled from the steering system. The vehicle's speed shall be measured by sensors and reported to the Microcontroller Unit for display to the user. This user feedback shall include either: LCD display, 7-segment LED display or the use of a galvanometer. The two former solutions are more likely as a speed estimate will be digitally stored within the MCU.

Open-loop speed control was achieved, with the desired speed command being measured from the joystick potentiometers. The voltage across the motors is proportional to the speed input command allowing the diwheel to drive forwards and backwards. Encoders were mounted on the drive-wheel brake discs to provide a feedback of the current motor speed to the Dragonboard which can be used to estimate the diwheel speed. The implementation of the speed feedback in the software was not completed due to project delays. As such, the open loop speed control goal has been achieved while the speed feedback to the user has not been completed.

Dynamic braking

The motor controllers shall be capable of 4-quadrant operation. This will be achieved by use of a H-bridge driver. The battery shall be capable of the current levels required to exert braking torque on the motor. The user shall be able to enable or disable this feature. If disabled the

braking current will be limited (e.g. motor terminals open circuit). When enabled, dynamic braking shall produce a noticeable increase in deceleration when both motors are turned off. The effect shall be designed to be comfortable for the driver.

The ROBOTEQ motor controller used in the final diwheel electronics is based on a H-bridge configuration allowing 4-quadrant operation. The regenerative current to the batteries during dynamic braking is limited by the controller to less than 100A to ensure the circuit breaker is not tripped. Disabling the dynamic braking during operation has not been implemented as the ROBOTEQ controller automatically uses dynamic braking. This is in contrast to initial designs incorporating open source motor controllers which gave greater control in enabling and disabling the dynamic braking through use of the Dragonboard. Should the power to the motors be cut via the emergency stop circuit, dynamic braking will be disabled and only mechanical braking may be applied. System proving has shown the dynamic braking to be significantly effective in stopping the diwheel quickly and comfortably.

Closed-loop slosh control

When this is disabled rapid acceleration/deceleration of the diwheel shall cause the inner ring to gerbil and deflect by some amount from the neutral position. Slosh control shall be implemented to damp this oscillation, improving user comfort. The success of this control shall be measured quantitatively and qualitatively through the use of a gyrosensor and driver reactions, respectively.

System proving illustrated the significant sloshing of the inner frame during harsh accelerations and decelerations. The implementation of the slosh controller showed substantial slosh reduction in both the VRML model and the physical system as outlined in Section 7.5 and Chapter 9, respectively. Logging of the slosh angular rate and feedback from driver reaction with slosh control implemented has shown that this goal has been achieved.

Adjustable acceleration and deceleration ramps

When closed-loop slosh control is disabled, the user shall be able to customize the acceleration and deceleration ramp times by altering default parameters in the MCU.

Following the derivation of the diwheel system dynamics, it was found that this goal is analogous to slosh control and allowing manual tuning of the slosh controller gain. Therefore this goal and the closed-loop slosh control goal are not mutually exclusive and a solution for one goal also solves the other.

Battery compensation

Both open loop and closed loop control require a fixed gain across the amplifier. A compensation circuit will be implemented to achieve a fixed gain, regardless of battery voltage. This circuit shall consist of the MCU and a low pass filter. The MCU will automatically compensate for the dropping battery voltage. If the voltage drops enough to indicate depletion of the batteries the MCU may disable the diwheel.

A battery compensation circuit consisting of two resistors forming a voltage divider has been implemented in the diwheel providing feedback to the MCU proportional to the battery voltage level, as shown in Section 5.3. A low pass filter was not required for the battery monitoring circuit as the control loop samples this voltage level at a low enough rate that any high frequency noise is not a significant issue. The output to the motor controller is multiplied by a gain proportional to the battery voltage, effectively compensating for the dropping battery voltage. The circuit that has been integrated into the diwheel meets the requirements of this goal.

10.1.3 Miscellaneous Goals

Mathematical Model of System / State space model

A mathematical model of the system shall be developed.

A full mathematical model of the diwheel is presented in Chapter 7 and incorporates forward and reverse translational dynamics, steering dynamics and slosh dynamics. The mathematical model has been derived using both an analytical method and mechanical method to provide verification of the results. The dynamics give system behaviour at a level of accuracy adequate for the design of the desired controllers and indicate the completion of this goal.

Virtual simulation model

A virtual simulation shall be created for the MATLAB *environment and operating features of the vehicle shall be reproduced in this simulation.*

A virtual model of the diwheel was created to provide visual feedback of the modelled system's response to command inputs. The final VRML model utilises the dynamics derived for the mathematical model and gives a good estimate of the behaviour that the physical system may exhibit from commands in open-loop, slosh and inversion control modes. The VRML model takes commands from a joystick identical to that used on the diwheel and the design strived to match the simulated model to the physical system. Section 7.2.7 depicts the final VRML model and environment which allows operating modes to be controlled and switched between in the same manner as on the diwheel. The completion of a fully functional VRML model demonstrates that this goal has been achieved.

10.1.4 Extension Goals

Regenerative Braking

The kinetic energy of the di-wheel at speed shall be returned to the batteries during braking if feasible.

The dynamic braking introduced automatically by the motor controller is believed to automatically provide charge to the batteries causing regeneration. This operation is guaranteed if

the motor controllers short circuit the motor when driven, however regeneration has not verified during system testing.

State Control of Pitch Angle

The mathematical model of the system shall be used to provide state-space control of the pitch angle.

State-space control of the inner frame angle has not yet been achieved, although the necessary controllers and control structures have been designed. The implementation of these controllers remains to be completed. The creation of an attitude reference system using a gyrosensor and accelerometer which estimates the inner frame angle has been created and tested, although the accelerometer was damaged towards the end of the project and needs to be replaced.

Closed-loop yaw rate control

The actual yaw rate shall be measured and compared to the desired yaw rate, and the error between the two shall be minimized. This shall require speed sensors on the two drive wheels. Two sensor options are: encoders and DC motors. Issues with accuracy at low speed may be encountered with the encoders.

Due to the problems arising when implementing motor speed feedback system using encoders and time limitations, the rotational speed of the motors was not able to the fed to the MCU. Thus the yaw rate was not able to the measured and closed-loop yaw rate control was not achieved. An encoder system to measure motor speed has been implemented on the diwheel using photo-detectors to sense infrared pulses broken by holes in the brake disc coupled to the rotor of the drive-wheel. However, this system was not successfully integrated with the control programming in time for the completion of this goal.

Dynamically stabilised pitch

The controller may be engaged to turn the user upside at standstill and maintain this unstable static equilibrium point against disturbances. This goal also requires the fitting of a harness to the seating arrangement.

The control strategies to invert the occupant and create static and dynamic stability while inverted have been designed for the mathematical model using fuzzy control for swing up and a linear quadratic regulator for stabilisation. Feedback sensor issues and time constraints have prevented this strategy from being implemented on the physical system. A racing seat and harness have been implemented to restrain the passenger during operation, and system proving has seen the diwheel perform full rotations of the inner frame while maintaining driver safety. These rotations have been achieved through manually rocking the inner frame back and forth, and by locking the mechanical brakes while traveling at full speed. During slosh testing, the slosh controller was changed to positive feedback with an increased gain causing the system to attempt to generate slosh rather than reduce it. This caused the inner frame to complete a full

revolution and illustrates a form of swing up control, however due to the absence of a balancing controller, full inversion control has not been completed.

Design of an alternative tire for the wheel

The alternate tire may consist of a pneumatic solution or solid 'foam-filled' solution.

A custom pneumatic or solid 'foam filled' solution for the outer wheel tyre of the diwheel proved infeasible. These alternative solutions were dismissed early in the design process as they were deemed to have been too expensive and problematic to implement.

Suspension system (AT)

There shall be some means of isolating the driver from the vibration levels experienced at the wheel.

The final diwheel prototype exhibits a working suspension system which uses automotive spring-dampers to allow movement in the idler wheels. This system provides significant movement of the inner frame relative to the outer wheels, and maintains full idler wheel contact with the outer wheels despite undulations in the circularity of the outer wheels. This reduces the vibration levels transmitted to the driver and provides good driver comfort indicating the accomplishment of this goal.

Real time Radio Control (BT)

The di-wheel shall be capable of Remote Control via an RF link. This shall enable command control and simulation of user input into the system.

Remote control of the diwheel was not achieved. However, the electronic hardware in place is conducive to the implementation of a RF link to control the diwheel remotely. This goal was not given high priority with respect to other goals and as such was not deemed to be feasible to implement within time constraints.

10.2 Cost Analysis

Throughout the project cost was a major driving factor in the selection of components and manufacturing techniques. Each group member is entitled to 200AUD from the University of Adelaide for use in the final year project. With five students in this group, the project budget without external sponsorship was 1000AUD. After external sponsorship was sought, only few parts were donated to the project, or sold at a reduced cost and no monetary sponsorship was obtained despite efforts.

A summary of the costs incurred throughout this project is given in Table 10.1 which includes the component and manufacturing costs. Parts which were obtained at no cost due to sponsorship or the recycling of parts from previous final year engineering projects are shown (in italics) but are not included in the total cost.

In the construction of the physical system, a large amount of labour was required from both the mechanical and electrical workshop at the University of Adelaide. A summary of the total workshop hours attributed to this project is give in Table 10.2 and summary of the working hours of each group member is provided in Table 10.3.

Table 10.1: Cost of parts for the EDWARD project

Category	Part	Cost ($AUD)
Outer Wheel	Tyre (materials and bonding)	200
	Rolled steel	583.5
Inner Wheel	Damper fitting plates	110
	Spring dampers (set)	*10000*
	Idlers	385
	Idler guards	108
	Idler guard brushes	80
Transmission	Drive-wheel	120
	Sprocket and chain	72
Space Frame	Frame	400
	Seat	170
	Harness	50
	Quick lock clamps (for joystick mount)	30
Brakes	Brake caliper	0
	Brake lever	25.9
	Brake cable	12.8
Miscellaneous	Bearings	210
	Paint	99
Processor	Dragon board	200
Power source	Battery (SLA GEL)	360
Sensors	Gyro	89.98
	Accelerometer	29.89
	Encoders	60
Speed/yaw control	Motor (Includes both sets)	1100
	Joystick	39.95
	Motor controller (Roboteq)	*850*
Other Electrical	Circuit boards, cables, components	384.01
	Total Cost ($)	4720.03

Table 10.2: University of Adelaide workshop hours.

	Total Hours
Mechanical Workshop	304
Electrical Workshop	98
Total Workshop Hours	402

Table 10.3: Student work hours.

	C. Dyer	E. Schumann	J. Harvey	K. Fulton	T. Zhu
March	19	54	46	41	69
April	40	82	30	37	72
May	62	113	75	67	143
June	30	55	30	4	61
July	41	27	31	29	30
August	62	35.5	31	45	60
September	47	37.5	67	50	49
October	78	98	87	71	68
Student Hours	379	502	437	344	552
Team Total Hours	2174				

11 Summary

11.1 Future Work

There are several modifications that can be implemented to improve the performance and functionality of EDWARD. These were not implemented due to the limited time frame caused by project delays.

- Implementing closed-loop speed and yaw control allowing a more intuitive drive. This can be achieved by reading speed feedback from the motors and providing it to the appropriate closed-loop controller.

- During strenuous testing, the motors were noted to become very hot, approaching 70°. This was caused by their small form factor and inability to dissipate heat quickly enough. Resolving this issue might involve implementing a passive or active cooling system or replacing them with motors that have improved thermal capabilities.

- An optical solution was selected to measure the speed of the motor, however these sensors can be vulnerable to stray light and dust particles. Incorporating a more robust sensor such as a magnetic solution or DC motor tachometer would eliminate these vulnerabilities.

- The implementation of inversion controllers as described in Section 7.6, would allow a better demonstration of EDWARD's full capabilities especially as a system for applied control.

- The implementation of an observer/estimator on the Dragonboard, used to provide an estimate of $\dot{\varphi} - \dot{\theta}$ without directly measuring it could be used in for small slosh angles, reducing the need for the encoder sensors. It could otherwise be used as a redundant speed estimate.

- The implementation of hydraulic brakes in order to eliminate differential braking has been considered as a viable option.

- The implementation of a flexible sound system for reporting the diwheel's states to the driver, as well as warning sounds and music.

- The implementation of a real time radio control. Allowing testing to be conducted at a safe distance, without a driver.

11.2 Conclusion

The aim of this project was to design and build an electric diwheel with active rotation damping. This has been achieved with the completion of a physical system which has undergone system proving and rotation damping (slosh reduction) testing with successful results.

An extensive review of literature relevant to the project has provided inspiration for both concepts of the mechanical design and control methods to achieve slosh and inversion control. The final physical model has complied with the high level of safety measures asscociated with the design in order to minimise the risk of any driver injuries. Redundancy in the form of an emergency stop circuit, has been added to give the driver sufficient safety measures to mitigate any issues that may occur during operation. The ergonomics considered during the design phase have resulted in a reasonable level of comfort considering the space constraints of the physical system and the aesthetics of the design have also been well recieved by the public.

The mathematical and VRML model of the diwheel have proved effective in giving insight into the predicted behaviour of the phyical system and when compared to testing of the physical system, have proved sufficiently accurate. The derivation of the mathematical model allowed tuning of the slosh controller to be performed, allowing immediate and effective implementation on the physical system. Furthermore, the testing of different slosh controller gains on the diwheel has shown the gains tuned in simulation to correlate very strongly to the physical system.

Braking of the diwheel has been achieved both electrically and mechanically to increase user control. Mechanical braking provides a method of deceleration in the event power to the motors is lost or cut. Dynamic electrical braking is the primary form of deceleration and occurs automatically under normal operation, as a result of upgrading to a commercial motor controller. The motor controller used in the final design also provides regenerative braking during normal operation, charging the batteries as the diwheel decelerates. Limitation on the current that may be sent to the batteries during regenerative braking has been implemented through the use of a circuit breaker.

Inversion control, although not a core objective of the project, was attempted in order to further increase the novelty of the diwheel. The design of this control was completed using the simulated VRML model, but was not able to be fully implemented on the physical system due to time constraints caused by project delays. Half of the inversion controller, the swing-up, has been achieved using a positive feedback control law.

The outcome of the project has seen the accomplishment of all core goals, and the construction of the first electric diwheels to implement active control. A conference paper detailing the derivation of the dynamics and control structures has also been submitted to the Austalian Conference on Robotics and Automation (ACRA). The presentation of Edward at the University of Adelaide, School of Mechanical Engineering, 15th Annual Honours Student Project Exhibition received the Caroma Dorf Industries Ltd. award for *Best General Mechanical Engineering Project*, and has attracted significant media attention being featured on Channel 10 News and Totally Wild. This attests to the amount of work undertaken in the project by the students and its overall success.

References

(2005). Pedal powered di-wheel concept vehicle. Viewed 7 April 2009.

(2008). Dezeen design magazine.

(2009). Direct plastics, nylon 6 rod.

Aboel-Hassan, A., Arafa, M., and Nassef, A. (2009). Design and optimization of input shapers for liquid slosh suppression. *Journal of Sound & Vibration*, Vol. 320:pp. 1–15.

Ardoino, P. L. (1984). Dynamics of the belted occupant, implications for protection. Technical report, International Center for Transportation Studies, Elsevier Science Publishers, Amsterdam.

Astrom, K., K.J. and. Furuta (2000). Swinging up a pendulum by energy control. *Automatica*, 36(2):287–295. doi:10.1016/S0005-1098(99)00140-5.

Baker, N., Brown, C., Dowling, D., Modra, J., and Tootell, D. (2005). *SON of EDGAR, State-space control of Electro-Drive Gravity-Aware Ride*. University of Adelaide.

Batchelor, A. and Stachowiak, G. (2005). *Engineering Tribology*. Butterwort Heinemann, UK.

Cardini, S. (2006). A history of the monocycle - stability and control from inside the wheel. *IEEE Control Systems Magazine*, 26:22–26.

Chang, Y.-H., Chang, C.-W., Yang, C.-H., and Tao, C. (2007). Swing up and balance control of planetary train type pendulum with fuzzy logic and energy compensation. *International Journal of Fuzzy Systems*, 9(2):87–94.

Christensen, J., McBarron, J., and McConville, J. (1995). Nasa man-systems integration standards (msis). *Anthropometry and Biomechanics*, Vol 1, Sec 3.

Clark, M. A., Field, J. B., McMahon, S. G., and Philps, P. (2005). Edgar, a self-balancing scooter. Technical report, The University of Adelaide.

Cooney, J., Xu, W., and Bright, G. (2004). Visual dead-reckoning for motion control of a mecanum-wheeled mobile robot. *Mechatronics*, Vol. 14:pp. 623–637.

Di-wheels (2009). The museum of retro technology. Viewed 14 March 2009.

Dodge, F. T. (2000). The new 'dynamic behavior of liquids in moving containers'. Technical report, San Antonio - Southwest Research Institute.

Dyer, C., Fulton, K., Harvey, J., Schumann, E., and Zhu, C. (2009). Electric Di-Wheel with Automatic Rotation Damping. Technical report, The University of Adelaide.

Ellis, G. (2000). *Control system design guide - using your computer to understand and diagnose feedback controllers*. Academic Press.

Esmailzadeh, E., Goodarzi, A., and Vossoughi, G. (2003). Optimal yaw moment control law for improved vehicle handling. *Mechatronics*, 13:659–675.

Gandhi, P. S., Joshi, K. B., and Ananthkrishnan, N. (2009). Design and development of a novel 2dof actuation slosh rig. *Journal of Dynamic Systems Measurement & Control*, Vol. 131:p. 5.

Genta, G. and Morello, L. (2009). *The Automotive Chassis: Volume 1: Components Design*. Springer, New York.

Grasser, F., D'Arrigo, A., Colombi, S., and Rufer, A. (2002). Joe: A mobile, inverted pendulum. *IEEE Transactions on Industrial Electronics*, 49(1):107–114.

Guerra, R. d. S. (2008). Kalman filter tutorial for balancing robot. Technical report.

Haskell, R. E. and Hanna, D. M. (2009). *Learning By Example Using C Programming the DRAGON12-Plus Using CodeWarrior*. LBE Books.

Hughes, A. (2006). *Electric Motors and Drives - Fundamentals, Types and applications*. Elsevier Ltd.

Jantzen, J. (1998). Design of fuzzy controllers (tech. report no 98-e 864 (design)). Technical report, Technical University of Denmark, Department of Automation.

Karwowski, W. (2006). *International encyclopedia of ergonomics and human factors*. CRC Press.

Lauwers, T., Kantor, G., and Hollis, R. (2006). A dynamically stable single-wheeled mobile robot with inverse mouse-ball drive. In *IEEE Int. Conference on Robotics and Automation*, pages 2884–2889. Orlando, FL. doi:10.1109/ROBOT.2006.1642139.

Li, Y., Gu, F., Harris, G., Ball, A., Bennett, N., and Travis, K. (2005). The measurement of instantaneous angular speed. *Mechanical Systems and Signal Processing*, Vol. 19:pp. 786–805.

Lygouras, J. (2000). Accurate velocity evaluation using adaptive sampling interval. *Microprocessors and Microsystems*, 24:265–269.

Lyons, R. G. (2005). *Understanding Digital Signal Processing*. Pearson education Asia Limited and China Machine Press.

Martynenko, Y. (2007). Motion control of mobile wheeled robots. *Journal of Mathematical Sciences*, 147(2):6569–6606. doi:10.1007/s10958-007-0496-4.

Martynenko, Y. and Formal'skii, A. (2005a). Theory of the control of a monocycle. *Applied Mathematics and Mechanics*, 69(4):516–528. doi:doi:10.1016/j.jappmathmech.2005.07.003.

Martynenko, Y. G. and Formal'skii, A. M. (2005b). Theory of the control of a monocycle. *Applied Mathematics and Mechanics*, 69:516–528.

Modaressi-Tehrani, K., Rakheja, S., and Stiharu, I. (2007). Three-dimensional analysis of transient slosh within a partly-filled tank equipped with baffles. *Vehicle System Dynamics*, 45:525–548.

Monowheels (2009). The museum of retro technology. Viewed 12 March 2009.

Munson, J. (2006). Dual current-sense amplifiers simplify h-bridge load monitoring. Technical report, Linear Technology.

Muskinja, N. and Tovornik, B. (2006). Swinging up and stabilization of a real inverted pendulum. *IEEE Transactions on Industrial Electronics*, 53(2):631–639. doi:10.1109/TIE.2006.870667.

Nichkawde, C., Harish, P. M. ., and Anathkrishnan, N. (2004). Stability analysis of a multibody system model for coupled slosh-vehicle dynamics. *Journal of Sound & Vibration*, 275:1069–1083.

Ottoson, A. L. and Lovsund, P. (1989). Protective level of safety harnesses combined with some racing car seats in frontal impacts-a laboratory study. *Pergamon Journals Ltd.*

Parks, B. (2005). *Makers: all kinds of people making amazing things in garages, basements, and backyards*. O'Reilly, California.

Riegel, R. (2003). *Riegel's handbook of industrial chemistry*. Spring Press.

Ruan, X. and Cai, J. (2009). Fuzzy backstepping controllers for two-wheeled self-balancing robot. In *International Asia Conference on Informatics in Control, Automation and Robotics*.

Santana, J., Naredo, J., Sandoval, F., Grout, T., and Argueta, O. (2002). Simulation and construction of a speed control for a dc series motor. *Mechatronics*, 12:1145–1156.

Serious-wheels (2005). Peugeot moovie concept. Viewed 11 May 2009.

Shigley, J. and Mischke, C. (2004). *Mechanical Engineering Design, 7th Edition*. McGraw Hill, New York.

Southall, D. (2009). Dave southall's shed projects.

States, J. D., G, S., and A., F. H. (1970). The medical aspects of driver protection systems and devices developed through automobile racing. Technical report, SAE technical paper series.

Tao, C. W., Taur, J. S., Hsieh, T. W., and Tsai, C. L. (2008). Design of a fuzzy controller with fuzzy swing-up and parallel distributed pole assignment schemes for an inverted pendulum and cart system. *IEEE TRANSACTIONS ON CONTROL SYSTEMS TECHNOLOGY*, 16:1277–1288.

Tarakameh, A. and Shojaie, K. n. (Year unknown). Modeling of a differential drive wheel mobile robot by newton-euler method. Technical report, Iran University of Science and Technology.

Tilley, J. (2004). *Understanding Solids: the Science of Materials*. John Wiley and Sons.

Unknown (1935). Gyro-wheel car. *Modern Mechanix*, June edition:87.

Vereycken, E. (1947). Véhicule à deux roues solidaires l'une de l'autre: Two-wheeled vehicle supportive of each other.

Wellstead, P. (Year unknown). Ball and hoop 1: Basics. Control-systems-principles.co.uk.

Wellstead, P. and Readman, M. (Year unknown). Ball and hoop 2: Control and analysis. Control-systems-principles.co.uk.

Wiley, J. (1988). *Inside the wheel: The Complete Guide to Monocycles*. Solipaz Pub Co.

Zheng, B. and Anwar, S. (2009). Yaw stability control of a steer-by-wire equipped vehicle via active front wheel steering. *Mechatronics*, 19:799–804.

A Publications Arising from this Thesis

In addition to the work done towards the Project Contract, the group has also produced a journal publication for the Australian Conference on Robotics and Automation (ACRA). This paper is included in the following pages.

Control of an electric diwheel

B. Cazzolato, J. Harvey, C. Dyer, K. Fulton, E. Schumann, T. Zhu and Z. Prime
University of Adelaide, Australia
benjamin.cazzolato@adelaide.edu.au

Abstract

A diwheel is a novel vehicle consisting of two large outer wheels which completely encompass an inner frame. The inner frame freely rotates inside the wheels using supporting idler wheels. The outer wheels are driven from the inner frame and forward motion is achieved through a reaction torque generated by the eccentricity of the centre of gravity of the inner frame. During operation, diwheels experience slosh (when the inner frame oscillates) and tumbling (when the inner frame completes a revolution). In this paper the dynamics of a generic diwheel are derived. Three control strategies are then proposed; slosh control, swing-up control and inversion control. Finally, simulations are conducted on a model of a diwheel currently under construction at the University of Adelaide.

1 Introduction

The diwheel is a device which consists of a two large outer wheels which completely encompass an inner frame. The inner frame is free to rotate within the wheels, and is typically supported by a common axle or idlers which roll on the wheels (see Figure 1). Diwheels, like their more popular cousins the monowheel, have been around for almost one and a half centuries [Self, accessed Aug 2009; Cardini, 2006]. All of these platforms suffer from two common issues affecting driver comfort; slosh and tumbling (also known as gerbilling). Sloshing is when the inner frame oscillates, and it occurs in all monowheels and diwheels where the centre of gravity of the inner frame is offset from the centre line of the wheels. It is very prevalent as these platforms typically have low damping between the wheel and the frame in order to minimise power consumption during locomotion. In addition, during severe braking or acceleration the inner frame will tumble relative to the earth centred frame, which obviously affects the ability of the driver to control the platform.

In March 2009, honours students in the School of Mechanical Engineering, at the University of Adelaide commenced the design and build of an electric diwheel. The vehicle was called Edward (Electric DiWheel with Active Rotation Damping) [Dyer *et al.*, 2009]. A rendered solid model of the platform is shown in Figure 1 and Figure 2 shows the current stage of construction of the platform. The outer wheels are rolled and welded stainless steel tube with a rubber strip bonded on the outer rolling surface. An inner frame supports the driver who is held in place by a five-point racing harness. The inner frame runs on the outer wheels with three nylon idlers and is coupled to the inner frame by suspension arms, which act to provide some suspension and also maintain a constant contact force between the idlers and the wheel. Two brushed DC motors each drive (via sprockets and a chain) a small motor cycle drive-wheel which contacts the inner radius of the outer wheel. Thus the vehicle can be driven forwards and backwards using a collective voltage in to the motors, and can be yawed when the motors are differentially driven. The vehicle is drive-by-wire, and the driver controls the vehicle via a joystick. There is also a mechanical foot brake which operates calipers on the drive-wheels (in case of electrical failure). There are three sensing systems on board, viz. a solid state gyroscope (for measuring pitch rate), a solid state DC coupled accelerometer (for state estimation of pitch angle) and incremental encoders on the two drive-wheels.

The scope of the project was to not only design and build the mechanical and electrical platform, but to also implement several control strategies to modify the dynamics. The first was a slosh controller, with the purpose of minimising the rocking motion that occurs as the vehicle is accelerated or decelerated when torquing the drive motors. This was deemed necessary after viewing videos of monowheels and diwheels in operation. If implemented correctly it would also allow maximum deceleration of the vehicle if necessary, which occurs when the centre of gravity of the inner frame is horizontally aligned

Figure 1: Rendered image of the EDWARD diwheel

Figure 2: Photograph of the EDWARD diwheel during construction

to the centre of the outer wheels. Another control mode was also considered with the aim to make the ride in the vehicle more exciting. This involved a swing-up controller followed by an inversion controller. The purpose of this controller was to invert the driver, then stabilise them enabling them to drive around upside down.

In this paper the dynamics of a generic diwheel using a Lagrangian formulation are derived. The control laws for the two control strategies are presented. Details of the EDWARD diwheel and its parameters are used in a numerical simulation, for which the open loop response and various closed loop responses are presented. Finally suggestions for future control strategies are made.

2 Dynamics of the 2DOF system

In the derivation of the diwheel dynamics that follows, motion has been restricted to the xy-plane. In this two degree-of-freedom model, the left and right wheel and left and right drive-wheels are combined into a single degree of freedom. In this way both pairs of wheels and drive-wheels rotate at equal speeds so that the diwheel does not yaw about the y-axis. A Lagrangian approach has been used for the derivation of the dynamic model of the diwheel, similar to that of shown in [Martynenko and Formal'skii, 2005].

The following assumptions have been made in the derivation of the dynamics.

- The motion is restricted to the xy-plane.
- Friction is limited to viscous friction, and the Coulomb friction arising from the idler rollers is neglected.
- The suspension arms are fixed, keeping the centre of gravity of the inner frame a fixed distance from the centre of the wheels.
- The inductance of the motor is negligible and therefore the current is an algebraic function of voltage and motor speed.
- The rotational and translational inertia from the motors and drive-wheels has been included in the inner frame.
- There is no slip between the drive-wheels and the outer wheels.
- There is no slip between the outer wheels and the ground.

The model has three coordinates, however the latter two are dependent:

- θ - rotation of the inner frame assembly about the z-axis.
- $\varphi_L = \varphi_R = \varphi$ - rotation of the wheels about the z-axis.
- x - the displacement of the diwheel (centre) about an earth centred frame.

The right-handed coordinate frame is located at the centre of rotation of the diwheel, as shown in Figure 3. The positive x-direction is to the right and positive y is down. Clockwise rotations about the centre are considered positive. The zero datum for the measurement of both the body angle θ and wheel angle φ is coincident with the positive y-axis.

Since the drive-wheel is fixed to the inner frame (body 2) the two masses may be lumped together. However, in the development that follows, the energy associated with the rotational velocity of the drive-wheel is omitted, as it is considered negligible.

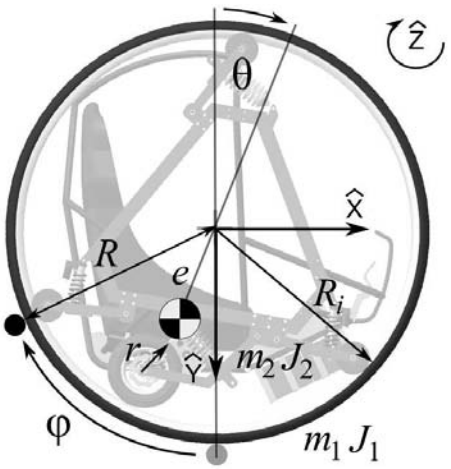

Figure 3: Schematic of a generic diwheel showing coordinate systems, mass distributions and states.

2.1 Non-linear dynamics

The Euler-Lagrange equations yield the dynamic model in terms of energy and are given by

$$\frac{d}{dt}\left(\frac{\partial L}{\partial \dot{q}_i}\right) - \frac{\partial L}{\partial q_i} = F_i \tag{1}$$

where the Lagrangian L is an expression of the difference in the kinetic and potential energies of the system, q_i are generalised coordinates (in this case θ and φ) and F_i are generalised forces. The solution of the Lagrange equation for each coordinate, q_i, yields an expression of the form:

$$\mathbf{M}(\mathbf{q})\ddot{\mathbf{q}} + \mathbf{C}(\mathbf{q}, \dot{\mathbf{q}}) + \mathbf{G}(\mathbf{q}) = \mathbf{F} \tag{2}$$

which summarise the system dynamics.

Velocities

The translational and rotational velocities of the bodies comprising the diwheel are presented below in preparation for the Lagrangian. The translational velocity of the wheel (body 1) in the x-direction is

$$v_{1x} = R\,\dot{\varphi}, \tag{3}$$

where R is the outer wheel radius and $\dot{\varphi}$ is the angular velocity of the wheel. The translational velocity in x-direction of the CoG of body 2 (the inner frame) is

$$v_{2x} = R\,\dot{\varphi} - \dot{\theta}\,e\,\cos(\theta)\,, \tag{4}$$

where e is the eccentricity between the inner frame CoG and the centre of the wheels, and $\dot{\theta}$ is the angular velocity of the inner frame relative to an earth centred frame. The corresponding velocity in y-direction of the inner frame CoG is

$$v_{2y} = -\dot{\theta}\,e\,\sin(\theta)\,. \tag{5}$$

The magnitude of the velocity of the inner frame CoG is thus

$$|v_2| = \left(\left(R\,\dot{\varphi} - \dot{\theta}\,e\,\cos(\theta)\right)^2 + \dot{\theta}^2\,e^2\sin(\theta)^2\right)^{\frac{1}{2}}. \tag{6}$$

Kinetic Energy

The kinetic energy of the diwheel has been separated into the following terms. First, the rotational energy of the wheel,

$$E_{1r} = \frac{J_1\,\dot{\varphi}^2}{2}, \tag{7}$$

where J_1 is the *combined* moment of inertia of both wheels about their centre.

Second, the translational energy of the wheel,

$$E_{1t} = \frac{R^2\,\dot{\varphi}^2\,m_1}{2}, \tag{8}$$

where m_1 is the *combined* mass of both wheels.

Third, the rotational energy of the inner frame,

$$E_{2r} = \frac{J_2\,\dot{\theta}^2}{2}, \tag{9}$$

where J_2 is the moment of inertia of the inner frame about its CoG.

Lastly, the translational energy of the inner frame CoG,

$$\begin{aligned} E_{2t} &= \frac{1}{2}m_2 v_2^2 \\ &= \frac{m_2\left(\left(R\,\dot{\varphi} - \dot{\theta}\,e\,\cos(\theta)\right)^2 + \dot{\theta}^2\,e^2\,\sin^2(\theta)\right)}{2}, \end{aligned} \tag{10}$$

where m_2 is the mass of the inner frame and $N = \frac{R}{r}$ is the ratio of outer wheel radius R to drive-wheel radius r.

Thus the total kinetic energy of this system is:

$$\begin{aligned} E_k &= E_{1r} + E_{1t} + E_{2r} + E_{2t} \\ &= \frac{m_2\left(\left(R\,\dot{\varphi} - \dot{\theta}\,e\,\cos(\theta)\right)^2 + \dot{\theta}^2\,e^2\,\sin^2(\theta)\right)}{2} \\ &\quad + \frac{J_1\,\dot{\varphi}^2}{2} + \frac{J_2\,\dot{\theta}^2}{2} + \frac{R^2\,\dot{\varphi}^2\,m_1}{2}. \end{aligned} \tag{11}$$

Potential Energy

The potential energy of the wheel is zero. Therefore the total potential energy (assuming zero potential energy at $\theta = 0$) is related to the change in height of the CoG of the inner frame and is given by

$$E_p = e\,g\,m_2\,(1 - \cos(\theta))\,, \tag{12}$$

where g is the gravitational acceleration.

Lagrangian

The Lagrangian for the diwheel is the difference in the kinetic and potential energies, $E_k - E_p$,

$$\begin{aligned} L &= \left(\frac{J_1}{2} + \frac{R^2\, m_1}{2} + \frac{R^2\, m_2}{2}\right) \dot{\varphi}^2 \\ &\quad -R\, e\, m_2\, \cos(\theta)\, \dot{\varphi}\, \dot{\theta} + \left(\frac{m_2\, e^2}{2} + \frac{J_2}{2}\right) \dot{\theta}^2 \\ &\quad -e\, g\, m_2 + e\, g\, m_2\, \cos(\theta)\,. \end{aligned} \tag{13}$$

This may be expressed compactly as

$$L = \frac{\hat{J}_1}{2}\dot{\varphi}^2 + a_R \cos(\theta)\, \dot{\varphi}\dot{\theta} + \frac{\hat{J}_2}{2}\dot{\theta}^2 + a_g\,(\cos(\theta) - 1)\,, \tag{14}$$

where $\hat{J}_1 = J_1 + R^2\ (m_1 + m_2)$ is the effective moment of inertia of the wheel and inner frame about the contact point with the ground, $\hat{J}_2 = J_2 + e^2\, m_2$ is the moment of inertia of the inner frame about the centre of the wheels (from the parallel axis theorem), and $a_R = -R\, e\, m_2$ and $a_g = e\, g\, m_2$ are constants of convenience.

Euler-Lagrange equations

The dynamics are found from

$$\frac{d}{dt}\left(\frac{\partial L}{\partial \dot{\theta}}\right) - \frac{\partial L}{\partial \theta} + b_{12}(\dot{\theta} - \dot{\varphi}) = -\tau, \tag{15}$$

$$\frac{d}{dt}\left(\frac{\partial L}{\partial \dot{\varphi}}\right) - \frac{\partial L}{\partial \varphi} + b_{12}(\dot{\varphi} - \dot{\theta}) + b_1\dot{\varphi} = \tau, \tag{16}$$

where b_{12} is a viscous damping coefficient related to the relative velocities of the inner ring (θ) and the outer wheel (φ), b_1 is the viscous damping constant associated with the wheel rolling (and is surface dependent) and τ is a differential torque applied to both the inner ring and the outer wheel by the drive-wheel/motor assembly.

Evaluating the terms for θ

$$\frac{d}{dt}\left(\frac{\partial L}{\partial \dot{\theta}}\right) = \hat{J}_2\, \ddot{\theta} + a_R\, \ddot{\varphi}\, \cos(\theta) - a_R\, \dot{\varphi}\, \dot{\theta}\, \sin(\theta)$$

$$-\frac{\partial L}{\partial \theta} = \sin(\theta)\, \left(a_g + a_R\, \dot{\varphi}\, \dot{\theta}\right).$$

Evaluating the terms for φ

$$\frac{d}{dt}\left(\frac{\partial L}{\partial \dot{\varphi}}\right) = -a_R\, \sin(\theta)\, \dot{\theta}^2 + \hat{J}_1\, \ddot{\varphi} + a_R\, \ddot{\theta}\, \cos(\theta)$$

$$-\frac{\partial L}{\partial \varphi} = 0.$$

Differential Equations Therefore the governing differential equations of the diwheel are given by

$$-\tau = \hat{J}_2\, \ddot{\theta} + b_{12}\left(\dot{\theta} - \dot{\varphi}\right) + a_g\, \sin(\theta) + a_R\, \ddot{\varphi}\, \cos(\theta) \tag{17}$$

and

$$\tau = \hat{J}_1\, \ddot{\varphi} + b_{12}\, \left(\dot{\varphi} - \dot{\theta}\right) + b_1\dot{\varphi} - a_R\, \dot{\theta}^2\, \sin(\theta) + a_R\, \ddot{\theta}\, \cos(\theta)\,. \tag{18}$$

It should be noted that the above differential equations are similar to the equations of motion derived for the monowheel by [Martynenko and Formal'skii, 2005; Martynenko, 2007] with the exception of the rolling resistance term b_1. It is also similar to that for the self-balancing two-wheel mobile robots [Grasser *et al.*, 2002; Ruan and Cai, 2009] and the ballbot [Lauwers *et al.*, 2006], where the only difference is that the gravitational term acts to stabilise the diwheel compared to the "inverted pendulum" robots which are unstable.

Solution to the Differential Equations of the Mechanical System

The system of differential equations may be solved in terms of $\ddot{\theta}$ and $\ddot{\varphi}$ to give

$$\begin{aligned} \ddot{\theta} &= -\frac{1}{D_1}\Bigg(\left(\hat{J}_1 + a_R \cos(\theta)\right)\left(\tau + b_{12}(\dot{\theta} - \dot{\varphi})\right) \\ &\quad - a_R \cos(\theta)\, b_1\dot{\varphi} \\ &\quad + a_R^2 \sin(\theta)\cos(\theta)\, \dot{\theta}^2 + \hat{J}_1 a_g \sin(\theta) \Bigg), \end{aligned} \tag{19}$$

where

$$D_1 = \hat{J}_1\, \hat{J}_2 - {a_R}^2 \cos^2(\theta)\,, \tag{20}$$

and

$$\begin{aligned} \ddot{\varphi} &= \frac{1}{D_1}\Bigg(\left(\hat{J}_2 + a_R \cos(\theta)\right)\left(\tau + b_{12}(\dot{\theta} - \dot{\varphi})\right) - \hat{J}_2 b_1\dot{\varphi} \\ &\quad + \hat{J}_2 a_R \sin(\theta)\, \dot{\theta}^2 + a_R a_g \sin(\theta)\cos(\theta) \Bigg). \end{aligned} \tag{21}$$

2.2 Fully Coupled Electro-Mechanical System

Electrical Dynamics

Permanent magnet DC electric motors have been used to power the diwheel. It has been assumed that the electrical inductance of the motors, L_m, is sufficiently small it may be neglected, and therefore the current in the motor coil is an algebraic function of the supplied voltage V_m and motor speed $\dot{\theta}_m = N n_s(\dot{\varphi} - \dot{\theta})$, and is given by

$$R_m i + K_m \dot{\theta}_m = V_m, \tag{22}$$

where R_m is the resistance of the armature of both motors wired in parallel (and equal to half the resistance of a single motor), K_m is the motor torque constant (which is equal to the back EMF constant for SI units) for each motor, $N = \frac{R}{r}$ is the ratio of the wheel radius to drive-wheel radius and n_s is the drive ratio from the motor sprocket to drive-wheel sprocket (when using a chain drive).

The differential torque acting on the wheel and the inner frame generated by the motor in terms of the armature current is given by

$$\tau = N n_s K_m i. \tag{23}$$

Combining Equations (22) and (23) gives the differential torque in terms of applied voltage

$$\tau = N n_s K_m \left(V_m - N n_s K_m (\dot{\varphi} - \dot{\theta}) \right) / R_m \tag{24}$$

Inserting Equation (24) into Equations (17) and (18) yields the differential equations of the fully coupled electro-mechanical system.

Solution to the Differential Equations of the Coupled Electro-Mechanical System

Equations (19) and (21) may be rewritten in terms of an input voltage to the motors by substituting Equation (24) to give

$$\begin{aligned} \ddot{\theta} &= -\frac{1}{D_1}\Bigg(- a_R \cos(\theta)\, b_1 \dot{\varphi} + \left(\hat{J}_1 + a_R \cos(\theta) \right) \\ &\times \left(\frac{N n_s K_m}{R_m} V_m + (b_{12} + b_m)(\dot{\theta} - \dot{\varphi}) \right) \\ &+ a_R^2 \sin(\theta)\cos(\theta)\,\dot{\theta}^2 + \hat{J}_1 a_g \sin(\theta) \Bigg), \end{aligned} \tag{25}$$

where $b_m = \frac{(N n_s K_m)^2}{R_m}$ is the effective damping from the back EMF, and

$$\begin{aligned} \ddot{\varphi} &= \frac{1}{D_1}\Bigg(\hat{J}_2 b_1 \dot{\varphi} + \left(\hat{J}_2 + a_R \cos(\theta) \right) \\ &\times \left(\frac{N n_s K_m}{R_m} V_m + (b_{12} + b_m)(\dot{\theta} - \dot{\varphi}) \right) \\ &+ \hat{J}_2 a_R \sin(\theta)\,\dot{\theta}^2 + a_R a_g \sin(\theta)\cos(\theta) \Bigg). \end{aligned} \tag{26}$$

2.3 Linearised Dynamics

The dynamics of the plant have been linearised about two operating conditions; the downward (stable) position and the upright (unstable) position.

Linearising about downward position

Using a Jacobian linearisation, the non-linear dynamics given by Equations (19) and (21) about the downward position $\theta = \dot{\theta} = \varphi = \dot{\varphi} = 0$ may be approximated by the linear state equations

$$\dot{\mathbf{x}} = \mathbf{A}\mathbf{x} + \mathbf{B}u, \tag{27}$$

where $\mathbf{x} = \begin{bmatrix} \theta & \varphi & \dot{\theta} & \dot{\varphi} \end{bmatrix}^T$ is the state vector, $u = \tau$ is the plant input and the state and input matrices are given by

$$\mathbf{A} = \frac{1}{{a_R}^2 - \hat{J}_1 \hat{J}_2} \times \begin{bmatrix} 0 & 0 & {a_R}^2 - \hat{J}_1\hat{J}_2 & 0 \\ 0 & 0 & 0 & {a_R}^2 - \hat{J}_1\hat{J}_2 \\ \hat{J}_1 a_g & 0 & (\hat{J}_1 + a_R) b_{12} & -(\hat{J}_1 + a_R) b_{12} - a_R b_1 \\ -a_g\, a_R & 0 & -(\hat{J}_2 + a_R) b_{12} & (\hat{J}_2 + a_R) b_{12} + \hat{J}_2 b_1 \end{bmatrix} \tag{28}$$

and

$$\mathbf{B} = \frac{1}{{a_R}^2 - \hat{J}_1 \hat{J}_2} \begin{bmatrix} 0 \\ 0 \\ (\hat{J}_1 + a_R) \\ -(\hat{J}_2 + a_R) \end{bmatrix}. \tag{29}$$

The poles of this plant are at $s = 0, -0.22 \pm 2.59i, -0.26,$, with the complex poles having a damping ratio of $\zeta = 0.083$. The transfer function from τ to θ exhibits one zero on the origin which is expected as at the steady state $\theta(s \to 0) \to 0$. It is interesting to note that the transfer function from τ to φ exhibits two undamped complex zeros at $s = \pm 3.44i$. The presence of lightly damped complex zeros is similar to that found in other systems exhibiting slosh such as the ball and hoop system [Wellstead, accessed Aug 2009]. The implication is that if the motor is driven with a sinusoidal input at the frequency of the zeros, then the wheel will stand still and only the inner cage moves.

Note that for the case of a voltage input, $u = V_m$, then the damping term arising from the differential velocity of the frame and wheel increases from $b_{12} \to b_{12} + b_m$ (resulting in open loop poles at $s = 0, -0.34 \pm 2.55i, -0.37,$) and the state input matrix $\mathbf{B}$ needs to be multiplied by $\frac{N n_s K_m}{R_m}$.

Linearising about upright (inverted) position

Linearising the non-linear dynamics given by Equations (19) and (21) about the upright position $\theta = \pi, \dot{\theta} = \varphi =$

$\dot{\varphi} = 0$ gives the linear state equations

$$\mathbf{A} = \frac{1}{{a_R}^2 - \hat{J}_1\hat{J}_2} \times \begin{bmatrix} 0 & 0 & {a_R}^2 - \hat{J}_1\hat{J}_2 & 0 \\ 0 & 0 & 0 & {a_R}^2 - \hat{J}_1\hat{J}_2 \\ -\hat{J}_1 a_g & 0 & (\hat{J}_1 - a_R)b_{12} & -(\hat{J}_1 - a_R)b_{12} + a_R b_1 \\ -a_g\, a_R & 0 & -(\hat{J}_2 - a_R)b_{12} & (\hat{J}_2 - a_R)b_{12} + \hat{J}_2 b_1 \end{bmatrix} \quad (30)$$

and

$$\mathbf{B} = \frac{1}{{a_R}^2 - \hat{J}_1\hat{J}_2} \begin{bmatrix} 0 \\ 0 \\ (\hat{J}_1 - a_R) \\ -(\hat{J}_2 - a_R) \end{bmatrix}. \quad (31)$$

The poles of this plant are at $s = 0, -0.25, 2.27, -3.07$. Note that for the case of a voltage input, $u = V_m$, then the damping term arising from the differential velocity of the frame and wheel increases from $b_{12} \rightarrow b_{12} + b_m$ (resulting in open loop poles at $s = 0, -0.34, 2.12, -3.40$) and the state input matrix $\mathbf{B}$ needs to be multiplied by $\frac{N n_s K_m}{R_m}$ as per the downward linearisation case.

3 Control strategies

In this section a number of different control strategies are presented for the two-dimensional diwheel model. It should be noted that no literature to date has been published on control laws for either monowheels or diwheels. This is not surprising given that previous diwheels and most monowheels were human or IC engine driven which are not amenable to automatic control, the latter having dynamics with similar time constants to the plant.

The parameters used for the model, and thus the controller designs, are detailed in Table 1. Most parameters were estimated from the solid model of the diwheel (and rider) with the exception of the damping terms which were measured.

3.1 Slosh control

The purpose of the slosh controller is to minimise the amount of rocking (sloshing) that the driver experiences when rapidly accelerating or decelerating. This has parallels with slosh control in liquid-fueled rockets, ships and tankers [Aboel-Hassan *et al.*, 2009; Readman and Wellstead, accessed Aug 2009; Wellstead, accessed Aug 2009]. Any number of suitable linear and non-linear control strategies can be used to suppress the rocking (sloshing) motion of the diwheel. [Readman and Wellstead, accessed Aug 2009] fed back the slosh angle of a ball in a hoop (equivalent to θ in the diwheel) to restrict the slosh, which was equivalent to increasing the torque arising from the offset in the CoG of the inner frame. It was found that this technique is effective as it drives two complex closed loop poles towards the plant zeros. An alternative and obvious solution is to increase damping to reduce slosh using velocity feedback. Another common technique is input (also known as command) shaping, which involves modifying the reference command by convolving it with a set of self-destructive impulses that act against the complex poles in the plant. This approach is effectively pole-zero cancellation and is not robust.

Table 1: Parameters used to define the model. Note that the terms for the wheels and motors account for both acting together.

Part	Parameter	Value
Wheels	m_1	50.3 kg
	J_1	26.1 kg.m^2
Frame	m_2	218 kg
	J_2	48.4 kg.m^2
Lengths	R	720 mm
	$R_i \approx R$	720 mm
	r	140 mm
	e	160 mm
Damping	b_{12}	30 Nm.s/rad
	b_1	12 Nm.s/rad
Motor	V_{sat}	48 V
	R_m	0.314 Ohms
	L_m	0.3 mHenry
	K_m	65 mNm/A
Transmission	$N = \frac{R}{r}$	5.14
	n_s	7

The approach used here was simply to feed back the angular rate of the inner frame, $\dot{\theta}$. This decision was based on simplicity and availability of a state measurement from a solid state gyroscope. The final controller was

$$u = V_m = [\ 0 \quad 0 \quad 31 \quad 0\ ]\mathbf{x} = 31\dot{\theta}, \quad (32)$$

and was chosen to make the poles (of the linearised dynamics) entirely real. Note that the positive sign for this term arises from the fact that a positive motor torque leads to a negative acceleration of the inner frame (see Equation (19)).

3.2 Swing-up control

The swing-up controllers developed for other underactuated non-linear planar mechanical systems (such as the inverted pendulum) are applicable to the swing-up of the diwheel, since their dynamics are similar [Astrom and Furuta, 1996; Yoshida, 1999; Wang and Fang, 2004]. Almost all early works on swing-up controllers used a bang-bang switching approach to drive the potential energy of the pendulum (in this case the in-

ner frame) to the inverted state. More recently, fuzzy control has been used to swing-up (and balance) inverted pendulums [Martynenko and Formal'skii, 2005; Chang *et al.*, 2007]. In this paper two approaches will be investigated; a simple positive velocity feedback controller and a fuzzy controller.

Positive velocity feedback

One very simple strategy to swing the inner frame to the upright position is to simply move the complex poles from the left hand of the s-plane to the right hand side by feeding back a positive velocity of the motor (to make it go unstable), giving a controller of the form

$$u = V_m = [\ 0 \quad 0 \quad -10 \quad 10\ ]\mathbf{x} = 10\left(\dot{\varphi}-\dot{\theta}\right) = 10\frac{\dot{\theta}_m}{Nn_s}, \tag{33}$$

where the gains were chosen such that they were as large as possible without severely saturating the motors.

Fuzzy Controller

Fuzzy control has been applied to the problem of balancing the inverted pendulum, first by [Yamakawa, 1989]. Since then, various fuzzy logic controllers have been applied to various aspects of balancing problems. [Chang *et al.*, 2007] have described fuzzy controllers for both the swing-up and balancing control of a planetary train type pendulum. Their swing-up controller consists of a bang-bang control scheme, with little regard to the velocity of the pendant link - however this strategy is not immediately amenable to the diwheel system, since such a strategy tends to fight with gravity. Finally [Martynenko and Formal'skii, 2005] describe a fuzzy swing-up controller, which they have used to swing up a pendulum by emulating an energy based approach.

About the controller The fuzzy controller developed here uses two inputs from the physical system, the angular position of the inner ring with respect to earth (θ) and the rate of the inner ring ($\dot{\theta}$). The single output consists of a voltage between -48V and 48V. In contrast to previous fuzzy controllers applied to the inverted pendulum, this fuzzy controller does not aim to limit the horizontal travel of the diwheel, and the two chosen inputs appear appropriate for the problem of swinging the diwheel up.

Membership functions The membership functions of the two inputs are shown in Figure 4, and are similar to those presented in [Martynenko and Formal'skii, 2005]. The range of θ is $[-\pi, \pi]$ and the range of $\dot{\theta}$ is $[-2\pi, 2\pi]$. The output voltage membership function consists of five singleton sets corresponding to $[-48, -10, 0, 10, 48]$ Volts.

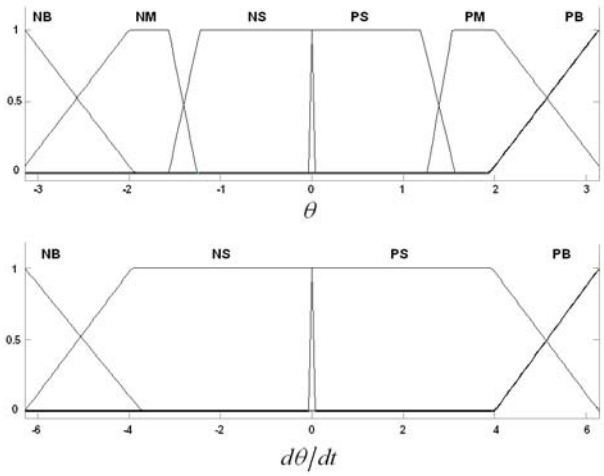

Figure 4: Membership functions

Rules The rules chosen for our initial fuzzy controller have been designed to force energy into the system in order to bring the inner ring to within $\pm 10°$of the inverted equilibrium point and are detailed in Table 2. The basic premise is to swing the inner ring hard until the back EMF of the motor develops sufficiently, and then to drive the motor so that it reinforces the fall of the inner ring due to gravity. For small angles ($|\theta| < \pi/2$) the action of the motor is determined according to the direction of the angular velocity, with regard to the fact that a positive motor voltage produces a negative reaction torque on the inner ring. For medium angles ($\pi/2 < |\theta| < 3\pi/4$) the motor is also driven hard when the angular velocity causes the inner ring to approach the balancing point. As the direction changes the motor direction is reversed. When the angle becomes large ($3\pi/4 < |\theta| < \pi$) and the angular rate is small, the motor action is made to cause the diwheel to 'drive underneath' the mass of the inner ring. For large angles and large angular rates the voltage is zero to allow the inner ring to slow down for capturing by the inversion controller.

3.3 Inversion control

A linear full-state feedback controller was used to keep the inner frame in the upright (open-loop unstable) position.

Linear Quadratic Regulator

A linear quadratic regulator (LQR) was used to stabilise the plant in its unstable position (Section 2.3). This approach has been used successfully in the inverted pendulum problem and its many variants [Lauwers *et al.*, 2006]. The cost function that was minimised is given by

$$J = \int_0^\infty \left(q_1\theta^2 + q_2\left(\dot{\theta} - \dot{\varphi}\right)^2 + R_1 V_m^2\right) dt \tag{34}$$

Table 2: Fuzzy rules

Rule 1	If (θ = PS) & ($\dot{\theta}$ = PS) then (V_m = NB)
Rule 2	If (θ = NS) & ($\dot{\theta}$ = NS) then (V_m = PB)
Rule 3	If (θ = PS) & ($\dot{\theta}$ = NB) then (V_m = PB)
Rule 4	If (θ = NS) & ($\dot{\theta}$ = PB) then (V_m = NB)
Rule 5	If (θ = PM) & ($\dot{\theta}$ = PB) then (V_m = NB)
Rule 6	If (θ = NM) & ($\dot{\theta}$ = NB) then (V_m = PB)
Rule 7	If (θ = PM) & ($\dot{\theta}$ = PS) then (V_m = NB)
Rule 8	If (θ = NM) & ($\dot{\theta}$ = NS) then (V_m = PB)
Rule 9	If (θ = PM) & ($\dot{\theta}$ = NB) then (V_m = NB)
Rule 10	If (θ = NM) & ($\dot{\theta}$ = PB) then (V_m = PB)
Rule 11	If (θ = PB) then (V_m = PS)
Rule 12	If (θ = NB) then (V_m = NS)
Rule 13	If (θ = PB) & ($\dot{\theta}$ = PB) then (V_m = Z)
Rule 14	If (θ = NB) & ($\dot{\theta}$ = NB) then (V_m = Z)

where q_1 and q_2 are the state penalties on the inner frame angle θ and the difference in the angular velocities between the frame and wheel $\dot{\theta} - \dot{\varphi}$ respectively. The purpose of the latter term is to restrict the speed of the drive motor which is rated to 2100RPM. The term R_1 is the penalty on the drive voltage. Using Bryon's rule, the state penalty matrix for the state vector given in Section 2.3 was set to

$$\mathbf{Q} = \begin{bmatrix} q_1 & 0 & 0 & 0 \\ 0 & 0 & 0 & 0 \\ 0 & 0 & q_2 & -q_2 \\ 0 & 0 & -q_2 & q_2 \end{bmatrix} = \begin{bmatrix} 36 & 0 & 0 & 0 \\ 0 & 0 & 0 & 0 \\ 0 & 0 & \frac{1}{36} & \frac{-1}{36} \\ 0 & 0 & \frac{-1}{36} & \frac{1}{36} \end{bmatrix} \tag{35}$$

and the effort penalty was

$$R_1 = \left(\frac{1}{\frac{1}{2}48} \right)^2 \tag{36}$$

Solving the continuous algebraic Riccati equation returns the optimal control gains

$$\mathbf{k} = [\ -193 \quad 0 \quad -44 \quad -11\ ]. \tag{37}$$

Pole placement (expensive control)
In parallel with the LQR controller described above, a state feedback regulator was developed by using the common method of pole placement. The placement involved reflecting all unstable poles about the imaginary axis so that they were stable. Note that this is equivalent to expensive LQR control, where the penalty on the control effort is infinite. The poles of the system were moved from those given in Section 2.3, viz. $s = 0, -0.34, 2.12, -3.40$, to $s = 0, -0.34, -2.12, -3.40$, resulting in a control vectors

$$\mathbf{k} = [\ -91 \quad 0 \quad -30 \quad -13\ ]. \tag{38}$$

4 Numerical Simulations

Numerical simulations were conducted on the differential equations derived in Section 2 within SIMULINK. To validate the differential equations and the implementation within SIMULINK, a parallel model was constructed using SIMMECHANICS. A virtual reality (VRML) model (shown in Figure 5) was built to aid in the visualisation of the plant.

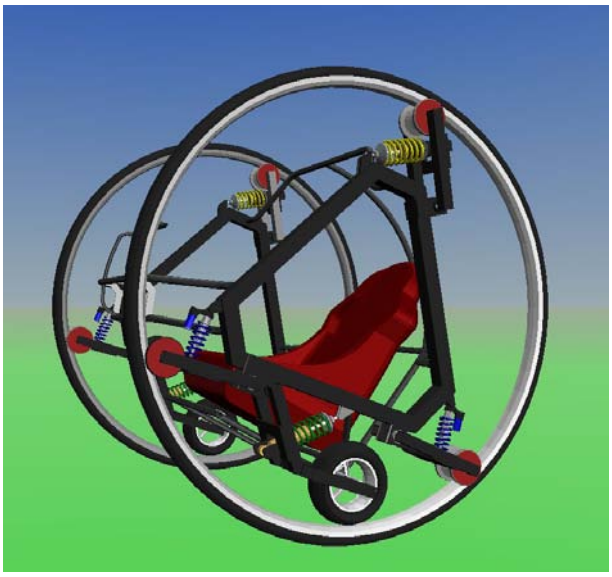

Figure 5: Rendered image of the VRML model

The various control strategies detailed in Section 3 were also integrated in to the SIMULINK model and the simulation results are presented following.

4.1 Open loop response

Figure 6 shows open loop response of the inner frame angle θ (and control voltage $V_m = 0$) when the inner frame was rotated to just less 180° and released. The slosh (rocking) is clearly evident.

4.2 Closed loop slosh control

Figure 7 shows the inner frame angle θ and control voltage V_m when the inner frame was rotated to just less 180°and released. Note that saturation of the motors just occurs and the slosh is dramatically curbed.

4.3 Swing-up control

The two swing-up controllers were investigated for the diwheel, when it was initially at rest and positioned at its stable equilibrium.

Positive velocity feedback
Figure 8 shows the response of the simple (positive velocity feedback) swing-up controller. Since it is based

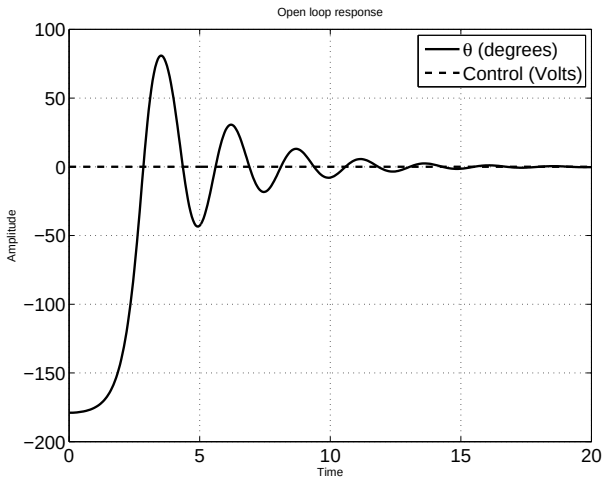

Figure 6: Open loop response when rotated to almost 180° and released

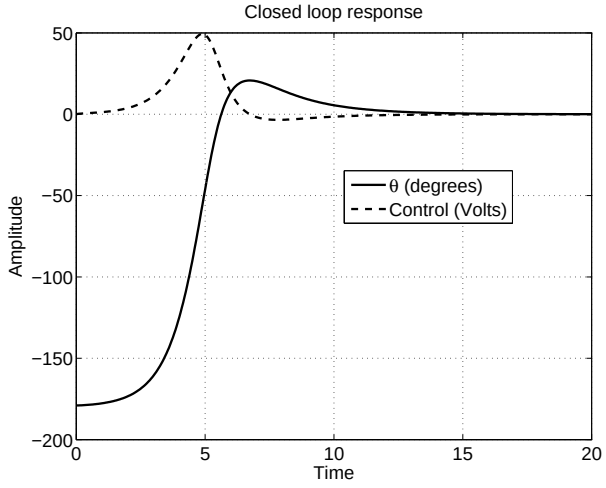

Figure 7: Closed loop response of slosh controller when rotated to almost 180° and released

on exponential growth (arising from the unstable pole), it takes a considerable time (16 seconds) to be captured by the inversion controller, even when starting from an initial state of $\theta_0 = 5°$.

Fuzzy controller

Figure 9 shows the response of the fuzzy swing-up controller. It can be seen from the magnitude of the control signal in Figure 8, that the simple method is no where near as effective as a bang-bang like fuzzy controller in Figure 9 for driving energy into the system.

4.4 Inversion control

Figure 10 shows the closed loop response of the frame angle θ and the control signal V_m to an initial pose of $\theta_0 = 170°$ when using the LQR given by Equation (37).

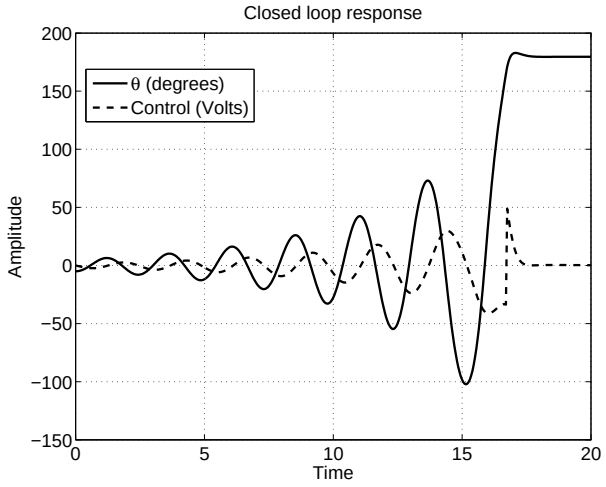

Figure 8: Closed loop response of positive velocity feedback swing-up controller

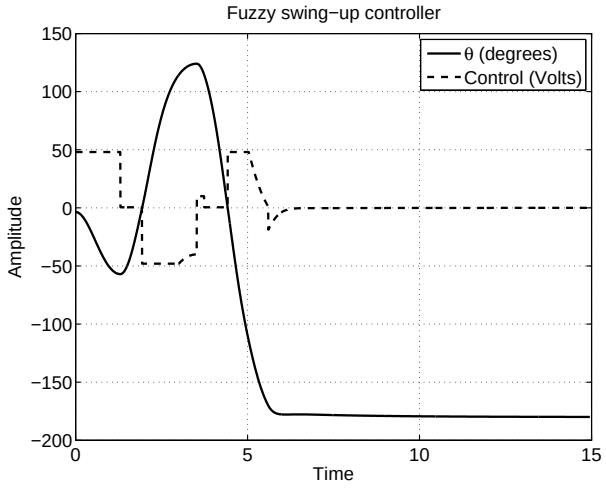

Figure 9: Closed loop response of fuzzy swing-up controller

The expensive control gains given by Equation (38) were analysed, and although they were able to stabilise the plant, the non-aggressive control law was unable to capture the inner frame upon swing-up for all but the most benign cases.

5 Conclusion and Future Work

In this paper the dynamics of the diwheel were derived, where it was seen that it exhibits behaviour seen in other nonlinear under-actuated unstable mechanical plants such as the inverted pendulum and self-balancing wheeled robots [Fantoni and Lozano, 2001]. Consequently, approaches applied to systems with similar dynamics are also applicable to the diwheel, which have been successfully demonstrated here.

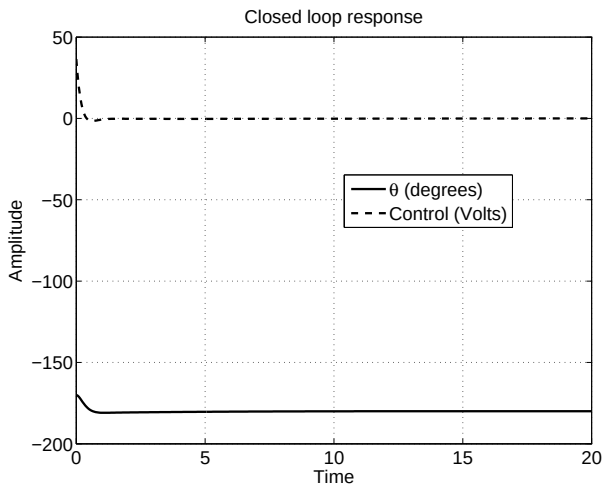

Figure 10: Closed loop response of inversion controller to an initial pose of $\theta_0 = 170°$

Future work will involve extension of the two-dimensional model to a fully coupled three-dimensional model, including yaw arising from differential motion of the wheels. In parallel to this work will also continue on the EDWARD diwheel, including the final assembly and commissioning, conducting a thorough system identification, testing the different safety systems, and then finally implementing and benchmarking the various control strategies.

Acknowledgments

The authors would like to acknowledge the support of the Bob Dyer and Phil Schmidt for their efforts in constructing the physical diwheel used as the basis of the model in this paper.

References

[Aboel-Hassan *et al.*, 2009] A. Aboel-Hassan, M. Arafa, and A. Nassef. Design and optimization of input shapers for liquid slosh suppression. *Journal of Sound & Vibration*, 320:1–15, 2009.

[Astrom and Furuta, 1996] K.J. Astrom and K. Furuta. Swinging up a pendulum by energy control. In *IFAC 13th World Congress*, 1996.

[Cardini, 2006] S.B. Cardini. A history of the monocycle - stability and control from inside the wheel. *IEEE Control Systems Magazine*, 26(5):22–26, 2006.

[Chang *et al.*, 2007] Y.-H. Chang, C.-W. Chang, C.-H. Yang, and C.W. Tao. Swing up and balance control of planetary train type pendulum with fuzzy logic and energy compensation. *International Journal of Fuzzy Systems*, 9(2):87–94, 2007.

[Dyer *et al.*, 2009] C. Dyer, K. Fulton, J. Harvey, E. Schumann, and C. Zhu. Electric Di-Wheel with Automatic Rotation Damping. Technical report, The University of Adelaide, 2009.

[Fantoni and Lozano, 2001] I. Fantoni and R. Lozano. *Non-linear Control for Underactuated Mechanical Systems*. Springer, 2001.

[Grasser *et al.*, 2002] F. Grasser, A. D'Arrigo, S. Colombi, and A.C. Rufer. Joe: A mobile, inverted pendulum. *IEEE Transactions on Industrial Electronics*, 49(1):107–114, 2002.

[Lauwers *et al.*, 2006] T.B. Lauwers, G.A. Kantor, and R.L. Hollis. A dynamically stable single-wheeled mobile robot with inverse mouse-ball drive. In *IEEE Int. Conference on Robotics and Automation*, pages 2884–2889, Orlando, FL., 2006.

[Martynenko and Formal'skii, 2005] Y.G. Martynenko and A.M. Formal'skii. Theory of the control of a monocycle. *Applied Mathematics and Mechanics*, 69(4):516–528, 2005.

[Martynenko, 2007] Y.G. Martynenko. Motion control of mobile wheeled robots. *Journal of Mathematical Sciences*, 147(2):6569–6606, 2007.

[Readman and Wellstead, accessed Aug 2009] M. Readman and P. Wellstead. Ball and hoop 2: Control and analysis. Technical report, Controlsystems-principles.co.uk., accessed Aug. 2009.

[Ruan and Cai, 2009] X. Ruan and J. Cai. Fuzzy backstepping controllers for two-wheeled self-balancing robot. In *International Asia Conference on Informatics in Control, Automation and Robotics*, 2009.

[Self, accessed Aug 2009] D. Self. Dicycles and diwheels. [Online - www.dself.dsl.pipex.com/MUSEUM/TRANSPORT], accessed Aug. 2009.

[Wang and Fang, 2004] Chen Y. Wang, Z. and N. Fang. Minimum-time swing-up of a rotary inverted pendulum by iterative impulsive control. In *American Control Conference*, pages 1335–1340. IEEE, 2004.

[Wellstead, accessed Aug 2009] P. Wellstead. Ball and hoop 1: Basics. Technical report, Control-systems-principles.co.uk., accessed Aug. 2009.

[Yamakawa, 1989] T. Yamakawa. Stabilization of an inverted pendulum by a high-speed fuzzy logic controller hardware system. *Fuzzy Sets and Systems*, 32(2):161–180, 1989.

[Yoshida, 1999] K. Yoshida. Swing-up control of an inverted pendulum by energy-based methods. In *American Control Conference*, pages 4045–4047, 1999.

B Appendix

B.1 Hertzian Idler Wheel Contact

The following solution for the contact pressures between two curves surface of different materials is an application of Hertzian contact theory. The outer and idler wheel are considered as two elastic bodies in contact with two dimensions of curvature shown in Figure B.1. The terms are defined below:

- The material of the outer wheel (body 1) and idler wheel (body 2) are steel and nylon respectively
- Young's moduli, $E_1 = 200\text{GPa}$ and $E_2 = 2\text{GPa}$, and the reduced Young's modulus, E'
- Poisson's ratio: $v_1 = 0.3$ and $v_2 = 0.4$
- R_{1x} is the radius of curvature of body 1 in the x direction and if a curvature is concave the radius is negative
- R' is the reduced radius
- The radii of the outer and idler wheel are are $R_{1x} = 0.03m$, $R_{1y} = -0.720m$, $R_{2x} = \infty$ and $R_{2y} = 0.04m$
- k_0, k_1, k_3, k_4 and k_5 are the contact coefficients
- $\theta = 90^o$ is the angle between the direction (x or y) of the largest radius of each body

The idler wheel design has two points of contact to support the overestimated 200kg of loading. These surfaces are at an angle of 51^o with the loading. Therefore the loading is halved and is subject to a $cos\theta$ factor

$$cos(90 - 51) = \frac{2000N/2}{W} \Rightarrow W = \frac{2000N/2}{cos(90 - 51)} \approx 1300N.$$

The reduced Young's modulus is given by

$$\frac{1}{E'} = \frac{1}{2}\left(\frac{1 - v_1^2}{E_1} + \frac{1 - v_2^2}{E_2}\right) = \frac{1}{2}\left(\frac{1 - 0.3^2}{200e9_1} + \frac{1 - 0.4^2}{2e9_1}\right)$$

$$\Rightarrow E' = 4.7109GPa.$$

The reduced radius is given by

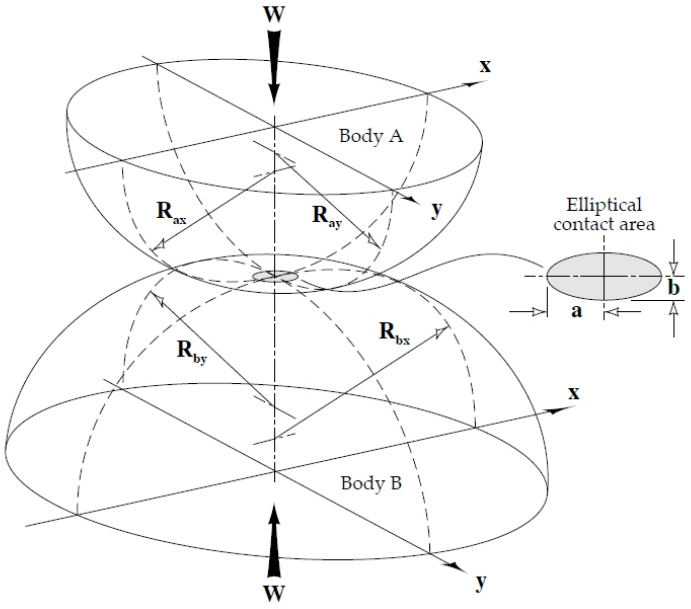

,

Figure B.1: Geometry of two convex elastic bodies in contact (Batchelor & Stachowiak 2005)

$$\frac{1}{R'} = \frac{1}{R_{1x}} + \frac{1}{R_{1y}} + \frac{1}{R_{2x}} + \frac{1}{R_{2y}} = \frac{1}{0.03} + \frac{1}{-0.720} + \frac{1}{0.04} + \frac{1}{\infty}$$

$$\Rightarrow R' = 0.01756m.$$

The contact coefficient k_0 is given by

$$k_0 = \frac{\sqrt{\left\{\frac{1}{R_{1x}} - \frac{1}{R_{1y}}\right\}^2 + \left\{\frac{1}{R_{2x}} - \frac{1}{R_{2y}}\right\}^2 + 2\left\{\frac{1}{R_{1x}} - \frac{1}{R_{1y}}\right\}\left\{\frac{1}{R_{2x}} - \frac{1}{R_{2y}}\right\} cos2\theta}}{\frac{1}{R_{1x}} + \frac{1}{R_{1y}} + \frac{1}{R_{2x}} + \frac{1}{R_{2y}}}$$

$$\Rightarrow k_0 = \frac{\sqrt{\left\{\frac{1}{0.03} - \frac{1}{0.720}\right\}^2 + \left\{\frac{1}{0.04} - \frac{1}{\infty}\right\}^2 + 2\left\{\frac{1}{0.03} - \frac{1}{0.720}\right\}\left\{\frac{1}{0.04} - \frac{1}{\infty}\right\} cos2\theta}}{\frac{1}{0.03} + \frac{1}{-0.720} + \frac{1}{0.04} + \frac{1}{\infty}}$$

$$k_0 = 3.4722.$$

k_1, k_2, k_3, k_4 and k_5 are then determined from k_0 using a set of graphs on page 300 of Engineering Tribology (Batchelor and Stachowiak 2005). The contact coefficients were determined to be $k_1 = 1.1$, $k_2 = 0.91$, $k_3 = 2.0$, $k_4 = 0.32$ and $k_5 = 0.52$. The radii of the elliptical contact, a and b (Figure B.1) are given by

$$a = k_1\sqrt[3]{\frac{3WR'}{E'}} = 1.1\sqrt[3]{\frac{3 \times 1300 \times 0.01746}{4.711e9}} = 2.685mm$$

$$b = k_2\sqrt[3]{\frac{3WR'}{E'}} = 0.91\sqrt[3]{\frac{3 \times 1300 \times 0.01746}{4.711e9}} = 2.221mm$$

The maximum contact pressure at the center of the contact region is given by

$$p_{max} = \frac{3W}{2\pi ab} = \frac{3 \times 1300}{2\pi \times 0.002685 \times 0.002221} = 104.1MPa$$

The maximum shear stress is then given by

$$\tau_{max} = k_4 p_{max} = 0.32 \times 104.1 = 33.3MPa$$

B.2 Drive-wheel Hub Bolt

The holes for the three hub bolts to connect the disc brake to the hub of the chosen drive wheel is shown in Figure B.2. The torque applied to the drive wheel from the brake is t. The shear force on each of the bolts in one plane of shearing is V. The bolt steel is assumed to be of the properties of 4.6/6 bolting category of the minimum tensile strength $f_{uf} = 400MPa$. The radius of each hub bolt from the center of rotation is $r = 20mm$.

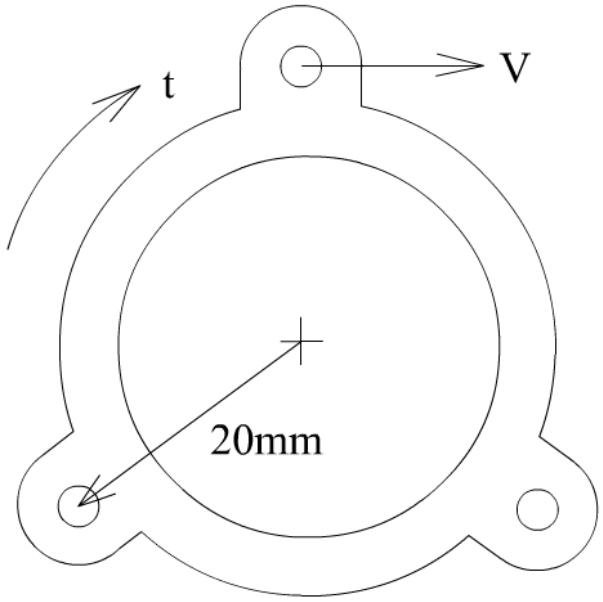

Figure B.2: The three hub bolts on the rim of the mini-moto drive wheels

From Australian Standard of Steel Structures (AS 4100) . the design sheer capacity is given as

$$\phi V = \phi 0.62 f_{uf} k_r (n_n A_c + n_x A_o)$$

Where:

- For a lap length of less than 300mm $k_r = 1$
- There are $n_n = 0$ shear planes through the thread

- There are $n_n = 1$ shear planes through the shank of area $A_c = 12.566mm^2$
- The design capacity factor is $\phi = 0.8$

The design capacity of each bolt is then

$$\phi V = 0.8 \times 0.62 \times 400 \times 1 \times (1 \times 12.566) \approx 2.49kN.$$

When applied to the three hub bolts there is a design torque capacity of

$$t = 3Vr = 3 \times 2490 \times 0.02$$

$$\Rightarrow t \approx 150Nm.$$

When compared to the motor torque and maximum braking torque of approximately 14Nm and 10Nm respectively the hub bolts seem adequate.

B.3 Mechanical Design Dynamic Analysis

To initially estimate the distance of the center of gravity from the center of rotation of the diwheel, a simplistic energy approach can be undertaken by assuming that all of the diwheel's kinetic energy traveling at 8km/hr is converted into potential energy in inverting the passenger by locking the brakes. The following terms are used in this calculation.

- Estimating the masses of the wheels to be: $m_w = 40kg$, and frame and passenger: $m_F = 200kg$, giving a total mass of $m_t = 240kg$
- KE_t is the total kinetic energy of the diwheel
- KE_{rotat} is the rotational kinetic energy of the outer wheels
- KE_{trans} is the total translation kinetic energy of the diwheel
- KE_F is the translational kinetic energy of the inner frame
- KE_W is the translational kinetic energy of the outer wheels
- $v = 8km/hr = 8/3.6m/s = 2.22m/s$ is the translational speed of the diwheel
- $R = 0.75$ is the radius of the outer wheels
- I_W is the moment of inertia of the outer wheels: $I_W = m_W R_W^2 = 40 \cdot 0.75^2 = 22.5kgm^2$
- PE is the gravitational potential energy of the inner frame
- h_c is the distance of the center of gravity from the center of rotation of the diwheel

The total kinetic energy is given by

$$KE_t = KE_{rotat} + KE_{trans} = KE_{rotat} + (KE_F + KE_W)_{trans}.$$

Which in a braking situation is converted to potential energy

$$PE = m_t \cdot g \cdot h_c$$
$$\Rightarrow KE_{rotat} + (KE_F + KE_W)_{trans} = PE$$
$$\Rightarrow \frac{1}{2} I_W \omega_W^2 + \left(\frac{1}{2} m_F v^2 + \frac{1}{2} m_W v^2\right)_{trans} = m_t \cdot g \cdot h_c$$
$$\Rightarrow h_{cg} = \frac{1}{m_t g}\left(\frac{1}{2} I_W \omega_W^2 + \left(\frac{1}{2} m_F v^2 + \frac{1}{2} m_W v^2\right)_{trans}\right)$$
$$\Rightarrow h_{cg} = \frac{1}{240 \times 9.81}\left(\frac{1}{2} \times 22.5 \times (2.22/0.75)^2 + \left(\frac{1}{2} 200 \times 2.22^2 + \frac{1}{2} 40 \times 2.22^2\right)_{trans}\right)$$
$$\Rightarrow h_{cg} = 0.294m.$$

With the center of gravity at this location, a locked braking situation at this speed will fully invert the diwheel into an unstable equilibrium which is then subject to control. The mechanical losses in the constructed diwheel wheel reduce it's ability to roll and so a greater speed will be needed to invert. This value is not a final goal and must be compromised with design restrictions of geometry and dynamic requirements.

The dynamics driving the design of the width between wheels of the diwheel is a worse case yawing situation. If one wheel locks and the diwheel yaws about this wheel, then a centrifugal force created from this rotation must balance with the weight of the diwheel to keep both wheels on the ground. The distance of the center of gravity from the center of rotation of the diwheel is estimated to be $h_c = 0.3m$ and the width of the Di-wheel is l. Other parameters used in the following calculation are shown in Figure B.3. If we assume that

- The translational velocity of the diwheel is $v = 10km/hr = 10/3.6m/s = 2.778m/s$
- The total mass of the diwheel is $m_T = 240kg$
- The weight of the diwheel is $w = m_T g$
- Centrifugal force of the diwheel about the locked wheel is F_c

The centripetal force around the locked wheel applied at the center of gravity is given by

$$F_c = \frac{m_t v^2}{l/2} = \frac{240 \times (\frac{10}{3.6})^2}{l/2} = \frac{3704}{l}.$$

If we take the moments around the point A (see Figure B.3)

$$\sum M_A = w \times \frac{l}{2} - F_c \times \left(\frac{R}{2} - h_c\right) = 0$$

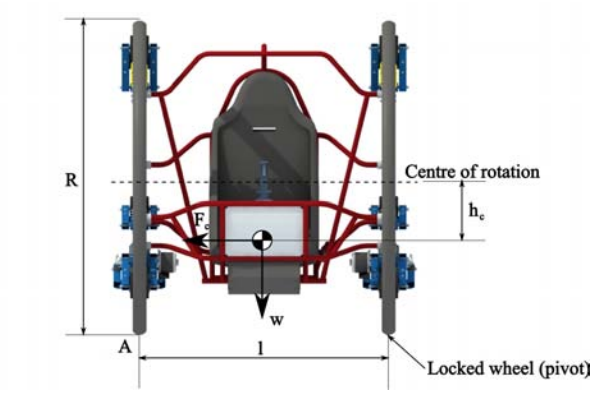

Figure B.3: Front view of EDWARD in a locked braking situation

$$\Rightarrow w \times \frac{l}{2} - \frac{3704}{l} \times \left(\frac{R}{2} - h_c\right) = 0$$

$$\Rightarrow l = \sqrt{2 \times \frac{F_c l}{m_T g} \times \left(\frac{R}{2} - h_c\right)} = \sqrt{2 \times \frac{3704}{240 \times 9.81} \times \left(\frac{1.5}{2} - 0.3\right)}$$

$$\Rightarrow l = 1.19m.$$

Therefore, for the worst case yawing situation, a width of $l = 1.2m$ will prevent the diwheel from losing contact to the ground with one of its wheels. This value was used as an initial estimate of the width of the diwheel. The width is not restricted to be greater than 1.2m in order to prevent tipping the diwheel on it's side, rather, it is only to prevent the loss of traction between one of the wheels and the ground. The width is also subject to space limitations and requirements.

B.4 Anthropometrics

There exist few available anthropometric databases for civilians due to vast population sizes and the lack of measurement techniques (Karwowski 2006). However, there exist anthropometric data for some selected groups. For example, extensive databases are maintained for military populations. An appropriate set of anthropometric data may be crucial for certain design situations, especially where safety is a factor. Therefore in order to select an appropriate database one must consider the possible user population and the data's application to the required design. For the design of the diwheel a comprehensive database has been selected from NASA's Man-Systems Integration Standards (Christensen et al. 1995). This database is free, unlike the many ISO and military anthropometric data sets, and comprehensive, representing a wide population of male and female 40 year old persons. Dimensions of the human form used from this document can be seen Figure B.4. The dimensions used in the design of the space frame are given in Table B.1 with reference to the numbers labeling the dimensions defined in Figure B.4.

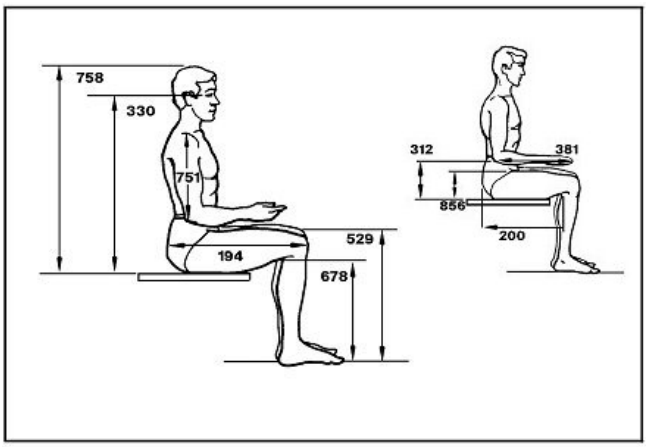

Figure B.4: Anthropometric dimensions and reference numbers for a male (Christensen et al. 1995)

Table B.1: Anthropometric measurements of various dimensions shown above of a 40 year old male (Christensen et al. 1995)

No.	Dimension	5th percentile (cm(in))	50th percentile (cm(in))	95th percentile (cm(in))
758	Sitting height	88.9 (35.0)	94.2 (37.1)	99.5 (39.2)
194	Buttock-knee length	56.8 (22.4)	61.3 (24.1)	65.8 (25.9)
529	Knee height, sitting	52.6 (20.7)	56.7 (22.3)	60.9 (24.0)
312	Elbow rest height	21.1 (8.3)	25.4 (10.0)	29.7 (11.7)
457	Hip breadth	32.7 (12.9)	35.8 (14.1)	39.0 (15.4)
223	Chest breadth	29.7 (11.7)	33.2 (13.1)	36.7 (14.4)
362	Foot length	25.4 (10.0)	27.3 (10.8)	29.3 (11.5)
356	Foot breadth	9.0 (3.6)	9.9 (3.9)	10.7 (4.2)
	Mass	65.8 kg	82.2 kg	98.5 kg

C FMEA, Risk Analysis and SOP

Failure Mode, Effects, and Criticality Analysis for the Diwheel

Project: Diwheel (Edward)

Supervisor: Benjamin Cazzolato

Symbols and abbreviation

S: Severity Rating from 1(no danger) to 10(important)

O: Occurrence Rating from 1 to 10

D: Detection Rating. This number represents the ability of planned tests and inspections at removing defects or detecting failure modes

CRIT: Criticality = S x O

RPN: Risk Priority Number = S x O x D

Function	Failure Mode	Effect of Failure	S	Potential Causes of Failure	O	Current Process Controls	D	CRIT	RPN	Recommended Actions
Outer Wheel Ring	Outer wheel ring deform excessively	Excessive deformation of outer ring structure can cause severe vibration of inner frame. Inner frame jams if the ring has poor circularity.	10	Excessive load on the inner frame or poor travelling surface condition	1	Design load is bigger than actual applied load. Include safety factor. Aviod operating on rough surface	1	10	10	Retain wheel circularity
	Out Side rubber surface demage	Decrease on max friction force Slip while turning or braking	8	Poor road condition. Oxidition. Rubber-metal bonding failure.	3	Aviod operating on bumpy surfacc Store in cool place	1	24	24	Fix rubber coating. Give enough time for glue to form adequate bond force.
Iner Rotation Frame	Too much deflection on SHS	Distortion of all frame components. Casters lose contact with outer wheel.	7	Excessive load on the inner frame or poor travelling surface condition.	1	Introduce design load and safety factor.	1	7	7	Straighten over-bent members or replace if necessary
	Butt weld failure	Structure failure and possible injuries.	10	Excessive load or unflat travelling surface	3	Regular inspections on all weld connections.	2	30	60	Reweld or use bolt connection instead.
	Bolt connection failure	Structure failure and possible injuries.	10	Excessive load or unflat travelling surface	1	Use friction connection principle	1	10	10	Change to stronger bolts or introduce reinforcement bars.
Joining Frame	Butt weld failure	Structure failure and possible injuries.	10	Excessive load or unflat travelling surface	3	Regular inspections on all weld connections.	2	30	60	Reweld or use bolt connection instead.
	Bolt connection failure	Structure failure and possible injuries.	10	Excessive load or unflat travelling surface	1	Use friction connection principle or introduce reinforcemet	1	10	10	Change to stronger bolts or introduce reinforcement bars.
Casters	Bearing failure	Severe vibration while running. Caster wheels fall off the wheel shaft.	8	Load excedes bearing's design load or inapproprite bearing type is used	3	Carefully select approperite bearing type for the job and install with correct method.	2	24	48	Replace damaged component and check whether the design is suitable or not.
	Caster arm weld failure	Inner stucture losses support and could fall out if the broken caster is at critical location	10	Load is excessive or sudden impact force such as running onto a kerb with very high speed	3	Regular inspections on welds and fix existing cracks	2	30	60	Reconnect broken parts with stronger welds or add reinforcement bars.
	Caster suspension fail	Caster loss contact with wheel	10	Spring stiffness is too low. Springs not locked in place.	2	Insure springs are strong enough and firmly in place.	1	20	20	Select stronger springs or use more in parallel.

Function	Failure Mode	Effect of Failure	S	Potential Causes of Failure	O	Current Process Controls	D	CRIT	RPN	Recommended Actions
Drive system (exclude motor)	Gears loss mesh	Causes partial or total loss of mechnical power and maybe unable to hold inner frame in place while operating in up side down condition. Generate noise.	9	Gear bearing failure. Gear shafts are not in right position. Gear wear out. Gearbox cover is loose and shafts slip out from bearing holes.	2	Tighten bolts and screws on gearbox. Regular inspection. Limit mechnical power in put so gears are not overloaded and slip	2	18	36	Change gears if they worn out. Tighten bolts and screws. Replace damaged bearings. Check if the failure is caused by design faults.
	Driving wheel slip	Causes partial loss of mechnical power. Outside rubber material wears quicker.	7	Wheel suspension is unable to provide enough contacting force for the driving wheel to transmit all motor power to outer wheel. Driving wheel rubber doesn't provide enough friction force.	3	Keep wheel surfaces (both outer wheel and drving wheel) clean and free of lubricating oil. The design actuating suspension force is more than enough to generate adequate friction force for motor.	1	21	21	Clean wheel contacting surfaces. Replace suspension springs with stronger ones if necessary. Coat inside of outer wheel with rubber if the above two didn't work.
	Drive system mounting failure	Driving wheel derail. Completely loss of mechnical power. Possible damage of motor.	6	Over deformed by unknown external force.	1	To be operated by authorized personel only.	1	6	6	Disassemble and fix or replace the damaged part.

PROJECT RISK ASSESSMENT:

This form is to be completed in conjunction with the Plant Hazard Identification Form and in accordance with the Hazard Management Policy/Procedure and Plant and Equipment Safety Management Policy/Procedure.

Overall risk rating (existing controls) highest score eg L, M, VH, H	**HIGH**

STEP 1: ENTER INFORMATION ABOUT THE ITEM OF PLANT/EQUIPMENT, IT'S LOCATION AND THE PEOPLE COMPLETING THE RISK ASSESSMENT

Campus	**School/Branch**	**Building**	**Room**	
North Terrace	School of Mechanical Engineering	Engineering South	Student & Mechanical Engineering Workshops.	**Date assessed:** 11/10/09
Plant (Include name and model) [i]	EDWARD (Electric) Di-Wheel			**Review date: 15/10/09**
Purpose of Plant	Honours student project-vehicle for driving and testing control structures			

AFFIX PHOTO HERE

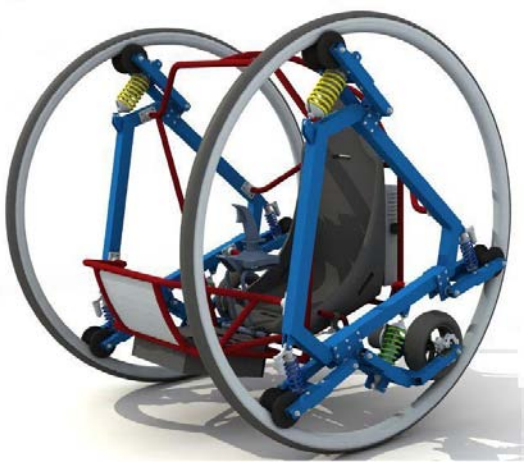

REGISTRATION/LICENCES/ COMPETENCIES
(Refer Appendix B)

Registration required?
☐ **Yes**
☒ **No**

Licence/ Trade certificate required?
☐ **Yes**
☒ **No**

Supervisor assessment required? (Induction required for this plant)
☒ **Yes**
☐ **No**

Other competency required?
☒ **Yes**
☐ **No**
Include in Safe Operating Procedure

LEGISLATION

OHS Legislation and/or Australian Standard to be used for further reference.
OHS Regulations (1995) Divisions:
- 1.2 OHS Responsibilities
- 1.3 Information, Instruction, Training, Induction, Supervision
- 2.10 Noise
- Part 3 Plant (including)
  - 3.2.25 Plant with moving parts
  - 3.2.15 Hazard Management
  - 3.2.17 Control of risk

AS 4024 - 2006 Safety of machinery
AS 1788 Abrasive wheels
AS 60204.1 electrical equipment for industrial machines

RISK ASSESSMENT TEAM

Operator: All project members

HSO/Manager: Tao Zhu

HSR: Tao Zhu

Other:

Other:

Risk assessment rating and action required endorsed by Head of School/Branch (see also Step 3)

11 / 10 / 09

朱涛

(Signature) **Tao Zhu** **(Name)**

Project No: 757 **Issue No: 1**

THE UNIVERSITY OF ADELAIDE AUSTRALIA

PROJECT RISK ASSESSMENT:

THE UNIVERSITY OF ADELAIDE AUSTRALIA

PROJECT RISK ASSESSMENT:

LEGEND		
❑ El = Elimination ❑ Su = Substitution ❑ En = Engineering	❑ Is = Isolation ❑ Ad = Administration ❑ PPE = Personal Protective Equipment	❑ CAR = Corrective Action Register

Hazard Identified	Likelihood	Consequence	Score	Comments (i.e. when and where hazard is present, task/activity)	Hierarchy of Control	Current Controls	Action Required? Y / N	Tfr to CAR Y / N
Can the following items become entangled (eg in moving parts)?								
☒ Yes (e.g. Hair, Jewellery, Clothing, Cleaning aids (cloth), Gloves or Other_____ ☐ No ☐ NA	Unlikely	First Aid	Low	Hair, Jewellery or Clothing may be entangled by the sprockets and chains	☐ El ☐ Su ☐ En ☐ Is ☒ Ad ☐ PPE	Requirements for operators • Clothing must be tight fitting • Long hair must be confined close to the head by an appropriate restraint • Finger rings and exposed loose jewellery (eg bracelets and necklaces) must not be worn. Medic Alert bracelet must be taped if exposed	N	NA
Are Emergency Stop buttons adequate?								
☒ Yes (within easy reach and clearly marked) ☐ No ☐ Other issues_____ ☐ NA	NA	NA	NA	Two Emergency Stop buttons are installed. One manually activated Stop button under joystick controller. One automatic micro switch on mechanical brake.	☐ El ☐ Su ☒ En ☐ Is ☐ Ad ☐ PPE	Emergency Stop buttons are tested before all operations.	N	NA

THE UNIVERSITY OF ADELAIDE AUSTRALIA

PROJECT RISK ASSESSMENT:

Hazard Identified	Likelihood	Consequence	Score	Comments (i.e. when and where hazard is present, task/activity)	Hierarchy of Control	Current Controls	Action Required? Y / N	Tfr to CAR Y / N
Can anyone be crushed by:								
☒ Plant falling or unexpected movement of the plant eg ☐ Tipping ☐ Falling ☐ Rolling over ☒ Rolling forward ☐ The plant's load ☐ Under/between plant and a structure eg wall ☐ Inability to apply brake ☐ Falling off the plant ☐ Part of the plant collapsing/changing shape ☐ Other issues _____ ☐ No ☐ NA	Possible	Major	High	Incidents may happen if people are around the diwheel while it is running. First aid or medical treatment may be required.	☐ El ☐ Su ☐ En ☐ Is ☒ Ad ☐ PPE	The Diwheel is only operated at open space where no unauthorized people are close by.	N	NA
Can anyone be cut, stabbed or punctured, amputated by coming into contact with:								
☒ Moving plant or parts ☐ Sharp or flying objects ☐ Work pieces ejected ☐ Work pieces disintegrating ☐ Other issues_____ ☐ No ☐ NA	Possible	First Aid	Medium	Only a few sharp edges present and protective guards are installed. Unlikely to cause any major injuries.	☐ El ☐ Su ☒ En ☐ Is ☐ Ad ☐ PPE	Protective guards are designed and applied on idler wheel pinch points.	N	NA

THE UNIVERSITY OF ADELAIDE AUSTRALIA

PROJECT RISK ASSESSMENT:

Hazard Identified	Likelihood	Consequence	Score	Comments (i.e. when and where hazard is present, task/activity)	Hierarchy of Control	Current Controls	Action Required? Y / N	Tfr to CAR Y / N
Can anyone be injured from an electrical shock?								
☐ Water near equipment ☐ Plant located near or in contact with exposed live electrical conductors ☐ Leads/switch in poor condition ☐ Overhead and underground wires ☐ Other issues_____ ☒ No ☐ NA	NA	NA	NA	Power source is only 12V batteries	☐ El ☐ Su ☐ En ☐ Is ☐ Ad ☐ PPE	NA	N	NA
Can anyone be injured by an explosion?								
☐ Gas ☐ Vapour ☐ Dust ☐ Liquid ☐ Other issues _____ ☐ No ☒ NA					☐ El ☐ Su ☐ En ☐ Is ☐ Ad ☐ PPE			
Can anyone be burnt due to Friction?								
☐ Contact with moving parts or surface of the plant ☐ Material handled by the plant ☐ Other issues _____ ☐ No ☒ NA					☐ El ☐ Su ☐ En ☐ Is ☐ Ad ☐ PPE			

THE UNIVERSITY OF ADELAIDE AUSTRALIA

PROJECT RISK ASSESSMENT:

Hazard Identified	Likelihood	Consequence	Score	Comments (i.e. when and where hazard is present, task/activity)	Hierarchy of Control	Current Controls	Action Required? Y / N	Tfr to CAR Y / N
Can anyone be struck by moving objects due to:								
☐ Plant/materials being ejected ☒ Plant/material movement ☐ Other issues _____ ☐ No ☐ NA	Unlikely	Minor	Low	All components are moving at low speed. No serious injury will occur	☐ El ☐ Su ☐ En ☐ Is ☒ Ad ☐ PPE	No contact is allowed with the running diwheel (except the operator) while it is running	N	NA
Can anyone suffocate due to:								
☐ Lack of oxygen ☐ Atmospheric contamination ☐ Engulfment ☐ Other issues _____ ☐ No ☒ NA					☐ El ☐ Su ☐ En ☐ Is ☐ Ad ☐ PPE			
Can anyone be burnt due to:								
☐ High/low temperature ☐ Naked flame ☐ Steam ☐ Laser beams ☐ Other issues _____ ☐ No ☒ NA					☐ El ☐ Su ☐ En ☐ Is ☐ Ad ☐ PPE			

THE UNIVERSITY OF ADELAIDE AUSTRALIA

PROJECT RISK ASSESSMENT:

Hazard Identified	Likelihood	Consequence	Score	Comments (i.e. when and where hazard is present, task/activity)	Hierarchy of Control	Current Controls	Action Required? Y / N	Tfr to CAR Y / N
Can anyone be affected by temperature extremes?								
☐ Exposure to high temperature ☐ Exposure to low temperature ☐ Other issues _____ ☐ No ☒ NA					☐ El ☐ Su ☐ En ☐ Is ☐ Ad ☐ PPE			
Can anyone slip, trip or fall due to:								
☐ The location of the plant ☐ Uneven work surfaces ☐ Lack of safe guards (eg rails) ☐ Slippery work surfaces ☒ Other issues: Inside frame rotation ☐ No ☐ NA	Unlikely	Major	Medium	Incidents may happen if belts are not applied properly.	☐ El ☐ Su ☐ En ☐ Is ☐ Ad ☐ PPE	Belts are inspected before every operation.	N	NA
Can anyone come into contact with Fluids or Gases under high pressure due to:								
☐ Failure of the plant ☐ Nature of the plant ☐ Other issues _____ ☐ No ☒ NA					☐ El ☐ Su ☐ En ☐ Is ☐ Ad ☐ PPE			

THE UNIVERSITY OF ADELAIDE AUSTRALIA

PROJECT RISK ASSESSMENT:

Hazard Identified	Likelihood	Consequence	Score	Comments (i.e. when and where hazard is present, task/activity)	Hierarchy of Control	Current Controls	Action Required? Y / N	Tfr to CAR Y / N
Can anyone injured due to Ergonomic issues due to:								
☐ Repetitive body movement or posture ☐ Insufficient space ☐ Excessive effort (push/pull) ☐ Working at a height ☐ Seating design ☐ Poor lighting ☐ Other issues _____ ☐ No ☒ NA					☐ El ☐ Su ☐ En ☐ Is ☐ Ad ☐ PPE			
Can anyone be injured or suffer ill health from exposure to other hazards?								
☐ Chemicals ☐ Radiation ☐ Fumes ☐ Dusts ☐ Vibration ☐ Noise ☐ Toxic gases or vapours ☐ Other issues _____ ☐ No ☒ NA					☐ El ☐ Su ☐ En ☐ Is ☐ Ad ☐ PPE			

THE UNIVERSITY OF ADELAIDE AUSTRALIA

PROJECT RISK ASSESSMENT:

Hazard Identified	Likelihood	Consequence	Score	Comments (i.e. when and where hazard is present, task/activity)	Hierarchy of Control	Current Controls	Action Required? Y / N	Tfr to CAR Y / N
Does the plant generate significant environmental hazards								
☐ Energy consumption ☐ Water consumption ☐ Hazardous waste ☐ Hazardous emissions ☐ Nuisance noise ☐ Produce ignition to the surrounding area ☐ Other issues _____ ☐ No ☒ NA					☐ El ☐ Su ☐ En ☐ Is ☐ Ad ☐ PPE			

STEP 3: ACTION REQUIRED BY MANAGER/SUPERVISOR/AUTHORISED PERSON (Note: Sign off required by Head of School/Branch on Page 1)

☐ All action items have been transferred to the Corrective Actions Register (RMSS)

☒ If no actions required and residual risk is medium to very high, the activity and the hazard(s) have been transferred to the Hazard Register and communicated to the relevant personnel.

RISK ASSESSMENT TABLES

Likelihood Table

CATEGORY	DESCRIPTION
Almost Certain	Incident will occur at some time (0 – 1 month)
Likely	Incident could occur at some time (1 month – 1 year)
Possible	Incident is possible to occur (1 year – 2 years)
Unlikely	Incident is possible, but unlikely to occur (2 years – 5 years)
Rare	Cannot imagine that this could occur (over 5 years)

Consequences Table

CATEGORY	DESCRIPTION
Minor	Effects unlikely to last until the next day.
First Aid	Likely to affect employee the next day.
Major	Medical Treatment injury needs formal medical treatment
Critical	Injury requiring extensive medical treatment and/or hospitalization
Catastrophic	Injury resulting in death or permanent incapacity

Risk Score Calculator

Likelihood	Consequences				
	Minor	**First Aid**	**Major**	**Critical**	**Catastrophic**
Almost certain	Medium	High	High	Very High	Very High
Likely	Medium	Medium	High	High	Very High
Possible	Low	Medium	High	High	High
Unlikely	Low	Low	Medium	Medium	High
Rare	Low	Low	Medium	Medium	High

Risk Priority Table

Descriptor	Priority	Action
Very High	1	Immediate action required. The activity should cease immediately and short-term safety controls implemented. Notify Manager and assess activity.
High	2	Implement short-term safety controls immediately. Notify Manager and assess activity
Medium	3	Short-term safety controls implemented to minimise risk of injury. Notify Manager and assess activity. Corrective Actions within one month.
Low	4	Notify Manager and assess activity. Corrective Actions within three months (if possible).

SAFE OPERATING PROCEDURE: EDWARD DIWHEEL

LOCATION DETAILS

School/Branch: School of Mechanical Engineering

TASK/ACTIVITY

Operation of EDWARD Diwheel	**Date: 10th October 2009**

PREPARED BY Name, Position and Signature (insert names of the supervisor, HSR, HSO and operator involved)

Name	Position	Signature
Benjamin Cazzolato	Supervisor & Vehicle Operator	
Christopher Dyer	Vehicle Operator	
Evan Schumann	Vehicle Operator	
Jonathon Harvey	Team Leader & Vehicle Operator	
Kane Fulton	Vehicle Operator	
Tao Zhu	Vehicle Operator	

HAZARD IDENTIFICATION:	**RISK ASSESSMENT**
See Risk Assessment dated: 10 / 10 / 2009	**HIGH**

SAFE OPERATING PROCEDURE DETAILS

STOP

DO NOT OPERATE VEHICLE IF: (1)YOU HAVE NOT COMPLETED THE COMPULSORY UNIVERSITY OF ADELAIDE OCCUPATIONAL HEALTH AND SAFETY INDUCTION COURSE, AND (2)YOU ARE NOT UNDER THE DIRECT SUPERVISION OF A PROJECT SUPERVISOR.

Preparation – operating area check:

- ❑ Area is free from grease, oil, debris and objects, which can be tripped over.
- ❑ Area is clear of unauthorised people before commencing any operation.

Personal Attire & Safety Equipment:

- ❑ Clothing must be tight fitting.
- ❑ Long hair must be worn up, preferably using a hair-net.
- ❑ Finger rings and exposed loose jewellery (eg bracelets and necklaces) must not be worn. Medical Alert bracelet must be taped if exposed.

Controller layout

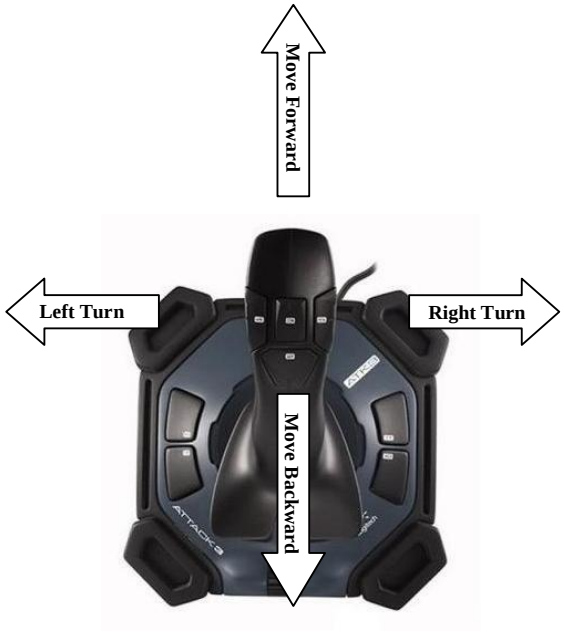

System self-diagnosis:

- ❑ Turn on the main switch.
- ❑ After 10 sec. read feedback information on control board LCD.
  Display: "All Test Passed" => All electronic and control states are normal.
  Display: "Test failed: (4 digit error code)" => Do not operate the vehicle and report the error code to project staff.
- ❑ Do not press START button at this stage.

Operation Of Emergency Stop Button:

- ❑ Fasten 5-Point driver seat safety belt/harness tightly after seated.
- ❑ Ask project staff to switch power on at the main switch on top of the electric box and start the vehicle.
- ❑ Press START button situated on the right side of the joystick controller.
- ❑ Moving the vehicle for a small distance by pushing the joystick SLIGHTLY FORWARD. (The 5 point safety belt must be worn during this process)
- ❑ Apply Emergency Stop Button and check that it is working correctly.
- ❑ Check that the mechanical brake Emergency Stop micro-switch is working.
- ❑ Release the Emergency Stop button in preparation for next Vehicle use.

Machine Pre-operational Safety Checks – Safety Precautions that MUST be Observed:

- ❑ Visual inspection of machine to verify it is in good operational order, ensuring no damage to any stationary or moving parts, electrical cords etc. Any unsafe equipment is to be reported to project supervisor, and other project members.
- ❑ Ensure that the 5 point safety belt/harness is worn tightly
  – WARNING: FAILURE TO PROPERLY APPLY SAFETY BELT MAY RESULT IN DEATH OR CRITICAL INJURY!
- ❑ Be aware of other activities happening in the immediate area.
- ❑ Ensure that no slip and/or trip hazards are present.
- ❑ Ensure that NO unauthorised personnel are close to the vehicle.
- ❑ Ask project staff to switch on the vehicle.
- ❑ Check that the Emergency Stop is working.
- ❑ Check that all machine guards, electrical interlocks and Emergency Stop micro-switch are correctly positioned, locked in place and in proper working condition.

IF IN DOUBT, ASK

Ensure:

- ❑ Knowledge of the location of Emergency Stop Button.
- ❑ Driver is aware of all functions of the joystick and controller buttons
- ❑ Driver is aware of the consequences of operating this vehicle at excessive speed.
- ❑ Driver is aware of the consequences of making sharp turns at high speed.
- ❑ Driver is aware of the consequences of locking the braking system.

Vehicle Operation:

- ❑ Do not switch on the main power before driver is seated and safely fastened into harness.
- ❑ Only operate vehicle in open areas, and ensure no unauthorised persons are within the operational area.
- ❑ Safety/harness belt is to be fastened at all times during operation.
- ❑ Never operate the vehicle at speed exceeding 15 km/h.
- ❑ Do not press any buttons for which the assigned functions are unfamiliar.
- ❑ **DO NOT** lock the brakes, unless unavoidable in an Emergency situation.
- ❑ Fast acceleration and deceleration is forbidden.
- ❑ **DO NOT** press stop button for normal braking purposes.
- ❑ **DO NOT** attempt to make contact with any moving parts.
- ❑ The swing-up function is only to be demonstrated by project staff, once supervisor is satisfied it is safe to do so.
- ❑ When stopping, at fully stopped condition, ask project staff to switch off main power before undoing the safety belt.

Operation of Brake:

- ❑ Press brake button for normal braking purpose.
- ❑ Mechanical brake is only to be used in Emergency conditions such as power failure or control malfunctioning. All power supply will be cut by applying mechanical brake.
- ❑ For both electric and mechanical braking systems, maximum braking efficiency is achieved when the centre of gravity is raised to the horizontal direction; where the seat back is parallel to the ground.
- ❑ Operator of Diwheel should be aware of the required braking distance at certain speeds. A schematic estimation of calculated minimum braking distances vs. travelling speeds is given in the following graph.

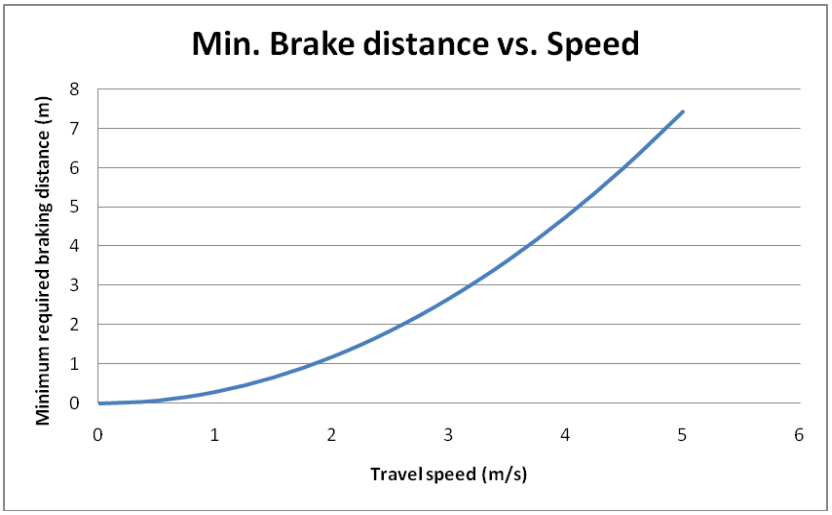

General Safety

- ❑ Visual inspection of plant prior to use. Unsafe plant to be tagged out and reported to Project Supervisor.
- ❑ Keep all parts of your body and attire safely clear of the rotating and moving parts, at all times.
- ❑ Ensure scheduled maintenance for this machine has been carried out; including scheduled testing of Emergency Stop.
- ❑ Only authorised and suitably qualified and competent persons to operate this machine.
- ❑ Guards must be correctly fitted to the machine at all times during operation. DO NOT attempt to open, or remove, guards while machine is being operated.
- ❑ Assistance from other project members to be sought when mounting and dismounting the vehicle.
- ❑ NEVER LEAVE EDWARD DI_WHEEL RUNNING WHILST UNATTENDED.
- ❑ Safety glasses must be worn at all times during the operation of this machine.
- ❑ Closed Toe Type Shoes must be worn during the operation of this machine.
- ❑ Loose hair to be securely tied back, loose clothing to be rolled up and/or secured, loose jewellery to be removed.
- ❑ Hearing protection to be worn, where appropriate to the task being performed.
- ❑ Leather Safety Gloves to be worn, where appropriate to the task being performed, and;
- ❑ Ensure feet, fingers and other body parts are kept clear of moving parts, and from pinch-points, during operation.
- ❑ Do not touch the electric motors after operation; allow time for them to cool down.
- ❑ Switch Off main switch of the vehicle before leaving it unattended.

Note: This Safe Operating Procedure must be reviewed:
a) after any accident, incident or near miss;
b) when training new staff;
c) if adopted by new work group;
d) if equipment, substances or processes change; or
e) within 1 year of date of issue.

D Mechanical Drawings

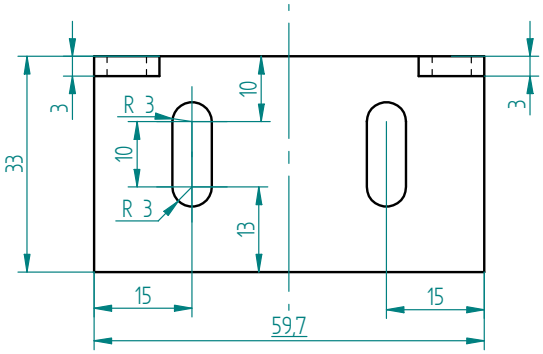

Please notice that the hole center distance need to be maintained at 50.5 mm to fit the brake calliper

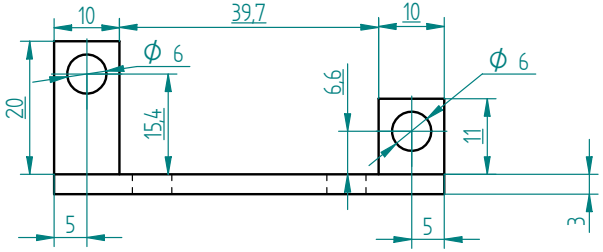

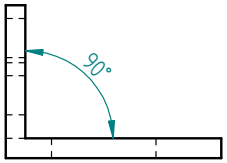

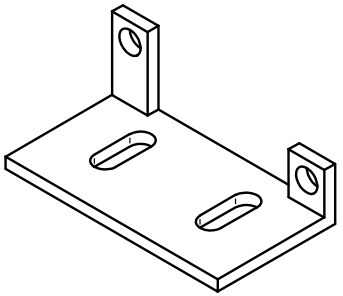

Item 1 Quantity 1

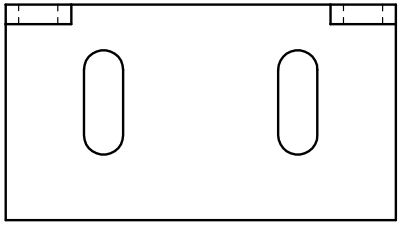

This item is exactly the same as above one except that fitting hole columns swaped places. refer to graph below

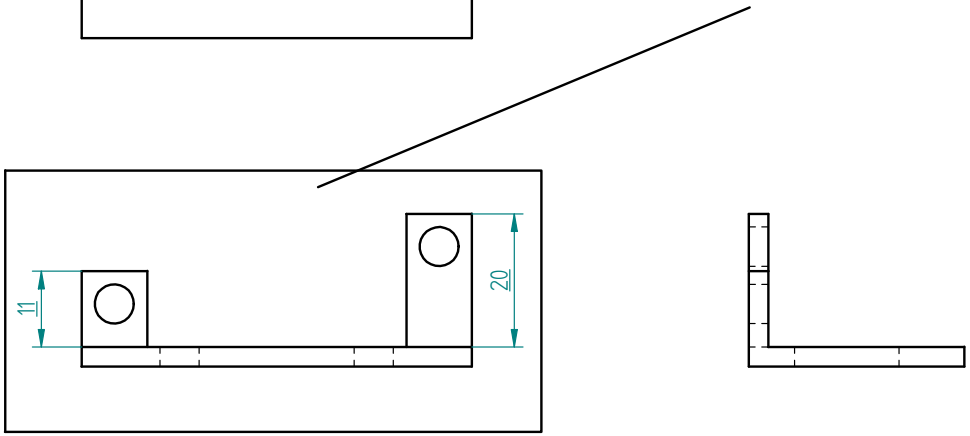

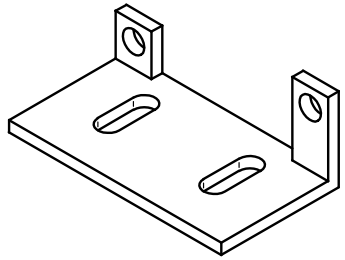

Item 2 Quantity 1

DRAWN	Charles	05/27/09
CHECKED	Ben Cazzolato	
CONTACT: 0413647219		
TOLERANCE ANGLES ±0.1° LENGTH ±0.1 UNLESS OTHERWISE SPECIFIED		

DIWHEEL WHEELBIKE
SUPERVISOR: Ben Cazzolato

TITLE : Brake calliper holder	Steel
SCALE: 1 : 1.3	QUANTITY: 1 for left and 1 for right

Material: all parts 8mm thick steel plate

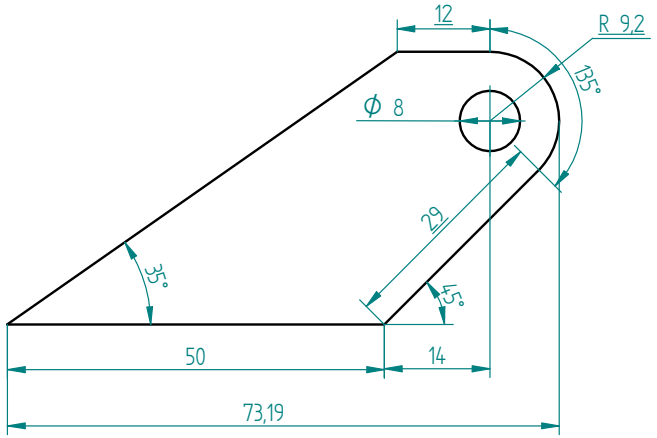

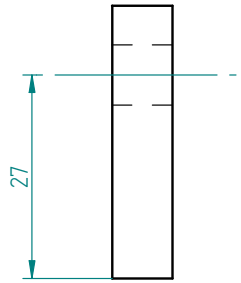

ITEM 1

Name: Damper fitting plate (top)
Quantity required: 4

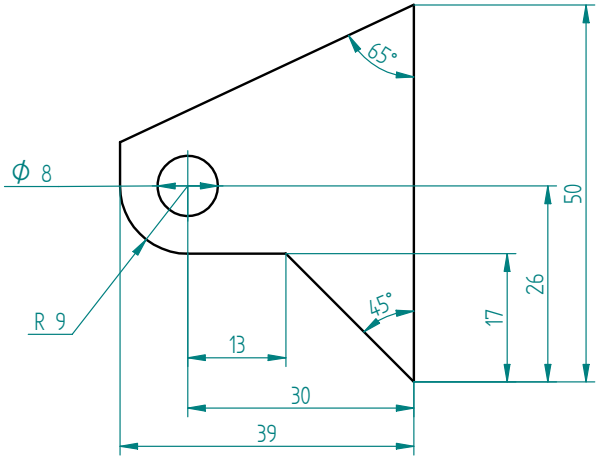

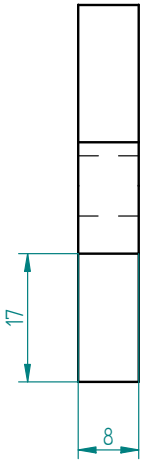

ITEM 2

Name: Damper fitting plate (sides)
Quantity required: 8

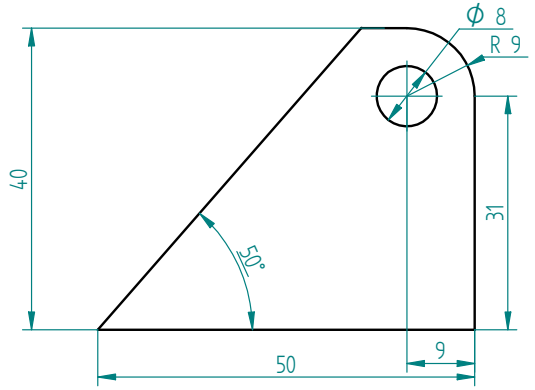

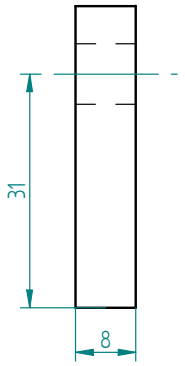

ITEM 3

Name: Damper fitting plate (bottom)
Quantity required: 4

DRAWN	Charles	05/26/09
CHECKED	Ben Cazzolato	
CONTACT: 0413647219		
TOLERANCE ANGLES ±0.1° LENGTH ±0.1 UNLESS OTHERWISE SPECIFIED		

DIWHEEL WHEELBIKE
SUPERVISOR: Ben Cazzolato

TITLE : Damper fitting plates (top sides and bottom)

SCALE: 1 : 1.5 | QUANTITY: top 4; sides 8; bottom 4.

Quantity: 4

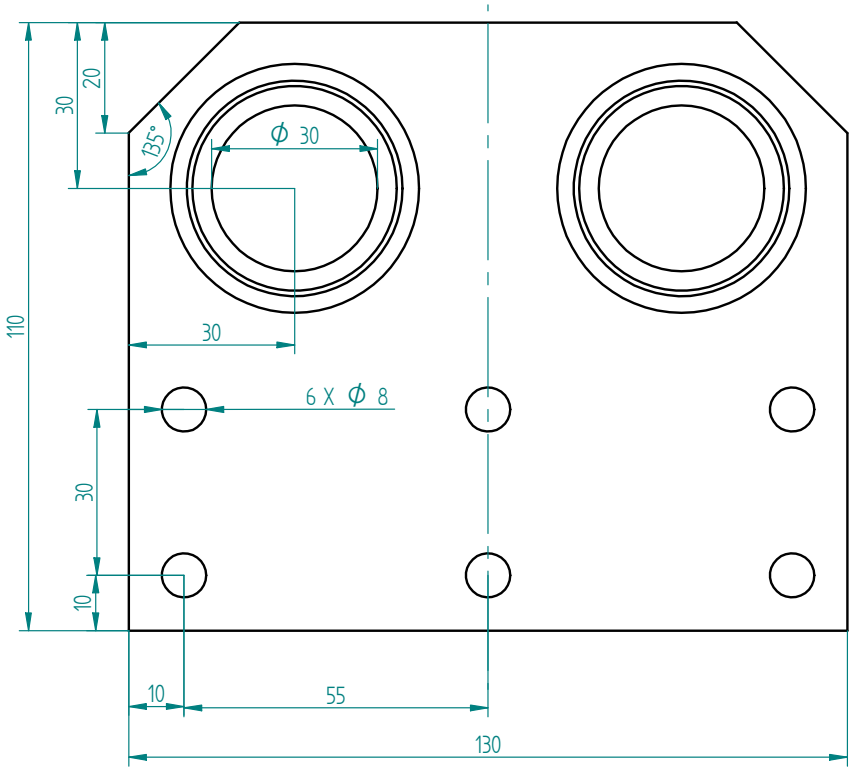

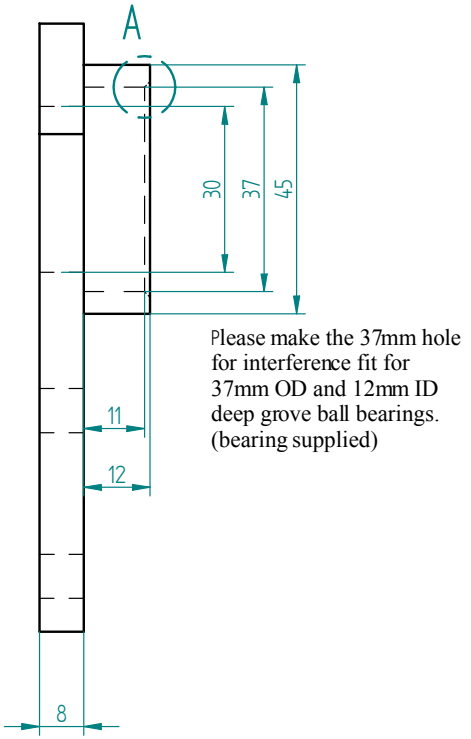

Please make the 37mm hole for interference fit for 37mm OD and 12mm ID deep grove ball bearings. (bearing supplied)

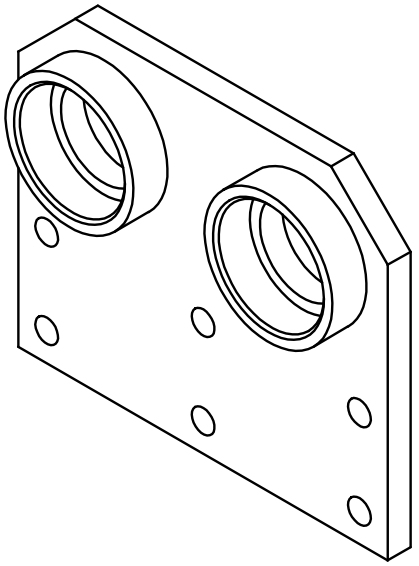

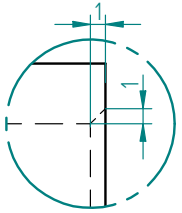

Chamfer with 1 mm setback

DETAIL A

DRAWN	Charles	05/26/09
CHECKED	Ben Cazzolato	
CONTACT: 0413647219		
TOLERANCE ANGLES ±0.1° LENGTH ±0.1 UNLESS OTHERWISE SPECIFIED		

DIWHEEL WHEELBIKE
SUPERVISOR: Ben Cazzolato

TITLE : Double bearing housing	Steel
SCALE: 1 : 1.1	QUANTITY: 4

Item	Quantity
Drive swing arm part 1	2
Drive swing arm part 2	1

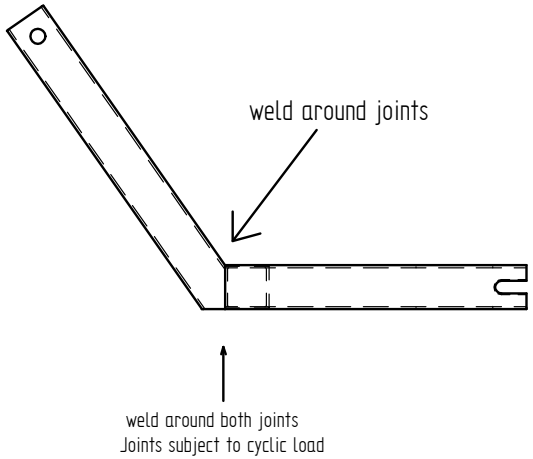

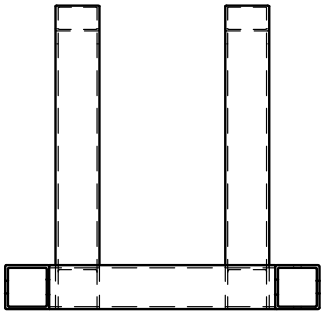

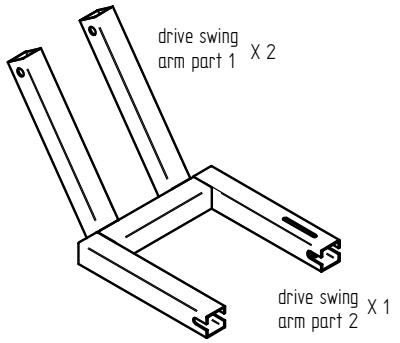

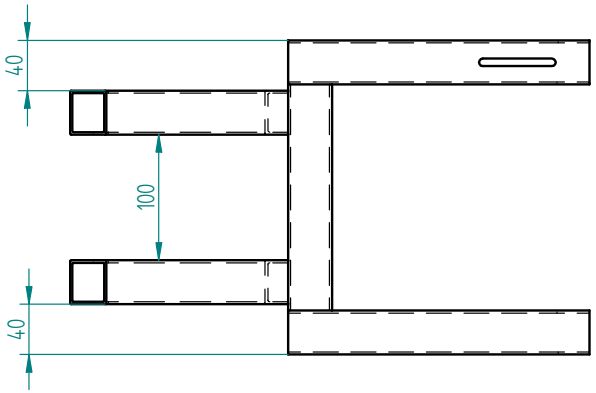

weld another Drive swing arm assembly with the "drive swing arm part 2" slot on the side. Shown in the graph below

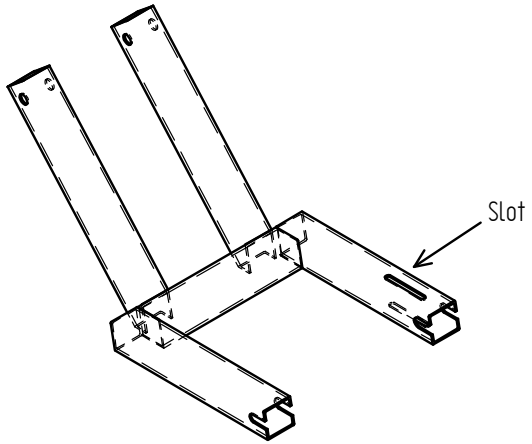

Quantity:
1 for slot on the left
1 for slot on the right

DRAWN	Charles	05/27/09
CHECKED	Ben Cazzolato	
CONTACT: 0413647219		
TOLERANCE ANGLES ±0.1° LENGTH ±0.1 UNLESS OTHERWISE SPECIFIED		

DIWHEEL WHEELBIKE
SUPERVISOR: Ben Cazzolato

TITLE : Drive swing arm assembly

SCALE: 1 : 0.25 | QUANTITY: 1 for left and 1 for right

make this item with 35mm side 3mm thickness steel SHS

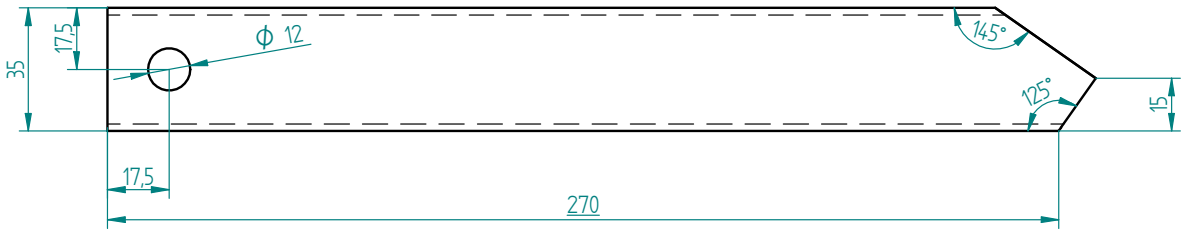

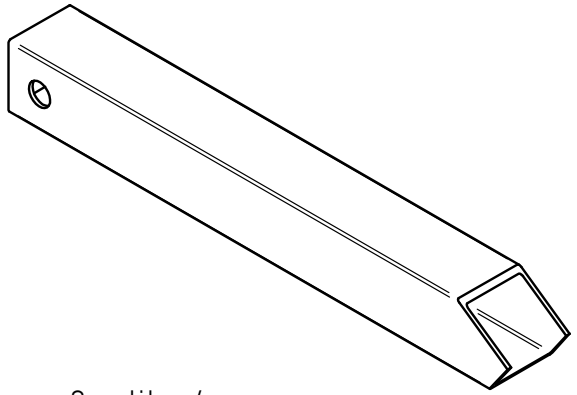

Quantity : 4

DRAWN	Charles	05/27/09
CHECKED	Ben Cazzolato	
CONTACT: 0413647219		
TOLERANCE ANGLES ±0.1° LENGTH ±0.1 UNLESS OTHERWISE SPECIFIED		

DIWHEEL WHEELBIKE
SUPERVISOR: Ben Cazzolato

TITLE : Drive swing arm part 1	Steel
SCALE: 1 : 0.7	QUANTITY: 4

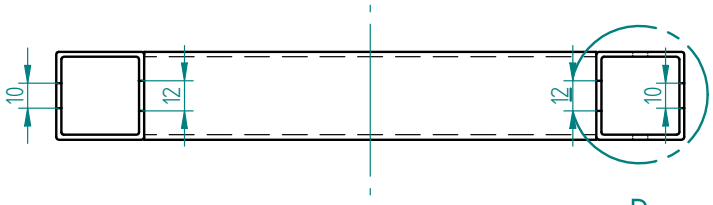

B

note that slots at the end of the parallel section are of different widths on two sides of the SHS. As shown in detail A&B.

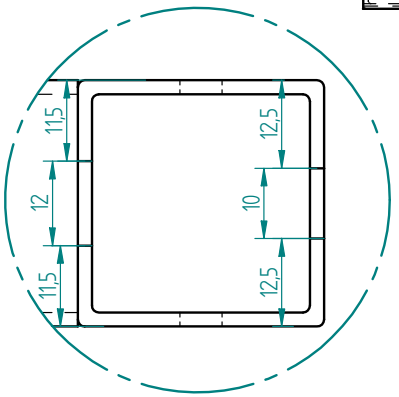

DETAIL B

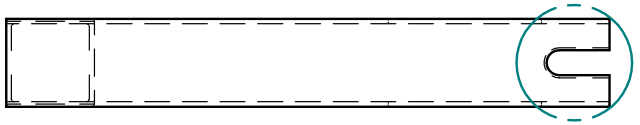

A

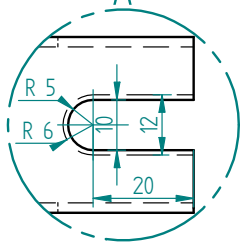

DETAIL A

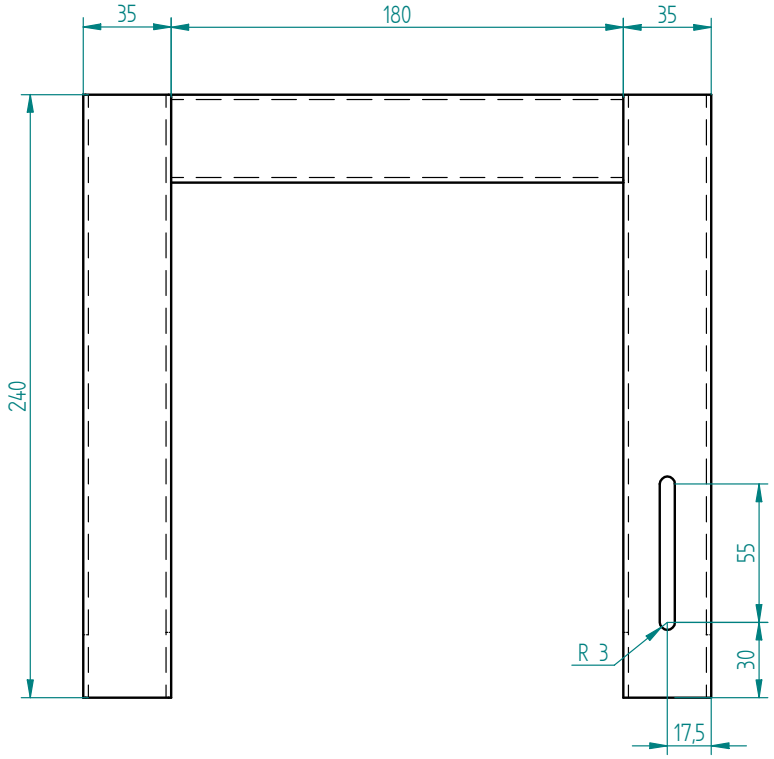

Please cut slot through the two sides of SHS

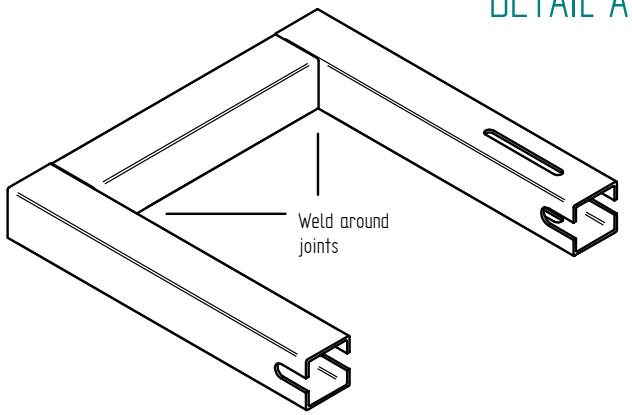

These sections are to be made with 35mm side 3mm thickness steel SHS. please weld the joints.

Quantity : 2

DRAWN	Charles	05/27/09
CHECKED	Ben Cazzolato	
CONTACT: 0413647219		
TOLERANCE ANGLES ±0.1° LENGTH ±0.1 UNLESS OTHERWISE SPECIFIED		

DIWHEEL WHEELBIKE
SUPERVISOR: Ben Cazzolato

TITLE : Drive swing arm part 2	Steel
SCALE: 1 : 0.5	QUANTITY: 2

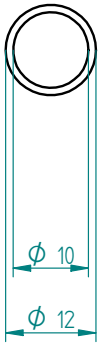

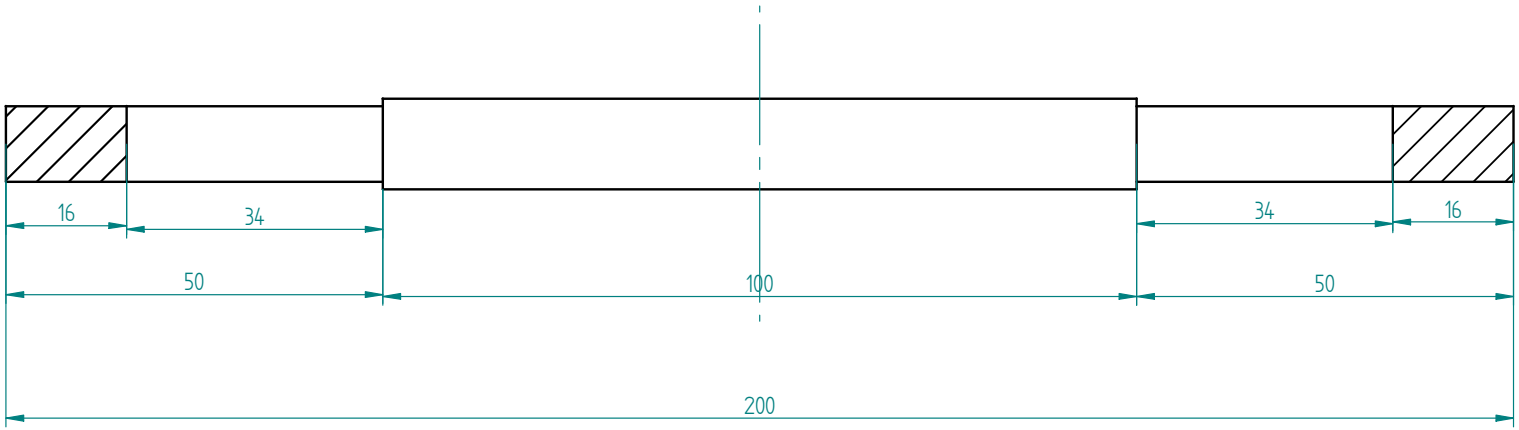

Shaded areas represent standard M10 threads.

Quantity : 14

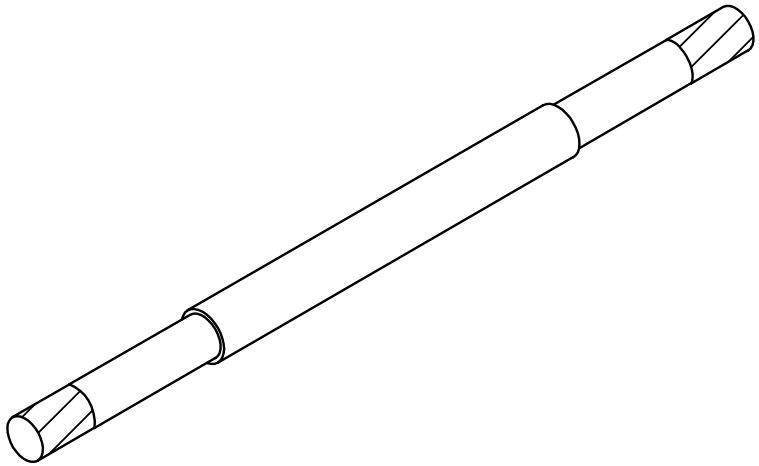

DRAWN	Charles	05/26/09
CHECKED	Ben Cazzolato	
CONTACT: 0413647219		
TOLERANCE ANGLES ±0.1° LENGTH ±0.1 UNLESS OTHERWISE SPECIFIED		

DIWHEEL WHEELBIKE
SUPERVISOR: Ben Cazzolato

TITLE : Idler wheel and suspension axial

SCALE: 1 : 1.5 | QUANTITY: 14

item	Quantity
Inner rotational frame memeber (short)	3
Inner rotational frame member (back)	1
Inner rotational frame member (front)	1
Inner rotational frame member (bottom)	1

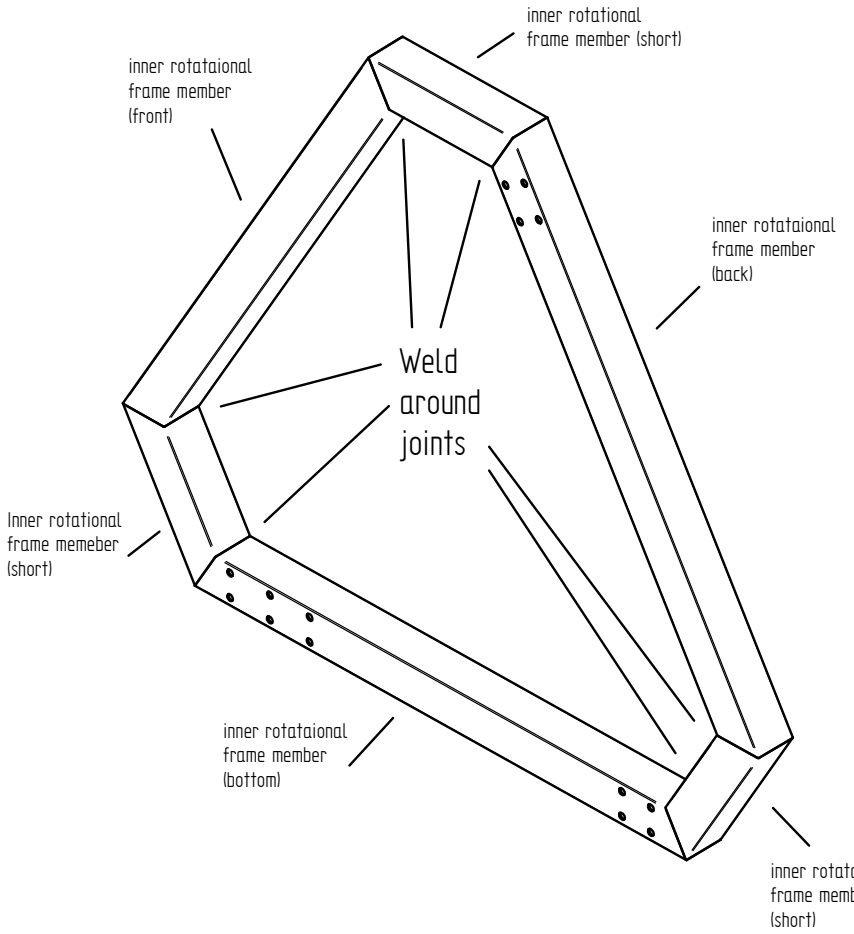

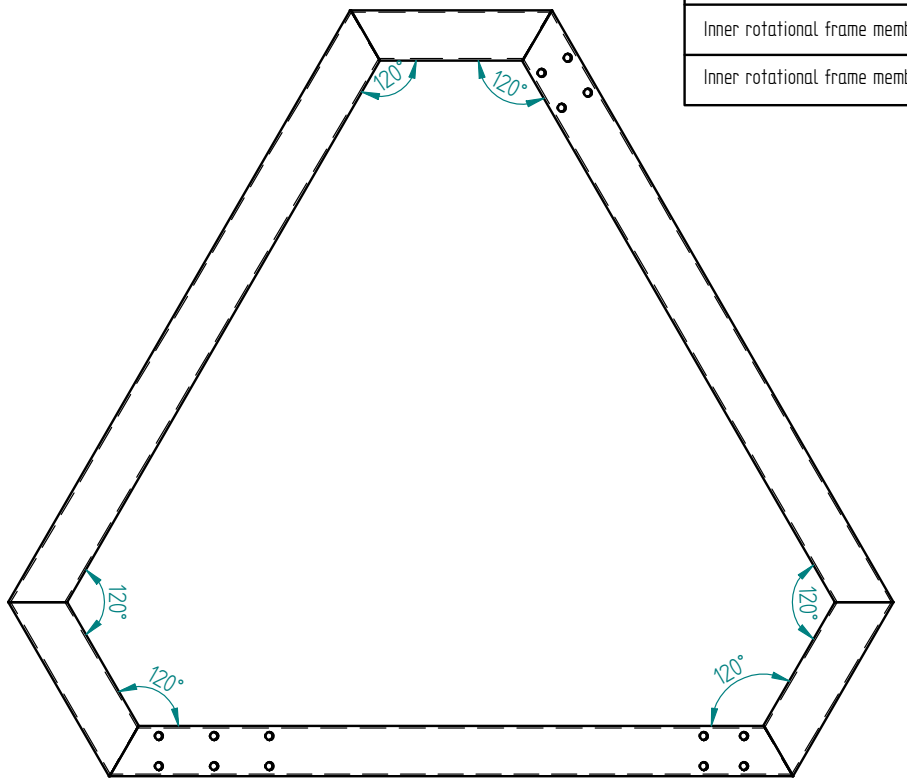

Weld all sections together as shown above, weld all around the joints if possible. please make sure holes are in the exact positions shown above.

Quantity of the frame assembly: 2

DRAWN	Charles	05/26/09
CHECKED	Ben Cazzolato	
CONTACT: 0413647219		
TOLERANCE ANGLES ±0.1° LENGTH ±0.1 UNLESS OTHERWISE SPECIFIED		

DIWHEEL WHEELBIKE
SUPERVISOR: Ben Cazzolato

TITLE : Inner ratational frame assembly 1

SCALE: 5 : 1 | QUANTITY: 2

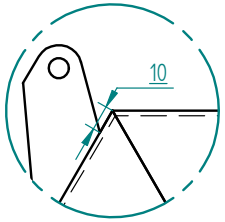

DETAIL C

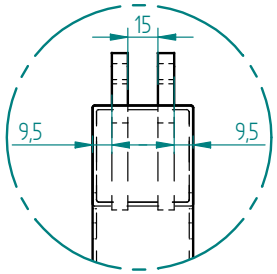

DETAIL E

Overview

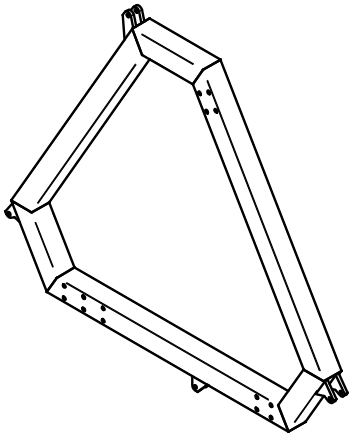

Item name	Quantity
Damper fitting (top)	2
Damper fitting (bottom)	2
Damper fitting (sides)	4
Inner rotational frame	1

All damper fittings are to be welded onto the main frame
Weld both sides fo each damper fitting plate

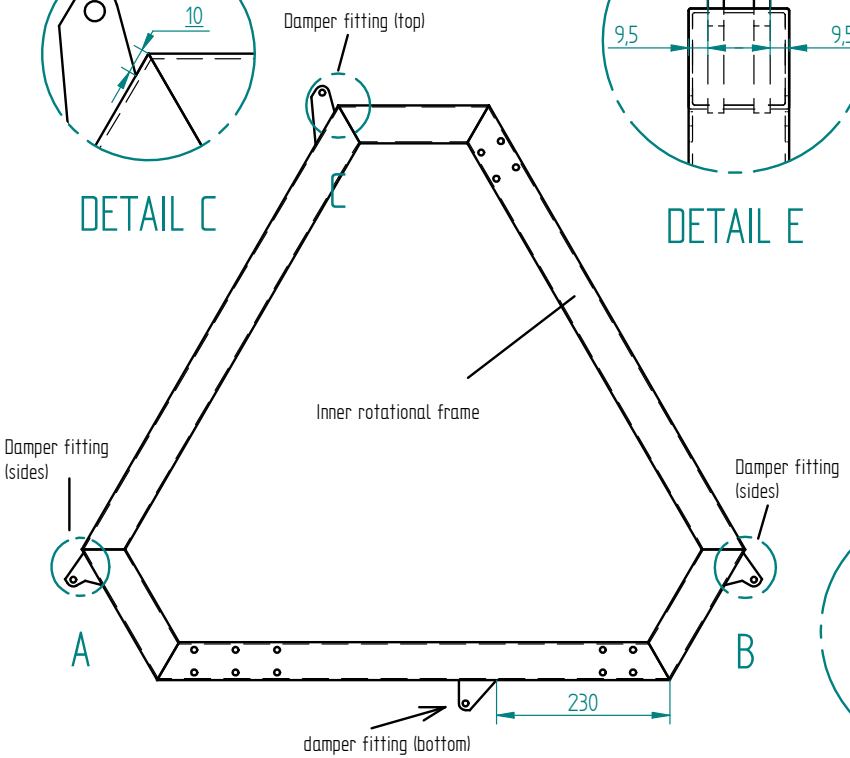

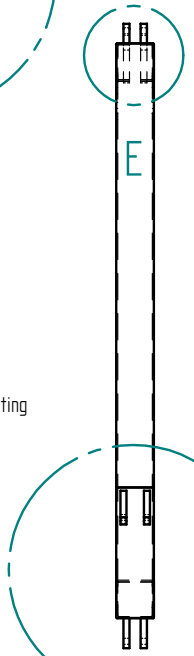

D

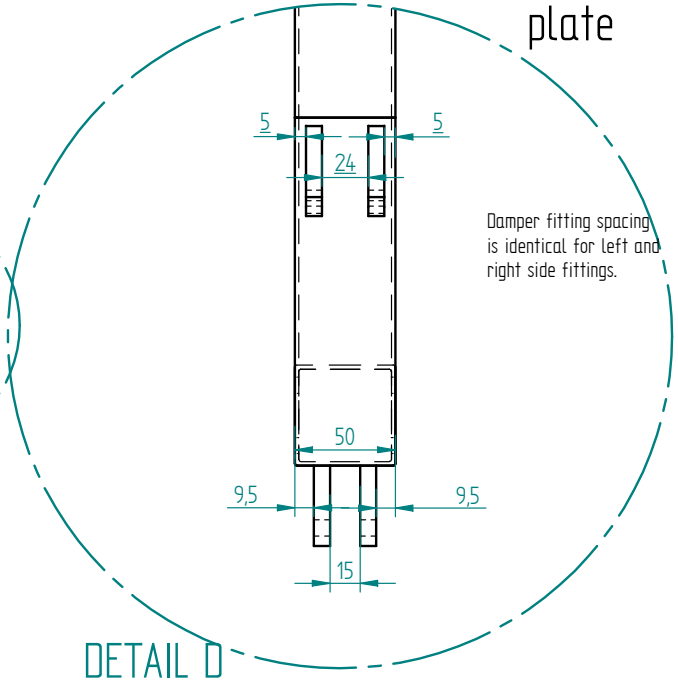

DETAIL D

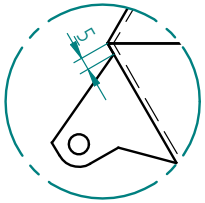

DETAIL A

Please note the 5 mm and 10mm clearances in detail A,B&C. so that welds of damper fittings do not intersect mainframe welds.

Damper fittings in detail A&B are item 2 damper fitting (sides)

All the paired fitting plates need to be maintained parallel, please control the weld distortion.

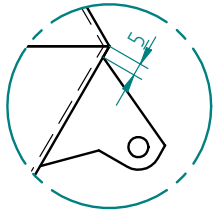

DETAIL B

DRAWN	Charles	05/26/09
CHECKED	Ben Cazzolato	
CONTACT: 0413647219		
TOLERANCE ANGLES ±0.1° LENGTH ±0.1 UNLESS OTHERWISE SPECIFIED		

DIWHEEL WHEELBIKE
SUPERVISOR: Ben Cazzolato

TITLE : Inner rotational frame ASM 2

SCALE: 1 : 0.15 | QUANTITY: 2

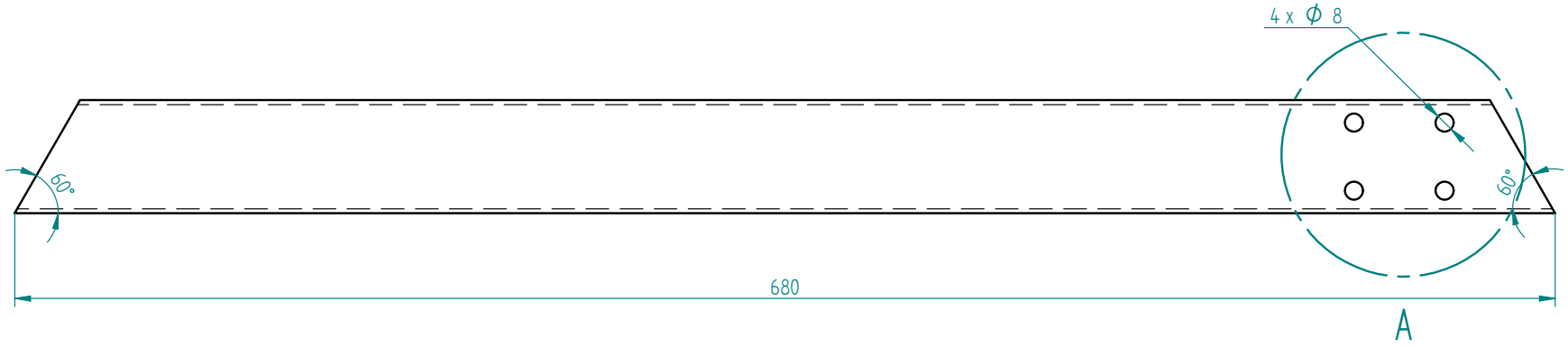

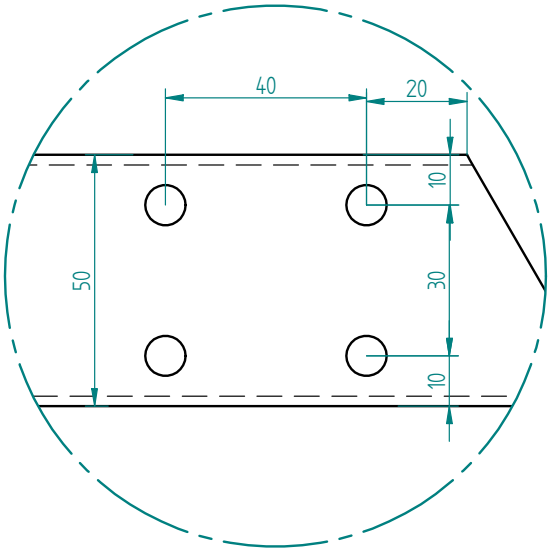

DETAIL A

This section is made of steel SHS (square hollow section) with 50mm side and 2mm wall thickness. Quantity required is 2

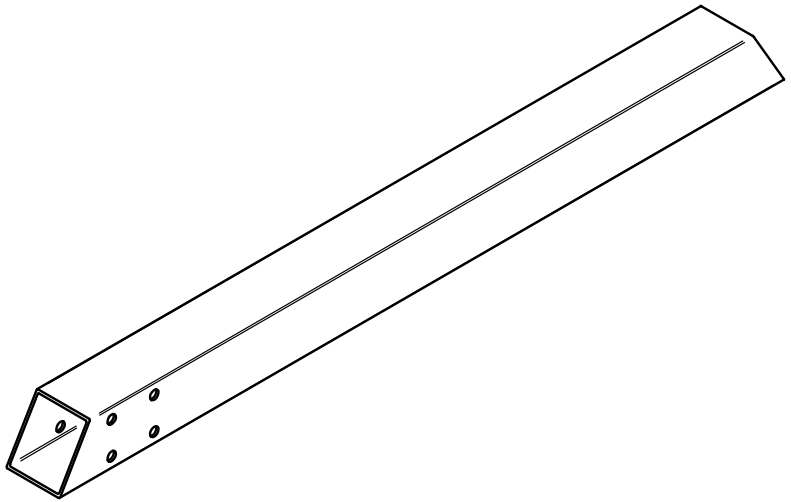

DRAWN	Charles	05/26/09
CHECKED	Ben Cazzolato	
CONTACT: 0413647219		
TOLERANCE ANGLES ±0.1° LENGTH ±0.1 UNLESS OTHERWISE SPECIFIED		

DIWHEEL WHEELBIKE
SUPERVISOR: Ben Cazzolato

TITLE: Rotational inner frame member (back)

SCALE: 1 : 0.5 | QUANTITY: 2

Quantity: 2

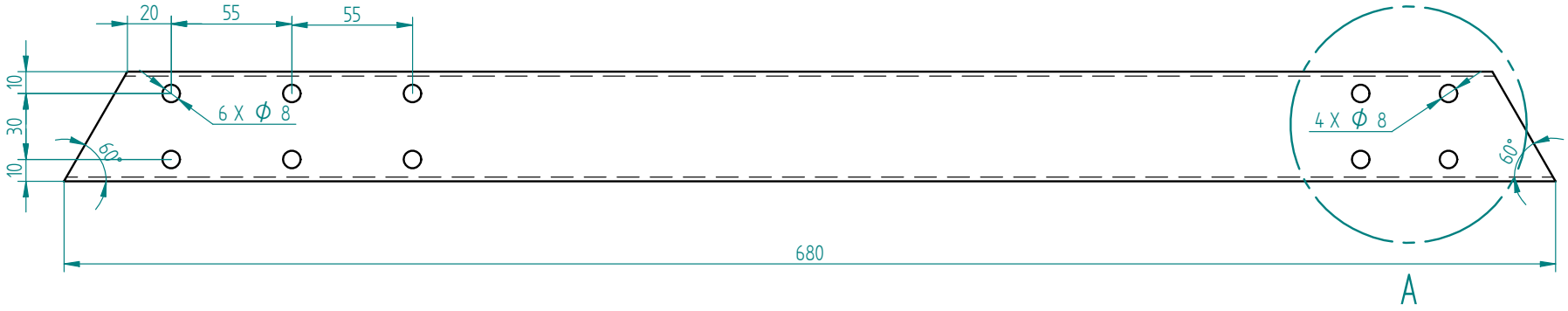

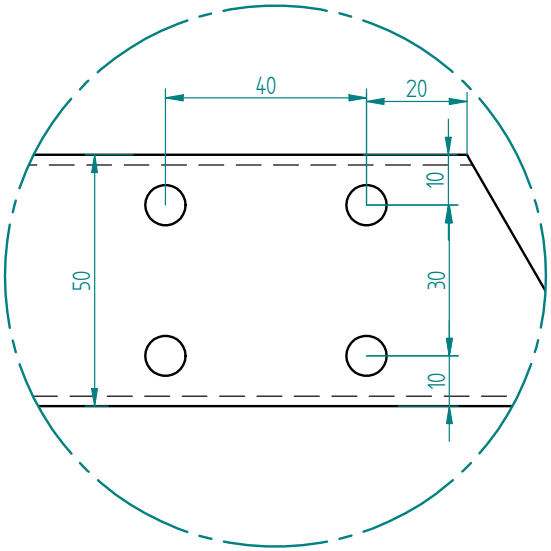

DETAIL A

This section is made of steel SHS (square hollow section) with 50mm side and 2mm wall thickness.

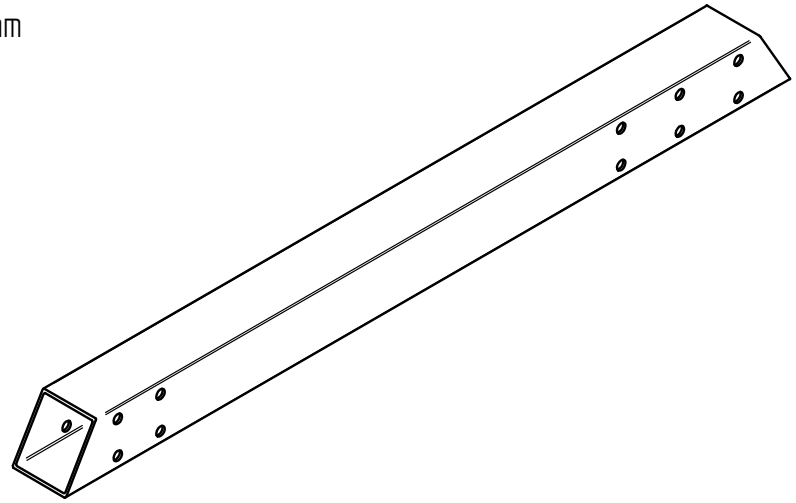

DRAWN	Charles	05/26/09
CHECKED	Ben Cazzolato	
CONTACT: 0413647219		
TOLERANCE ANGLES ±0.1° LENGTH ±0.1 UNLESS OTHERWISE SPECIFIED		

DIWHEEL WHEELBIKE
SUPERVISOR: Ben Cazzolato

TITLE: Rotational inner frame member (bottom)

SCALE: 1 : 0.5 | QUANTITY: 2

Quantity required is 2

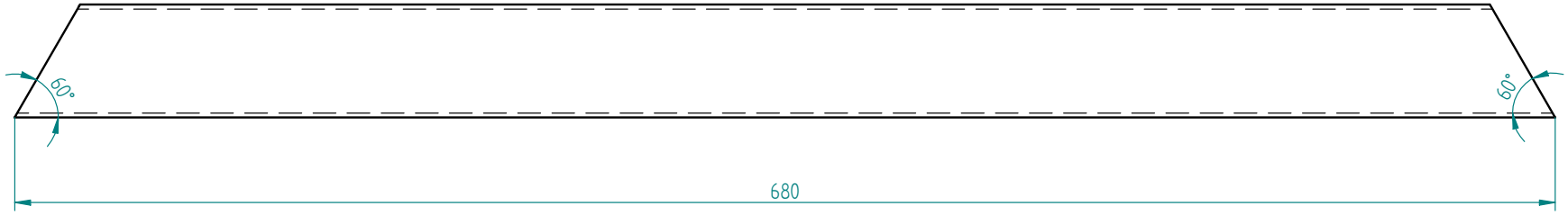

This section is made of steel SHS (square hollow section) with 50mm side and 2mm wall thickness.

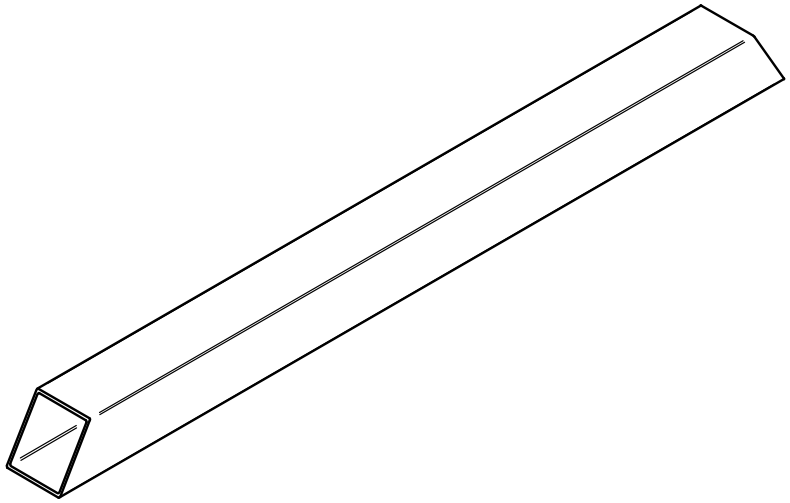

DRAWN	Charles	05/26/09
CHECKED	Ben Cazzolato	
CONTACT: 0413647219		
TOLERANCE ANGLES ±0.1° LENGTH ±0.1 UNLESS OTHERWISE SPECIFIED		

DIWHEEL WHEELBIKE
SUPERVISOR: Ben Cazzolato

TITLE: Rotational inner frame member (front)

SCALE: 1 : 0.5 | QUANTITY: 2

Quantity: 6

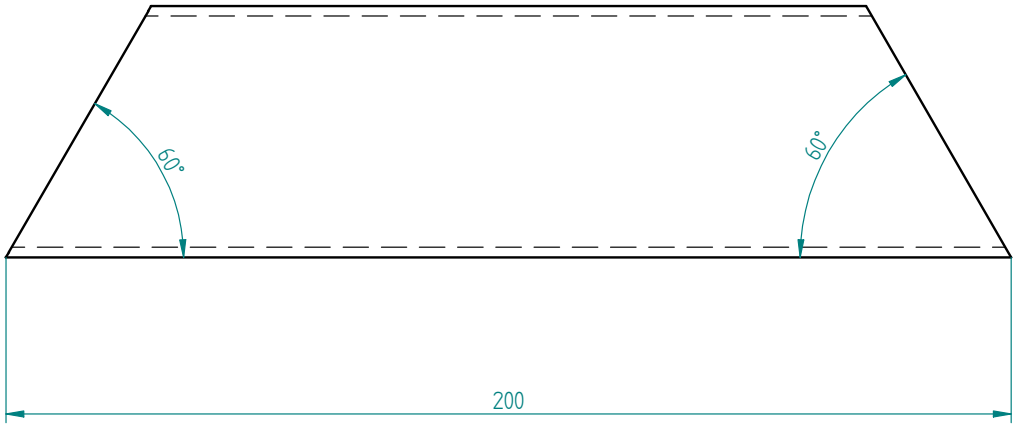

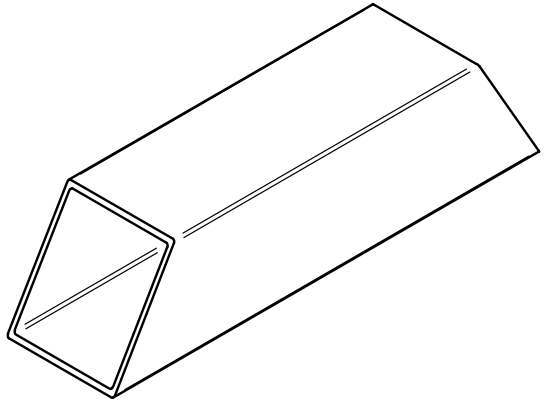

make this section with 50mm steel SHS (square hollow section) with 2mm wall thickness.

DRAWN	Charles	05/26/09
CHECKED	Ben Cazzolato	
CONTACT: 0413647219		
TOLERANCE ANGLES ±0.1° LENGTH ±0.1 UNLESS OTHERWISE SPECIFIED		

DIWHEEL WHEELBIKE
SUPERVISOR: Ben Cazzolato

TITLE Inner rotational frame member (short)

SCALE: 1 : 1	QUANTITY: 6

Please make the 37mm hole for interferencely fit for 37mm OD and 12mm ID deep grove ball bearings. (bearing supplied)

Quantity: 8

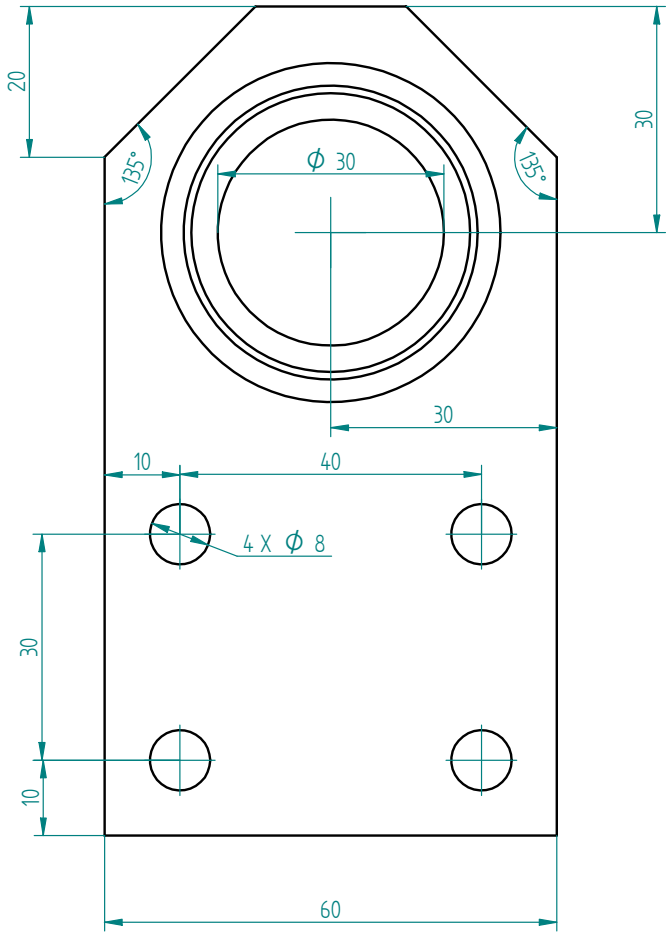

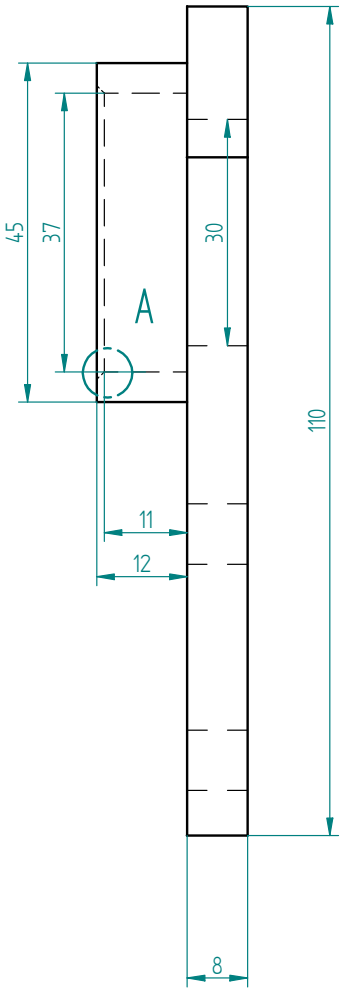

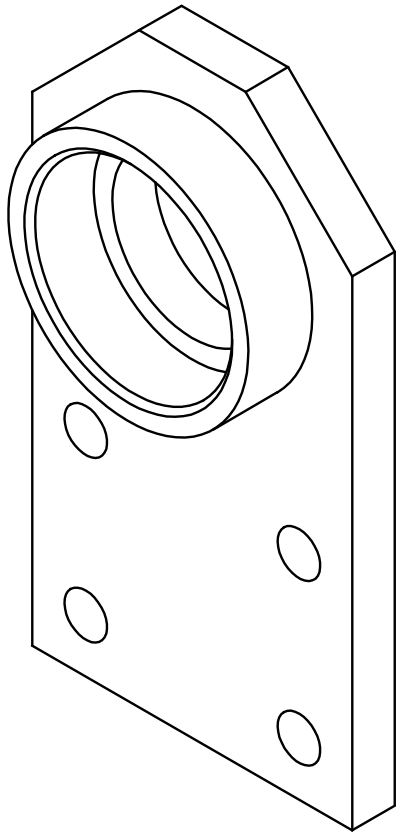

DETAIL A

Chamfer with 1 mm setback for installing bearing

DRAWN	Charles	05/26/09
CHECKED	Ben Cazzolato	
CONTACT: 0413647219		
TOLERANCE ANGLES ±0.1° LENGTH ±0.1 UNLESS OTHERWISE SPECIFIED		

DIWHEEL WHEELBIKE
SUPERVISOR: Ben Cazzolato

TITLE: Single bearing housing

SCALE: 1 : 1.5 | QUANTITY : 8

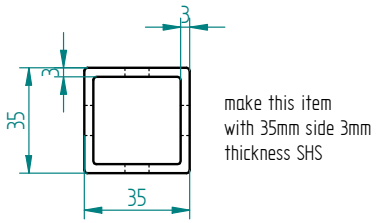

make this item
with 35mm side 3mm
thickness SHS

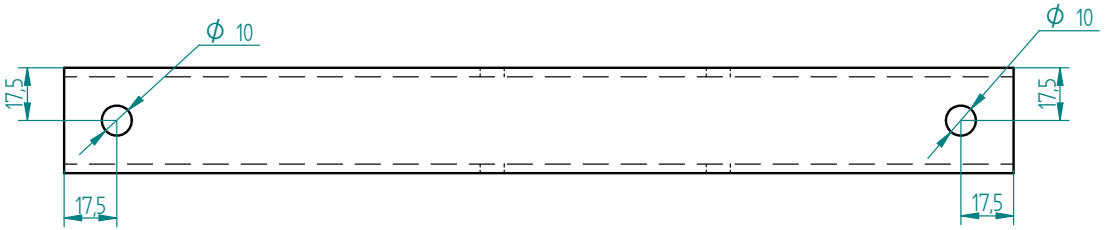

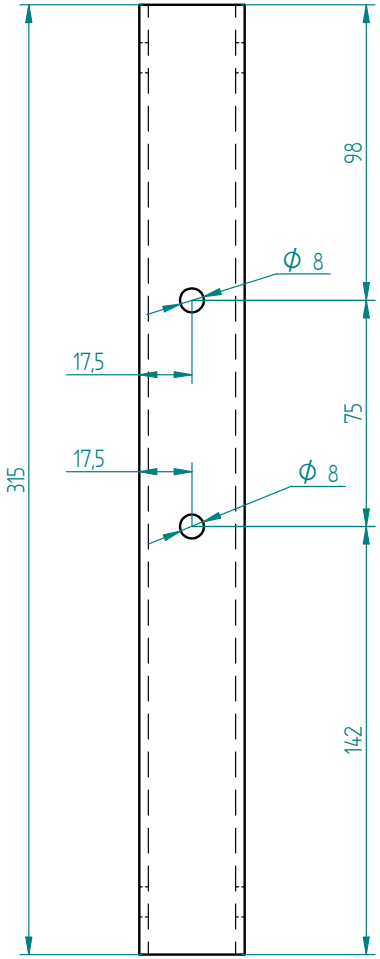

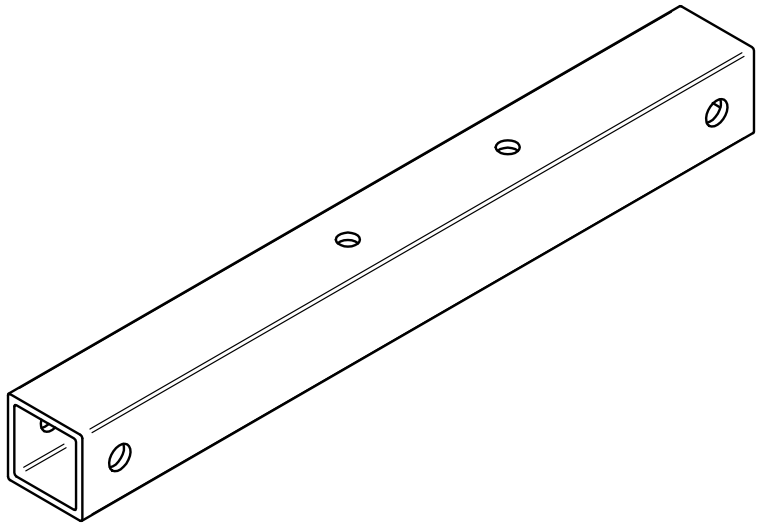

Quantity : 8

DRAWN	Charles	05/26/09
CHECKED	Ben Cazzolato	
CONTACT: 0413647219		
TOLERANCE ANGLES ±0.1° LENGTH ±0.1 UNLESS OTHERWISE SPECIFIED		

DIWHEEL WHEELBIKE
SUPERVISOR: Ben Cazzolato

TITLE : Suspension bridge member (sides)	Steel
SCALE:1 : 0.6	QUANTITY: 8

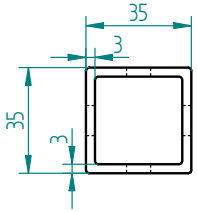

make this item
with 35mm side 3mm
thickness SHS

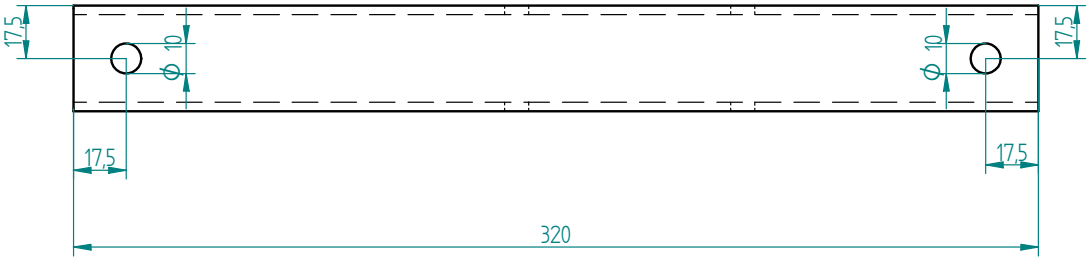

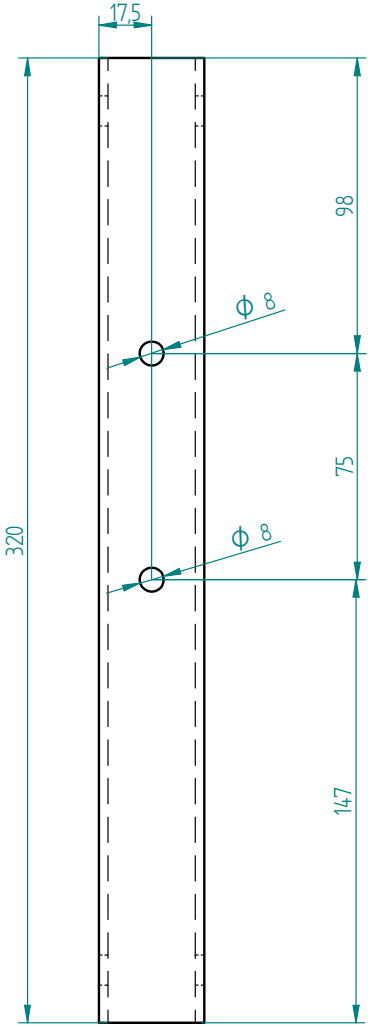

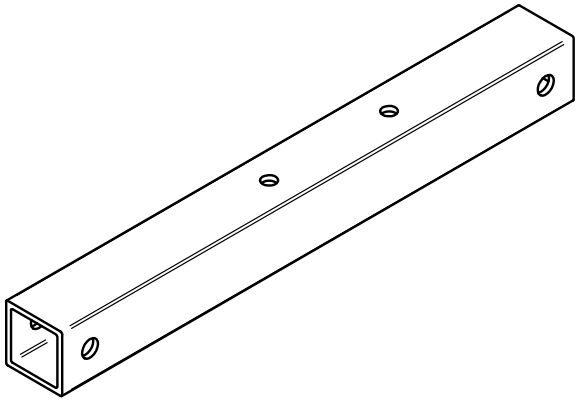

Qua ntity : 4

DRAWN	Charles	05/27/09
CHECKED	Ben Cazzolato	
CONTACT: 0413647219		
TOLERANCE ANGLES ±0.1° LENGTH ±0.1 UNLESS OTHERWISE SPECIFIED		

DIWHEEL WHEELBIKE
SUPERVISOR: Ben Cazzolato

TITLE: Suspension bridge member (top)	Steel
SCALE: 1 : 0.6	QUANTITY: 4

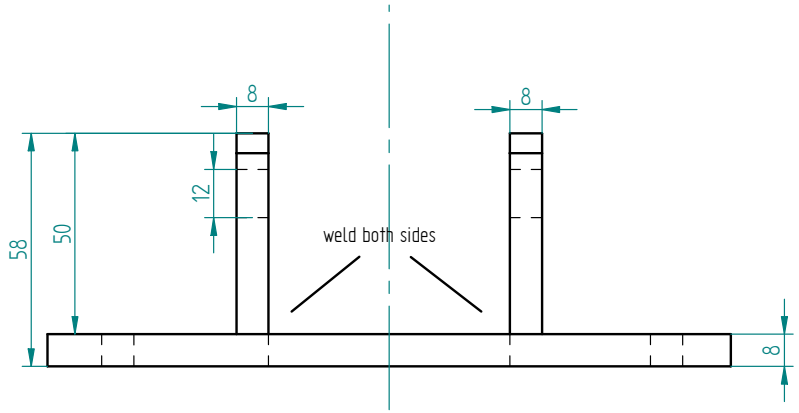

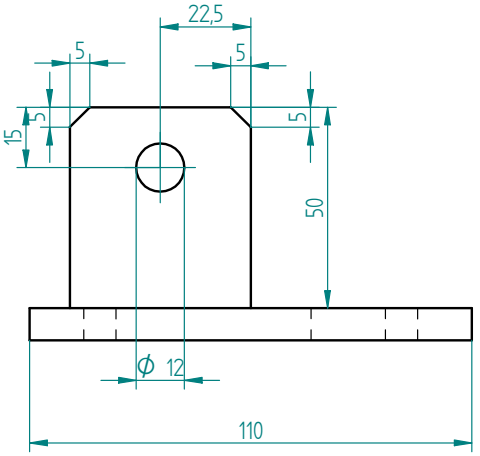

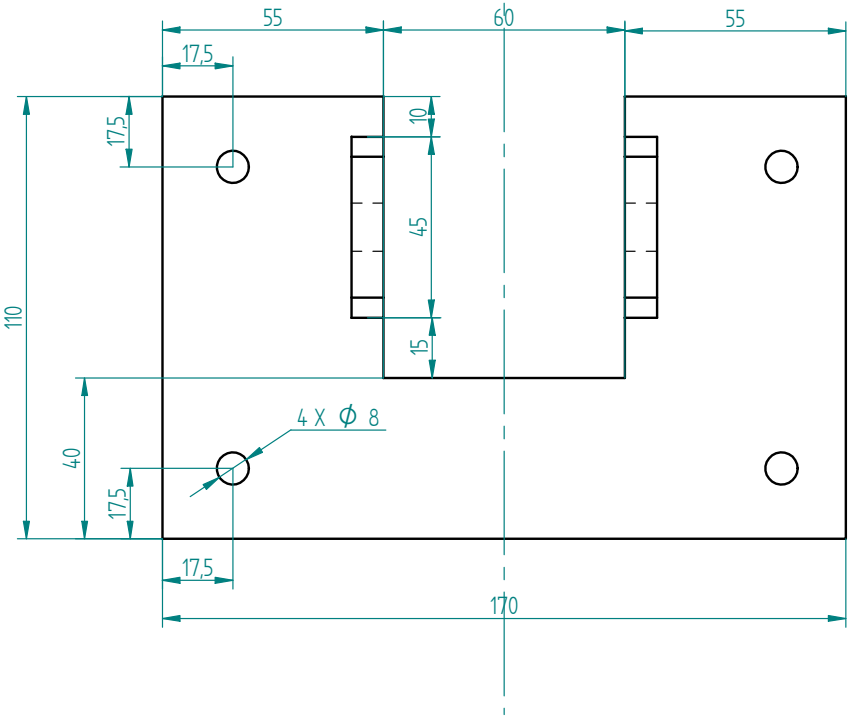

Quantity: 2

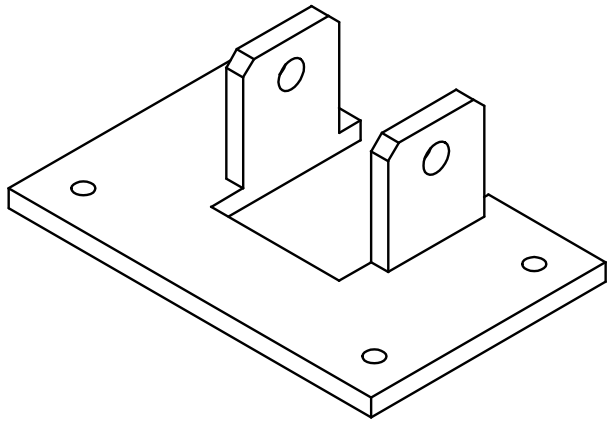

DRAWN	Charles	05/26/09
CHECKED	Ben Cazzolato	
CONTACT: 0413647219		
TOLERANCE ANGLES ±0.1° LENGTH ±0.1 UNLESS OTHERWISE SPECIFIED		

DIWHEEL WHEELBIKE
SUPERVISOR: Ben Cazzolato

TITLE : Suspension bridge plate (bottom)

SCALE: 1: 0.8 | QUANTITY: 2

Quantity: 4

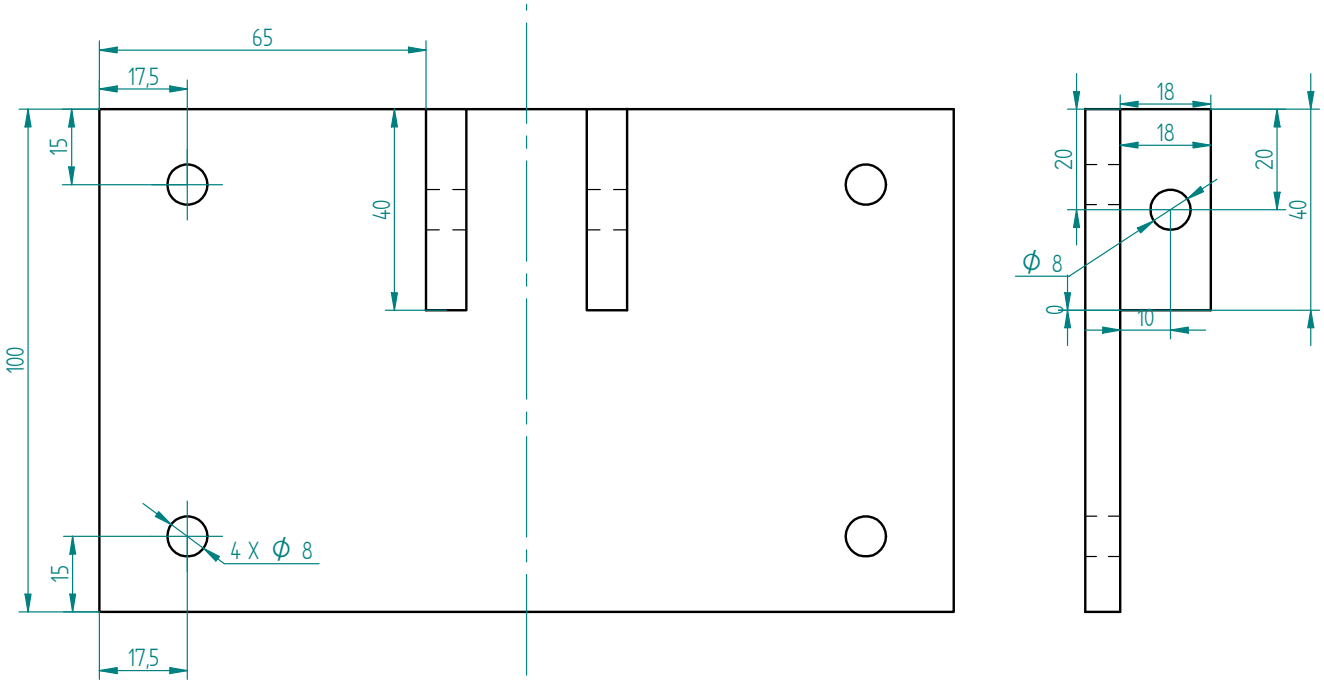

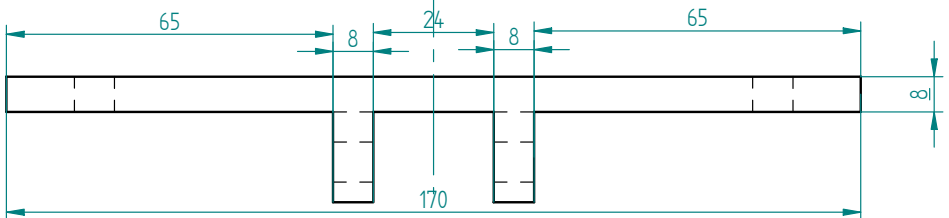

need to be maintained parallel when welding

Weld both sides of both plates, leave enough space between hole and base plate for M8 bolt head and nut on outer side of both plates.

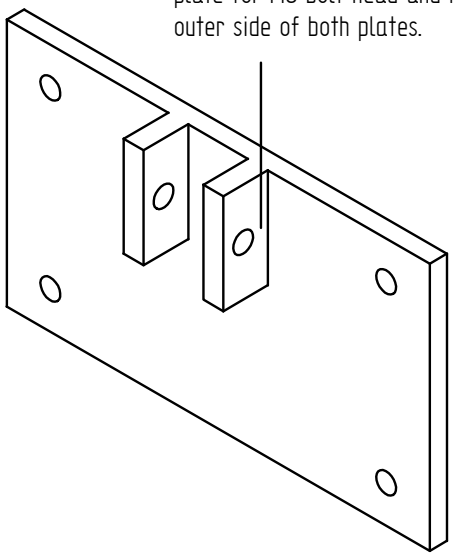

DRAWN	Charles	05/26/09
CHECKED	Ben Cazzolato	
CONTACT: 0413647219		
TOLERANCE ANGLES ±0.1° LENGTH ±0.1 UNLESS OTHERWISE SPECIFIED		

DIWHEEL WHEELBIKE
SUPERVISOR: Ben Cazzolato

TITLE : Suspension Bridge plate (sides)

SCALE: 1 : 1 | QUANTITY: 4

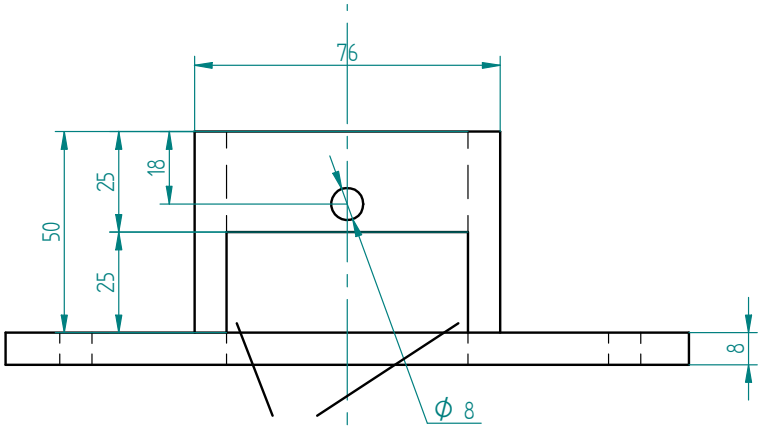

Weld both sides

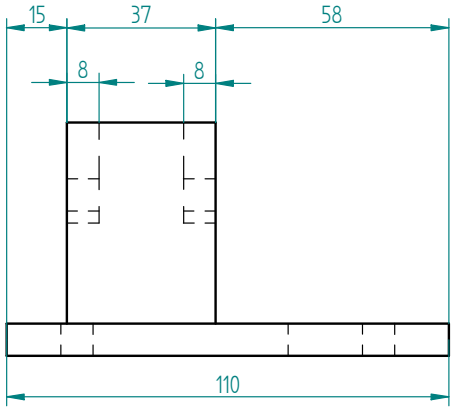

This item will be subjected to heavy cyclic load.
All the joints need to be strong.

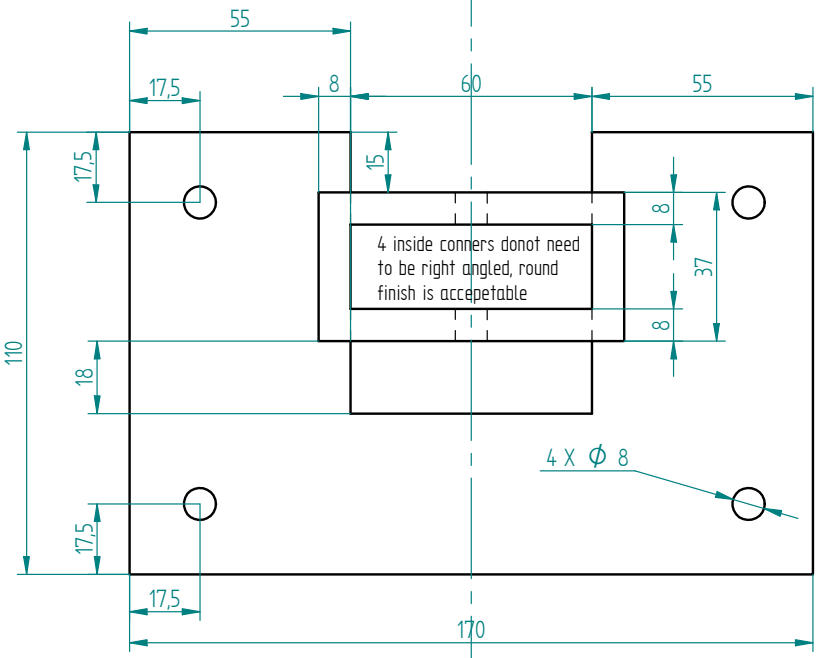

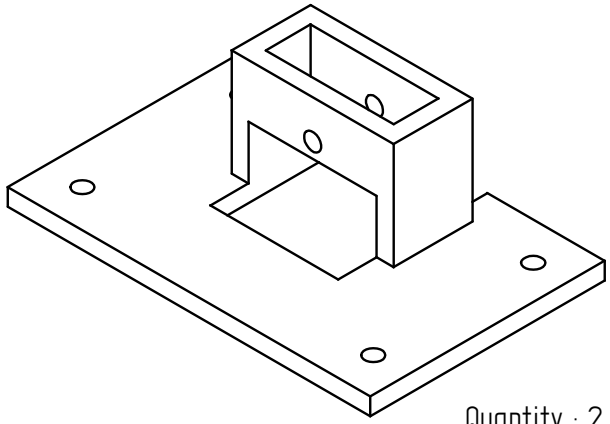

Quantity : 2

DRAWN	Charles	05/26/09
CHECKED	Ben Cazzolato	
CONTACT: 0413647219		
TOLERANCE ANGLES ±0.1° LENGTH ±0.1 UNLESS OTHERWISE SPECIFIED		

DIWHEEL WHEELBIKE
SUPERVISOR: Ben Cazzolato

TITLE : Suspension bridge plate (top)	Steel
SCALE: 1 : 0.8	QUANTITY: 2

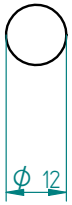

Shaded areas represent standard M12 threads

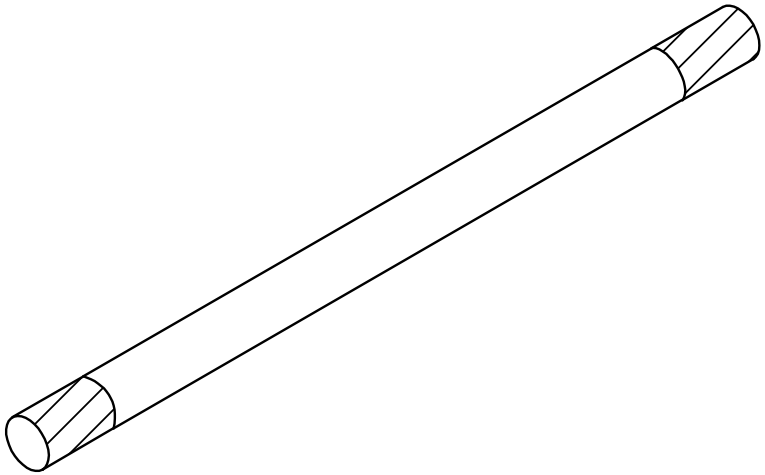

DRAWN	Charles	05/26/09
CHECKED	Ben Cazzolato	
CONTACT: 0413647219		
TOLERANCE ANGLES ±0.1° LENGTH ±0.1 UNLESS OTHERWISE SPECIFIED		

DIWHEEL WHEELBIKE
SUPERVISOR: Ben Cazzolato

TITLE : Swing arm pin joint axial

SCALE: 1 : 1 | QUANTITY: 2